

Materials and anti-adhesive issues in UV-NIL

Achille Francone

▶ **To cite this version:**

Achille Francone. Materials and anti-adhesive issues in UV-NIL. Materials. Institut National Polytechnique de Grenoble - INPG, 2010. English. NNT : . tel-00666073

HAL Id: tel-00666073
https://theses.hal.science/tel-00666073

Submitted on 3 Feb 2012

HAL is a multi-disciplinary open access archive for the deposit and dissemination of scientific research documents, whether they are published or not. The documents may come from teaching and research institutions in France or abroad, or from public or private research centers.

L'archive ouverte pluridisciplinaire **HAL**, est destinée au dépôt et à la diffusion de documents scientifiques de niveau recherche, publiés ou non, émanant des établissements d'enseignement et de recherche français ou étrangers, des laboratoires publics ou privés.

THESE DE L'UNIVERSITE DE GRENOBLE

Délivrée par l'Institut Polytechnique de Grenoble

N° attribué par la bibliothèque
|__|__|__|__|__|__|__|__|__|__|

T H E S E

pour obtenir le grade de

DOCTEUR DE L'UNIVERSITE DE GRENOBLE

Spécialité : « 2MGE Matériaux, Mécanique, Génie civil, Electrochimie »

préparée au Laboratoire des Technologies de la Microélectronique (LTM-CNRS)

dans le cadre de **l'Ecole Doctorale** « I-MEP2 Ingénierie Matériaux Mécanique Energétique Environnement Procéés Production »

présentée et soutenue publiquement par

Achille FRANCONE

Le 9 Décembre 2010

Materials and anti-adhesive issues in UV-NIL

Directeur de thèse: BOUSSEY Jumana

JURY

Président	M.me AUZELY-VELTY Rachel	Prof. à Université Joseph Fourier, Grenoble (France)
Rapporteur	M. SCHLATTER Guy	Prof. à Université de Strasbourg, Strasbourg (France)
Rapporteur	M. SOPPERA Olivier	Chargé de recherche CNRS-IS2M, Mulhouse (France)
Directeur de thèse	M.me BOUSSEY Jumana	Chargé de recherche CNRS-LTM, Grenoble (France)
Examinateur	M. ZELSMANN Marc	Chargé de recherche CNRS-LTM, Grenoble (France)
Examinateur	M. KEHAGIAS Nikolaos	Postdoctorant ICN , Bellaterra (Espagne)
Invité	M.me IOJOIU Cristina	Chargé de recherche CNRS-LEPMI, Grenoble (France)

Acknowledgments

Although a lot of efforts were necessary to write this PhD thesis, I feel really satisfied about the final result. A lot of persons contributed directly and indirectly, more or less, to the achievement of this work.

I am grateful to all the persons that accepted to participate to the jury of my thesis: Pr. AUZELY-VELTY Rachel, Dr. KEHAGIAS Nikolaos, Dr. IOJOIU, Cristina, Dr. ZELSMANN Marc, Dr. BOUSSEY Jumana, Dr. SOPPERA and Pr. SCHLATTER Guy, with the last two that accepted to evaluate my manuscript as rapporteurs.

I really appreciated the hospitality shown during this three-year thesis work at the Laboratoire des Technologies de la Microélectronique (LTM) in Grenoble (France) inside the CEA-LETI-Minatec center. I would like indeed to thank Dr. JOUBERT Olivier t, LTM Head, for enabling me to carry out this work in an excellent technical and scientific environment.

I am grateful to Région Rhône-Alpes for financing my three years PhD fellowship.

Special thanks go to Dr. BOUSSEY Jumana my thesis director for having made this work possible. She launched me on this adventure, and I have received high-value support from her throughout the thesis. Her patience in front of difficult situations taught me a lot.
Sincere thanks go to Dr. ZELSMANN Marc, my daily supervisor at LTM lab, with whom I have spent uncountable hours engaged in enjoyable and enriching discussions. His broad background in physics and engineering, his sportive spirit, his rigorous work and his methodology have contributed significantly to my scientific and human apprenticeship.

Then, I would like to thank a group of persons for the nice collaborations we had during my PhD, managing to get interesting results during different kinds of experiments. These persons are: Dr. POULAIN Christophe during nanoindentation experiments at CEA Grenoble-LETI-DIHS-Laboratoire de Caractérisation et de Fiabilité des Microsystèmes; LOMBARD Christophe and Dr. PEPIN-DONAT Brigitte during electron spin resonance experiments at CEA Grenoble-INAC- Laboratoire de Structure et Propriétés d'Architecture Moléculaires; Dr. IOJOIU, Cristina during Fourier Transform Infrared Spectroscopy experiments at CNRS-Grenoble Laboratoire d'Electrochimie et de Physicochimie des Matériaux et des Interfaces.

During my Phd I had also the possibility to collaborate and to run experiments away from Grenoble. In particular I had the pleasure to collaborate with Dr. ZOMPATORI Alberto, dependent of SOLVAY Solexis S.p.A., who hosted me in the Italian research and development centre at Bollate to select an anti-adhesive commercial product. His collaboration continued during all the experiments run on the product, giving precious advices over the interpretation of the results.
Many thanks go to HAATAINEN Tomi, that although several difficulties allows to me to run a week demolding force experiments in the Finnish VTT technical research centreat Espoo.
Particular acknowledgments go to Pr. SOTOMAYOR TORRES Clivia who allowed to me to join her Spanish group, ICN Phononic and Photonics Nanostructures Group, at Bellaterra. I spent seventh months of my Phd working with this group and it was a great experience under human and professional point of view. I found a wonderful atmosphere thanks to Nik, Vincent, Olivier, Damien, John, Michael, Sinead.

I cannot forget about all the friends that shared unforgettable experiences with me in Grenoble (sports, parties, trips, etc.) and that determined my positive judgment over the time I spent in France during my PhD.

A million thanks to my beloved family members back home in Italy, that encouraged me throughout the PhD time, sharing positive and negative moments.

Last but not least, my sincere thanks go to my lovely girlfriend Chiara, which gave me the moral support and motivations to go on, especially during the most critical moments of the PhD thesis writing period.

Preface

The works of research obtained after my three year Phd were well valorized. In fact, the results were presented during different events (international conferences, scientific day, summer school) and in different manners (journal publications, poster and oral presentations). These are listed below.

Journal Publications

1) D. Boutry, R. Galand, A. Beaurain, **A. Francone**, B. Pelissier, M. Zelsmann, and J. Boussey, "Mold cleaning and fluorinated anti-sticking treatments in nanoimprint lithography", Microelectron Eng, 86 (4-6), p. 669-672, 2009.

2) M. Zelsmann, C. Alleaume, D. Boutry**, A. Francone,** A. Beaurain, B. Pelissier and J. Boussey, "Degradation and surfactant-aided regeneration of fluorinated anti-sticking mold treatments in UV nanoimprint lithography", Microelectron Eng, 87 (5-8), p. 1029-1032, 2010.

3) M. Zelsmann, D. Boutry, **A. Francone**, C. Allaume, I. Kurt, A. Beaurain, B. Pelissier, B. Pépin-Donat, C. Lombard and J. Boussey , "Double-anchoring fluorinated molecules for anti-adhesion mold treatment in UV nanoimprint lithography", J. Vac. Sci. Technol. B, 27(6), p. 2873-2876, 2009.

4) **A. Francone**, C. Iojoiu, C. Poulain, C. Lombard, B. Pépin-Donat, J. Boussey and M. Zelsmann, "Impact of the resist properties on the antisticking layer degradation in UV nanoimprint lithography", J. Vac. Sci. Technol. B, 28(6), p. C6M72-C6M76, 2010.

5) N. Kehagias, **A. Francone**, M. Chouiki, M. Zelsmann, V. Reboud, R. Schoeftner and C. Sotomayor Torres, "Low temperature direct imprint of polyhedral silsequioxane (PSSQ) resist", to appear in Microelectron Eng.

Poster Presentations

All the works of research above listed as journal publications were presented as well during international conferences. Those published in Microelectronic Engineering were exposed as poster presentations during the same year edition of Micro and Nano engineering conference; those published in Journal of Vacuum Science & Technology B were exposed as poster presentations during the same year edition of Electron, Ion, Photon Beam Technology and Nanofabrication conference. Another poster was presented, as follows:

N. Kehagias, R. A. Farrell, M. Zelsmann, **A. Francone**, M. Chouiki, V. Reboud, J. D. Holmes, M. A. Morris and C. Sotomayor Torres, "PSSQ templates fabricated by RUVNIL technique for graphoepitaxy", Nanoprint and Nanoimprint Technology conference, Copenhagen (Denmark), Oct 13-15, 2010.

Oral Presentations

1) **A. Francone**, "Materials and process development of UV-based nanoimprint lithography", NanoSciences Summer school, Tremblay (France), Jun 23-28, 2008.

2) **A. Francone**, "Développement de la lithographie par nano-impression assistée par UV (UV-NIL)", Cluster Microéléctronique, Nanosciences et Nanoélectronique Scientific day, Grenoble (France), Oct 10, 2009.

3) M. Zelsmann, C. Alleaume, D. Boutry**, A. Francone,** A. Beaurain, B. Pelissier and J. Boussey, "Degradation and surfactant-aided regeneration of fluorinated anti-sticking mold treatments in UV nanoimprint lithography", Micro and Nano Engineering conference, Ghent (Belgium), Sept 28-Oct 1, 2009.

INTRODUCTION **9**

CHAPTER I. LITHOGRAPHY AND UV-ASSISTED NANOIMPRINT LITHOGRAPHY **11**

1 INTRODUCTION 11
2 LITHOGRAPHY IN MICROELECTRONICS 13
2.1 Optical lithography *13*
2.2 Optical lithography evolution *15*
2.3 Future of lithography *18*
2.4 Next Generation Lithographies (NGLs) *20*
2.5 Nanoimprint lithography techniques *23*
3 UV-ASSISTED NANOIMPRINT LITHOGRAPHY 27
3.1 Process details and variants *27*
3.2 Resist flow in thin layers *29*
3.3 Imprinting examples, resolution and applications *29*
3.4 Imprinting tools *33*
3.5 Industrialization issues *33*
4 IMPRINTING MATERIALS FOR UV-NIL 36
4.1 UV-assisted polymerization process *36*
4.2 UV-curable resists for UV-NIL *41*
4.3 Resist shrinkage *42*
4.4 Plasma etching processes and resists stripping *43*
5 MOLD FABRICATION AND ANTISTICKING ISSUES 45
5.1 Mold fabrication and characterization *45*
5.2 Antisticking issues *46*
5.3 Mold treatments *47*
5.4 Fluorinated mold treatment-resist interactions *49*
5.5 Resist-oriented antisticking strategies *49*
6 CONCLUSION 51

CHAPTER II. ANTISTICKING ISSUES IN NANOIMPRINT LITHOGRAPHY **53**

1 ANALYSIS OF FLUORINATED ANTISTICKING LAYERS (F-ASLS) BEFORE IMPRINTING 53
1.1 F-ASLs deposition procedure *53*
1.2 Fluorinated layers characterization techniques *54*
1.3 X-ray Photoelectron Spectroscopy (XPS) details *55*
1.4 Optool DSX characteristics after deposition *56*
2 ANALYSIS OF THE F-ASL DEGRADATION DURING IMPRINTING 58
2.1 Introduction *58*
2.2 F-ASL aging in a standard UV-NIL process *58*
2.3 Direct impact of UV exposure *60*
2.4 Impact of the mold nature and history *61*
2.5 Impact of the resist's free radicals *65*
2.6 Impact of the UV intensity and dose *67*
2.7 Conclusion *69*
3 EVALUATION OF OTHER F-ASLS 70
3.1 Fluorolink® S10: two anchoring end groups *70*
3.2 F_{13}-TMS: shorter chain *73*
3.3 Conclusion *76*
4 IMPACT OF THE UV-CURABLE RESIST ON THE F-ASL DEGRADATION 77
4.1 Comparison of UV-NIL and thermal-NIL *77*
4.2 Impact of type and number of polymerizable groups *82*
4.3 Impact of fluorinated additives in the UV curable resist *92*
4.4 Conclusions *96*
5 CONCLUSIONS OF CHAPTER II 97

CHAPTER III. APPLICATION OF UV CURABLE RESISTS IN A REVERSE UV-NIL PROCESS **99**

1 INTRODUCTION 99
2 BLOCK COPOLYMERS FOR NANOPATTERNING 100
2.1 Nomenclature *100*
2.2 Microphase separation *100*
2.3 How can we align thin film diblock copolymers? *102*

2.4 Graphoepitaxy 103
3 REVERSE UV-NIL EXPERIMENTS 105
3.1 Description of the process used 105
3.2 Hybrid mold fabrication 106
3.3 UV-curable functional resist 107
4 FIRST RESULTS 109
4.1 Graphoepitaxy on SSQ resists 109
4.2 Development of a dedicated solid SSQ resist 110
5 CONCLUSION 111
GENERAL CONCLUSION AND PERSPECTIVES 113
RESUME EN FRANÇAIS 115
REFERENCES 133

Introduction

The nanotechnology revolution has opened up new potential for producing miniaturized devices with reduced cost, less materials and better performance. Miniaturized devices such as microprocessors, micro-optics, biochips, microarrays and microfluidic components consist of micro / nanostructures of functional materials which can be made either using the "bottom up" or the "top down" approach. The bottom up approach fabricates materials and devices at the atomic or molecular scale, possibly using self-assembly methods, while the top down approach etches or mills smaller structures from larger ones. Currently, fabrication processes of most micro / nanostructures for micro / nanodevices are based on the established semiconductor industry manufacturing technology, which leads to the creation of electronic products widespread in modern times. Few examples are personal computers, mobile phones, televisions, DVD players and digital cameras. Although their different function, all of them are made with integrated circuits (ICs).
The fundamental building block of these modern electronic devices is the transistor. First ICs became commercially available in 1961 and at that time they hosted only one transistor; in 2010, Intel commercialized the Xenon 7500 processor series containing 2.3 billion of transistors. The key element responsible of this important progress is lithography, i.e. the technique used in the semiconductor industry to define the transistors. The process of miniaturization is still undergoing and standard projection optical lithography, used today in industry, will reach a resolution limit. This is why there is a need to develop Next Generation Lithographies (NGLs) able to propose an increased resolution at a reasonable cost. One of these NGLs is Nanoimprint lithography (NIL). It consists in the replication of a mold shape by pressing it into a thin layer of soft imaging material. Two main variants of nanoimprint lithography exist: thermal NIL and UV-assisted NIL (UV-NIL), demanding a thermoplastic (or thermo-curable) and a UV-curable resist respectively as soft imaging layer. UV-NIL is the most promising approach due to a lower process time and better alignment capabilities. However, number of issues has to be solved to bring this technology to an industrial maturity. Among these we have: the imaging material (resist) availability, the high resolution fused silica mold availability, the proper understanding of the resist flow during the process and all sticking-related problems that appear at the contact between the resist and the mold.

The *Laboratoire des Technologies de la Microélectronique*, in *Grenoble*, *France*, is a *CNRS* laboratory hosted in the *CEA-LETI-Minatec* center, one of the most attractive sites for applied research in Europe. During my three years PhD work in this lab, I tried to address the specific issues cited above, with a special emphasis on the antisticking issues, which is, I believe, the most critical aspect in this technology. Also, during the end of my second year, I stayed 6 months in the Catalan Institute of Nanotechnology in Barcelona, Spain, in the group of Prof. *C. M. Sotomayor Torres*, where I worked on the application of UV-NIL resists dedicated to the fabrication of templates for long-range ordering of di-block copolymers. Moreover, I had the possibility to collaborate and perform experiments in Finland, at the *VTT - Technical Research Centre* in *Espoo*.

This manuscript is divided into three chapters as follows:

- Chapter I presents the general context of lithography in microelectronics and the reason why it is needed to develop alternative lithography techniques. Process details and specific issues of UV nanoimprint lithography are given, along with a state-of-the-art on UV-NIL resists.

- Chapter II is the central chapter of my work. Results on antisticking issues in UV-NIL are presented. We tried to quantify and understand the mold treatment degradation occurring during the process. Also, original approaches are proposed to limit and possibly solve this very critical issue.

- Chapter III presents results on the synthesis and use of a hybrid organic-inorganic UV-NIL resist dedicated to a special application, i.e. the fabrication of templates for the long-range organization of di-block copolymers. Results are obtained in collaboration with the Catalan Institute of Nanotechnology and University College Cork, in Ireland.

Chapter I. Lithography and UV-assisted nanoimprint lithography

1 Introduction

An Integrated Circuit (IC) is an electronic circuit consisting of one silicon semiconductor substrate on which a number of electronic components (the main building blocks are transistor, diodes, resistors and capacitors) are mounted. ICs can be classified based on the degree of integration (the number of elements mounted on a single chip) and they can be grouped into four basic categories based on functions:

- Memories are ICs that store data and programs.
- Microcomputers are ultra-small computers incorporating Central Processing Units (CPUs) (which perform calculations as well as logical operations), memories and interface circuits.
- Application-Specific Integrated Circuit (ASICs) are ICs designed and manufactured to provide specific functions for electronic devices (such as mobile phones) and deliver superior performance and functionality.
- The System on Chip (SoC) refers to integrating all components of a computer or other electronic system into a single chip. It offers the highest degree of functionality and comprises microprocessors, chip sets, memories and video chips. This single chip boasts all of the functions of a computer. SoCs deliver benefits such as reduced mounting space, lower power consumption and higher cost-efficiency.

In general, it is possible to distinguish two main sections in integrated circuit manufacture, as indicated in Figure I. 1 (left): *front-end processing*, which refers to the formation of the transistors on the silicon substrate and *back end processing*, which refers to the formation of metal interconnecting wires. These interconnects are stacked today in multiple levels (between 5 and 10); the distance between these metal lines at the first level is called the pitch, and logically, the half-pitch is half that distance. The half-pitch of the metal lines on the first and densest level is special, because that distance was what once defined not only the half-pitch but also the gate and, consequently, the node. But by 2000, it was a dicey relationship. The half-pitch was becoming bigger than the node.

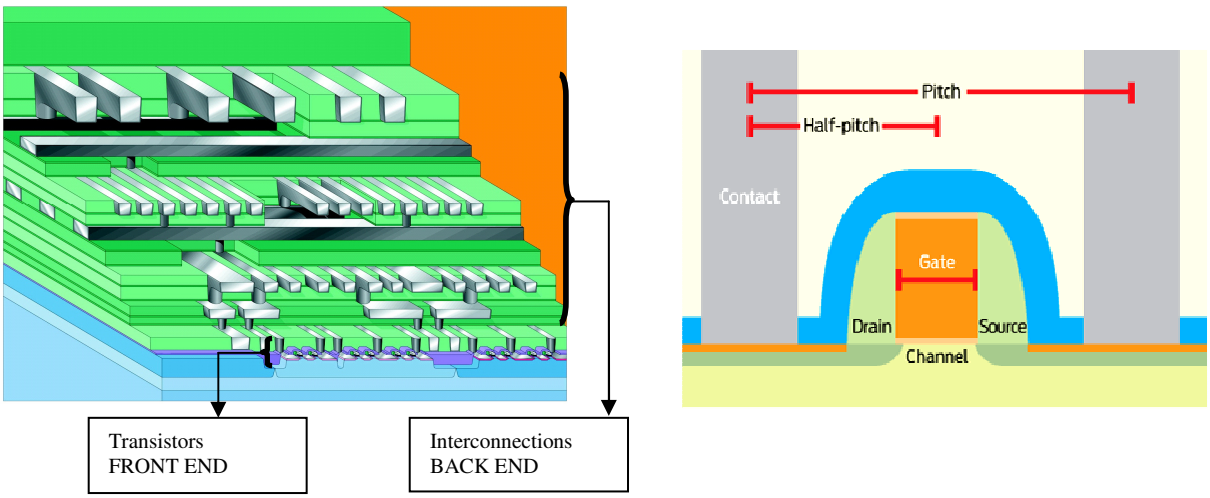


Figure I. 1: Cross-section of an integrated circuit, characterized by two distinguished sections *front end* and *back end* (left side); Picture showing the elements of a typical MOSFET transistor and the meaning of "pitch" and "half-pitch" (right side).[1]

The transistor is defined as MOSFET (Metal–Oxide–Semiconductor Field-Effect Transistor) and it presents specific elements in its structure, i.e. the drain, the source, the gate and the channel (which are separated by the gate insulator), as illustrated in Figure I. 1(right). Modern computers are manufactured using CMOS (Complementary Metal Oxide Semiconductor) technology, that uses a combination of p-type and n-type MOSFETs. Frank Wanlass successfully patented CMOS in 1967.
Today ICs has become incredibly small due to the reduction of the transistor's dimensions, representing the most important element for the speedup of microelectronic devices. The integration level of integrated circuits has risen according to Moore's Law, formulated in 1965[2] which says that the number of transistors integrated per chip doubles about every two years. This steady increase in integration level, illustrated in Figure I. 2, has made possible smaller ICs, faster processing, better reliability, lower heat dissipation and other performance improvements. At the same time, the larger number of chips which can be manufactured at once has resulted in slashed IC prices, accelerating the adoption of chips in many fields.

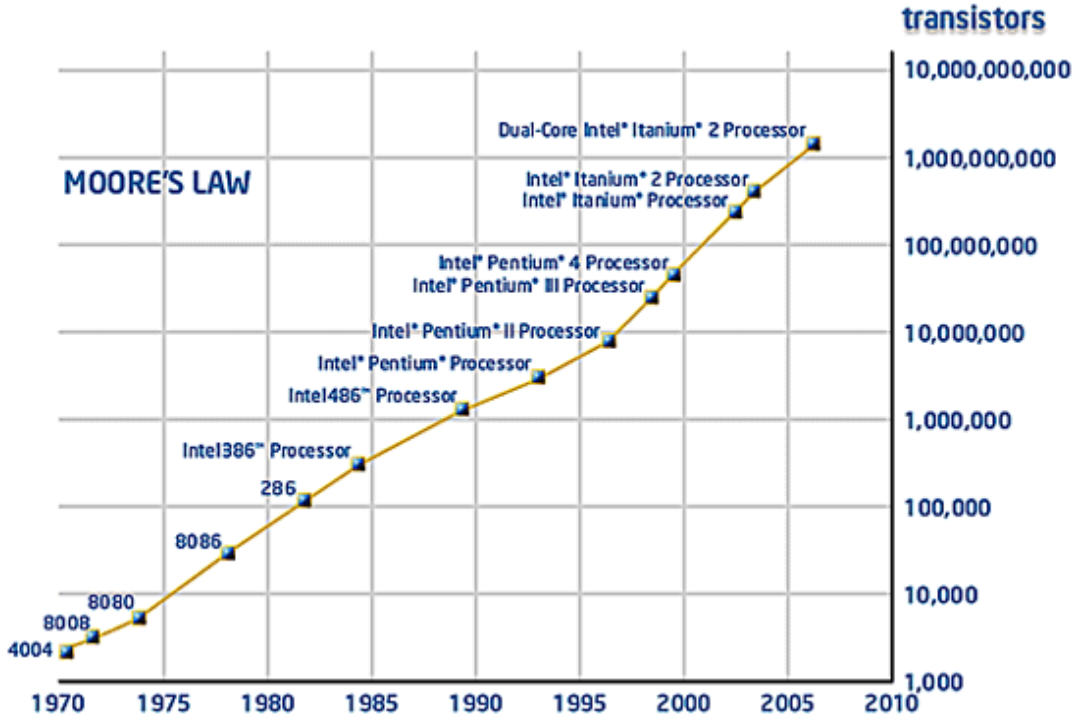


Figure I. 2: Increase in the number of integrated transistor per die from early 1970's till 2010 following Moore's law prediction.[3]

As will be presented in this chapter, this trend was made possible by the improvement of the photolithography capabilities during the last decades in microelectronics. Nevertheless, the continuous improvement of optical lithography's resolution is now becoming excessively expensive and there is a need of development of alternative technologies. In microelectronics, these alternative technologies are called Next generation Lithographies (NGLs). One of these NGLs is Nanoimprint Lithography (NIL), developed not only for the microelectronics field, but also as a general fabrication technique in application fields where electron-beam lithography or state-of-the-art photolithography cannot propose a sufficiently high resolution at a reasonable cost; or where the capability of 3D imprinting or imprinting in a functional material is needed.

2 Lithography in microelectronics

Lithography (from Greek λίθος - lithos, 'stone' and γράφω - grapho, 'to write') is a method for reproducing text and image using a stone or a metal plate with a completely smooth surface. Invented in 1796 by Alois Senefelder as a low-cost method of publishing theatrical works,[4] lithography can be used to print text or artwork onto paper or another suitable material.

In the semiconductor industry, lithography is the key technique whereby the circuit patterns are defined on an imaging layer. For multi-level circuits, semiconductor industry employ optical lithography's planar fabrication technology in which integrated circuits are built by stacking one layer of circuit elements on top of another. These make the fabrication process complicated and expensive. Roughly 35% of device costs are attributed to repetitive lithography processes.[5]

From the early 1960s till today ICs were patterned employing optical elements, so that we can talk about optical lithography. A lot of improvements in the optical lithography were necessary to achieve a constant miniaturization in the features, evolving from micro to nano-scale. In this section, I will introduce the basis of optical lithography, followed by the technical evolution that brought to the actual use of water immersion lithography.

2.1 Optical lithography

Steps involved in the optical lithography (also called "photolithography") process are: wafer cleaning, barrier layer formation, photoresist application, soft baking, mask alignment, exposure and development, and hard-baking, as illustrated in Figure I. 3:

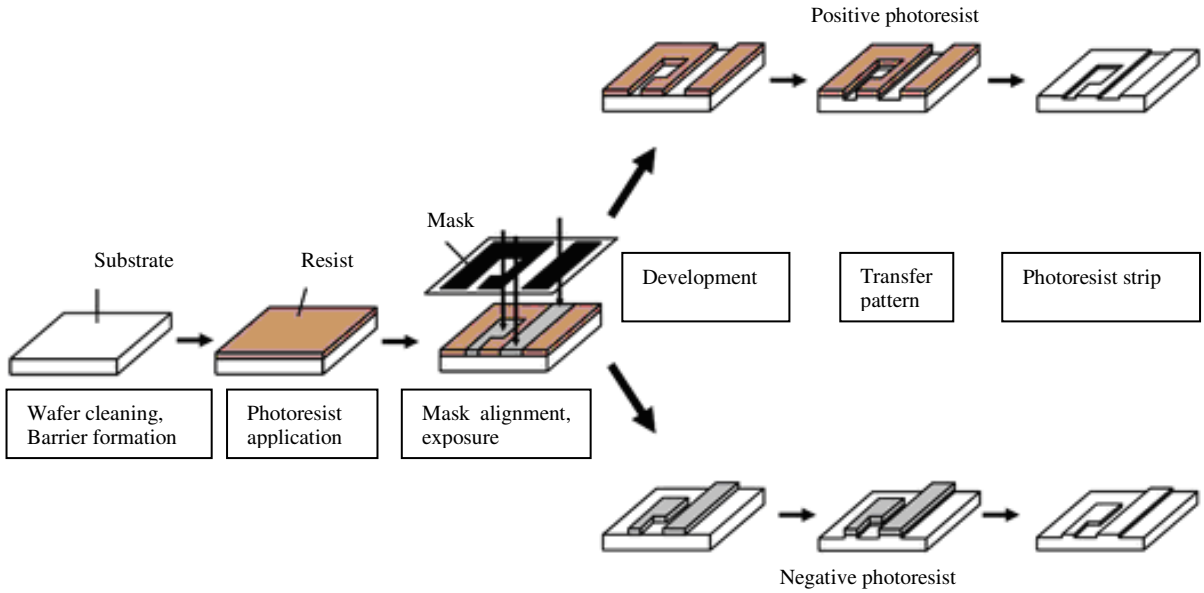


Figure I. 3: Schematic diagram showing the lithographic process used to fabricate microelectronic devices.[6]

Wafer Cleaning, barrier formation and photoresist application

In the first steps, the wafers are chemically cleaned to remove particulate matter on the surface as well as any traces of organic, ionic and metallic impurities. After cleaning, silicon dioxide, which can serve as a barrier layer, can be deposited or formed on the surface of the wafer. Then, photoresist is applied to the surface of the wafer by "spin coating", a technique that ensures a thin uniform resist film.

Positive and negative photoresist

There are two types of photoresist: positive and negative. For positive resists, the resist is exposed with UV light wherever the underlying material is to be removed. In these resists, exposure to the UV light changes the chemical structure of the resist so that it becomes more soluble in the developer. The exposed resist is then washed away by the developer solution, leaving windows of the bare underlying material. The mask, therefore, contains an exact copy of the pattern which is to remain on the wafer.

Negative resists behave in just the opposite manner. Exposure to the UV light causes the negative resist to become polymerized, and more difficult to dissolve. Therefore, the negative resist remains on the surface wherever it is exposed, and the developer solution removes only the unexposed portions. Masks used for negative photoresists, therefore, contain the inverse (or photographic "negative") of the pattern to be transferred.

Soft-baking

Soft-baking is the step during which almost all the solvent is removed from the photoresist coating. Oversoft-baking will degrade the photosensitivity of resists by either reducing the developer solubility or actually destroying a portion of the sensitizer. Undersoft-baking may prevent light from reaching the sensitizer. Then, a positive resist is incompletely exposed and will be attacked by the developer in both exposed and unexposed areas, causing less etching resistance.

Mask alignment and exposure

One of the most important steps in the photolithography process is mask alignment. A mask or "photomask" is a square glass plate with a patterned chrome film on one side. The mask is aligned with the wafer, so that the patterns can be transferred onto the resist surface at the desired location. Each mask after the first one must be aligned to the previous pattern. Once the mask has been accurately aligned with the pattern on the wafer's surface, the photoresist is exposed through the pattern with appropriate ultraviolet light intensity.

There are several primary exposure methods, and they will be presented later on, inside the next paragraph 2.2 Optical lithography evolution.

Development

One of the last steps in the photolithographic process is the development. Figure I. 4 below shows response curves for negative and positive resist after exposure and development.

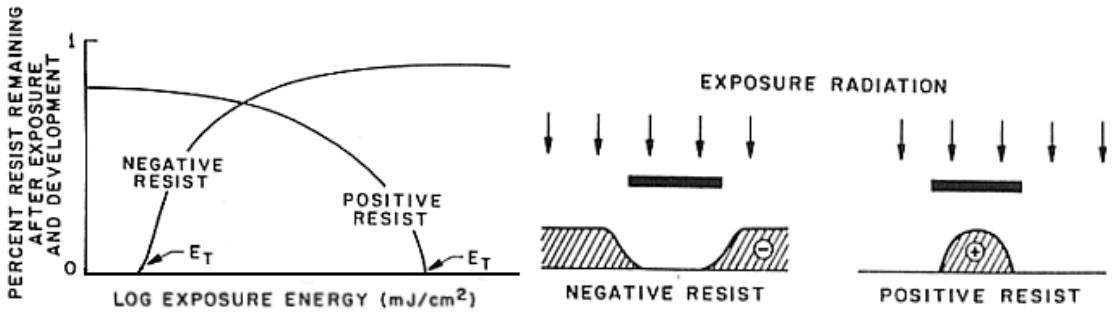


Figure I. 4: Resist exposure characteristics (left) and resist profiles after development (right).[7]

At low-exposure energies, the negative resist remains completely soluble in the developer solution. As the exposure is increased above a threshold energy E_T, more of the resist film remains after development. At exposures two or three times the threshold energy, very little of the resist film is dissolved. For positive resists, the resist solubility in its developer is finite even at zero-exposure energy. The solubility gradually increases until, at some threshold, it

becomes completely soluble. These curves are affected by all the resist processing variables: initial resist thickness, prebake conditions, developer chemistry, developing time, and others.

Final steps
Generally, the developed resist can have two functions: final coating layer or functional material. In the former case, hard-baking is the final step and it is necessary in order to harden the photoresist and improve its adhesion to the wafer surface. In the latter case, the resist acts as a temporary template for one of several methods of image transfer; these include plating and deposition (additive processing), chemical etching or physical milling (subtractive processing) or bombardment with energetic ions that are implanted into the substrate surface (doping by ion implantation). The remaining resist is removed or stripped after the image transfer step.

2.2 Optical lithography evolution

There are three primary exposure methods: contact, proximity and projection as illustrated in Figure I. 5. Each of them played an important role in the optical lithography evolution, finalized to keep a constant feature miniaturization.

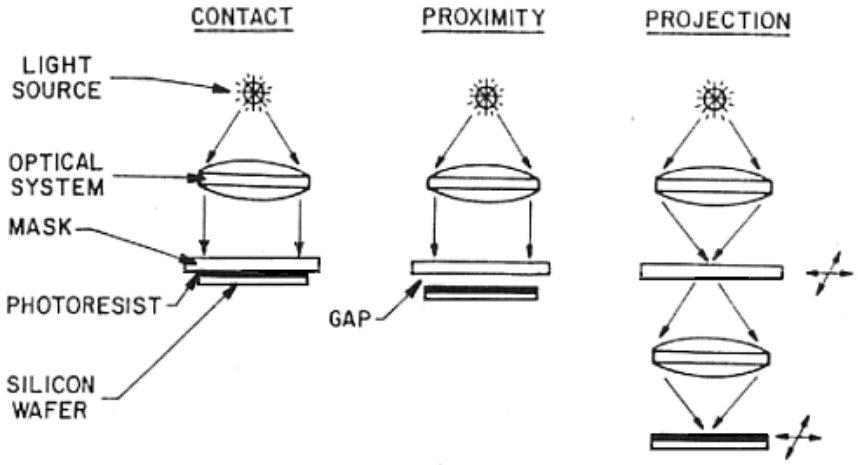


Figure I. 5: Optical lithography methods.[7]

Contact lithography
In the early 1960s, the first integrated circuits were patterned by contact lithography, where the resist-coated silicon wafer is brought into physical contact with the glass photomask. The wafer is held on a vacuum chuck, and the whole assembly rises until the wafer and mask contact each other. The photoresist is exposed with UV light while the wafer is in contact position with the mask. Because of the contact between the resist and mask, high resolution is possible in contact printing (e.g. 1 µm features in 0.5 µm thick positive resist).
The problem with contact printing is the contamination of the mask by resist residues and that particles, trapped between the resist and the mask, can damage the mask and cause defects in the pattern.

Proximity lithography
Proximity printing was contact printing successor. The proximity exposure method is similar to contact printing except that a small gap, between 10 and 25 µm, is maintained between the wafer and the mask during exposure. This gap minimizes (but may not eliminate) mask damage. Approximately 2- to 4-µm resolution is possible with proximity printing.

Projection lithography and its improvements

Proximity printing left the place to projection printing with the construction of Perkin Elmer Micralign tool in 1973. In this technique, which avoids mask damage entirely, an image of the patterns on the mask is projected onto the resist-coated wafer, which is a few centimeters away. In order to achieve high resolution, only a small portion of the mask is imaged. The image on the mask is projected onto the substrate through a system of optical lenses to properly control the light propagation for better feature resolution. Projection mask systems use a reduction factor (i.e. 4 or 5), which means that the projected image on the substrate is smaller (by that factor) than the image on the mask, unlike than contact and proximity printing.

Resolution limit in optical lithography is determined by the following Rayleigh's equation:

$$R = k_1 \times \frac{\lambda}{NA} \qquad \textbf{(Eq. 1)}$$

where R is the resolution (minimum resolvable feature), λ is the exposure wavelength, NA is the numerical aperture of the optical system and k_1 is a constant that depends on the specific resist material, process technology and image-formation technique used.

It follows from the Eq. 1 that resolution can be improved in three ways: by shortening the exposure wavelength, by decreasing the value of k_1 and by increasing the numerical aperture. The reduction in the wavelength light source was the easiest and most economical solution to realize. For this reason the semiconductor industry has moved from 436–365 nm (two strong lines, g and i, of the mercury arc) to 248–193 nm (KrF and ArF excimer lasers). It was proving extremely difficult to go further. One reason is that a unique advantage of ultraviolet and visible wavelengths is the existence of material that is transparent and mechanically rigid (usually fused silica in the case of ultraviolet wavelengths) for both the mask substrates and refractive lenses. An attempted move to 157 nm was aborted because the glass required by lenses, crystalline calcium fluoride, proved to have residual birefringence, which made it impractical[8]. The wavelength light actually used in the semiconductor industry is 193 nm as indicated in Figure I. 6, where it is possible to observe that since 1994 till today the resolution of the minimal feature was constantly smaller than the wavelength of the used light.

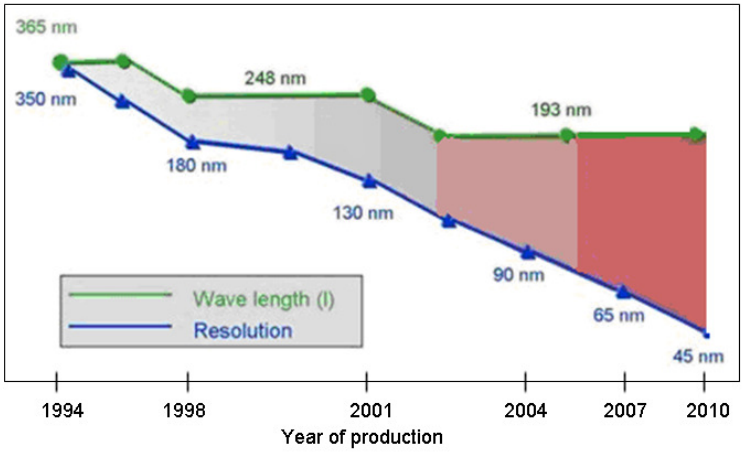


Figure I. 6: Evolutions in projection lithography concerning resolution (half-pitch) and wavelength in the last 20 years.

Several measures were taken to decrease the k_1 factor, once understood[9] the main causes affecting this parameter, most precisely:

- Imperfection in the imaging system: stray light, vibration, lens aberrations.
- Imperfect conditions at the recording media, i.e. the photoresist and the substrate (causing reflection and standing waves).

It was possible to reduce k_1 factor acting mainly on the illumination system (off-axis illumination) and on the mask (phase shift mask).

The numerical aperture is defined as follows:

$$NA = n \times \sin\theta = n \times \left(1.22 \times \frac{\lambda}{D}\right) \qquad \textbf{(Eq. 2)}$$

where θ is the angular resolution, i.e. the half-angle of the image-forming light cone at the image side; n is the index of refraction of the medium between the lens and the photoresist-coated wafer; D is the diameter of the lens and 1.22 is a factor derived from a calculation of the position of the first dark ring in the diffraction pattern.
To increase NA value, lens designer have created larger diameter lenses and lens elements that collect more light from the light source. Unfortunately, increased NA also results in reduced depth of focus. Depth of focus is the range of distances from the lens for which the image is in focus on the wafer. The variations in surface heights of the silicon wafer must be less than the depth of focus for proper treatment. Therefore, for high resolution lithography, the surface must be as flat as possible.
The alternative for increasing NA is changing the refractive index of the medium in front of the wafer as it can be seen from Eq. 2. Air has a refractive index equal to 1 at 193 nm wavelength, while that of water is equal to 1.436 at this wavelength. This brought to the introduction of water immersion lithography and to its adoption at industrial level.

Immersion lithography

The current technology adopted in semiconductor manufacturing industry is 193 nm water immersion lithography. A detailed global view over the typical elements present in this technique is showed in Figure I. 7.

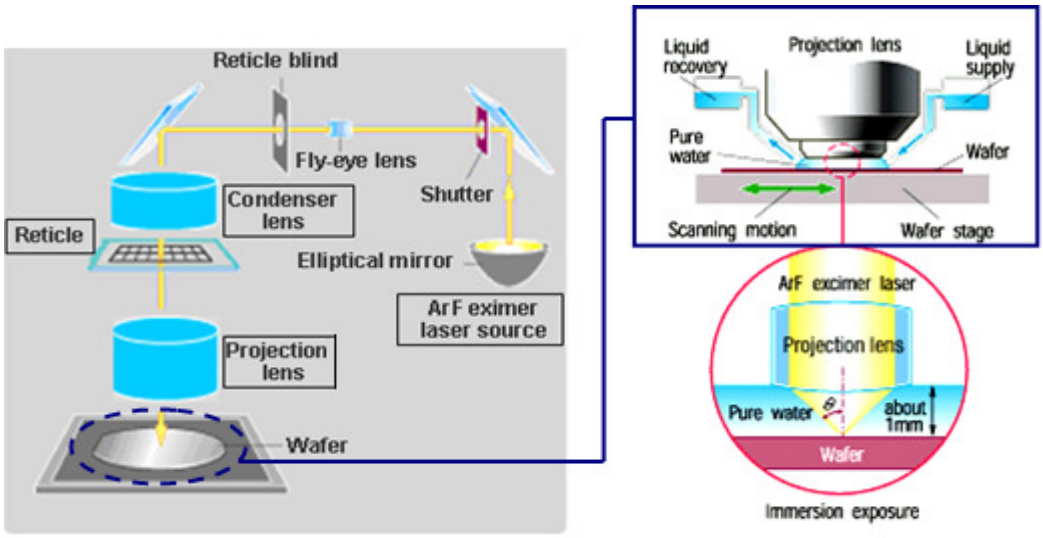


Figure I. 7: Images showing optical elements (left side), liquid dispensing system (right side top) and zoomed view of wafer / projection lens interface (right side bottom) for 193 nm water immersion lithography.[10]

The optical system (light source, fly-eye-lens, condenser lens, projection lens) is the same as for dry 193 nm lithography: this is the most important reason that allowed industry to move from dry to water immersion. However, the creation of a system that supplies and recovers the liquid between the lens and resist surface introduced several complications. For instance, the liquid has to flow continuously, not to leave any droplet on the resist that may lead to imaging defects, and has to be maintained at constant temperature with high precision to minimize any

imaging artifacts arising from water's refractive index change with temperature.[11] Several other issues are related to imaging under water immersion.[12] Of particular concern are the extent of resist components extraction (leaching) from the resist film into the immersion liquid and the water permeation into the resist. The application of a thin overcoat film was the solution adopted to suppress material exchange between resist and fluid and also to increase water's receding contact angle at fast scan speeds.
Water-based immersion lithography using 193-nm ArF illumination provides optical solutions as far as the 45-nm node (with a $k1$ of 0.31) but is not able to achieve further nodes as currently defined. Achieving these lithographic nodes will require new, higher-refractive index fluids to replace the water used in first-generation immersion systems. Therefore, there has been extensive research to develop second-generation ($1.44 \leq n_{(193nm)} \leq 1.65$) and third generation ($1.65 \leq n_{(193nm)} \leq 1.8$) 193 nm immersion fluids.

2.3 Future of lithography

In the near future term microelectronics industry could improve minimum features resolution adopting new techniques based on the use of existing exposure tools. These techniques are double exposure lithography (DEL) and double patterning lithography (DPL),[13] both illustrated in Figure I. 8.

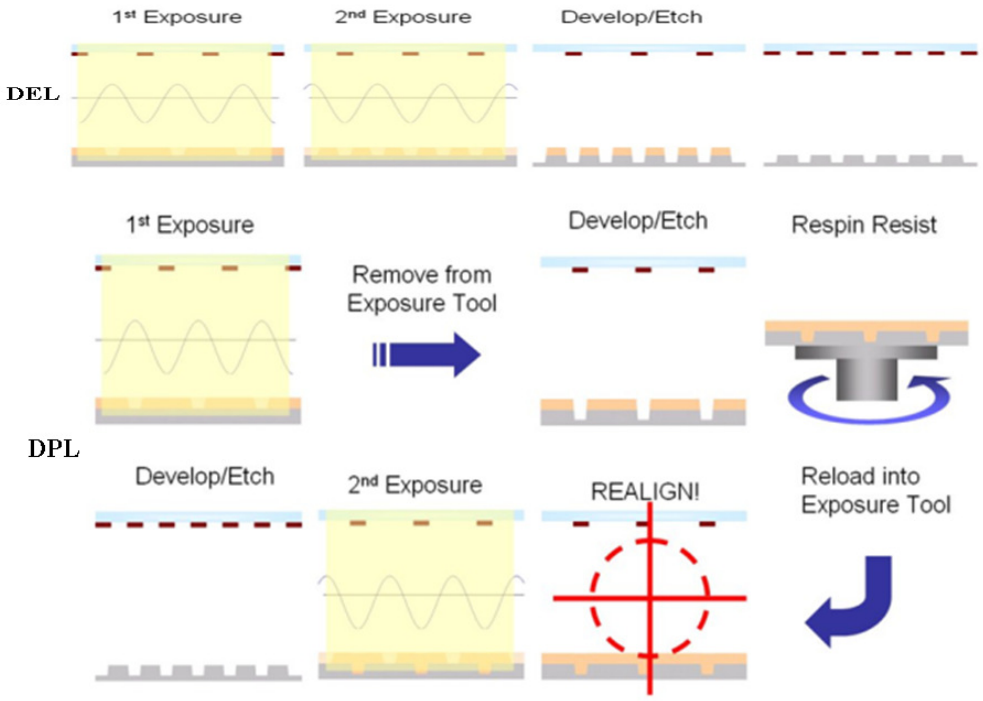


Figure I. 8: Double exposure lithography (DEL, top), and double patterning lithography (DPL; bottom).[13]

DEL is defined as a two exposure pass lithographic process that does not require the removal of the wafer from the exposure tool chuck between passes. DPL is defined as a two exposure pass lithographic process that requires a chemical development of the photoresist layers and possibly an intermediate etch step. The DPL processing approaches will require the removal of the wafer from the exposure tool chuck which may lead to a loss of overlay registration.
The benefits of DEL and DPL principally include the ability to use existing exposure tools to print technology nodes below the NA limit for single exposure processes. This could mean a lower cost of ownership as these techniques can in principle be deployed without costly capital investment. However, the two exposure passes require doubling the number of masks and reduced throughput due to increased processing time.

The process time is dramatically increased in the DPL process because of the additional process steps compared to the DEL process. In addition, the removal of the wafer from the wafer chuck between exposures poses severe overlay issues that may be difficult to overcome, especially at the CDs where this technology will be implemented. The DEL process only introduces an additional exposure pass, and, since the wafer is not removed from the imaging tool between exposures, the overlay issues are minimized. The reduced cost of ownership of DEL suggests that it would be the preferred technique. However, this technology is not possible without the development of new materials with nonlinear response to exposure dose.

In Table I. 1 are illustrated last guidelines contained in the ITRS[14] (International Technology Roadmap for Semiconductors) for near term future lithography, till 2019. The overall objective of the ITRS, since its first publication in 1999, is to present industry-wide consensus on the best current estimate of the industry's research and development needs out to a 15-year horizon. As such, it provides a guide to the efforts of companies, universities, governments, and other research providers or funders. The ITRS has improved the quality of R&D investment decisions made at all levels and has helped channel research efforts to areas that most need research breakthroughs.

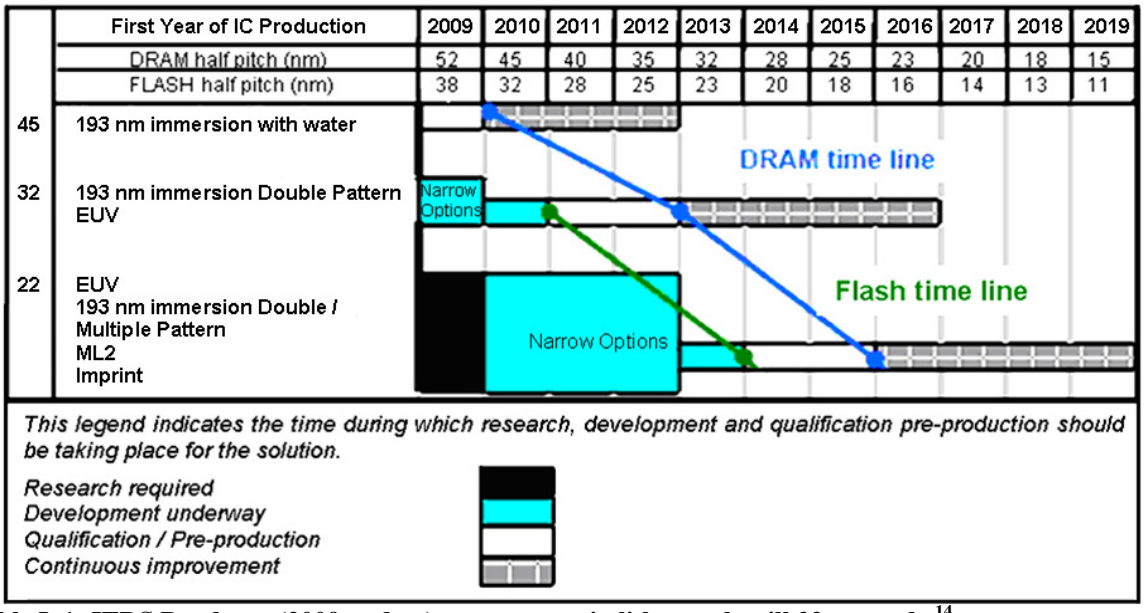


Table I. 1: ITRS Roadmap (2009 update) at near term in lithography till 22 nm node.[14]

In previous editions of the ITRS, the term "technology node" was used in an attempt to provide a single, simple indicator of overall industry progress in integrated circuit feature scaling. It was specifically defined as the smallest half-pitch of contacted metal lines on any product. Historically, DRAM (Dynamic random access memory) has been the product which, at a given time, exhibited the tightest contacted metal pitch and, thus, it "set the pace" for the ITRS technology nodes. However, we are now in an era in which there are multiple significant drivers of scaling and believe that it would be misleading to continue with a single highlighted driver, including DRAM.

For example, along with half-pitch advancements, design factors have also rapidly advanced in flash memory cell design, enabling additional acceleration of functional density. It is, in fact, possible to get in flash memory architecture a half-pitch smaller than in DRAM. For this reason, in Table I. 1, there are time lines concerning the half-pitch evolution for both kind of memory; furthermore, the first colon on the left of Table I. 1 indicates the microprocessor gate length. Several technologies are indicated near each gate size as candidates to achieve the

targeted value; the order of the options represents the probability of a particular technology to be the dominant solution. As shown, 193 nm immersion lithography with water is the technology actually adopted by industry and 193 nm immersion double patterning is presented like its successor, together with Extreme Ultra Violet (EUV) lithography (that will be presented in paragraph 2.4.b).
Beyond the 32 nm DRAM half pitch, optical lithography may not be useful because it is no longer economical to continue with a technology that has approached its ultimate limits. There are a number of lithographic technologies that have potential as the successor to optical lithography.
The next generation lithography (NGL) techniques will be discussed next.

2.4 Next Generation Lithographies (NGLs)

2.4.a MaskLess Lithography (ML2)

Maskless lithography (ML2) has been developing renewed interest as the cost (up to around $1 million per mask set!) and challenges of optical lithography masks increase. The interest in this technology is that the optical mask in traditional lithography systems can be replaced by the deflection mechanisms of the ML2 approaches. Since the deflection can be changed for each and every chip, if so desired, the potential of ML2 is the replacement of expensive photomasks that take considerable time to built and deliver. There is a worldwide effort in both charged particle maskless (CP-ML2) and optical maskless (O-ML2).[15]
The primary driving force behind the O-ML2 efforts are Micronic Laser Systems. Figure I. 9 (left side) shows a schematic of the system being developed by them. The traditional photomask is replaced with an addressable array of light modulating elements that are controlled in real time to produce the desired image. The type of modulating elements can be of many forms but either piston or tilting micro-mirror spatial light modulators are favored in today's development.
The basis for the e-beam version of CP-ML2 is derived from the early e-beam direct write (EBDW) systems that were in turn derived from scanning electron microscopes and optical mask writers. EBDW has been shown to be able to produce very fine features, with resolutions of 20 nm being possible today. Much smaller resolutions can be achieved, but there is a price to pay in longer exposure times. These systems are generally slow, expensive and inadequate to provide 24 / 7 operation at speeds approaching one wafer per hour. The development of CP-ML2 systems addresses the limitation of the single e-beam writing of the EBDW systems by providing multiple imaging sources at the wafer. An example of a CP-ML2 system is shown in Figure I. 9 (right side). This is a traditional approach of having the column vertical and the wafer being exposed under the column on a stage capable of high-speed motion with extreme accuracy of repositioning.

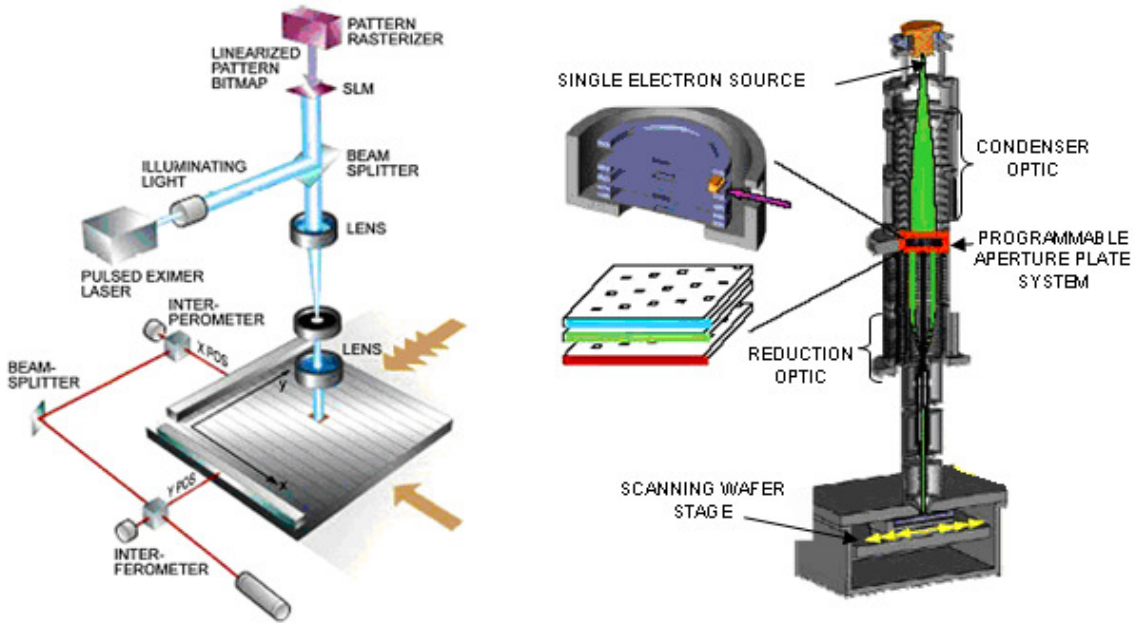


Figure I. 9: Example of O-ML2 (left side) and of CP-ML2 system (right side).[15]

The first consideration is that the throughput of the system should be equal to existing optical tools. Since this speed is in excess of a hundred 300 mm diameter wafers per hour, and current systems being developed are projected to achieve 10 wafers per hour, there is a gap that needs to be closed.
Different charged particles can be employed, as follows:[16]
Multi electron beams: various projects are being conducted worldwide; there are two projects in Europe that are dedicated to development of the multi beam tool. One called MAPPER is managed by a company Mapper, Holland and another called PML2 directed by Leica, Germany.
Multi ions beams: IMS Vienna develops a multi focused ion beams for lithography application or material patterning (ion milling) within the frame work of CHARPAN project of the European Community.

2.4.b EUV

EUV (Extreme Ultra Violet) lithography seems to be the favorite candidate as NGL of semiconductor industries and has been backed by major players in the semiconductor industry such as AMD, Intel and Motorola[17], because this technology is based on an extended optical lithography technique, but with a shorter wavelength (13.4 nm) of light illumination. However, a wavelength of 13.4 nm is a long x-ray and as such is easily absorbed in most materials. In this system, refractive optics are no longer feasible, instead, reflective optics such as the Bragg reflector system are used. Figure I. 10 shows the schematic of a EUV lithography (EUVL) system where the EUV light is generated from a 45 eV plasma created when a 1700 Watts pulsed Ytterbium-Aluminum-Garnet (YAG) solid state laser illuminates a supersonic jet of Xenon gas. The EUV light is collected and focused on a 4X reflective mask by a series of condenser mirrors (C1 - C4). The mask image is projected onto the wafer by a 4X reduction camera (M1 - M4) while the mask and wafer are simultaneously scanned. The entire operation takes place in a high-vacuum environment enclosure. All other offline optical lithography tools are still relevant to this technology, but the unresolved issues such as source brightness, mask defect inspection and repair and immature resist performance have delayed the deployment of this technology into high volume manufacturing line.[18]

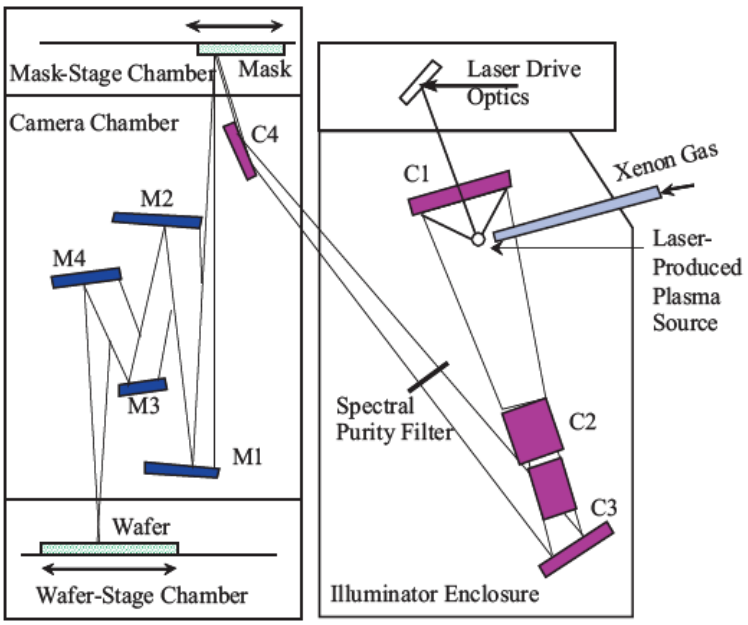


Figure I. 10: Schematic diagram of an EUVL system.[19]

At the moment, optical lithography is still the dominant lithography technology, but its future is uncertain. Even though EUVL was the first candidate to appear in the NGL elite group and had been named as a potential heir to lithography technology, its cost has ruined its reputation. Apparently not many parties could afford to own a EUVL system because of its high cost of about $USD 50 million per system, meaning only a few giant companies had the privilege of owning a EUVL system. Furthermore, EUVL has been under development for more than 20 years, however as of now, only a few beta EUVL tools are available in the world; located in the USA[20], Europe (ASML, IMEC)[21, 22] and Japan[23] for process characterization purposes. The large costs of electrical consumption, large footprint, costly parts, and process stability issues have hindered the progress of this technology.

2.4.c Nanoimprint lithography

NanoImprint Lithography (NIL) is an ancient patterning technique, as shown by imprints of pre-historic creatures found on fossils. In the nanofabrication field, NIL was first proposed by S. Chou in 1995,[24] as a high resolution and high throughput lithography technique based on the mechanical deformation of a resist layer with a stamp (or mold) presenting a surface topography (including eventually three-dimensional (3D) features). This technology is considered as a newcomer to semiconductor industry. In the year 2003, the ITRS had mapped out imprint as one of the lithography candidates for nodes beyond 32 nm. This has attracted research teams around the world to explore its potential. The requirements for NIL technology have been updated during following ITRS editions and the last ones notified in 2009[14] are mainly over surface roughness, defect level of the fabricated molds as well as timeline and capability of equipment infrastructure. Other issues of this technology include contamination, resist sticking on the mold surface, mold crack and bubbles in the imprinted resist layer.
Globally, we can find a large number of investments from government agencies, technology companies and higher education institutions, in setting up businesses and researches based on NIL technologies. In the USA, *Molecular Imprint Incorporated* and *Nanonex Corporation* are examples of companies providing equipments, processes and NIL related materials. Similar companies such as *EV Group* (Austria), *Obducat AB* (Sweden) and *Suss Microtec* (Germany) in Europe and many others around the world are progressing in this technology. Important

investments have been poured into it, and nowadays we can find many research and some manufacturing tools for NIL technologies available on the market.
The progress made in the last years has shown that NIL is not only a serious NGL candidate, but also a platform for one of ten technologies in the MIT Technology Review being evaluated to change the world.[25]

2.5 Nanoimprint lithography techniques

Two main families can be distinguished: thermal NIL[24] and UV-assisted NIL[26] (generally named UV-NIL); both processes are illustrated in Figure I. 11.

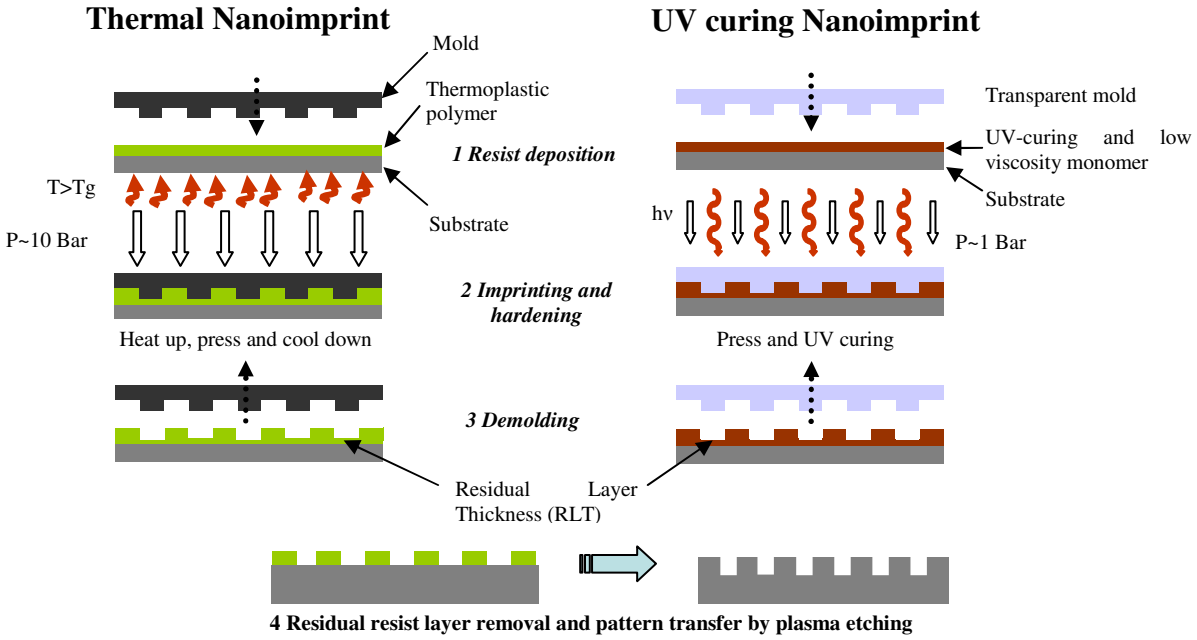


Figure I. 11: Schematic of nanoimprint process: thermal NIL (left side) and UV-NIL (right side).

In thermal NIL, a silicon mold is usually pressed into a thin (from few hundred nm to few hundred µm) thermoplastic polymer film (generally deposited on a silicon substrate) heated above its glass transition temperature (Tg) where the polymer can flow under quite high pressure (about 10 - 50 bar). The viscosity of the thin heated polymer layer (about thousands of Pa.s) remains a few orders of magnitude higher than those of a monomer layer (about hundreds of mPa.s or even less),[27,28] but the mold is generally made of silicon, using more advanced and established processes from the microelectronics industry. Furthermore, the non-flatness of the mold and / or substrate is in general compensated by the quite high imprinting pressure used. Finally, thermoplastic polymers needed for thermal NIL are more readily available (already used in electron-beam or photolithography).
On the other hand, in UV-NIL, a low viscosity monomer resist is pressed, at room temperature, with a transparent mold, under a limited pressure (around 1 bar) and later polymerized by UV light to form solid structures. In this case, the rigid and UV transparent (in general fused silica) mold fabrication is a more difficult point. In addition, only few dedicated resists are commercially available and flatness issues are more critical due to the low viscosity resist used.
After the patterns formation, one may use the polymer layer as a resist mask for additional processing steps (transfer etching in the substrate, ion implantation, material deposition, lift-off…), or this layer may be used as it is as a functional material. A residual resist layer is

always observed under the mold protrusions after imprinting. This layer might be removed with an anisotropic plasma etching step to obtain a conventional lithography resist mask.
Nevertheless, key advantages of UV-NIL make it a very attractive process for industrial applications:

- UV-NIL can be performed at room temperature, there is no need to heat and cool the mold / wafer stack as compared to thermal NIL. This is an advantage in term of throughput (UV curing can be performed in a few seconds) and in terms of imprinted patterns fidelity. (Thermal expansion mismatch of materials used in thermal NIL might induce distortions of the printed patterns. For this reason, it is mandatory to use the same material for the mold and for the substrate in thermal NIL).
- Due to the use of UV-transparent stamps, high accuracy alignment between different lithography levels is easier to implement in UV-NIL.[29]
- Low viscosity resists allow an improved resist flow and redistribution leading to an improved printing uniformity, especially when the mold design includes micro- and nanometer features at the same time or areas with different densities and variable fill factor. Additionally, due to these low-viscosity resists, UV NIL can be performed at low pressure (< 1 bar). This is essential for molding films onto delicate substrates and releases constrain on the mold mechanical properties.
- A step and repeat process allow the fabrication of smaller (i.e. cheaper) stamps and a better control of the placement accuracy.[30] Such a process is easier to implement with a UV system than with a thermal system.
- Finally, the properties of the cured polymer after imprinting can be adapted to dedicated applications by changing the resist's formulation or the irradiation time.

NIL techniques can be distinguished essentially considering mold characteristics (material, profile, and size) as well as the surface where the resist is deposited before imprinting, as follows.

Mold material: The mold employed can be a "hard mold", with high Young's modulus (around 130 GPa for silicon and 75 GPa for fused silica ones), or a "soft mold", made mainly from poly(dimethylsiloxane) (PDMS), whose Young's Modulus is less than 2 MPa. PDMS molds are transparent to UV light, so they can be used either with thermal- or UV-curable resists. NIL processes using soft molds are named "soft lithography". On the other hand, the mold can also have a Young's modulus between the two extremes; in this case it can be defined as "rigiflex" molds, like for instance ethylene-tetrafluoroethylene (ETFE) (about 1.2 GPa) molds.[31]

Mold profile: A mold can be planar or cylindrical. In the latter case we talk about roll lithography, and it can be performed using a planar (roll-to-plate lithography, R2PNIL) or circular (roll-to-roll lithography, R2RNIL) substrate as illustrated in Figure I. 12 (together with examples of large area patterned substrates). In general, roll lithography employs a soft mold, able to adapt its surface to the waviness of a wafer surface to achieve a conformal contact.

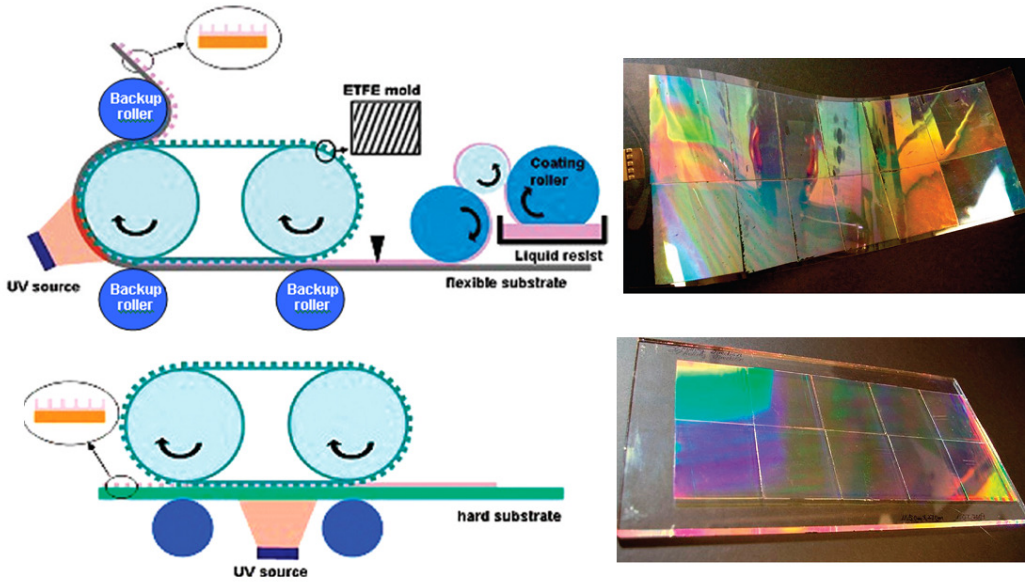


Figure I. 12: Schematics of R2RNIL (top) and R2PNIL (bottom) process, both employing UV curable materials, and examples of patterned substrates.[32]

Mold size: This consideration is applicable only to planar molds. It can have a size smaller or equal to the substrate, as detailed described in H. Schift's review.[28] In the first case, the imprinting process works in step and repeat mode, i.e. it is necessary to print n dies in n times before to have a fully patterned substrate. Each time, the mold is first put into contact with the substrate, afterwards the resist is cured, and then the mold is separated from the substrate and finally shifted to side to perform another cycle.

Surface where the resist is deposited before imprinting: All the above mentioned NIL techniques described till now referred to a process working with a resist that was deposited on the substrate. A variant is represented by the "Reverse NIL" process where the resist is spin-coated on the mold surface and then transferred onto the substrate. Reverse NIL can be performed either using a thermal[33] or UV curable resist,[34] and either on patterned or unpatterned surface (as showed in Figure I. 13). The reverse-imprinting technique represents a simple method to fabricate 3D polymer nanostructures by simply repeating the process to build up the structure in a layer-by-layer fashion.[35]

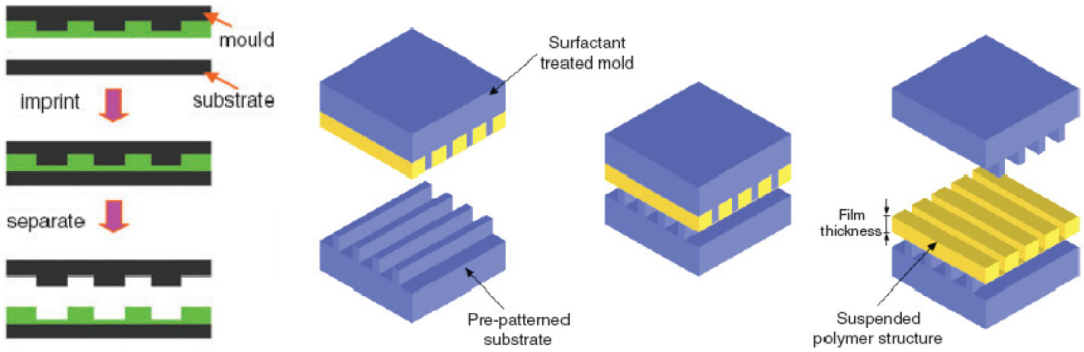


Figure I. 13: Schematic of the reverse nanoimprint lithography process on an unpatterned surface (left side) and patterned surface (right side).

One of the common aspect of all the above presented NIL techniques is the thickness of the resist deposited on the substrate and processed. This layer is, in fact, very thin (thickness ranging from few nanometers to hundreds of microns). This is an important point since it is at

the origin of many issues, such as printing non-uniformity and limited resist flow. Nevertheless, for a lithography purpose, it is absolutely necessary to use a resist layer as thin as possible to be able to use imprinted resist patterns as a conventional lithography resist mask, i.e. for example to transfer the features in the underlying substrate by plasma etching.

3 UV-assisted nanoimprint lithography

3.1 Process details and variants

In UV-NIL, a liquid material is coated onto a substrate and pressed, at room temperature, against a rigid UV-transparent mold. The low viscosity resist displacement takes place not only due to the imprinting pressure applied (squeeze flow of the resist), but also due to the capillary forces in the system. Consequently, only a limited pressure (< 1 bar) is sufficient to fill the mold cavities. Furthermore, this low force ensures a uniform imprint. Indeed, mold and substrate can be assumed to be completely rigid so that they are approaching in a perfectly parallel manner, insuring a uniform residual layer. Nevertheless, this ideal case is only working with perfectly flat surfaces, which is a difficult point to obtain in real experiments. To ease the process and to be able to imprint over topography, planarization layers might be necessary.[36,37] Also, imprinting at low force using two rigid surfaces is facilitated when the contact area is limited, this means, in general, when working with small molds. This is also an advantage in terms of mold fabrication, as it is easier and cheaper to write a limited area for example by electron-beam lithography (defect inspection and repair are also facilitated on smaller stamps). This is the reason why UV-NIL is often developed in a step and repeat process, where the mold has dimension in the range of 25*25 mm^2.
To apply resists onto wafers in step and repeat mode, two techniques are used: spin-coating and drop-dispensing (both illustrated in Figure I. 14).

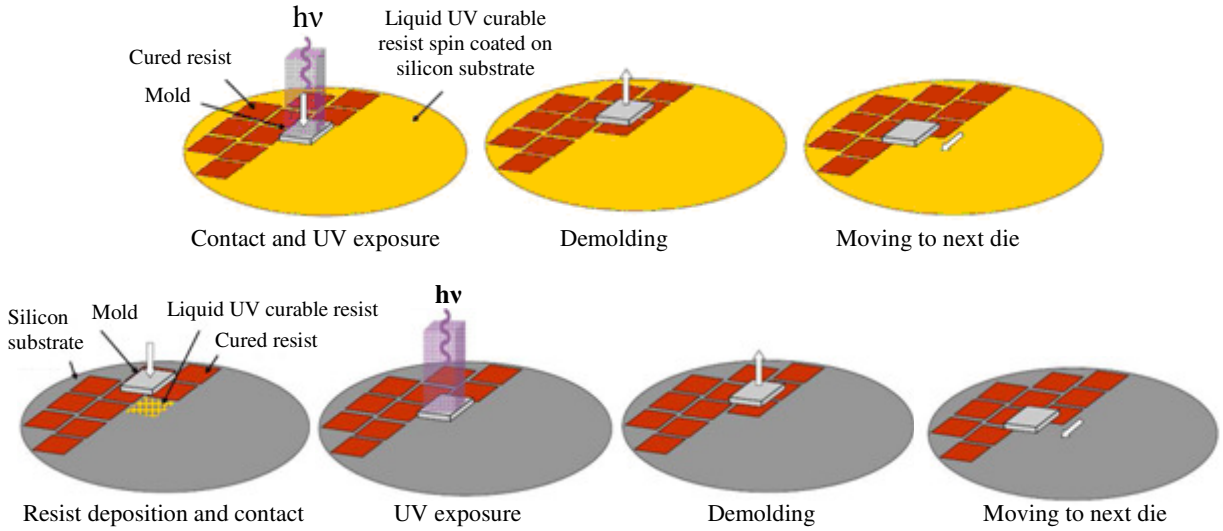


Figure I. 14: Two different methods to depose UV curable resist for UV-NIL process in step and repeat mode: spin coating (on top) and drop dispense (at bottom).

Spin-coating is already used in standard lithography and its main advantage is its excellent thickness uniformity over large areas. In UV-NIL, as liquid low-viscosity resists are used, the formation of a stable thin liquid layer by spin-coating is not straightforward. The resist has to wet the substrate surface, which is not always possible, depending on the resist used, and might require a special wafer treatment. Additionally, low-viscosity resists has to be chosen with a limited vapor pressure to be sure that all dies will have the same initial resist layer thickness and or to be able to imprint in vacuum. In practice, this means that the viscosity cannot be smaller than about 30 mPa.s.
On the other hand, resist can be drop-dispensed on the wafers. This can be done for only one imprinting area just before contact with the mold, limiting the possible evaporation of resist and allowing working with resist viscosities as low as a few mPa.s.[38] Furthermore, drops as

small as 1 pL can be used,[39] which corresponds to individual imprinted area of about 10*10 μm^2 on the wafer (depending on structure size and density; corresponding to about 60,000 drops per die in standard step and repeat conditions). This large number of drops gives the possibility to the user to adapt the resist quantity to the mold design in the die itself, conducting to an improved printing uniformity, and or shorter imprinting times, due to the limited resist flow. (The combination of step and repeat processing with tunable drop-dispensing (drop-on-demand™) has given rise to "step and flash™" imprint lithography (S-FIL) and lately to "jet and flash™" imprint lithography (J-FIL), trademarks of *Molecular Imprint Inc*.[40,41]) Also, the multidroplet geometry seems to favor filling of the mold cavities.[42] When the mold approaches the coated substrate, the fluid droplets spread out and fill the cavities under capillary action and the capillary force around each drops attract the mold, enhancing the effective imprinting force. Concerning the drop size, it was shown that smaller drops (~ pL) induce an improved capillary action but are more difficult to produce at high speed with good placement accuracy, generating issues on the drop dispensing unit. On the other hand, larger drops (~ 100 pL) are more difficult to displace (longer flowing time), inducing constrains on the mold design, and will obviously generate a larger quantity of expelled resist at the mold edges. Nevertheless, all the resists are not able to be drop-dispensed, especially in small drops. This depends on their visco-elastic properties and might be a limitation, in particular in applications where special dedicated resists are formulated.
Another development of S-FIL is S-FIL reverse[41,43] (S-FIL/R, see Figure I. 15). In this case, a purely organic resist is first imprinted as in SFIL. Then, a more plasma-etch-resistant resist (silicon-containing) is spin-coated onto imprinted features acting as a planarization layer. Finally, this stack is etched in a plasma reactor to produce the patterned resist mask. This technique is able to generate higher aspect ratio features and is less sensitive to non-uniformities in the imprinted residual resist layer. Also, it allows the fabrication of patterns with the same polarity as on the mold and, due to the two-layer resist, a lift-off process is possible. Additionally, there is no need to imprint the silicon-containing etch-resistant resist. Then, resist contaminations on the mold are easier to remove since the mold is in contact only with a purely organic resist. Finally, the silicon-rich resist does not have to present a low viscosity and can be applied with high uniformity by spin-coating.

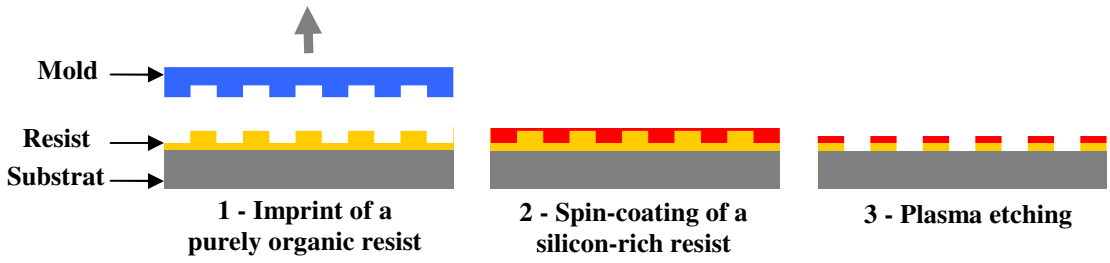


Figure I. 15: Schematic of the S-FIL/R nanoimprint process.

Alternatively to the step and repeat process, UV-NIL is also used with larger stamps.[44,45] In this case, the used imprinting pressures are in general much larger than in the step and repeat process to ensure a conformal contact between molds and substrates. In order not to induce too much imprinting non-uniformities, it is then very important that the tool used is able to apply a uniform (isotropic) imprint pressure even on non-flat surfaces. This is possible using soft pistons or membranes. Another alternative to have a conformal contact, even with quite low imprint forces, is to use a soft stamp.[46] Nevertheless, with these techniques, it becomes more difficult to realize high accuracy alignments of successive lithography levels due to the tool architecture or to the fact that the mold is not stiff enough.

3.2 Resist flow in thin layers

In UV-NIL, the resist displacement takes place not only due to the applied imprinting force (squeeze flow), but also due to the capillary forces. The balance between both phenomena is not yet clear and depends strongly on process conditions (mold treatment, wafer treatment, resist viscosity and surface energy and resist coating type (spin-coated or drop-dispensed)) in UV-NIL, due to the increased effect of capillarity. Nevertheless, the squeeze flow of a supposed perfectly viscous resist can be described quite simply in a first approximation by the so-called Stefan's law,[47] presented in Figure I. 16. For a line, the imprinting time can be written as:[48]

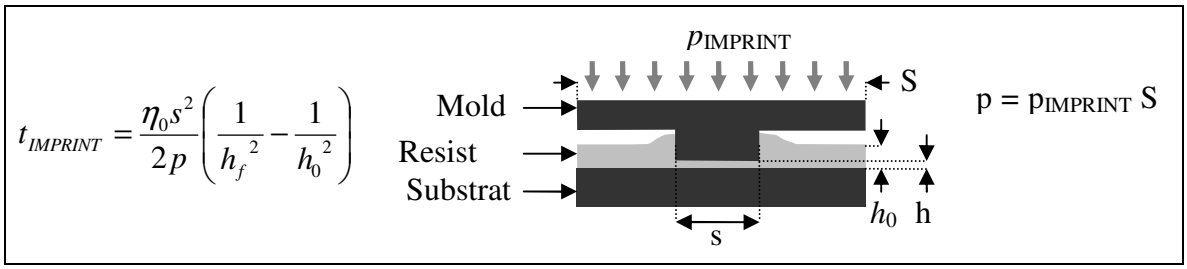


Figure I. 16: Stefan's law for a one-dimensional line.

where η_0 is the zero sheer viscosity of the resist, s the width of the line, h_0 the initial resist layer thickness, h_f the final resist layer thickness (residual layer) and p the effective imprinting pressure on the line. We observe that a shorter imprinting time can be inversely proportionally compensated by a larger imprinting pressure and vice-versa. Furthermore, the linewidth s as well as the residual resist thickness h_f plays a large role. Indeed, for a mold containing isodense 100 nm lines and spaces, a resist viscosity of 10 mPa.s and an imprint pressure of 1 bar, the time needed to press the resist from a 100 nm thick layer to a 15 nm thick one is about 1 µs. (In comparison, in the case of thermal NIL, where the viscosity is higher than 1000 Pa.s, the imprinting time in the same conditions is larger than 0.1 s.) This time is extremely short, but if the linewidth is thousand times larger (100 µm), the viscosity ten times higher (100 mPa.s, classical case of spin-coated resists) and if a residual layer of 10 nm is targeted, then the imprinting time becomes 0.2 s (2000 s in the case of thermal NIL). In the case of UV-NIL, the process is still very fast. Nevertheless, as the mold and substrate are assumed to be perfectly rigid due to the low imprinting pressure, the sinking rate of the mold will be governed by the largest protrusions. Thus, large protrusions (> 100 µm) have to be avoided on the total surface of the mold, or fake cavities have to be included in the mold design, in order to reduce the maximal linewidth.

As an example, with a 1000 mPa.s viscosity resist, a 13 bar pressure and an optimized initial resist thickness (final residual layer < 20 nm), the mean free path (or flowing distance) of a resist molecule could be experimentally estimated to be about 1 mm.[49] This value is important for the mold design which therefore has to present the same density (protrusion to cavity area ratio) on any 1 mm^2 areas on its surface in order to favor a uniform residual layer. In this example, the resist redistribution area is quite small but, when using lower viscosity resists (η_0 < 50 mPa.s), this area should reach almost the stamp size in the case of small stamps.

3.3 Imprinting examples, resolution and applications

In Figure I. 17, some examples of imprinted resist layers, made in the lab on an *EVG 770* step and repeat system, are reported. With an optimized initial resist thickness and knowing the mold design, an excellent contrast between the features height and the residual layer thickness can be obtained, which is a very important point in the case of additional process steps.

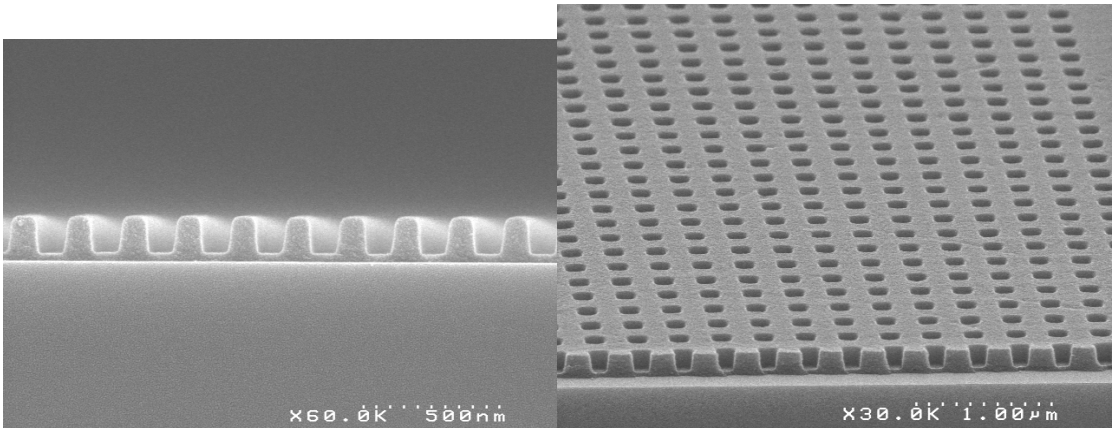


Figure I. 17: Examples of UV-NIL imprinted patterns (left: 100 nm lines, right: 100 nm contact holes).

Already in the first NIL experiment by S. Chou[24] a very high resolution of 25 nm was demonstrated using thermal NIL. The fabricated polymer mask could be used successfully in a lift-off process. In UV-NIL, a resolution of 5 nm linewidth and 14 nm pitch using NIL and lift-off was demonstrated in 2004, also by the group of S. Chou.[50] Here, the mold used was a cleaved facet of a sample containing molecular-beam epitaxy-grown superlattices. The same year, Hua et al. demonstrated that it is even possible to reproduce the shape of a single-wall carbon nanotube into a polymer (Figure I. 18).[51] Indeed, the surface roughness of the mold is in general very well reproduced into the polymeric material during the molding process. The resolution of the molding technique itself is not the blocking point for the overall resolution of the technique, but much more the high resolution mold availability and the pattern transfer (as will be detailed in § 4.4 Plasma etching processes and resists stripping).

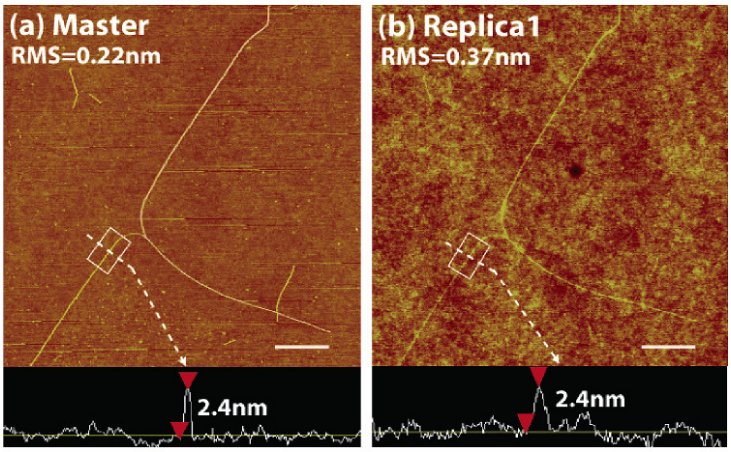


Figure I. 18: Demonstration of single-wall carbon nanotube reproduction using UV-NIL.[51]

Molds are in general fabricated with high resolution techniques, mainly electron-beam lithography,[52] allowing NIL to achieve resolutions beyond the limitations set by the light diffraction in optical projection lithography. Furthermore, due to a parallel fabrication of features over large areas, a high throughput production is possible. As a consequence, NIL is not only considered as a NGL technique in the microelectronics industry for the fabrication of integrated circuit,[53] but also developed as a fabrication technique in application fields where electron-beam lithography or state-of-the-art photolithography cannot propose a sufficiently high resolution at a reasonable cost; or where the capability of 3D imprinting or imprinting in a functional material is needed. Indeed, depending on the application, the UV curable materials used could either serve as etch masks for pattern transfer into the underlying substrate or be used as they are. In the later case issues like mechanical stability, electrical

conductivity, and optical properties (transparency, refractive index, etc.) play an important role for their selection. Example of application fields where UV-NIL has already today a real potential are as follows:

Interconnects for integrated circuits

UV-NIL can be adopted by microelectronics industry not only for "front-end processing" (the main reason for its candidature as NGL, as previously explained) but for "back-end" as well. Multilayer interconnects for integrated circuits present stacked layers of metal linked by vias and trenches. Conventional process (dual damascene process) requires separate lithography and etching steps to pattern separately the vias and trenches. However, this approach is complex since it requires the stacking and alignment of many layers, as described elsewhere.[54] An innovative approach based on imprinting lithography could allow to fabricate via and trench simultaneously for each level of metal using double-deck mold geometry (Figure I. 19 (a)), and thereby reduces the total number of processing steps. The use of UV-NIL in the dual-damascene approach is even more advantageous when using imprintable photocurable low-*k* dielectric material,[55] as depicted in Figure I. 19 (a).

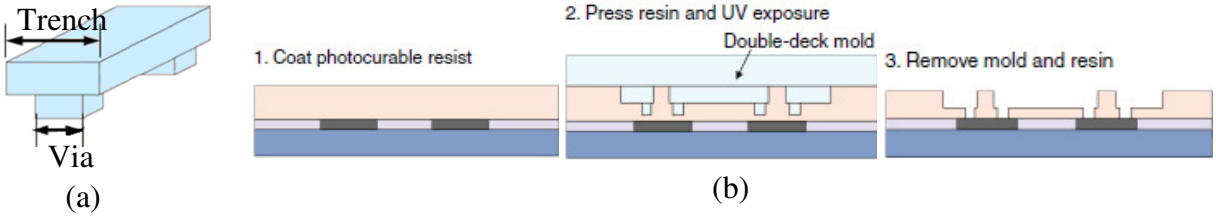


Figure I. 19: Double-deck mold geometry (a) for the dual damascene process using UV-NIL and imprintable low dielectric constant imprintable material (b).[56]

Patterned magnetic media

The ever-increasing storage density of hard disk drives is approaching an apparent limitation imposed by the superparamagnetic effect (thermal instability of individual magnetic domains in a continuous magnetic layer). The practical limitations of superparamagnetism can be avoided by patterning the magnetic material (with individual pillars of around 15 nm in diameter) as depicted in Figure I. 20. Industrial forecasts suggest that the market demand for hard disk recording media will reach 10^9 units / years in the next few years around the world. Fabrication of patterned media to meet this demand will require a large supply of imprint templates. As the lifetime of a single imprint template is anticipated to be approximately 10^4 imprints, suggesting that at least 10^5 templates will be required, it is envisaged to use a "master" template, created directly with an electron-beam tool, that will be replicated many times to produce the required supply of working templates. The *Molecular Imprints Imprio HD2200* tool, based on the UV-NIL process (most precisely on the S-FIL one), has been developed to meet the requirements of feature resolution, pattern precision and cost-efficiency for master template replicas and bit patterned media fabrication.[57]

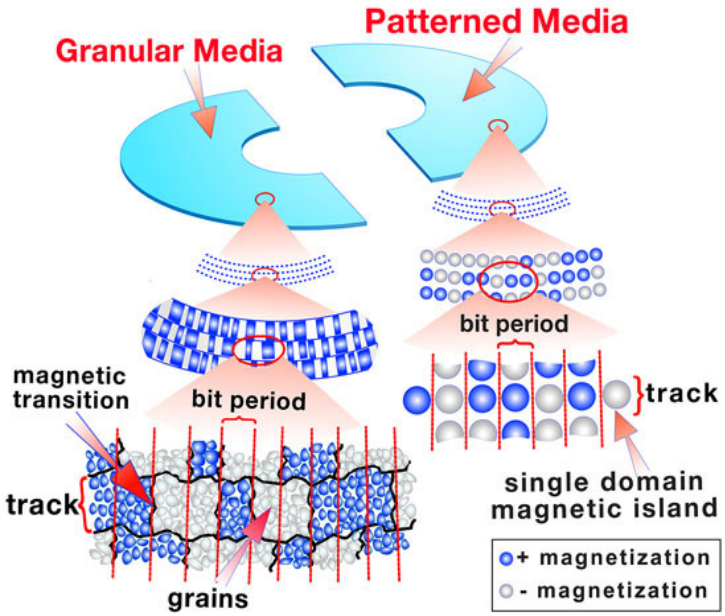


Figure I. 20: Conventional magnetic media (left) and patterned magnetic media (right).[58]

Non-volatile memory

NIL might also be used to realize next generation non-volatile memories. Here, the device structure consists of a resistance switching material sandwiched between two metal nanoelectrodes. Bottom and top electrodes are aligned perpendicular to each other building a crossbar array structure, as indicated in Figure I. 21. A significant advantage of these future devices in addition to their simplicity is the high integration density. Crossbar arrays with 200 nm electrodes and single cross junctions with 30 nm electrodes were achieved using UV NIL. The bottom electrodes were embedded and planarized by spin on glass, such that an even surface for the realization of the top electrodes by UV NIL could be obtained. Finally electrical measurements demonstrated the function of the fabricated devices.

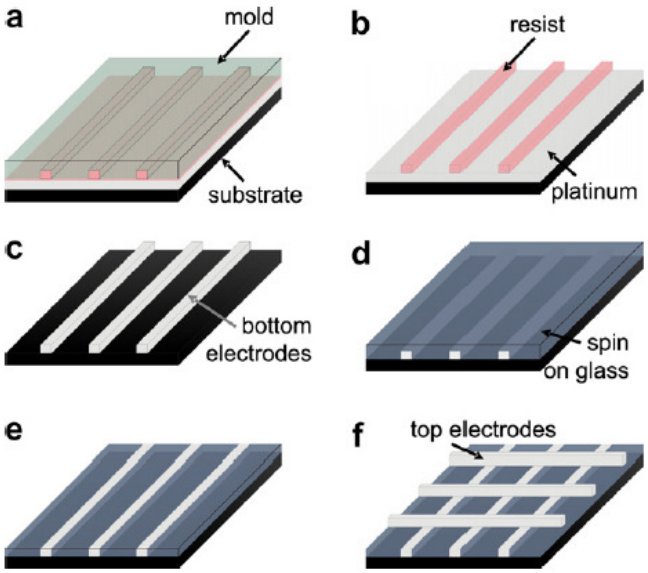


Figure I. 21: Process flow for the realization of crossbar arrays: a: molding, imprinting and UV exposure; b. removing resist residual layer; c. resist etching into platinum layer, giving bottom electrodes; d. surface planarization by spin on glass; e. spin on glass etching till bottom electrodes surface is exposed; f. top electrodes processed in the same way as the bottom electrodes. [59]

Biomedical applications
The physical and chemical properties of hydrogels make them valuable materials for a variety of biomedical applications such as bio-sensing or drug delivery. In this last case, they have been extensively used for cell and tissue engineering to encapsulate and release drugs. By micro- and nanopatterning hydrogels surfaces, it is possible to tailor topographic, chemical and physical properties interesting for protein attachment or cell confinement. UV-NIL is a rapidly emerging technique which is particularly suitable for this type of biotechnological applications. However, the current library of materials has been designed for microelectronic applications and they are often not yet compatible with biological systems.[60]

3.4 Imprinting tools

As described in more details in the review by H. Schift**Errore. Il segnalibro non è definito.** there exists quite a lot of different tool architectures in NIL, depending on the process used or on the targeted application. In planar UV-NIL, two main types of tools can be identified as already introduced before. The first one is step and repeat tools. Main commercial actors are *Molecular Imprints*, *EVG*, and *SET/Karl Süss*. In this case, hard stamps and substrates with excellent flatness are brought into contact at low pressure. Advantages of these tools are the possibility to fabricate stamps with smaller active areas (in general around 25*25 mm^2) and the possibility to implement more easily a high accuracy alignment system. Indeed, a high accuracy alignment (< 30 nm) is only possible, during the imprinting process, when the mold is already in contact with the resist and then requires a mold with a high mechanical stiffness.
The second type of tools is composed of equipments using soft pistons and full wafer molds. Here, flexible membranes are used on only one side or on the two sides of the wafer / mold stack in order to apply an isotropic imprinting pressure. The higher imprinting pressure used (up to more than 100 bars) is bending the mold and substrates and ensures a conformal contact between them. Known commercial actors in this field are *Nanonex*, *Obducat*, *Molecular Imprints*, *EVG*, and *SET/Karl Süss*. Main advantages of these tools are a lower incidence of the substrate and mold flatness quality and the possible very high throughput (full wafer imprint). Nevertheless, alignment is more problematic due to the larger molds and to the soft piston tool architecture.
Finally, some other industrials (*Toshiba*, *Hitachi*) have reported on the fabrication of UV-NIL tools as well, but for internal use and especially developed for microelectronic or bit patterned media applications.[61,62]

3.5 Industrialization issues

In a research laboratory, nanoimprint lithography works very well, but if one wants to use this technique in an industrial process at high throughput and high yield, specific issues has to be solved or tolerated. Among these, we have:

Air entrapment, evacuation and dissolution
This problem is dependent on the tool and process conditions used. Indeed, depending on the mold design, the flow front arrest at high aspect ratio features edges might create bubbles. Also, the resist drops placement geometry in the case of drop-dispensing and the geometry of the contact plays an important role (An inclined template descent or a mold bending may enhance bubble evacuation, especially for larger molds). Air bubbles are able to dissolve in the liquid resist, but, depending on their initial size, this phenomenon might limit the speed of the global imprinting process. The bubble dissolution rate in the resist might be enhanced when working in special gases environments (small helium molecules[63] or carbon dioxide[64] dissolve quite well in organic materials). The use of pentafluoropropane, which condensation

starts when the gas pressure exceeds 0.15 MPa, was also demonstrated.[65] Another possibility is to work in vacuum.[66] Then, one has to take care of the resist evaporation.

Flatness issues
At low imprinting force, the imprint quality is dependent on the mold and substrate flatness. For the step and repeat process, the 6.35 mm thick fused silica generally used can be prepared with a sufficient flatness. For the substrates, double-side polished wafers are preferable to single-side polished ones due to their better flatness and reduced total thickness variation. The wafer chuck flatness has also to be very well controlled.

Local geometry of the mold features
The geometry of the mold features might induce some problems. In particular, some applications in microelectronics are very sensitive to the line edge roughness. The shape of the features (vertical or inclined sidewalls, undercuts) may also induce demolding problems (possible rip-off of the structures, increased demolding force).[28]

Mold inspection and repair
Fabrication of defectless molds is extremely difficult. Some applications, in microele
ctronics for example, will require molds with almost no defects (defect density lower than 10^{-2}/cm²). For this, automatic mold inspection and repair tools are being developed. This is not a simple task due to the very high resolution involved (much smaller than in photolithography mask inspection as no reduction coefficient exists in NIL) and to the fact that the mold material is, in general, insulating (the use of scanning electron microscopy is more problematic due to charge effects).

Mold design issues
A uniform residual layer is obtained more easily when large protrusions are avoided in the mold design and when the mold density is as uniform as possible to avoid resist displacement over longer distances. On the other hand, one may use a reduced initial resist thickness (much less than the mold depth) to avoid long resist displacements and to compensate large density variations in the mold design. Then, larger cavities will be only partially filled. Nevertheless, and especially in UV-NIL where capillary phenomena are very important, this is not a good solution. Indeed, the resist will not stay flat in the incompletely filled cavities, but will create capillary bridges between the mold and the substrate, leading to unwetted areas.[67]

Mold and mold treatment lifetime, mold contamination
This point is essential in UV-NIL. Almost all results presented in this thesis are related to this issue (cf. Chapter II Antisticking issues in nanoimprint lithography) and a state-of-the-art on this topic will be given in § 5 of this chapter.

All the aforementioned issues may lead to defects in the imprinted resist.[68,69] Additionally, defects may also come from atmospheric particle contamination. Indeed, in NIL, a simple particle trapped between the mold and substrate will produce a very large non-contacted area. This is the reason why it is absolutely necessary to work in a very high quality clean environment. Another issue concerns the distance between imprinted dies in the step-and-repeat process. It is not possible to stitch adjacent die due to the expelled resist at the stamp border and a distance of about 100 µm or more has to be taken between the die. Also, this resist excess at the die border is a problem for the resist stripping step (removal of the resist mask or residues after use) because of its increased thickness. Additionally, imprinting uncompleted die at the border of a wafer is difficult without damaging or contaminating the

mold. Finally, real time measurement and simulation tools (including all interfacial aspects) would be of great help to understand more precisely some of the different phenomena.[70]

4 Imprinting materials for UV-NIL

In this part, I will first introduce the UV polymerization process in general and present the state-of-the-art of UV-curable materials used in UV-NIL.

4.1 UV-assisted polymerization process

In a UV-assisted polymerization process, the source of curing is UV radiation, defined in Figure I. 22 as the portion of the electromagnetic spectrum between X-rays and visible light, i.e., between 100 and 400 nm in wavelength. The UV light sources generally adopted by industry to cure a photocurable formulation are basically of two types: arc light and laser light. The former includes mercury and xenon lamps for example. The medium-pressure mercury lamp is currently the overwhelming industry choice because of its high power (up to about 300 W/cm^2) and intense emission lines which are absorbed by most commercially available photoinitiators.[71]

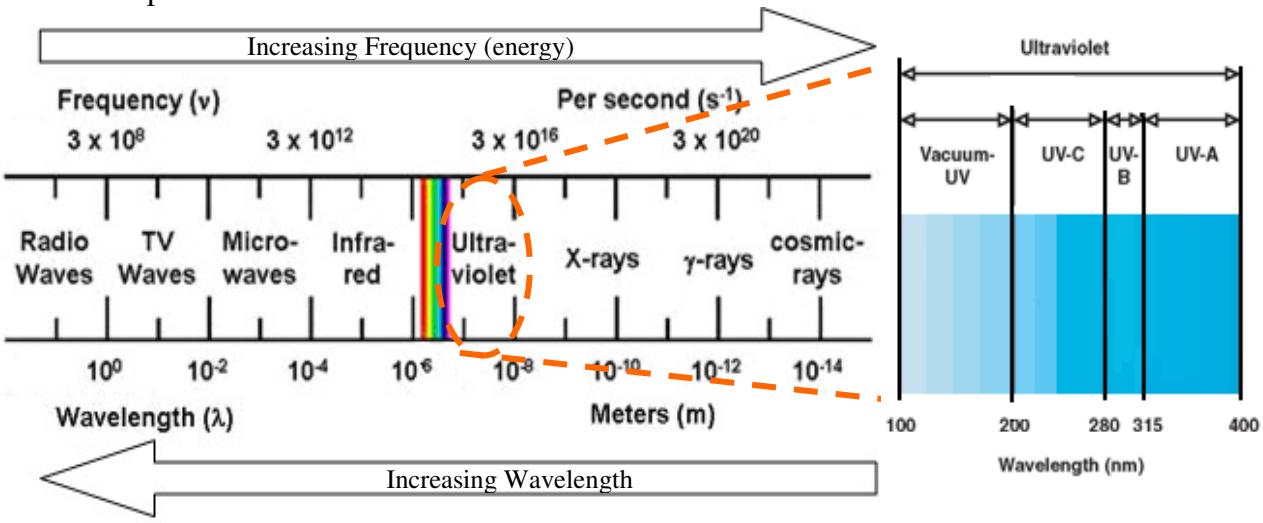


Figure I. 22: Electromagnetic spectrum (left side) with a focused view over the UV portion (right side).[72]

A photocurable formulation contains in general a photoinitiator, one or more oligomers, monomers and solvents. The photoinitiators absorb the UV energy from the light source and is fragmented into reactive species, setting in motion a chemical reaction that quickly converts the liquid formulation into a solid, cured film. It is therefore mandatory that the emission spectrum of the UV light source overlaps the absorption spectrum of the chosen initiator.
A photoinitiator can be categorized in different ways, according to:

- the produced reactive species (free radical or cationic)
- its state (liquid or solid)
- its adsorption spectrum (UV light or visible light)
- its depth of cure (thick or thin layer)
- its application (clear, pigmented or white)[71]

Monomers are low molecular weight materials. They can be mono- or multifunctional molecules, depending on the contained number of reactive groups. Functional monomers become part of the polymer matrix in the cured coating because their reactive groups undergo polymerization during exposure to UV light. Monomers also function as diluents in the formulations, used to adjust the system viscosity, and are sometimes referred to as reactive diluents. Because some monomers have a rather high molecular weight, the difference between monomers and oligomers is not sharply defined.
Oligomers are also often called (telechelic) prepolymers. They tend to present a higher viscosity and a higher molecular weight and are the main components of a formulation.

Molecular weight ranges from several hundred to several thousand grams / molecule or even higher. Usually, the type of oligomer backbone determines the final properties of the coating such as flexibility, toughness, etc... These backbones can be epoxy, polyether, polyester, polyurethane or other types. The functional groups that provide linkage between molecules are generally located at both ends of the oligomer molecules and will generate a 3D structure after polymerization. The functionality found to be most effective is the acrylate functional group.
Two main types of polymerization systems are used in UV-NIL:

The free radical polymerization system (acrylates and methacrylates)
In free radical polymerization, the whole process starts with the photoinitiator. This molecule is split into two fragments under UV radiation: the pair of electrons in the bond which is broken is so separated, giving two molecules with unpaired electrons, called *free radicals*. These unpaired electrons are instable and tend to react to be paired; if they can find any electrons to pair up with, they will do so. The carbon-carbon double bond in a vinyl monomer, like ethylene, has a pair of electrons which is very easily attacked by the free radical. The unpaired electron, when it comes near the pair of electrons, swipe one of them to pair with itself. This new pair of electrons forms a new chemical bond between the initiator fragment and one of the double bond carbons of the monomer molecule. This electron, associates itself with the carbon atom which is not bonded to the initiator fragment. This whole process, the breakdown of the initiator molecule to form radicals, followed by the radical's reaction with a monomer molecule is called the *initiation* step of the polymerization, as illustrated in Figure I. 23 taking benzoyl peroxide as free radical photoinitiator.

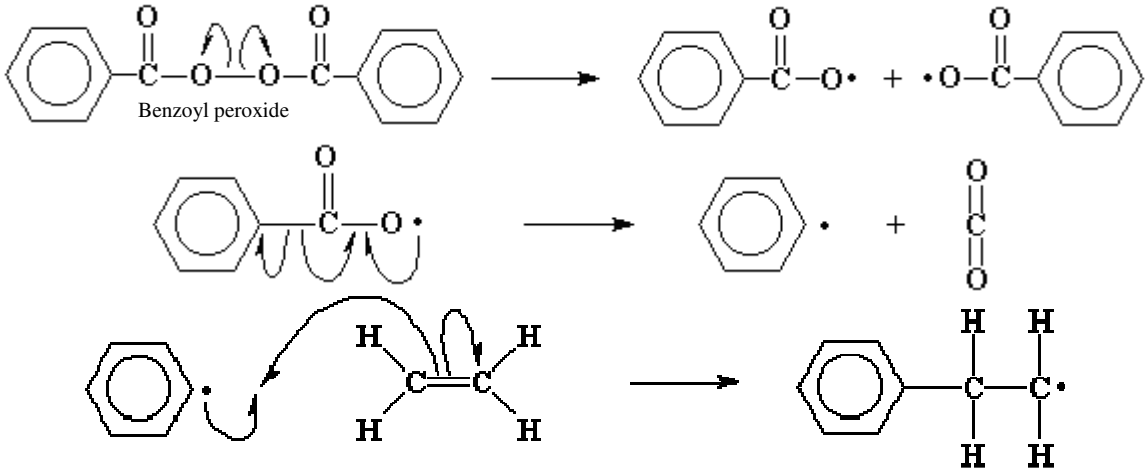


Figure I. 23: *Initiation* step in free radical polymerization. (When a line is drawn between two atoms, this represents a pair of electrons the atom share. Sharing one pair of electrons makes a single bond. Sharing two pairs makes a double bond, shown by two lines. The curved arrows show the motion of a pair of electrons).

This new radical obtained after *initiation* reacts with another ethylene molecule in the same way as the initiator fragment did, always generating another radical when this reaction takes place over and over again. This process, the adding of more and more monomer molecules to the growing chains, is called *propagation*, as shown in Figure I. 24.

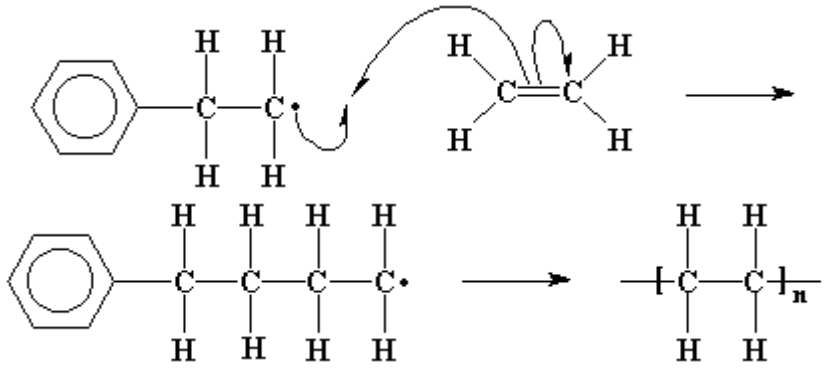


Figure I. 24: Propagation step in free radical polymerization.

In free radical polymerization there are two different mechanisms that can stop the growing polymeric chain and shut down the whole polymerization process; these are called respectively *coupling* and *disproportionation*. The former is the result of the interaction between two growing chain end radicals that join together and give rise, as illustrated in Figure I. 25, to a polymeric chain containing no new radical.

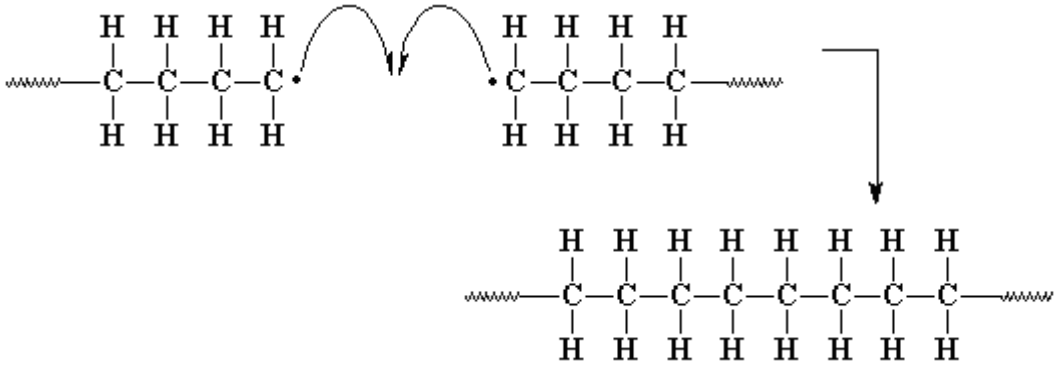


Figure I. 25: *Coupling*: first mechanism of *termination* step in free radical polymerization.

In the latter, presented in Figure I. 26, when two growing chain ends come close together, the unpaired electron of one chain does something different from simply joining with the unpaired electron of the other chain. It can react with the carbon-hydrogen bond of the carbon atom next to the other carbon radical. The unpaired electron grabs not only one of the electrons from this bond, but the hydrogen atom as well. As a result, the first chain has no unpaired electrons and the end carbon now shares eight electrons. The polymer chain which lost its hydrogen atom remains with two carbon radicals next to each other, which join their unpaired electrons to form a pair, and thus form a double bond between the two carbon atoms at the end of the polymer chain.[73]

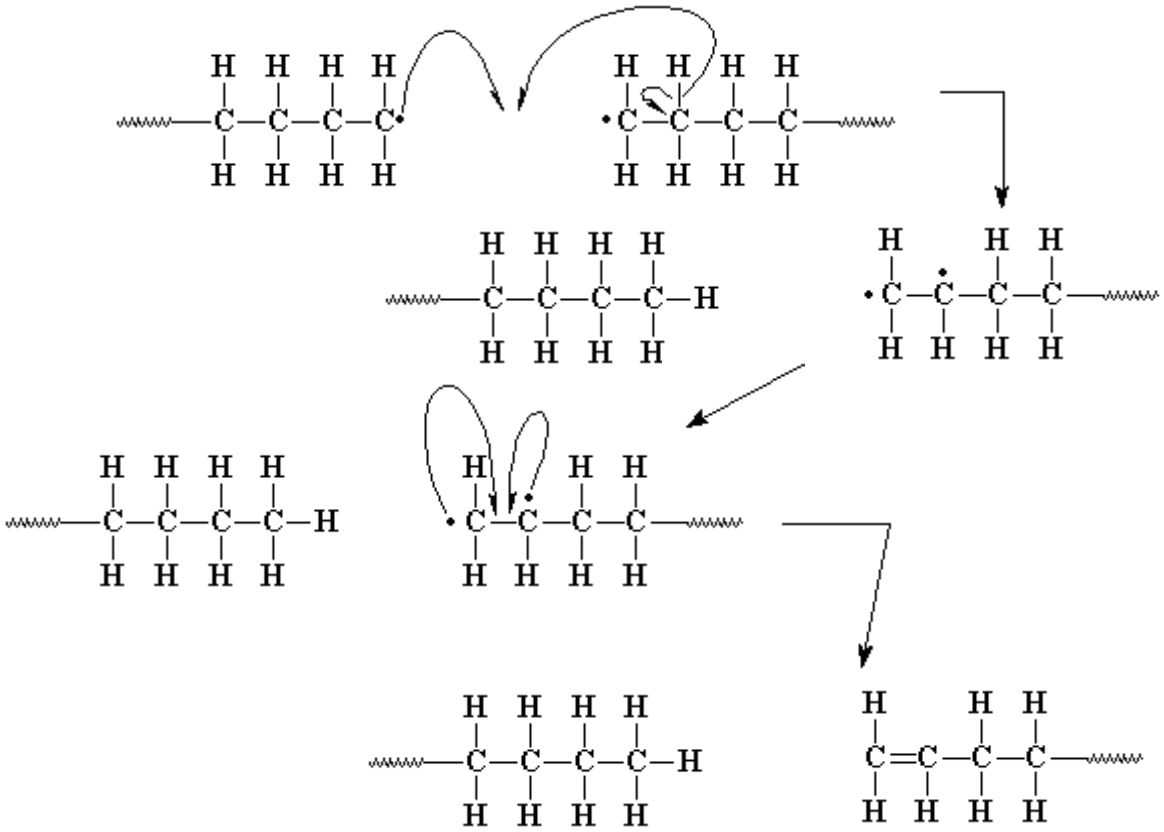


Figure I. 26: *Disproportionation*: second mechanism of *termination* step in free radical polymerization.

The cationic polymerization system (epoxies and vinylethers)

In cationic polymerization, the initiator is a cation, which is an ion with a positive electrical charge. Different kinds of cationic photoinitiator can be employed to start the process. Aluminum trichloride, or $AlCl_3$, is taken to present cationic polymerization steps. The aluminum atom in $AlCl_3$ is sharing electron pairs with only three other atoms, leaving it with only six electrons (two less than those necessary to complete the outermost shell, according to octet rule) and a whole empty orbital. A very small amount of water is usually present in the system; the oxygen atom in water has two unshared pairs of electrons, and it donates a pair to the aluminum atom, forming an $AlCl_3$ / H_2O complex.

Oxygen, being very electronegative, will tend to pull the electrons it shares with the hydrogen atoms toward itself, leaving the hydrogen atoms with a slight positive charge. This leaves them rape for an attack by a pair of electrons from the double bond of a monomer molecule. The monomer in this way can swipe the hydrogen, making itself a cation, and the $AlCl_3$ / H_2O complex becomes its compliment anion $AlCl_3OH^-$. This whole process by which the $AlCl_3$ / H_2O complex forms and reacts with the first monomer molecule is called *initiation*, as illustrated in Figure I. 27.

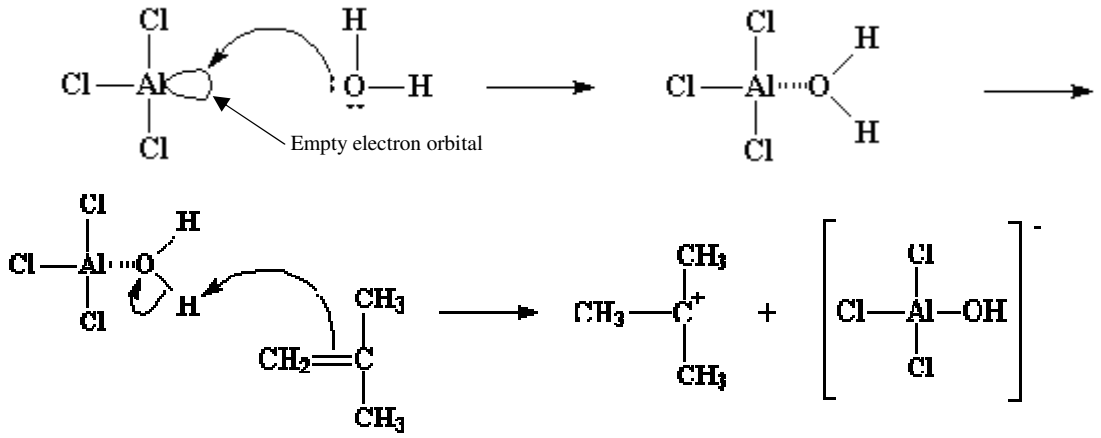


Figure I. 27: *Initiation* step in cationic polymerization.

After *initiation*, a carbocation (a cation where the positive charge is on a carbon atom) is created. Carbocations are very unstable because the carbon atom in a carbocation only has six electrons in its outermost shell. In presence of a monomer molecule containing a carbon-carbon double bond (and a pair of electrons for each bond as well), the carbocation swipes a pair of electrons and in doing so forms a single bond with the monomer molecule. It also generates another carbocation, which can react with another monomer, and then another, and so on. This process, illustrated in Figure I. 28, is called *propagation*.

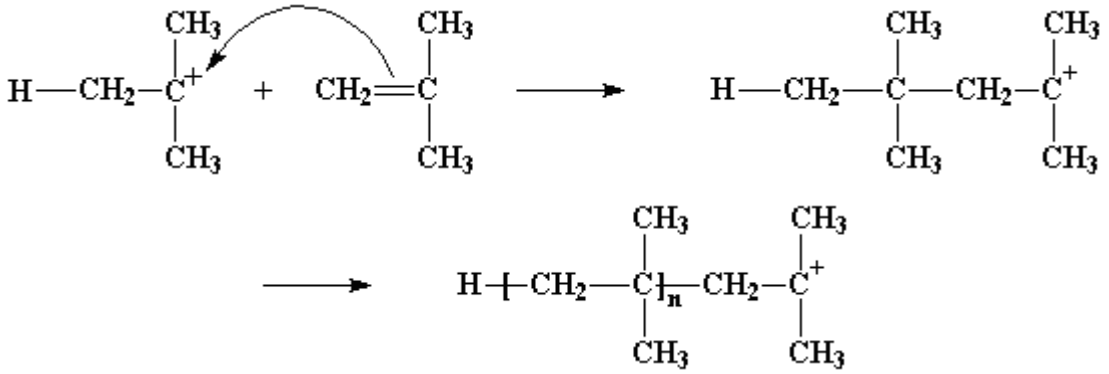


Figure I. 28: *Propagation* step in cationic polymerization.

Instead of reacting with a monomer molecule, the growing cationic chain can also react with the old anion of the initiating cation. When this reaction brings to no new chain creation, the polymerization is over and this process is called *termination*, as presented in Figure I. 29.

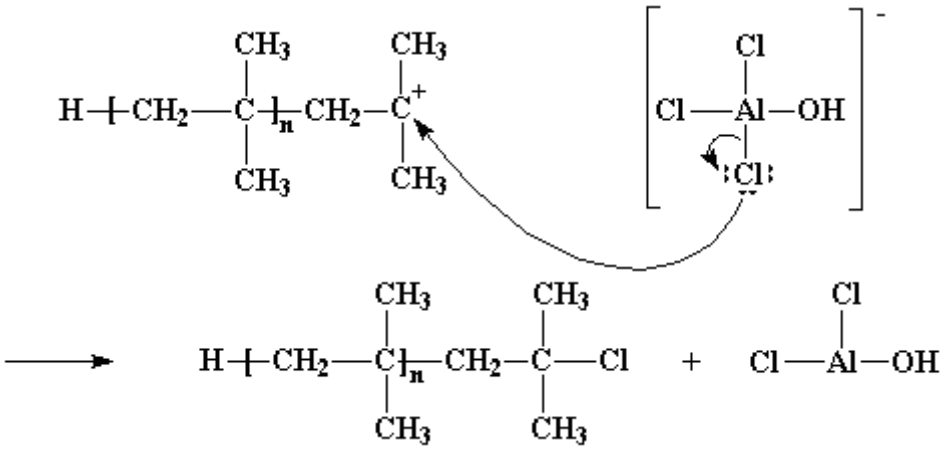


Figure I. 2

In the case of aluminum trichloride, *termination* can occur when the unshared pairs of electrons from a chlorine atom react with the cationic carbon atom. The end of polymer chain contains after reaction a chlorine atom, which will not start a new polymer chain growing.[74]

4.2 UV-curable resists for UV-NIL

Resists developed for UV-NIL have to present following, eventually specific, characteristics: low viscosity, high curing speed, high etch-resistance, high adherence to the substrate, low adherence to the mold, good film formation (spin-coated resists), reduced contraction during photopolymerization, adapted mechanical properties and finally a low evaporation rate (reduced vapor pressure). In general, they are composed of monomers and a UV-sensitive photoinitiator. Additionally, they may contain sensitizers[75] (to improve UV light absorption), surfactants[76] (for example fluorinated surfactants to reduce their adherence to the mold), more than one photoinitiator[77] (to improve the speed of conversion and the conversion ratio), inhibitors (to reduce the effect of free radical annealing by scavengers like oxygen) and finally solvents (to be able to adjust the thickness of the spin-coated layer). Solvents are not used in the case of drop-dispensing in order to maintain initial spherical drop shapes, facilitating the resist flow and limiting the bubble entrapment.

About the monomers used, they may present one or more polymerization sites. In the case of one polymerization site only, the cured material will be composed of linear chains and will remain soluble in common solvents. This may lead to a lower mechanical stiffness and lower plasma etching resistance, but will present the advantage of being easily removed from the mold (contamination cleaning) or wafer (resist stripping) surface. In the case of more than one polymerization site, the material will present a 3D crosslinked network.

Three main monomer families are used in UV-NIL. The first one is epoxy monomers.[75,78] In general, they present the advantage of insensitivity to oxygen during the polymerization (cationic mechanism) and a higher mechanical stiffness, but the polymerization does not proceed very rapidly as compared to acrylates or vinyl-ether formulations. Acrylates are most often used, mainly because of their extensive commercial availability, low viscosity, and capability for rapid polymerization via radical propagation. However, oxygen is a strong radical inhibitor. Dissolved oxygen in the resist may slow down the polymerization mechanism, or some uncured resist contamination might appear at the border of the template where resist might be in contact with air. Vinyl ethers are the third category of monomers used in UV-NIL.[79] Their polymerization proceeds also via a cationic mechanism, which is insensitive to oxygen and very rapid. In addition, vinyl ether monomers have even lower

viscosities than acrylates at otherwise comparable molecule composition.[80] Nevertheless, there is not a large choice of commercial raw materials and vinyl ether resists adhere more strongly to molds and enhance the required release force[80]. This last limitation is partly overcome by the higher tensile strength of vinyl ether formulations.[81] Finally, the UV-sensitivity is not a limiting point of UV-NIL since exposure times of 1 s or less are reported using acrylates or vinyl ether formulations.[82]

Concerning the mechanical properties, a high crosslinking of the material after UV exposure may bring improved plasma etch resistance[83] as well as improved mechanical properties. This last point is important for the demolding process. However, a long UV exposure time may cause excessive shrinkage and brittleness of the resist, increasing the possibility of features breaking and mold contamination. On the other hand, insufficient UV curing will lead to a low cohesive strength of the polymer, increasing the probability of pattern distortion and collapse.[84] This means that the irradiation dose may have to be optimized for each material and pattern type in order to achieve appropriate mechanical properties.

In addition, some resist are developed for special application and with special properties. This is the case for example in microelectronics, where special low-dielectric constant and high thermal and mechanical resistant hybrid organic-inorganic materials are being developed for the simplification of the dual damascene electrical interconnection process.[85] Also, resists loaded with functional nanoparticles can be patterned using NIL.[86]

On the commercial side, a few products are available from *Nanonex*, *Obducat*, *micro resist technology*, *Molecular Imprints*, *AMO*, *Toyo Gosei*, or *AGC* for example. It has to be noted that some manufacturers will sell their resists only with a proprietary process and equipment. Then, it is difficult to compare the properties of these commercial products on the same equipment and in similar conditions.

Adhesion of low viscosity thin films of monomer solutions to the surface of silicon (or fused silica) substrates can be enhanced by using an intermediate adhesion promoter applied prior to resist dispensing. The adhesion promoter can be a thin polymeric film that shows a high adhesion to the substrate as well as a high affinity with the used monomers. Also, this thin layer can play the role of compliant / planarization layer. However, its thickness might be as high as a few tens of nm and will increase the residual resist thickness, but it may help the pattern transfer (for lift-off processes for example[87]). An alternative approach consists in functionalizing the silicon substrate's surface with a self assembled monolayer (SAM) whose molecules are designed to fulfill two requirements: one headgroup bonds covalently to the silicon surface via a silanization reaction with hydroxyl groups while the other headgroup is able to copolymerize with the UV-NIL resist during UV exposure. This solution has been adopted by Hewlett Packard's research group since 2005 and has allowed 30 nm half pitch dense lines imprinting and transfer using a methacrylate based resist.[88]

4.3 Resist shrinkage

During UV curing, the resist volume shrinks. Due to a ring opening polymerization, epoxy resist have a very limited shrinkage rate, in general around 3 %. On the other hand, acrylates and vinyl-ether resists show shrinkage rates of around 10 % in most cases.[89] For high aspect ratio features embossed in a thick UV-curable material, resist shrinkage was demonstrated to facilitate demolding[90] and it seems that an optimum level of shrinkage exists at which the stress experienced by the polymer during demolding is minimized.[91] Such phenomena were not yet demonstrated in UV-NIL and large resist shrinkages are something that has to be avoided. Indeed, due to the thin residual resist thickness and the mechanical rigidity of the substrate, the bottom of the fabricated structures is not able to relax. Consequently, the resist shrinkage will induce a change in the top lateral dimensions and height of the features,

reducing their lateral slope. This is a problem for the control of critical dimensions, especially when an additional plasma etching transfer step is required.
In order to limit the shrinkage, resist formulations are made with monomers presenting a reduced shrinkage. For this, steric hindrance might be used. Another possibility is to include an oligomer or a polymer in the resist formulation as a binder,[92] but one has to be careful not to increase too much the resist viscosity in this case.

4.4 Plasma etching processes and resists stripping

Imprinting in a polymeric material is technically not very complicated, even at very high resolution when a mold is available, but using the fabricated polymer features in a real device by transferring them in an underlying substrate is more critical. One has to control the resist flow in order to limit the number of defects and ensure a thin and uniform residual resist layer. Then, the polymer layer can be used as a mask in a plasma etching equipment.
First, a "breaktrough" etch is performed in order to remove the residual resist layer. In general, a pure oxygen plasma is used here which is very reactive with organic materials and will not etch conventional substrates like silicon or silica. Addition of ammonia (NH_3) or larger atoms (Cl or Ar) in the plasma was shown to improve the anisotropy of the process and to reduce the etching speed of the resist, leading to an improved control of the process.[93] Even with an anisotropic etching process, it is important to have a uniform residual layer. Indeed, in the case of an over-etch intended to compensate the non-uniformity of the residual layer, reactive species at locations were the resist layer is already removed will react isotropically with the surrounding features and change their lateral dimensions.
Then, the obtained "opened" resist mask can be used to etch the underlying substrate. In the case of silicon or silica, plasmas with fluorine (mainly CF_4 and SF_6 gases), bromine (HBr) or chlorine (Cl_2, HCl) can be used. To achieve transferred features with a usable aspect ratio (in general larger than 1, meaning a feature height larger than its linewidth), imprinted resists has to present a correct selectivity to the underlying material (this means that the etch rate of the resist in the considered plasma has to be sufficiently small as compared to the etch rate of the substrate in order to be able to fabricate the desired features).
In general, in UV-NIL, the material is crosslinked due to the use of monomers with multiple photopolymerizable groups. This is an advantage compared to the photolithography case (in particular positive tone resists). Indeed, very correct etching resistance can be obtained when choosing hybrid organic-inorganic monomers (in general molecules containing siloxane bonds, characterized by their weight percentage of silicon atoms), perfluorinated monomers or monomers containing aromatic cycles (benzenic or norbornene cycles for example). As an example, 40 nm wide lines could be etched 120 nm deep in silicon using a 80 nm thick layer of the commercial product *AMONIL*, from *AMO*, which is a silicon-containing resist (Figure I. 30, before removing the resist residues).

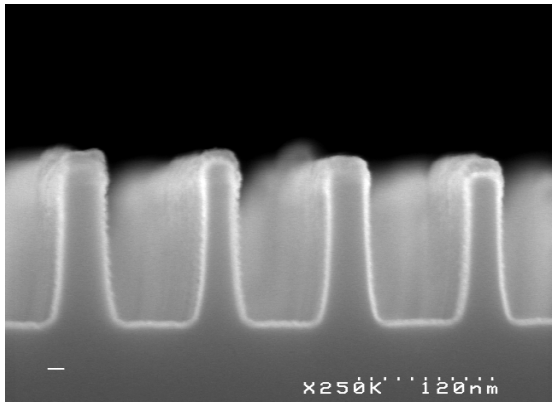


Figure I. 30: Example of 40 nm wide lines etched 120 nm deep in silicon using a silicon-containing resist.

In Figure I. 31, examples of silicon etching using three different resists in exactly the same conditions (same imprinting conditions, same mold, same etching plasmas, same resist thickness and same resist removal process) are reported. We observe that for the purely organic product, the plasma etching resistance was not sufficient leading to a "faceting" of the silicon lines (left). In the case of silicon-containing or perfluorinated resists, non-facetted line profiles are observed (centre and right). Indeed, incorporation of fluorine rich monomers in the UV curable resist may enhance the etch properties. The work conducted by Kim et al.[94] where an acrylate-based formulation was doped with a fluorine-substituted acrylate chain reported that the incorporation of 20% of fluorinated monomers increases the oxygen plasma etching rate of the photo-polymerized material by more than 15%. But another example reported by *AGC*[95] highlighted a weakening of the adhesion to the substrate when the amount of fluorinated monomer increases necessitating applying suitable adhesion promoter onto the substrate.

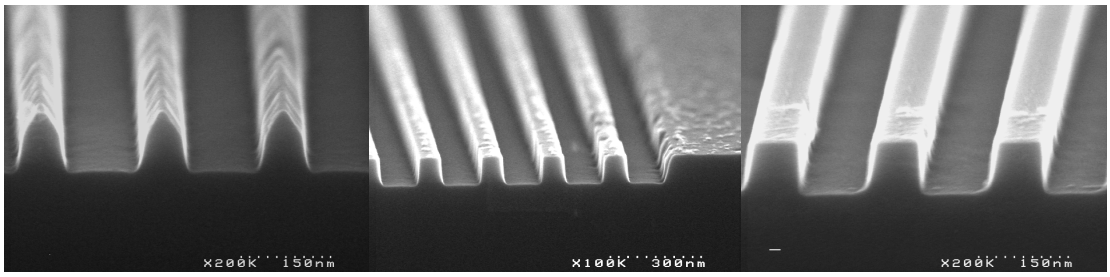


Figure I. 31: Examples of silicon etched with different UV-NIL resists in exactly the same conditions (left: purely organic resist, centre: silicon-containing resist, right: perfluorinated resist).

The resist removal process, or resist stripping, is done in general with pure oxygen plasma and or using an acid solution (mixture of hydrogen peroxide and sulphuric acid for example). Additionally, a dip in hydrofluoric acid (HF), removing silica-like compounds, may help to remove the passivation layers and resist residues that appears during silicon etching. In the case of Figure I. 31, resist stripping was done with an oxygen plasma and HF dip. We can observe that a large number of residues still exist on the wafer surface for the silicon-containing material. Indeed, removing resist residues of crosslinked materials is difficult; especially for those presenting a very high etch resistance. Perfluorinated materials seem to present both a sufficient etch resistance and ease of stripping. Alternatively, a very elegant method allowing an efficient resist stripping process for crosslinked materials is the development of "degradable crosslinkers".[96]

5 Mold fabrication and antisticking issues

5.1 Mold fabrication and characterization

As already described, in UV-NIL, molds can be made of organic materials (using for example polymers or elastomeric materials) or inorganic materials (using glass, fused silica, transparent conductive oxide such as Indium Tin Oxide[97] (ITO, to overcome charge problems), sapphire[98], fluorinated diamond-like carbon[99], boron nitride[100] or silica-like electron-beam inorganic resist such as Hydrogen SilsesQuioxane[101] (HSQ)). Indeed, using HSQ, one can fabricate directly the features without etching as the resist reaches almost the composition and density of silica after thermal treatment.

Among all these inorganic transparent materials, ¼ in. thick, 6 in. square fused silica plates are mostly used as base material for UV-NIL stamps fabrication thanks to their commercial availability, their high degree of purity, their excellent flatness and their inert behavior with respect to photo curable monomers solutions. In addition, mask shops have acquired, for the purpose of phase shift masks fabrication, accurate and reliable electron-beam writing as well as plasma etching processes on such type of plates.[102,103,104] Moreover, fused silica stiffness is high enough to avoid nano-features deformation during the imprinting sequence which may induce unacceptable misalignment in mix and match lithographies. However, the resolution needed here is much smaller than those required for optical masks, as NIL is a 1X lithography technique and it is more difficult to etch an insulating material like silica to very small dimensions in a plasma (as compared to silicon for example) due to surface charge issues.

Details on fused silica mold fabrication are illustrated in Figure I. 32 and detailed elsewhere.[105] In general, a resist is patterned using electron-beam lithography and then transferred into a thin (between 8 and 20 nm) chromium layer with a Cl_2/O_2 plasma. Afterwards, fused silica is etched in a fluorocarbon plasma using the chromium layer as a hard mask. Finally, this hard mask is removed in a wet or dry process.

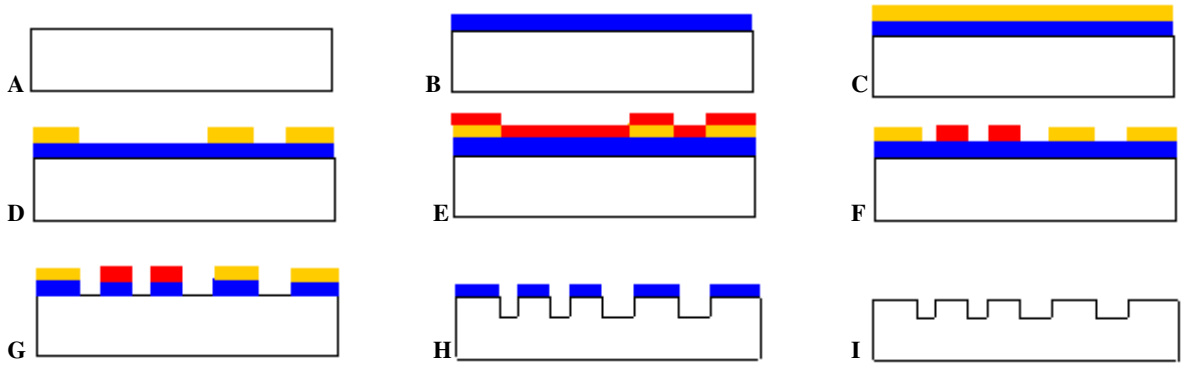


Figure I. 32: Description of a combined optical and electron-beam lithography mold fabrication process on a fused silica wafer (A); (B) chrome layer deposition; (C-D) optical lithography; (E-F) electron beam lithography; (G) chrome dry etching; (H) silica dry etching; (I) chrome stripping and anti-sticking treatment.

A different solution to fabricate molds consists in copying an initial master mold into a daughter mold using a polymeric transparent material which bulky properties confer good release characteristics. Furthermore, master molds could be fabricated in silicon using standard tools and processes from the microelectronics industry. *AGC* has elaborated fluorinated high transparency polymers (*F-template*) that can be embossed by thermal NIL to replicate a master template, made of either silicon or fused silica[95] into a working stamp presenting a water contact angle higher than 100°C. Other research teams have also synthesized thermally[106] and UV[107,108] curable formulations for the need of template

replication. Nevertheless, to be definitely adopted, this alternative solution has to be finely characterized in terms of mold degradation and mechanical properties.
Also, when no high accuracy alignment is needed and due to the low pressure used in UV-NIL, mechanical properties of the mold can be relaxed. Then, mold copies can also be obtained by replicating elastomeric materials like PDMS, which is UV-transparent within the 340-600 nm wavelength region[109,110]. Finally, the ultimate stamp copy process was presented by *Obducat* with the *Intermediate Polymer Stamp.*[111] Here, the polymer stamp is used only once, avoiding any mold contamination or erosion issues.

Mold inspection[112] and repair[113] are mandatory in applications, like microelectronics, requiring a very low defectivity. Some specific commercial tools, derived from wafer and mask inspection equipments, are under development.[114,115] Also, the Line Edge Roughness (LER) is an important characteristic of fabricated templates and becomes a critical issue when the dimensions are shrinking. One powerful method, used in our lab, to characterize the roughness of fabricated UV-NIL molds is three-dimensional atomic force microscopy (AF-ASL3D). Such a tool is able to reconstruct completely a 3-dimensionnal surface (see example in Figure I. 33) and to measure directly the LER. Also, AF-ASL3D can be used to follow the roughness of NIL fabricated features at the different steps of the process (after imprint, after residual layer etching, after transfer and finally after stripping).

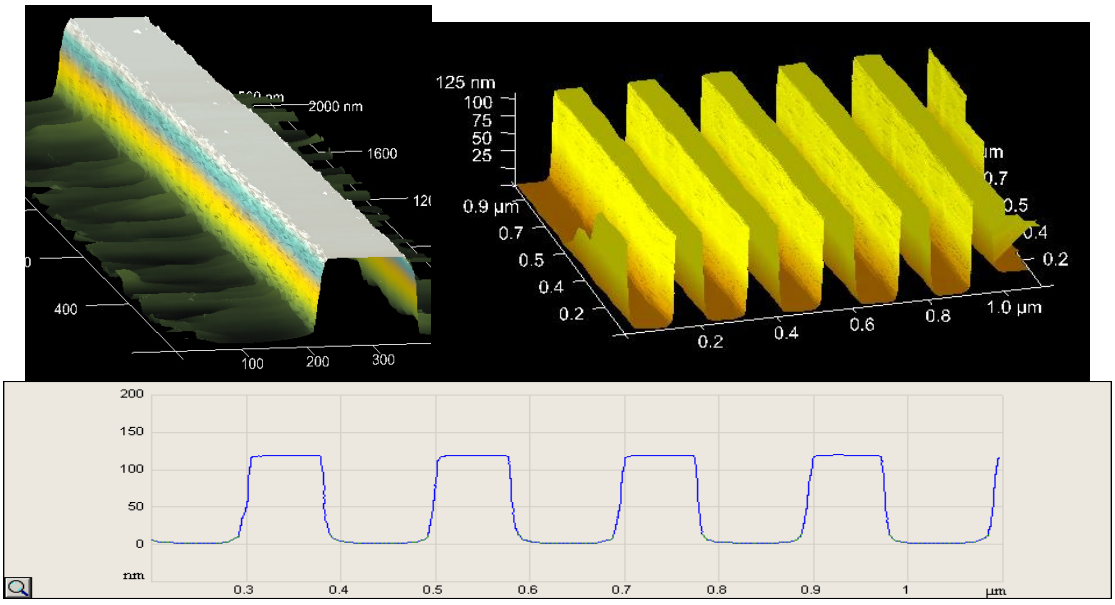


Figure I. 33: Example of AF-ASL3D mold characterization (100 nm wide lines).

5.2 Antisticking issues

A major challenge of the nanoimprint technique is to perform a correct detachment of the mold from the cured resist. This difficulty is inherent to the high density of nanoscale protrusions patterned on the mold's surface which effectively increases the total area that contacts the UV-cured resist. Therefore, sticking between imprinted polymeric structures and mold's surface can lead to the three following detrimental consequences:

- Improper release of the polymer film from the template creates defects in the imprinted layer.
- Any residual photopolymer that remains on the template from a previous incomplete release creates defects in subsequent imprinted patterns. (Some work has shown a

"self-cleaning" effect of the mold,[116] removing contaminants after a few imprints, but this is not very clear and seems to depend on the contaminant size and on the process used).

- Finally, attempts to systematically remove photopolymer residues from the mold's surface by wet or dry chemistry are not only time consuming processes but also harmful to the template integrity and lifetime.

As an example, Figure I. 34 shows imprinted features performed in the lab with and without mold treatment using the same imprinting conditions. In the case of the untreated mold, the imprinted resist layer is clearly not usable. The origin of this problem is either a weak adhesion of the UV curable resist thin film to the substrate, a strong adhesion of the cured materials to the mold, a poor mechanical resistance of the material or, more likely, a combination of all. However, improving adhesion of the resist thin film to substrate and tuning the resist's mechanical properties cannot totally prevent the sticking issues. That's why much work has been done to reduce the mold-resist sticking by minimizing the interfacial energy.

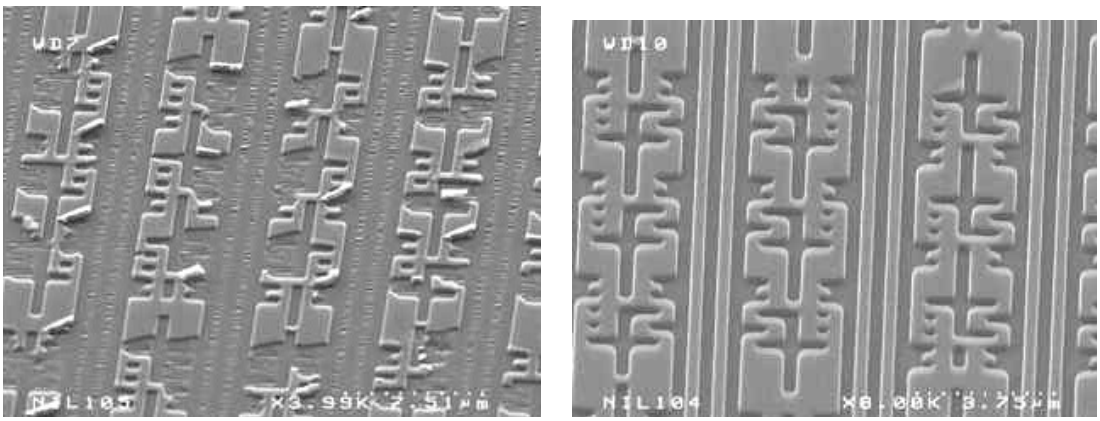


Figure I. 34: Resist layer imprinted with an untreated (left) and a treated (right) mold in the same conditions.

Fused silica is a hydrophilic material exhibiting a rather high surface free energy (~ 50 mJ/m^2) facilitating the adhesion of cured resist to its surface. According to industrial criteria in terms of process throughput and cost of ownership, a fused silica template should be able to undergo thousands of imprinting sequences with a reproducible behavior before being cleaned (or eventually replaced). To meet such severe requirements, different approaches were proposed. They are essentially: a) to treat the mold surface with an AntiSticking Layer (ASL); b) to modify the resist formulation; or c) to make a "low-cost" copy of the stamp as described in the previous paragraph.

5.3 Mold treatments

Fused silica templates can be coated with an anti-adhesion layer that lowers effectively its adherence to cured resist. In addition to this major criterion, this layer must have a good adhesion to the template surface, should be deposited in a conformal way onto the mold's features, should have good mechanical properties (high stiffness) and should not reduce excessively the UV transmittance properties of the mold. Moreover, in the case of sub-100 nm features patterned on the molds surface, the thickness of this layer should not exceed a few nanometers and its surface roughness has to be as low as possible and should not increase the mold's initial roughness.

Diamond-Like Carbon (DLC) coatings, also known as amorphous carbon coatings, have been considered as a good choice for this application due to the combination of relative

hydrophobicity with outstanding mechanical properties.[99] They can be easily obtained by plasma enhanced chemical vapor deposition (PECVD) of hydrocarbon gases (methane) and exhibit a lower surface energy than silica (~ 40 mJ/m²) and high stiffness (20 GPa). However, the deposition rate of those films is still important (few nm/sec) which makes it difficult to obtain uniform and conformal layers thinner than 20 nm, making them unsuitable for sub-100 nm features. Besides, the transmittance of such DLC films is low at typical wavelengths used in the UV-NIL process (13% transmittance for a 100 nm thick layer, 50 % for a 10 nm-thick one).[117]

Other attempts have been done in order to improve optical properties of DLC coatings via a partial doping during vapor phase. N_2 or Si doping has proven to enhance the UV transmittance of ion beam synthesized DLC coatings,[118] but the stiffness was noticeably reduced.

Alternatively, a recent work by F. Houle et al.[119] showed that thin metal oxide compounds coatings, with water contact angles lower than 50°, can be good candidates for antisticking layers with well controlled behavior when used with free radical or cationic resists.

Teflon like thin films deposited by plasma show a very good hydrophobic performance but suffer from a poor adhesion to the template surface.[120] More generally, the trade-off between the tribological properties, chemical composition, surface energy and optical band gap is critical in defining the performance of these coating materials for UV-NIL applications.

Another approach, used in my work (and the most used in the literature), are fluorinated silane molecules treatments able to covalently bond to the mold's surface. The grafting principle will be detailed in § Chapter II.1.1. Several fluorinated molecules are reported as being release agents for NIL templates. Among them, tridecafluoro-1,1,2,2-tetrahydrooctyltrichlorosilane [CF_3-$(CF_2)_5$-$(CH_2)_2$-$SiCl_3$], 1,1,2,2-perfluorodecyltrichlorosilane [CF_3-$(CF_2)_7$-$(CH_2)_2$-$SiCl_3$], 1H,1H,2H,2H-perfluorooctyltrimethoxysilane [CF_3-$(CF_2)_5$-$(CH_2)_2$-$SiO(CH_3)_3$, F_{13}-TMS], or perfluoropolyether molecule (*Optool DSX* from *Daikin Chemical* or *Fluorolink S10* from *Solvay Solexis* for example) are the most used. All these molecules lead, when properly deposited, to a water contact angle higher than 100° and a free surface energy on the order of 10 mJ/m², able to reduce adhesion between the treated mold surface and the cured resist. These Fluorinated AntiSticking Layers (F-ASLs) can be deposited either in liquid phase, by dipping directly the mold in a diluted solution of antisticking molecules,[121] or in a vapor phase process. This latest can be done either by thermal evaporation of the liquid precursor at atmospheric pressure[122] or by vacuum evaporation at room temperature.[123] In the case of chloro-silane molecules, these are very reactive and are able to polymerize in presence of water (water vapor in air is sufficient), producing particles that can precipitate onto the mold's surface. This is why it is preferable to use the vapor phase process with this type of molecules, leading to smoother surfaces.[124]

Compared to inorganic deposited films, F-ASLs have several advantages:

- Their thickness is very low. Experimental values reported in the literature and confirmed during my work vary from 0.3 nm for a F_{13}-TMS based layer[122] up to 3 nm for an *Optool DSX*-based one.[125] (After a large number of observations it is now widely admitted that the presence of this very thin layer of F-ASL does not significantly change the critical dimensions of nanostructures elaborated on the mold surface.)
- These layers have a very low surface energy and effectively give very good release properties in the NIL process.
- Their adhesion to the mold is excellent due to a covalent bonding of the molecules.

- Deposition parameters like the dip time, the concentration and the temperature of the solution, the evaporating time and pressure can be monitored quite easily to optimize roughness and density of the deposited layer.
- F-ASL deposition can easily be implemented in an industrial environment.
- Finally, if necessary, F-ASL treatments are cleanable and can be entirely removed from silica surfaces by a suitable combination of wet and or dry etching processes without altering the mold surface roughness. Then, the mold can be retreated with a new layer. This property enhances the ability of F-ASL treatments to be implemented in a whole repetitive and reliable patterning process and increases the mold's lifetime.

Despite these interesting properties, it has been widely noted and reported, mainly by research teams from academia, that even the best F-ASL is not very durable. Indeed, sticking problems between a treated mold and a UV-cured resist may appear after less than twenty imprints. This releasing default is clearly accompanied by an increase of the template's surface energy and a decrease of the fluorine surface concentration as will be detailed in the results presented in this chapter. With optimized conditions and using the *Molecular Imprint Inc.* process, a mean lifetime of the release layer of about 800 was reported[28] (i.e. 6 wafers in the used conditions). Although this last value represents a good durability for a treated stamp, its efficiency is still far from the requirements of the ITRS and can seriously impede the spread of UV-NIL as large volume nanopatterning technique.[126]

5.4 Fluorinated mold treatment-resist interactions

Since the last few years, several studies have aimed at determining the accurate mechanisms that are responsible for this premature degradation but their conclusions do not systematically converge.[125,127] Tada et al. supposed that the main cause limiting the lifetime of a treated mold surface is the mechanical interaction with the resist. In fact, when the mold is pressed on the resist, resist molecules may penetrate through the release layer, since the density of the release layer is relatively low, leading to the entanglement of ASL chains into the cured resist. So, when the mold is detached from the resist, the chains of ASL are broken by the resist.[125] However, outlines of numerous studies confirm a chemical reactivity between the F-ASL and the cured resist either with acrylate or vinyl ether formulations.[127] The species that are presumed to attack fluorinated molecules are free radicals or cationic charges generated during photopolymerization. However, there is no experimental procedure that can correlate these reactive species to the deterioration of the antisticking layer yet.

Other works have also highlighted the impact of the resist's formulation on the F-ASL degradation rate and mechanisms. In particular, the incorporation of crosslinkers or silicon containing components seems to have a clear impact on the adhesion between mold and cured resists.[128]

Even if some experimental trends are not fully understood (in particular the balance between chemical and mechanical degradation), it comes out that fluorinated release layers have a limited lifetime when imprinting conventional acrylate or vinyl-ether resists. The only criterion of low surface energy therefore is not enough to guarantee durable and effective antisticking behavior.

5.5 Resist-oriented antisticking strategies

Other strategies can be adopted to minimize the interaction between the UV-curable resist and the template surface, such as the modification of its formulation; two resist-oriented solutions are reported.

The first consists in adding fluorine-containing monomers in the UV curable mixture: it was demonstrated that hydrophobic properties of the UV cured resist are enhanced and allow an easier repetitive demolding.[95,129] Besides, the viscosity of the UV curable mixture is not

degraded because fluorine-containing monomers are available at viscosities as low as 10 mPa.s. Also, when associated with F-ASL template antisticking treatments, the use of fluorine rich resist seems to slow (but not eliminate) its degradation.[129]
The second possibility is the use of fluorinated surfactants in the resist composition. Surfactants are small molecules that will not participate to the polymer network and are able to move in the resist before curing.[130] According to this explorative work in the field of NIL, it seems that, to fully take advantages of their incorporation, surfactant migration from the resist to the resist / template interface has to be effective. This is possible only with low surface energy templates. Indeed, fluorinated surfactants are segregated at the resist / template interface only if these molecules have an affinity with the considered interface.[76] For the same reason, and when used in relatively small quantities, surfactants will not degrade the adhesion of the resist to the substrate.

6 Conclusion

At a lab scale, when taking care of the mold design, resist quantity and formulation, resist flow, environmental contamination and flatness issues, UV nanoimprint lithography is able to produce very high resolution features at quite high throughput and low cost potentially on any surface. Nevertheless, to go a step further in development and industrialization, some critical issues has to be considered like air inclusions, fast and uniform curing, mold inspection and repair, distance between imprinted dies and border imprinted dies in the step-and-repeat process. Some solutions exist but will need further development to be really effective. Also, one of the major problems is the sticking between the mold and cured resist which may lead to additional defects, mold contamination, mold abrasion and time-consuming mold cleaning and re-treatment. It is this issue that I will address in the next chapter. I will present experimental results performed using fluorinated antisticking layers. We will first focus on aspects concerning grafting and cleaning procedures of the fluorinated antisticking layer. Then, experimental results concerning its degradation as a function of imprint number and resist composition will be presented and discussed. Emphasis will be put on the precise measurement and understanding of this degradation and possible ways to reduce it.

Chapter II. Antisticking issues in nanoimprint lithography

1 Analysis of Fluorinated AntiSticking Layers (F-ASLs) before imprinting

In this section we will first describe the F-ASL deposition procedure as well as the characterization techniques used to access to physical, mechanical and chemical properties of the F-ASL. All the work presented in this section was performed before the imprinting step.

1.1 F-ASLs deposition procedure

For all the experiments presented in this PhD thesis we decided to apply F-ASLs on the mold surface by a liquid phase deposition technique. Contrarily to the vapor phase deposition technique, this technique has the advantage of simplicity and does not require any specific equipment (but is in practice not applicable to chloro-silane molecules as explained above). It aims at putting the F-ASL molecules on the fused silica surface under suitable conditions of temperature and humidity allowing a covalent bonding between the fluorinated molecule end groups and the silanol groups on the mold surface. In the case of *Optool DSX* molecules, the anchoring groups are methoxysilanes as illustrated in Figure II. 1.

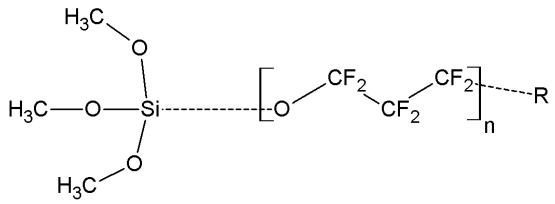


Figure II. 1: Chemical formula of *Optool DSX* (30<n<40). "R" radical and dashed bonds corresponds to very limited unknown groups.

Prior to the ASL deposition, molds are cleaned using a "CARO" solution (2:1 volume mixture of H_2SO_4 (96 %) and H_2O_2 (30 %)) for 15 min. This solution removes organic compounds from the surface and promotes the creation of –OH bond. Then, the used liquid phase deposition technique itself includes three steps as illustrated in Figure II. 2. The mold is first soaked in a low concentration *Optool DSX* solution (1 ‰ wt into perfluorohexane) during 1 minute. It is then placed in a water-saturated environment at 65°C for one hour before being rinsed in perfluorohexane during 10 minutes (to remove all excess of un-grafted fluorinated molecules). Finally, molds are dried with a dry nitrogen gun.

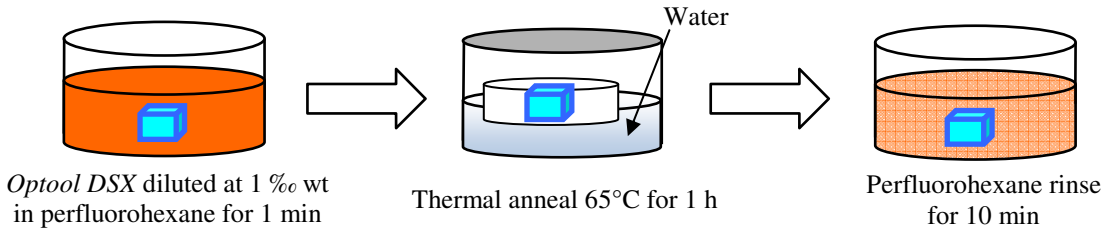


Figure II. 2: Illustration of fluorinated monolayer liquid phase deposition on the mold surface.

In the case of a virgin and perfectly clean fused silica surface, the grafting mechanism is supposed to occur as illustrated in the schemes of Figure II. 3. When the mold is placed in

presence of fluorosilane compounds, the hydrophilic anchoring head -Si(OCH_3)$_3$ comes spontaneously in contact with the water film present at the mold's surface (Figure II. 3 (a)). Water reacts with the precursor to form -Si-(OH)$_3$ silanol terminations (Figure II. 3 (b)). During the thermal annealing, the mobility of molecules into the water layer is increased which allows the formation of covalent Si-O-Si bonds between the molecules and the surface of the mold (Figure II. 3 (c)) and the condensation of first neighbors (Figure II. 3 (d)), leading to a 3D comb-like structure. This scheme is supposed to be valid also in the case of virgin silicon mold as silicon surface is naturally coated with a thin native silicon oxide film.

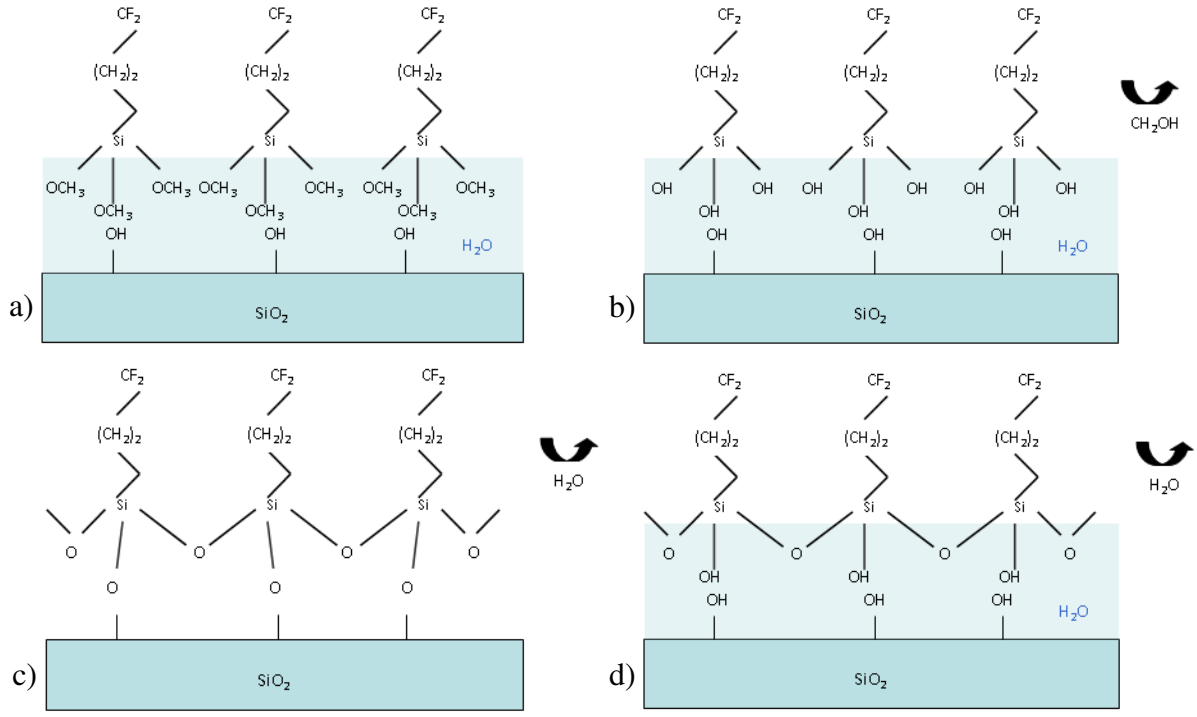


Figure II. 3: Grafting scheme of a fluorosilane monolayer. Several steps are supposed to occur during the process: (a) Physisorption, (b) Hydrolysis, (c) Covalent grafting to the substrate, (d) In-plane reticulation.

1.2 Fluorinated layers characterization techniques

After deposition, the so obtained anti-sticking layers have to be characterized. One needs to know their intrinsic properties and performances before starting their degradation analysis as a function of imprinting and resist parameters. Many characterization techniques are reported in the literature and can be classified into three groups:

- Morphological characterization tools: Atomic Force Microscope (AFM), Ellipsometry, X-ray reflectometry and Scanning Electron Microscopy (SEM).
- Adhesion characterization tools: In-situ demolding force measurement in the nanoimprint stepper, 4-point bend method, double cantilever crack method and, in some extend, AFM.
- Physico-chemical characterization tools: surface energy measurement by contact angle measurements, X-ray Photoelectron Spectroscopy (XPS), Fourier Transform InfraRed spectroscopy (FTIR) and Electron Spin Resonance (ESR).

I used almost all these characterization techniques during my work as will be detailed in the following sections.

1.3 X-ray Photoelectron Spectroscopy (XPS) details

To get an idea of the chemical composition of the *Optool DSX* layer, we had to select a suitable characterization tool. Also, we wanted to compare the grafting mechanism on silicon and on fused silica, before investigating if the substrate type could have an impact during the imprinting step. Optical absorption based methods (in visible and infra-red domains) were excluded because silicon and silica are not transparent in the same wavelength ranges. Moreover, the signal collected would be the result of two contributions: the fluorine layer one and the bulk substrate one. Additionally, we were looking for a non-destructive technique capable to inform us about chemical bonds present at the top surface (the first few nm) of the sample. X-Ray Photoelectron Spectroscopy[131] is the method of choice to fulfill these requirements.

The XPS tool used was the *Theta 300* spectrometer from *Thermo Electron Corporation* using a high resolution monochromatic Al Kα X-ray source (1486.6 eV photons). The X-ray spot, corresponding to the analyzed surface, has a diameter of 400 µm. After the acquisition of the global spectrum (reported in Figure II. 4), concentrations of C, F, Si and O atoms were systematically extracted from the C1s, F1s, Si2p and O1s core level energy regions respectively. Using a numerical fitting procedure, the energy spectra were fitted in order to extract the different binding contributions in the acquired energy regions. Each element concentration was then obtained by dividing calculated peak areas by the corresponding sensitivity factors (C1s: 1.0, F1s: 4.43, Si2p: 0.82, O1s: 2.93). Acquisition of the four relevant elements (C, F, Si and O) was necessary to have quantitative data on the surface composition. Nevertheless, the carbon, with its multiple chemical environments, gave us the most information on the grafted molecules. Consequently, carbon spectra were mostly considered.

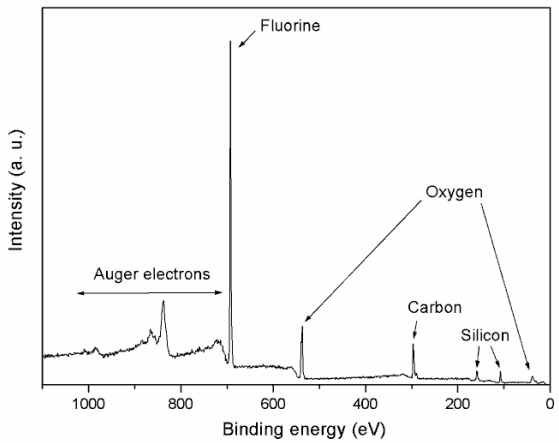


Figure II. 4: XPS spectra of an *Optool DSX* layer grafted on a fused silica surface. All chemical elements of the F-ASL are identified.

In the case of insulating samples (like fused silica transparent molds), the release of photoelectrons gives rise to a positively charged zone around the X-rays spot and constitutes an energetic barrier for subsequently released photoelectrons. As a consequence, their kinetic energy is lowered and shifted by a value ranging between a few eV up to 100 eV. An electron gun was used to compensate this charge effect. This took more or less time (between 20 min up to a few hours) depending mainly on the contact between the analyzed sample and its holder. Generally, charge compensation on insulating samples has to be carried out during a few hours before starting spectra acquisition. As a consequence, we pointed out that during such a long acquisition time, fluorinated molecules grafted on the mold's surface were affected by the XPS measurement conditions and more precisely by the incident X-ray beam (We excluded other possible causes like the electron charge compensation or the ultra-high

vacuum). This effect is illustrated in Figure II. 5 where Carbon 1s spectra of *Optool DSX* grafted on both fused silica and silicon are reported after different X-ray exposure times. A great decrease of the peaks between 290 and 295 eV is observed between the first (t_0) and the last acquisition (t_0 + 3 hours), corresponding to the disappearance of fluorinated compounds from the mold's surface.

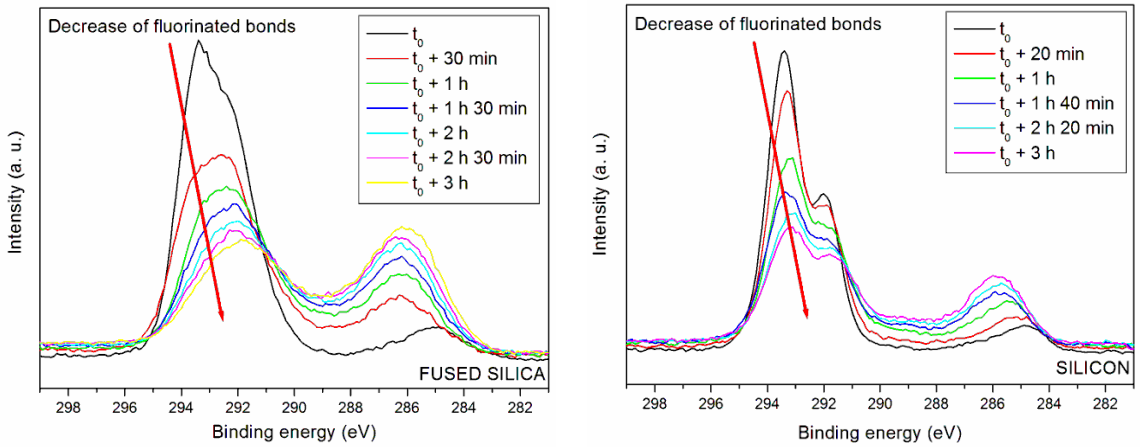


Figure II. 5: Carbon 1s spectra evolution of *Optool DSX* grafted on fused silica (left) and silicon (right) after different X-ray exposure times.

This discovery was of major importance especially when we keep in mind that XPS analysis was chosen to be our investigation tool to follow up F-ASL degradation. At that stage, it became legitimate to have a doubt about the validity of literature reported results involving XPS analysis and treating of the antisticking layer degradation on fused silica molds.
To avoid this experimental error during spectra acquisition, the charge compensation was conducted on a large surface (3 mm diameter spot) compared to the X-ray beam spot (400µm). Afterward, when the complete charge compensation is achieved, the mold holder was slightly shifted and the spectra acquired from a non damaged area located at the vicinity of the initial X-rays beam spot.

1.4 *Optool DSX* characteristics after deposition

1.4.a Layer thickness and surface energy measurements

According to the chemical formula of *Optool DSX* (see Figure II. 1) and by calculating the length of one molecule, it results that the chain length of *Optool DSX* is about 15 nm. Using spectroscopic ellipsometry, the thickness of the *Optool DSX* treatment on a silicon surface was measured to be in the range of 2.5 to 3.5 nm. The difference observed between the theoretical chain length and the thickness of the deposited *Optool DSX* layer suggests that the chains of *Optool DSX* are not self-organized on the surface of the mold like a self-assembled monolayer but that molecules lie down on the surface. These ellipsometry measurement where performed on silicon because there is only a low optical index contrast between fused silica and the *Optool DSX* layer and this does not allow to measure the thickness of such thin layers with a sufficiently low error. Equipment used was a *Jobin Yvon UVISEL* ellipsometer on a 200 - 800 nm wavelength range using the "new amorphous" model of the *Jobin Yvon Delta Psi 2* software.
The surface free energy of the as-deposited *Optool DSX* layer on a fused silica or silicon surfaces was measured with a drop shape analyzing system (*DSA 100* from *Krüss*) and using the *Owens-Wendt* model. Obtained results were in the range of 9.5 to 11 mJ/m² and the mean value of the water contact angle was 113°. For each sample, three liquid were used (water,

diiodomethane and diethyleneglycol) and 5 or more measurement points were taken for each liquid.

1.4.b Surface chemistry results by XPS

With the modified XPS acquisition procedure explained above, we analyzed the surface of both a fused silica and a silicon mold treated with *Optool DSX*. Obtained Carbon 1s XPS spectra are reported on Figure II. 6.

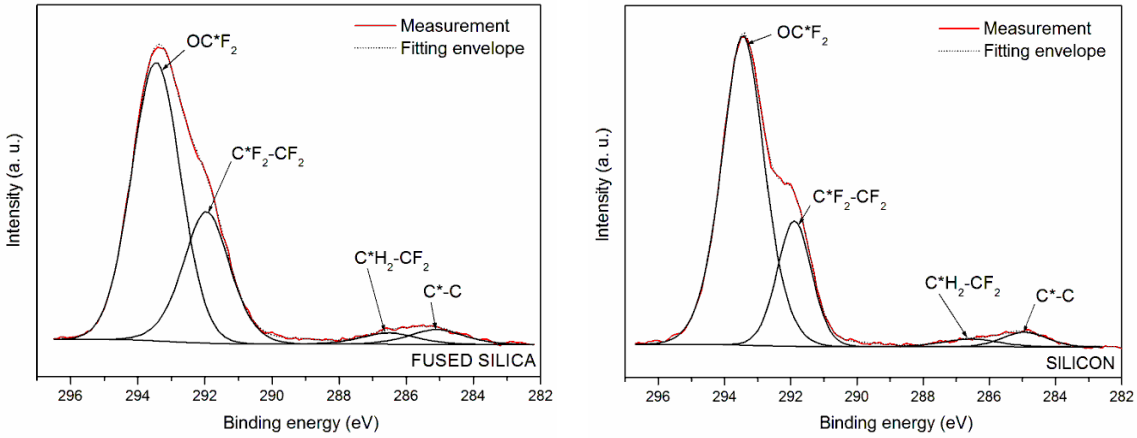


Figure II. 6: Carbon 1s XPS spectra of *Optool DSX* grafted on fused silica (left) and silicon (right), and the associated chemical bond contributions (black curves)

The measurement resolution is better on silicon than on silica due to the fact that the charges are evacuated more efficiently in this case. This resolution is estimated to be below 1 eV on silicon and below 2 eV on silica. Errors on the peak positions were estimated to be below 0.4 eV on silicon and below 0.7 eV on silica, depending strongly on the peak intensity and width.
All binding energy peaks of F-ASL molecules could be identified for both substrates. Values are reported in Table II. 1 along with corresponding binding energy values from the NIST (National Institute of Standards and Technology).

	Binding energy value (eV) as listed by NIST	Our results (eV) on silicon	Our results (eV) on fused silica
C*-C	285	285	285
C^*H_2-CF_2	286.3	286.4	286.5
C^*F_2-CF_2	292.6	291.9	292.0
O-C^*F_2	293.9	293.4	293.5

Table II. 1: Peak identification for a deposited *Optool DSX* layer on silicon and fused silica substrates compared with NIST references.

Peaks around 292 eV are related to the presence of fluorocarbon bonds. The largest contributions comes from OC^*F_2 and C^*F_2-C^*F_2 bonds, in accordance with the chemical formula in Figure II. 1. The peak around 285 eV is attributed to C-C bonds coming from the molecule it-self and also from atmospheric pollutants adsorbed on the surface; the one around 287 eV is attributed to C^*H_2-CF_2 bonds present in the *Optool DSX* molecule.
These spectra prove the presence of well-anchored molecules at the surface of the two types of substrates (molds) and the efficiency of the F-ASL deposition procedure.

2 Analysis of the F-ASL degradation during imprinting

In this part, we investigate the *Optool DSX* mold treatment degradation when used in an imprint process. The photocurable resist considered here is a simple mixture of a diacrylate monomer (*Laromer 8765* from *BASF*) with 1 wt % of a photo-initiator (*Irgacure 379* from *Ciba*).

2.1 Introduction

Thanks to the work previously described, we were able, at this stage, to use the XPS as an accurate and reliable tool to monitor the mold surface chemistry (for both silicon and fused silica cases) as a function of the imprints number and conditions. Although the topics of our research is dedicated to the UV-NIL materials and process, we carried out the F-ASL degradation study by taking into account both thermal and UV-NIL configurations (i.e. with fused silica and silicon molds, as well as with UV-NIL resist and thermoplastic polymers). This strategy is motivated by the fact that the results reported in literature on the durability of F-ASL in thermal NIL suffer some discrepancies and are not always conducted under well identified experimental conditions. For instance, when Yamada et al.[132] have investigated the evolution of the antisticking properties of unpatterned silicon molds treated with a F-ASL and imprinted it into thin films of a commercial polymer heated at 150°C, they did not notice any significant degradation of the release properties and decided to stop their analysis at 180 imprints. On the other hand, Hirai et al.[133] pushed this investigation a step further when they analysed, using a home developed de-molding apparatus, the degradation of release properties using patterned molds with various feature shapes. By comparing the relative contribution of adhesion and friction forces occurring when a silicon mold is being separated from its resist replica, they found out that friction forces are predominant and concluded therefore that the surface roughness of the mold features has to be minimized.

Even though those studies were very interesting from a fundamental point of view, their outlook was never considered as a threaten for the expansion of thermal NIL techniques because the majority of the early envisioned thermal NIL applications were small and medium series production that did not necessarily require a high throughput and can cope with regular cleaning and anti-sticking treatment of silicon molds. With the advent of the UV-NIL techniques at the last 90's, the context has totally changed, and worsened making necessary to perform more details studies on this topics.

After an investigation of the mold treatment degradation during a standard imprinting process, a comparative approach was conducted to investigate the impact on the F-ASL degradation of the following parameters:

- the direct UV exposure
- the mold nature and history
- the resist's free radicals
- the UV intensity and dose
- the type of process (thermal-NIL vs. UV-NIL)

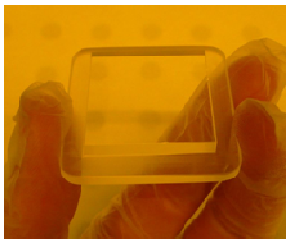
2.2 F-ASL aging in a standard UV-NIL process

A standard UV-NIL process was performed with our 1st generation *EVG770* step and repeat imprinting equipment with unpatterned fused silica molds. A picture of this tool, along with one of the mold shape used and one of an imprinted wafer, is reported in Figure II. 7.

The resist used has a viscosity of 740 mPa.s at room-temperature. To obtain the desired thickness after spin-coating on a wafer, ethyl-L-lactate may be used as a solvent. Here, 8 g of resist is diluted in 92 g of ethyl-L-lactate in order to obtain a 200 nm thick resist layer after spin-coating at 1850 rpm for 30 s. The UV exposure lamp used is a mercury lamp emitting

from 350 to 410 nm in wavelength at a power density of 11 mW/cm^2 at the mold / resist interface. The exposure time was set to 1 second which guaranties a conversion ratio of 75% for this acrylate-based resist.[83]





Mold:
Printing area: 25x25 mm²
Step height: 3 mm
Total thickness: 6.35 mm
Total area: 35x35 mm²

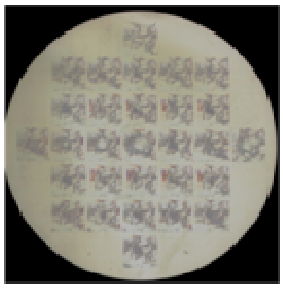


Figure II. 7: Pictures of the 1st generation *EVG770* step and repeat imprinting system (left), of the mold shape used in this tool (center) and of an imprinted 200 mm wafer (right).

Carbon 1s XPS spectra of the surface of an *Optool DSX* treated fused silica mold are reported in Figure II. 8 (left) before imprinting, after 1 imprint and after 10 imprints. C*-C bonds are observed at low binding energies coming from the treatment but also from unavoidable carbonate atmospheric contamination which lead to a very thin C-C type layer adsorbed at the extreme surface of the sample. At higher binding energies, peaks related to fluorine (mainly OC*F_2 and C*F_2 bonds) are observed. By increasing the number of imprints, their intensity is decreasing and a larger decrease is observed after the first imprint than between the first and 10th imprint. Furthermore, no real change in the peak contributions (i.e. in the spectral shape) could be identified. This seems to indicate that, in a first phase, fluorinated molecules are removed from the mold's surface but not degraded ("rinsing" effect). This is confirmed by the measurement of the Carbon 1s spectra of the resist's surface reported in Figure II. 8 (right). OC*F_2 and C*F_2 groups from *Optool DSX* molecules are visualized on the resist's surface along with groups attributed to the resist (C*-C, C*-O and C*=O).

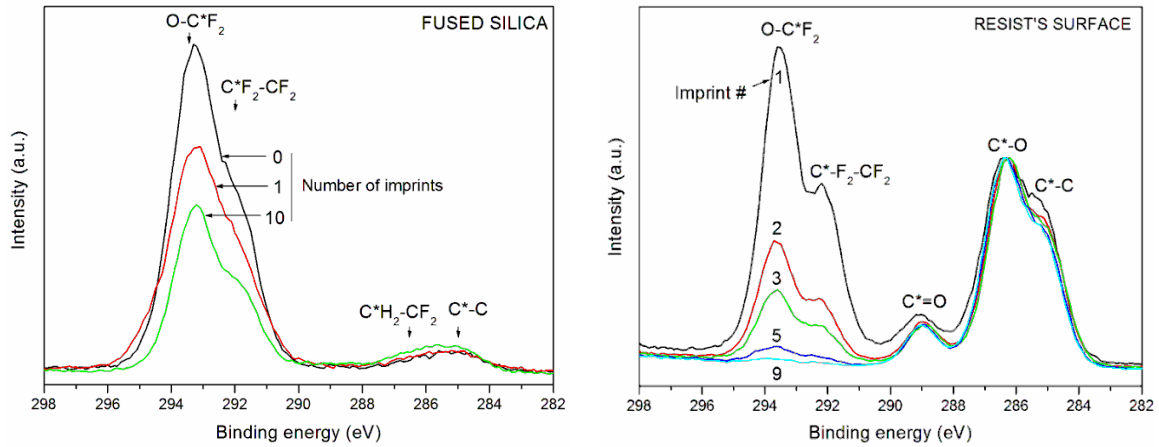


Figure II. 8: Carbon 1s XPS spectra of <u>right:</u> a fused silica mold treated with *Optool DSX* before imprint (black curve), after 1 imprint (red curve) and after 10 imprints (green curve); <u>left:</u> the resist's surface after the first, the second, the third, the fifth and the ninth imprints with an *Optool DSX* treated fused silica mold. Arrows indicates the positions of the different bonding contributions.

After 5 imprints, almost no more fluorine is observed on the resist's surface whereas the fluorinated treatment continue to be degraded (no more fluorine could be detected on the stamp after 75 imprints with the used conditions). This indicates that the first loss of fluorine detected after initial imprints is the removal of ungrafted *Optool DSX* molecules that were present on the stamp's surface. Then, antisticking molecules still disappear from the mold's surface but are no more transferred to the resist's surface. This means that, at this stage, molecules are degraded in shorter volatile species.
The corresponding free surface energy evolution of the stamp's surface is reported in Figure II. 9. We can observe a continuous and regular increase of the free surface energy during the first 40 imprints until it reach the value of an untreated fused silica surface.

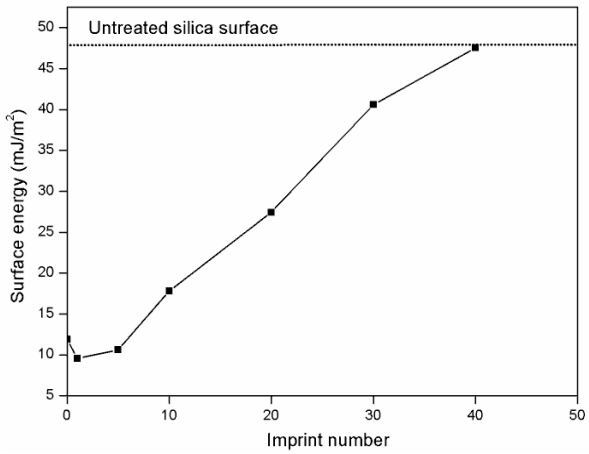


Figure II. 9: Surface energy of an *Optool DSX* treated fused silica mold as a function of the number of imprints.

In conclusion, we observe a very rapid degradation of the release properties of a fused silica surface when used in a standard imprinting process. A good correlation exists between the disappearance of fluorine from the mold's surface observed by XPS and the increase of the free surface energy. Nevertheless, due to the length of the *Optool DSX* molecules, we were not able to distinguish a change in the surface chemistry during the degradation process (as observed by XPS) that could inform us on the real degradation mechanism that is taking place. This will be possible with shorter fluorinated chains as detailed in a following section.

2.3 Direct impact of UV exposure

Published literature has confirmed that grafted *Optool DSX* molecules are no degraded by temperatures up to 500°C.[134] Giving that almost all thermoplastics are imprinted at a temperature ranging between 100°C and 300°C, it comes out that the thermal budget provided during thermal NIL is not harmful for the *Optool DSX* F-ASL. In UV-NIL, the imprints are conducted at room temperature. However, the UV exposure may bring certain amount of energy that may deteriorate the F-ASL chains. To investigate the hypothesis of a direct degradation of *Optool DSX* molecules by exposure to UV, 3 fused silica molds were treated with *Optool DSX*, put in contact with an uncoated silicon substrate and exposed for a variable time in the imprint stepper tool. Surface energies were then measured. Results are reported in Table II. 2. An exposure during 1000 s corresponds to 1000 imprinted dies in the standard UV-NIL conditions as described in the previous paragraph. Looking at the surface energy evolution, we can unequivocally say that UV exposure doesn't affect at all the antiadhesive properties of this F-ASL.

Stamp	UV expo. time [s]	Contact angle with [°] Water	Diethylene-glycol	Di-iodomethane	Surface energy [mJ/m^2]
N°1	0	114.8	99.5	98.5	9.34
N°2	1000	114.2	100.3	97.7	9.41
N°3	2000	114.2	100.3	97.7	9.41

Table II. 2: Surface energy evolution of an *Optool DSX* treated fused silica surface when exposed to UV irradiation for various durations.

2.4 Impact of the mold nature and history

In this part, we investigate the possible impact of parameters like the mold nature (fused silica or silicon) and cleaning procedures on the durability of the antisticking layer.

2.4.a Influence of the mold material

According to XPS data presented in Chapter II.1.4, *Optool DSX* molecules seams to bond similarly to silicon and to silica surfaces. Nevertheless, the durability of the release properties might be different for the two surfaces due, for example, do the electrical conductivity difference between the two materials. Indeed, in practice, we observe important electrostatic induced phenomena (attractive forces or contactless resist flow) between a fused silica mold and a resist coated silicon substrate, which might indicate that the F-ASL degradation might be correlated to electrostatic effects.
The experimental procedure followed here is a manual imprint of a resist drop (the same as in the stepper) with both silicon and fused silica molds of dimensions in the order of 2*2 cm^2. A schematic of these experiments is given in Figure II. 10. In the case of a silicon mold, fused silica substrates are used to be able to expose the UV-sensitive resist trough the substrate, whereas silicon substrate are used in the case of fused silica molds. The exposure lamp, intensity and dose are the same as in the step and repeat system. Imprints were run manually, putting firstly into contact the mold and substrate, then waiting until the resist wetted completely the mold surface and finally exposing it to UV radiations. In this way, we ensured a reproducible full contact area between resist and mold surfaces.

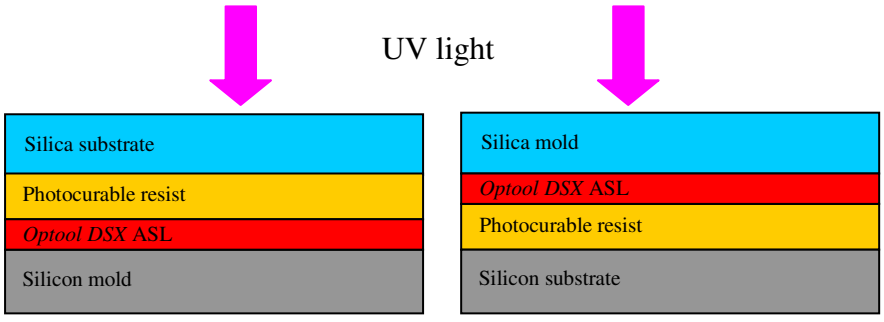


Figure II. 10: Schematic conditions for the comparative study between silicon and fused silica release properties degradation.

After imprinting and manual demolding, mold surfaces were first characterized by their water contact angle (10 measured drops per sample). Average results are listed in Table II. 3 and show that the contact angle evolution was exactly the same on both surfaces.

Mold nature	Freshly treated, no imprint	After 1 UV-NIL imprint	After 10 UV-NIL imprints
Fused silica	113.2°	112.4°	110.5°
Silicon	113°	112.2°	110.3°

Table II. 3: Evolution of average water contact angle value as a function of the UV-NIL imprints on molds of different nature treated with *Optool DSX*.

Mold's surfaces are then investigated by XPS. To compare the degradation occurring on silicon and fused silica, we calculated the ratio of the CF bonds contribution (fluorine environment) over the CC bonds contribution (carbonate environment). Table II. 4 summarize the values obtained before imprinting, after 1 and after 10 imprints. Although a small difference is found on newly treated molds, CF / CC values after one and 10 UV-NIL imprints were found to be very similar for both molds, which finally makes possible to state that the conductivity of the mold seems not to impact the F-ASL degradation. This result confirms also that the ASL grafting is very similar on silicon and silica surfaces, well in accordance with the literature, where the concentration of -OH sites present on an oxidized silicon surface is shown not to depend on the nature of this oxide (native oxide on a silicon surface or fused silica).[135]

Mold	No imprint	After 1 imprint	After 10 imprints
Fused silica	11.9	9.9	4.8
Silicon	13	9.4	4.8

Table II. 4: Evolution of the XPS measured CF / CC ratio on the surface of fused silica and silicon molds treated with an *Optool DSX* F-ASL as a function of UV-NIL imprints number.

2.4.b Influence of the pre-cleaning procedure

Once demonstrated that the grafting mechanism and the ASL degradation are not dependant on the nature of the mold, we decided to analyze the possible influence of other experimental parameters. Here, we focus on the mold's surface preparation before the F-ASL application and on its possible impact on the final release performance.

We performed two types of chemical wet cleaning before applying the F-ASL. The standard one, as presented in Chapter II. 1.1, is the wet cleaning with a CARO solution for 15 min. The second cleaning procedure is also a very common process in the microelectronics industry for wafer cleaning and resists stripping. It consist of the same CARO treatment, followed by a "SC1" bath composed of ammonium hydroxide, hydrogen peroxide and deionized water in 1:1:5 ratio, heated up to 70°C and for 15 min. While the CARO treatment is usually conducted to remove all organic residues from a surface, the SC1 treatment is known to increase the silicon surface hydrophilicity by growing ultrathin silicon dioxide layer on its top.

The impact on the *Optool DSX* F-ASL degradation deposed on such pre-cleaned samples was tested twice for each treatment. The evolution of the mold's surface energy is monitored by contact angle measurements as a function of imprint number as reported in Figure II. 11. The imprinting parameters were the same already presented in the previous paragraph, i.e. manual imprints with small samples, but using always exposure conditions that are the same as on the stepper.

It comes out that the surface energy of molds pre-cleaned only with the CARO solution remains lower after the same number of imprints compared to molds pre-cleaned with both a CARO and a SC1 solution. This result might be explained by the fact that the SC1 cleaning

procedure is less effective to produce –OH bonds on a surface than a CARO solution, resulting in a lower F-ASL molecule concentration grafted on the surface. According to this result we continued applying only a CARO treatment prior to the first F-ASL deposition.

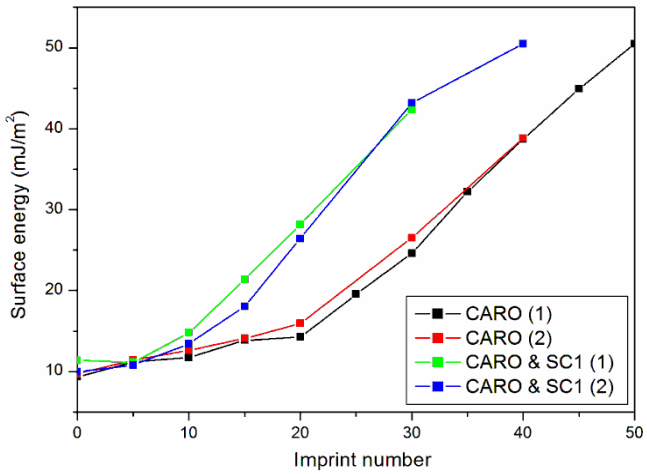


Figure II. 11: Surface energy evolution as a function of imprint number for *Optool DSX* treated fused silica molds previously cleaned following two different procedures. Both experiments where repeated twice.

2.4.c Mold cleaning and retreatment

In the previous experiments, I investigated the influence of the pre-cleaning of molds with new fused silica surfaces. But, in my experiments, I observed that, in the case were I was cleaning an re-treating used molds, the cleaning procedure was not straightforward and that it had an influence on the ASL aging. This is the reason why we investigate here the cleaning mechanism to be used to remove the *Optool DSX* layer from the mold's surface. Also, we investigate the durability of the *Optool DSX* layer in the imprint process as a function of a previous mold surface cleaning.

The classical cleaning procedure applied in the lab on already used silicon molds in the case of thermal NIL consists in the following: soaking the silicon mold in a CARO solution as already described and then exposing it to an oxygen plasma in a standard plasma asher (Branson IPC 33, 2 min, 750 W, 250 °C, 700 mtorr, 800 sccm) in order to remove all possible traces of both polymers and F-ASL residues. Then, a new F-ASL can be applied according to the procedure described earlier in Chapter II.1.1. This sequence is known to work properly for silicon molds. We applied this cleaning procedure to fused silica and silicon molds, newly treated with *Optool DSX*. Cleaned surfaces were then analyzed by XPS. Surprisingly, fluorinated molecules are still identified after cleaning in the case of fused silica molds (Figure II. 12, left). Indeed, there is almost no change in the Carbon 1s XPS spectra after the cleaning. On the other hand, in the case of silicon molds, almost all fluorinated species are removed during the cleaning procedure (Figure II. 12, right). The amount of fluorine decreases from 57 % ± 5 down to 53 % ± 5 only on silica, whereas it decreases from 55 % ± 5 down to 6 % ± 5 on silicon. The observed differences between the two substrate types are attributed to the insulating nature of the fused silica. Indeed, a local charge accumulation will appear at the surface of fused silica stamps decreasing the plasma efficiency.

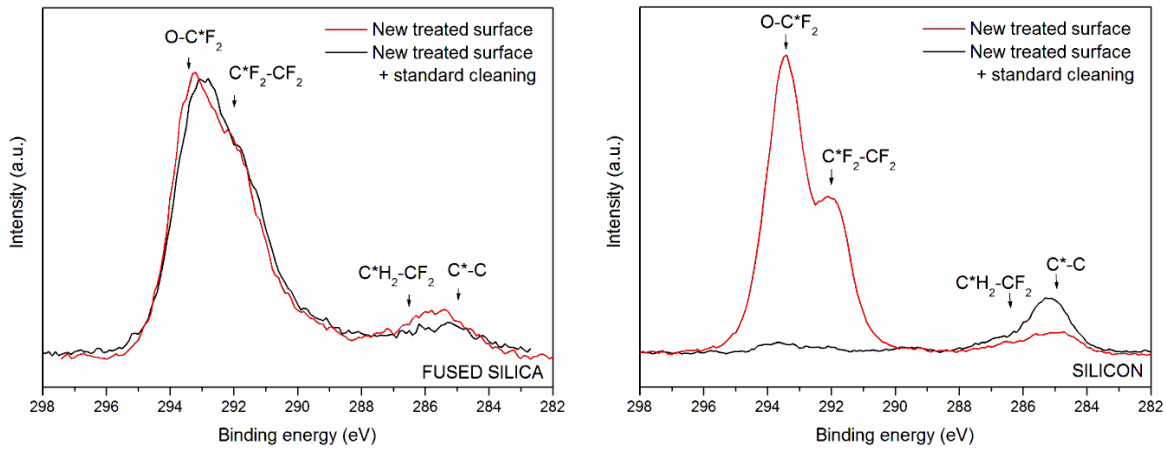


Figure II. 12: Comparison of the cleaning efficiency of the standard cleaning process for both silica (left) and silicon molds (right) previously treated with an Optool DSX layer. Red curves: before cleaning; black curves: after cleaning.

To try to solve this issue for fused silica molds, we elaborated a new cleaning procedure including an Argon ion bombardment during the oxygen plasma cleaning step. Then, as illustrated in Figure II. 13, the removal of the F-ASL was proven to be much more efficient. Nevertheless, this Ar bombardment was not tested on a mold with nanometric patterns and we are not sure if this treatment erodes or not the topography on the mold. To avoid this risk, we showed that a much longer pure oxygen plasma (10 min instead of 2 min) is able to achieve almost the same result.

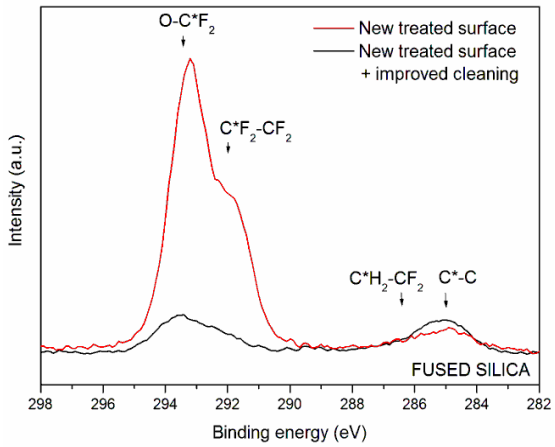


Figure II. 13: Cleaning efficiency of the modified cleaning process including Ar bombardment for silica molds previously treated with an Optool DSX layer. Red curve: before cleaning; black curve: after cleaning.

To assess the importance of such an improved plasma cleaning procedure, we compared the efficiency of the re-treatment in the UV-NIL process. A newly treated mold and a mold treated, used in a UV-NIL process, cleaned with the standard CARO / O_2 plasma and re-treated, were used in the same imprinting conditions (as described before). Just after the treatment, no differences are observed by XPS between these two molds. Surface chemistries of the templates were then recorded after 10 imprints, as illustrated in Figure II. 14. Here we can see that the fluorinated antisticking layer of the newly treated sample (top curves) is not affected extensively after 10 imprints. The shape of the fluorinated bonds is almost unchanged compared to a virgin one. On the other hand, for the sample cleaned using the standard O_2 plasma (bottom curves on Figure II. 14), a premature degradation is observed: the peak related to OC*F_2 bonds is drastically reduced. This can be explained by the fact that the poor

cleaning has not removed all the siloxane groups between the fluorinated part of the molecules and the substrate. Therefore, when the stamp is re-treated, new F-ASL molecules can't be linked to the substrate because the remaining parts of F-ASL molecules avoid all other molecules to be anchored. On the other hand, no difference could be observed by XPS between a newly treated mold and an efficiently cleaned and re-treated mold, indicating that the recycling procedure adopted is fully efficient.

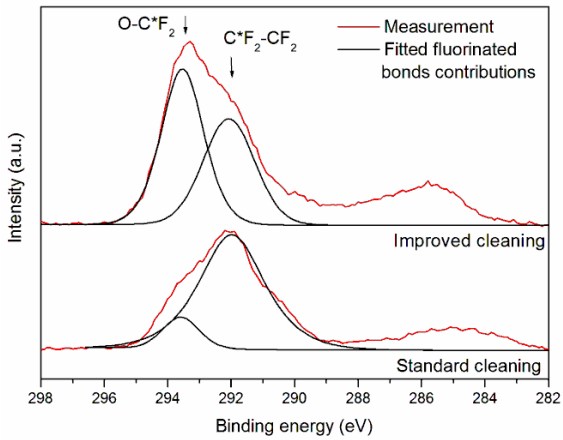


Figure II. 14: *Optool DSX* treatment after 10 imprints with a newly treated fused silica mold (top, black curves) and after 10 imprints with a mold cleaned with a standard O_2 plasma and re-treated (bottom, grey curves).

2.5 Impact of the resist's free radicals

Several research groups addressed the underlying origin of the ASL degradation, but their conclusions were not convergent and their experimental conditions are not always comparable. In their work Tada *et al.*[125] used XPS and X-ray reflectivity to monitor the thickness, density, and chemical composition of a fluorinated antisticking layer grafted on a silicon stamp as a function of the UV-NIL experimental conditions. They did not point out any noticeable effect of UV radiation neither of photoinitiator free radicals on the chemical and structural properties of the F-ASL. Therefore, they concluded that the only cause of the fluorinated layer degradation is the mechanical contact with the resist. This assumption is in contradiction with the exhaustive work of Houle *et al.*[128] who confirmed that a F-ASL applied to a fused silica template is rapidly and easily degraded when used for UV-NIL patterning. Indeed, by carrying out this study with three types of UV-curable resist chemistries (acrylates, methacrylates, and vinyl ethers), they assumed a chemical reactivity of the UV-curable resist system toward the F-ASL. However, the accurate nature of involved chemical reactions is not experimentally determined.

Our approach was to find out a characterization technique able to quantity the chemical reaction intensity occurring at the mold / resist interface during the UV exposure. For the first time, we propose to use Electron Spin Resonance (ESR) on this kind of systems. Thanks to its sensitivity to unpaired electrons, it can be used to characterize and quantify free radical species formed by UV exposure in free radical polymerization systems.

The used ESR experimental setup (belonging to the *INAC-SPrAM* laboratory in the *CEA-Grenoble* center) requires the analyzed matter to be sealed inside few millimeters-diameter cylindrical silica tubes. Therefore, instead of bulk silica stamps, which would be hardly introducible into thin glass tubes, spherical fused silica beads, with a granulometry in the range of 60 to 200 µm (*Geduran Si* from *Merck*) were used to simulate the reactive system (i.e., the mold surface treated with F-ASL brought into contact with the UV-curable resist). Here, a mixture of resist and silica beads is introduced in the ESR tubes, as indicated in Figure

II. 15. Tubes were loaded with always the same resist / beads ratio (60 wt % of beads and 40 wt % of resist) and with sufficient material to completely fill the ESR cavity in order to ensure comparative analysis between the investigated samples. They were prepared in a glove box under argon atmosphere in order to prevent oxygen inclusion into the mixture which would, afterwards, inhibit the free radical polymerization process. Silica beads were treated with *Optool DSX*, following the same procedure adopted for the molds, as described in § 1.1 of this chapter.

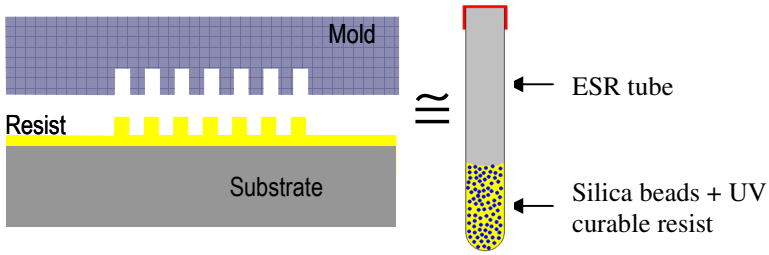


Figure II. 15: Schematic illustration of an ESR tube filled with fused silica beads and resist to reproduce the mold / resist interaction of a UV NIL process.

Free radicals of the UV-curable resist were visualized by ESR with the following parameters. The *X*-band (9 GHz) ESR spectrum were recorded at room temperature with an *EMX Bruker* spectrometer equipped with a rectangular ER41005DR double TE 104 cavity. The microwave irradiation power (0.5 mW), magnetic field modulation amplitude (0.5 mT), and frequency (100 kHz) were set to avoid signal saturation and kept constant.
The UV source and the photocurable formulation were the same already presented in this section. A dedicated illumination system (illustrated in Figure II. 16) was used to make sure that the samples were irradiated in a reproducible way and to try to have a comparable exposure dose as in the stepper equipment (i.e. 11 mJ/cm^2 in the plane of the tube). It consists in a dark plastic block with two holes and an internal channel linking the holes. The first hole hosted the filled ESR tube, while the second one the fiber connected to the UV lamp.

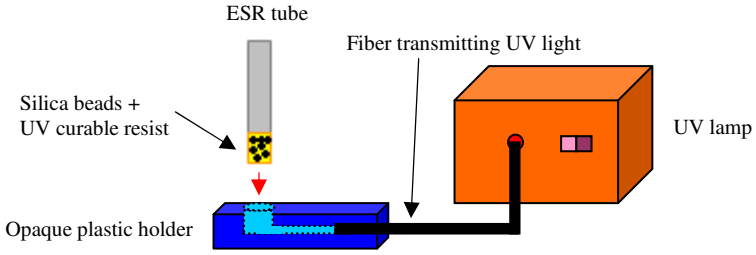


Figure II. 16: Schematic illustration of the illumination system adopted during UV irradiation of ESR tubes before ESR spectra acquisitions.

All the samples were first analyzed in the dark to verify that no free radicals are present in the system before exposure (green curve in Figure II. 17). Then, samples were irradiated during 1 second and analyzed by ESR. Time needed for the spectrum acquisition was about 1 min and it was not possible to visualize, under the above described conditions, the ESR signal in real time during UV exposure. Consequently, the observed free radicals are those with a sufficiently long lifetime, i.e., those trapped into the vitrified polymer matrix.

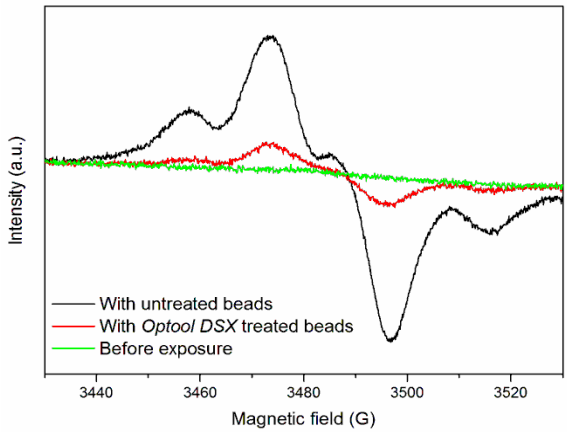


Figure II. 17: Typical flat ESR spectrum before irradiation (green curve), ESR spectrum of resist containing micrometric untreated silica beads after 1s UV irradiation (red curve) and of resist containing micrometric *Optool DSX* treated silica beads after 1s UV irradiation (black curve).

The recorded ESR spectra after irradiation are shown on Figure II. 17 in the case of a resist mixed with untreated beads (black curve) and in the case of *Optool DSX* treated beads (red curve). Three resonance peaks, occurring respectively at 3457, 3474, and 3485 G, were clearly detected and are attributed to ester acrylate end-groups,[136] i.e. to free radicals of the polymer chains of the resist. In the case of treated beads, a decrease of about 77 % of the radical concentration is observed in comparison with the untreated beads (This ratio is calculated from the relative height of the highest peak at 3474 G as there is no apparent modification in the signal shape.). This drastic decrease was therefore attributed to a chemical reaction between the grafted fluorinated molecules and the resist free radicals, consuming them. Consequently, ESR experiments show that resist radicals created during photopolymerization had an interaction with *Optool DSX* and should play an important role in the F-ASL degradation during the UV-NIL process.
When beads are present in the analyzed samples, a significant and reproducible increase in the signal is observed compared to the resist alone, as listed in Table II. 5. This phenomenon can be explained by the free radicals confinement effect induced by the beads. Indeed, more free radical species are observed in this case because they are localized in small areas between the beads and their ability to recombine is decreased.

Sample composition	ESR intensity after 1s UV irradiation (a.u.)
Pure UV-curable resist	2800
Resist+ untreated silica beads	20250
Resist+ *Optool DSX* treated silica beads	4700

Table II. 5: ESR signal peak height (arbitrary units) at 3474 Gauss after 1s UV irradiation for pure resist, resist mixed with untreated beads and resist mixed with *Optool DSX* treated beads.

Finally, by using ESR spectroscopy, we demonstrated for the first time that it is possible to quantify the chemical interaction that exists between fluorinated mold treatments and resist's free radical in the UV-NIL process. Then, ESR can be used to choose F-ASL – resist couples presenting the lowest interaction.

2.6 Impact of the UV intensity and dose

Until now, we used always the same resist and tried to be in the more comparable UV exposure conditions for all the conducted experiments. Here, we will investigate the influence of the reduction of the UV exposure intensity on the F-ASL degradation. 200 mm diameter

fused silica molds were imprinted in a thin UV-curable resist film coated on 200 mm diameter silicon wafers. The contact between the two wafers is performed under vacuum, at room temperature, with an imprint force of 10 kN during 3 min in an *EVG 520* imprinting tool (depicted in Figure II. 18, left). UV exposure was performed out of the tool, using an opaque plastic box (as indicated in Figure II. 18, right) on the full wafer with an intensity of 0.4 mJ/cm^2 for 360 s (corresponding to a dose of 144 mJ/cm^2). The UV source was the same already presented in the paragraph 2.4.a of this chapter. Previously used exposure conditions where an intensity of 11 mJ/cm^2 for 1 s (corresponding to a dose of 11 mJ/cm^2).

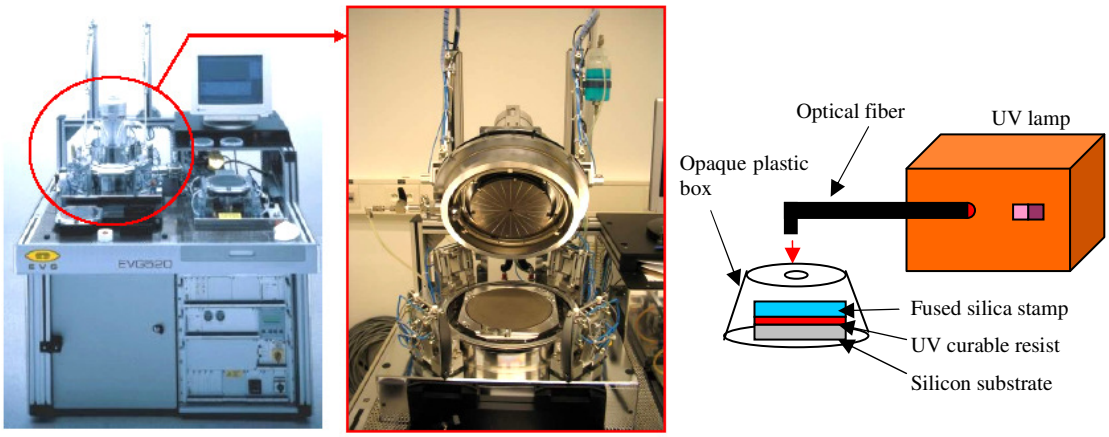


Figure II. 18: EVG 520 imprinting tool (left) and schematic illumination system adopted to cure the mold / resist stack after assembly in the EVG 520 (right).

After photo-polymerization, mold and substrate are separated manually by inserting a thin blade between the two wafers. The evolution of the mold's surface free energy is monitored by contact angle measurements after several imprints. Results are presented in Figure II. 19. We can observe that the UV exposure conditions have a large impact on the mold treatment aging. For the lower UV intensity (but a much larger dose), the degradation starts later than in the standard case. Nevertheless, when started, the degradation rate seems to be the same. This phenomenon might be explained by the fact that a lower excess of free radicals are created in the case of the lower intensity exposure, leading to a reduced reaction with the *Optool DSX* molecules. Also, another explanation is that the resist's mechanical properties are different in both cases, inducing a different mechanical stress / degradation on the treated surface. This kind of mechanical aspects will be investigated later in this chapter.

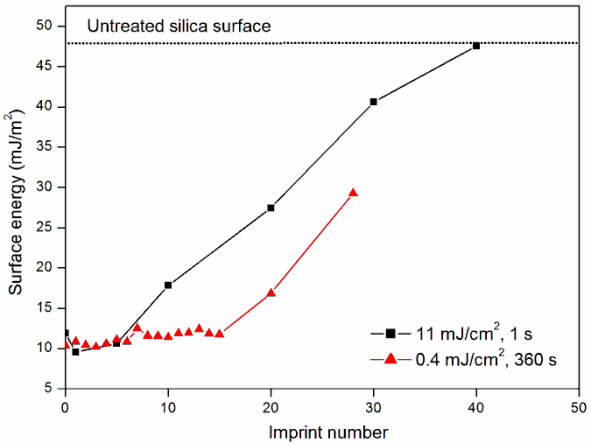


Figure II. 19: Evolution of the surface energy of an *Optool DSX* treated 200 mm diameter fused silica mold after several UV-NIL imprints for two different exposure conditions.

2.7 Conclusion

In conclusion, in this section, we have investigated the degradation of an *Optool DSX* antisticking layer when imprinted in a simple diacrylate resist. With our standard UV-NIL process, we observe a very fast degradation of this layer, with a maximal number of imprints in the order of 40. This degradation might be due to the chemical interaction that exists between the mold treatment and the resist's free radicals, as evidenced for the first time by ESR. We showed also that this fluorinated treatment is not subject to a direct degradation under the UV light in the used conditions and that it is grafted equivalently to silicon or fused silica. Also, care has to be taken during the pre-cleaning, the cleaning and the re-treatment of molds in order to have an efficient grafting. Finally, we observed an influence of the UV intensity on the treatment degradation that might be explained by a reduced chemical interaction (less free radicals are created) as well as a reduced mechanical interaction (due to different resit's mechanical properties).

3 Evaluation of other F-ASLs

Once evaluated the impact of several parameters on the *Optool DSX* treatment aging, we decided to test two other fluorine anti-adhesive treatments presenting a different chemical structure but identical grafting groups. The first one was *Fluorolink® S10*, exhibiting two anchoring end groups and a perfluoropolyether chain similar to the one of *Optool DSX*. The second one was a molecule presenting a short fluorocarbon chain (called F_{13}-TMS) that should enable to perform a more precise XPS study of the degradation. The photocurable resist used is here the same as before (mixture of a diacrylate monomer with 1 wt % of a photo-initiator).

3.1 *Fluorolink® S10*: two anchoring end groups

3.1.a Presentation

To go further in the comprehension of mechanical and or chemical degradation mechanisms, we evaluated a new type of perfluoropolyether molecule (*Fluorolink® S10* from *Solvay Solexis*) in comparison to *Optool DSX*. The particularity of this molecule is that it has two anchoring ends groups (see Figure II. 20), allowing two covalent grafting sites of the molecule to the mold's surface. Consequently, the treatment is expected to have a better mechanical resistance.

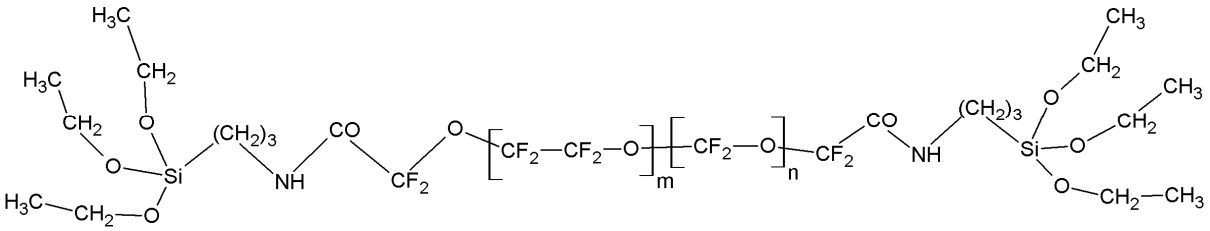


Figure II. 20: Chemical formula of *Fluorolink® S10* (m/ n= 1.5 - 2.5, 2 < n < 5, 5 < m < 9).

Fluorolink® S10 was also applied in liquid phase as follows: molds were first washed with isopropylalcohol (IPA) and dried with dry nitrogen. Then, they were dipped in a solution containing 0.1 wt % of *Fluorolink® S10*, 0.1 wt % of hydrochloric acid (37 wt % solution), 0.4 wt % of water and 99.4 wt % of IPA. Finally, molds were placed in a water-saturated environment at 150°C for 15 minutes.

The grafting after deposition and the aging of this F-ASL were monitored as a function of imprinting number using surface energy measurements, XPS and ESR. Results are compared with those obtained for *Optool DSX*. Imprints were performed manually using the same procedure and parameters already presented in the paragraph 2.4 of this chapter.

3.1.b Contact angle analysis

As illustrated in Figure II. 21, we measure a clear increase in surface energy values after repeated imprints. Indeed, after 40 imprints, the surface energy of the fused silica mold treated with *Fluorolink® S10* reached a value of about 45 mJ/m^2, which is a value comparable to those obtained for *Optool DSX*. Also, the overall degradation rate is very similar for the two products.

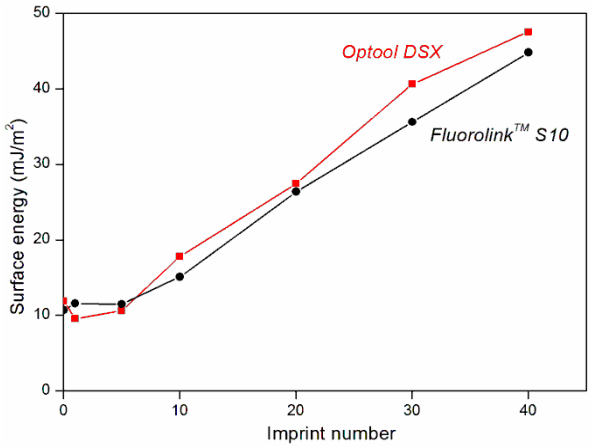


Figure II. 21: Surface energy of silica templates treated with *Optool DSX* (red curve) and *Fluorolink® S10* (black curve) when newly treated and after several imprints.

3.1.c XPS analysis

In Figure II. 22, the Carbon 1s spectrum of a newly *Fluorolink® S10* treated mold is reported, allowing to confirm the grafting of the molecule onto the mold as well as its chemical composition. We assigned the seven fitted peaks with the help of the National Institute Standard and Technology (NIST) binding energies database. Peaks with the larger binding energies, from 291 eV to 296 eV, were related to the presence of fluorocarbon bonds. Peaks centered at 295, 293.5 and 292.9 eV were attributed to O-C*F2-O, O-C*F2-CF2 and O=C-C*F2-O environments, respectively. Below 291 eV, all the peaks were attributed to aliphatic carbon environments. We observed at 289 eV the N-C*=O links, at 286.5 eV the C*-N links, at 285 eV the C*-C links and finally at 284.5 eV the Si-C* groups.

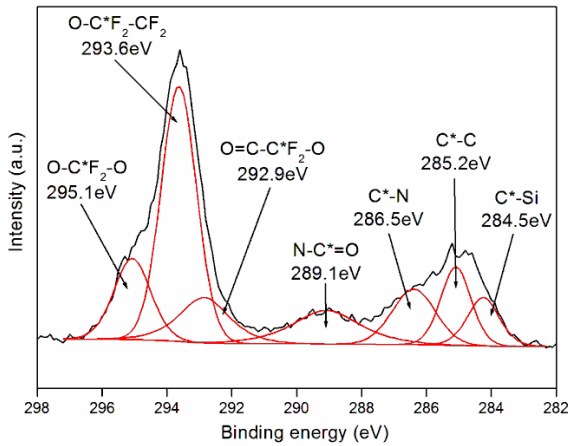


Figure II. 22: Carbon C1s XPS spectrum of a fused silica mold newly treated with *Fluorolink® S10* (black curve) along with all the fitted bonding contributions (red curves).

The Si-C*, C*-C, C*-N, N-C*=O and O=C-C*F2-O peaks were fitted with the same area because the *Fluorolink® S10* molecule contains the same proportion of each link. The area of the two other peaks representing the O-C*F2-CF2 and the O-C*F2-O contributions were not fixed because of the variable number of these links ($2 < n < 5$, $5 < m < 9$). After fitting, all the attributed links were quantified. Two carbon atoms correspond to 9.4 % of the total quantity. Consequently, the number of O-C*F2-O groups could be estimated to a mean value of 2.8 (it represents about 13 % of the total signal) and the number of O-C*F2-C*F2-O groups could be estimated to a mean value of 4.3 (it represents about 40 % of the total signal (2 times 20 %

due to the two identical carbon atoms)). These two estimations were close to the range given by the chemical supplier.
By increasing the imprint number, it was possible to follow the degradation of the antisticking treatment, which provokes a gradual decrease of fluorocarbon bonds as shown in Figure II. 23. We clearly observed that O-C*F_2-O links completely disappeared between 10 and 40 imprints and that the O-C*F_2-CF_2 contribution decreases. Therefore, a large quantity of fluorinated groups localized in the middle of the molecular chain is degraded during the imprint process and molecules may be broken during this process. On the other hand, a new link seems to appear near 291.7 eV (which may be due to a recombination of the broken links with a less electronegative group) and the two peaks at 286.5 and 285 eV are increasing. The most probable created group could be -CF_2-$(CH_2)_n$-, as the binding energy of the C*F2-CH2 link is about 291 eV. Furthermore, the presence of C*H_2-CF_2 and C*-C links would explain the increased peak intensities at 286.5 and 285 eV, respectively. This hypothesis is in agreement with the large surface energy increase observed (Figure II. 21). These hydrophilic –$(CH_2)_n$- groups may come from both an interaction with the resist's molecules and from resist residues.

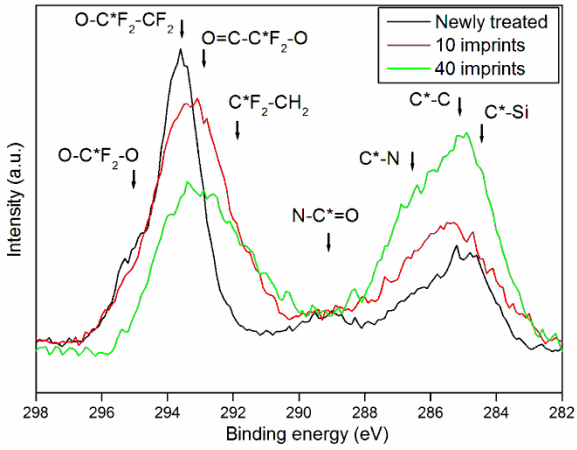


Figure II. 23: Carbon C1s XPS spectra of a fused silica mold treated with *Fluorolink® S10* before imprint (black curve), after 10 imprints (red curve) and after 40 imprints (green curve). Arrows indicates the positions of the different bonding contributions.

3.1.d ESR analysis

It is clear that *Fluorolink® S10* molecules break during repeated imprints. To try to evaluate if this degradation comes mainly from a chemical reaction or from a mechanical process, we performed ESR measurements following a similar protocol than previously described for *Optool DSX*. Due to slight changes in the exposure conditions (change of the UV lamp bulb and of the exposure tube holder), *Optool DSX* was measured another time in exactly the same conditions as for *Fluorolink® S10*. ESR results are reported in Figure II. 24 after 1 s UV illumination for untreated silica beads, *Fluorolink® S10* treated silica beads and *Optool DSX* treated silica beads. We clearly observe a difference in intensity between the three samples. For the non-treated beads, free radicals did not react with the silica surface: a large quantity of radicals was present in the mixture (curve with the higher intensity). On the other hand, the two anti-sticking treatments seem to react with free radicals from the resist since their signals are weaker than the reference. But *Fluorolink® S10* was more affected by the chemical reaction with the free radicals of the resist compared to *Optool DSX*. This could be due to the presence of C=O and C-N bonds in this molecule (that are not present in the *Optool DSX* molecule as evidenced by XPS measurements) that might be more affected by free radicals.

However, the two antisticking treatments degraded with the same rate as observed by contact angle measurements (Figure II. 21). One explanation may be that *Optool DSX* has a weaker mechanical resistance compared to *Fluorolink® S10*. Due to its only one grafting end on the mold, at the demolding step, the free end of the molecule might have a larger chance to be trapped in the polymerized network of the cured resist than *Fluorolink® S10*, which had two grafted ends and might form a "bridge" structure on the mold that may minimize the penetration of the molecule into the resist.

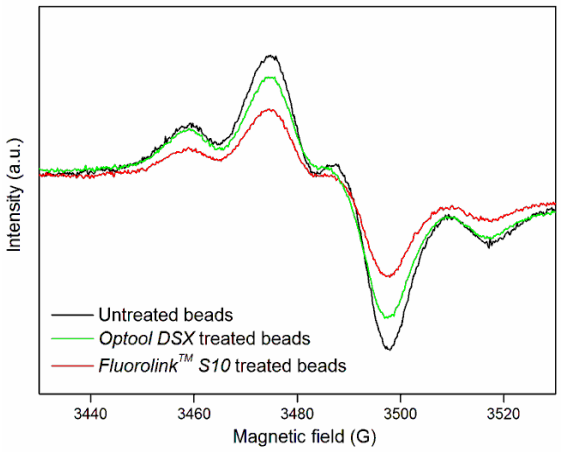


Figure II. 24: ESR spectra of resist and silica beads mixture irradiated 1s for untreated beads (solid curve), *Optool DSX* treated beads (dashed curve) and *Fluorolink® S10* treated beads (dotted curve).

In conclusion, chemical and mechanical degradation occur on the two molecules but it seems that a chemical degradation dominated in the case of *Fluorolink® S10*. Based on these experimental results, one can think that, during the photopolymerization process, resist free radicals (-CH_2•) react with *Fluorolink® S10*, increasing the surface energy of the mold and creating CF_2-CH_2 links on its surface. The two anchoring groups seem to minimize the mechanical breaking of the molecule, probably because of an improved grafting and or a conformation that decreases the mechanical interaction between the treatment and the resist.

3.2 F_{13}-TMS: shorter chain

3.2.a Presentation

1H,1H,2H,2H-Perfluorooctyltrimethoxysilane (F_{13}-TMS), supplied by ABCR, is a fluorinated molecule with a much shorter perfluorinated carbon chain (-$(CF_2)_5$-CF_3) containing 13 fluorine atoms and the same trimethoxysilane anchoring group -Si-$(O\text{-}CH_3)_3$ as the two other F-ASLs tested before. Its chemical formula is presented in Figure II. 25.

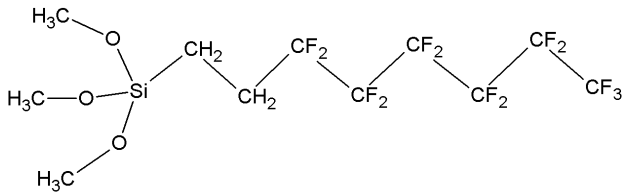


Figure II. 25: Chemical formula of F_{13}-TMS.

The deposition procedure followed for this product was the same as for *Optool DSX*, i.e. the liquid phase deposition as described in Chapter II.1.1. The thickness of the layer after deposition on a silicon substrate and measured by spectroscopic ellipsometry was observed to be between 1 and 2 nm. This value is close to the chain length of the molecule, which is about

1 nm. This means that F_{13}-TMS, thanks to its shorter chain, is anchored vertically on the substrate surface, and might be considered as a self-assembled monolayer, while *Optool DSX* molecules lies down on the surface as illustrated in Figure II. 26.

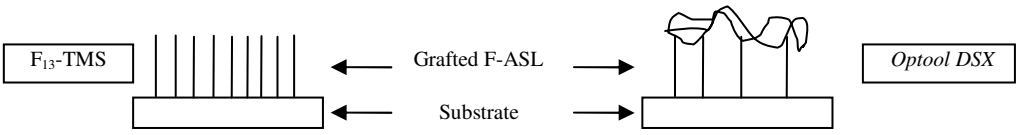


Figure II. 26: Schematic illustration showing the possible different conformation of F_{13}-TMS and *Optool DSX* molecules on the mold's surface.

We monitored the grafting mechanism after deposition and the aging of this F-ASL as a function of imprinting number using the same methods as for the previous cases (*Optool DSX* and *Fluorolink® S10*). Imprints were run manually adopting the procedure and parameters already presented.

3.2.b XPS analysis

Optool DSX, with its long chain and relatively thick layer, was seen not to be well adapted to perform a precise degradation study by XPS. This is the reason why we choose to work with these shorter F_{13}-TMS molecules. XPS experiments were performed on fused silica molds when newly treated, after 1 imprint and after 10 imprints. Resulting fluorine surface concentrations are given in Table II. 6 for both *Optool DSX* and F_{13}-TMS. After the first print, only a small quantity of fluorine is removed from the mold with shorter molecules compared to *Optool DSX*. All the molecules are well anchored to the mold's surface and the "rinsing" problem met with *Optool DSX* is not observed. Already at the first imprint, only the degradation phenomenon should be observed. After 10 imprints, the percentage of remaining fluorine on the fused silica stamps is higher for *Optool DSX* than for F_{13}-TMS. This is attributed to the higher initial thickness of *Optool DSX*.

% F	*Optool DSX* on fused silica	*F_{13}-TMS* on fused silica
freshly treated	100	100
After 1 UV-NIL imprint	92.2	99.4
After 10 UV-NIL imprints	76.6	29.4

Table II. 6: Percentage of remaining fluorine on fused silica molds treated with *Optool DSX* and F_{13}-TMS after one and ten imprints, determined by XPS and relative to a newly treated mold.

A Carbon 1s XPS spectrum for the F_{13}-TMS treatment before imprint and on fused silica is reported in Figure II. 27 along with all chemical bonding contributions (black curves). With this shorter and simpler molecule, it is easier to distinguish all contributions. C*-C, C*H_2-CF_2 and C*O bonds are present at lower binding energies whereas C*F_3, C*F_2-CF_2 and C*F_2-CH_2 bonds are observed at higher energies. For a new treatment, all these contributions come from the fluorinated layer and are consistent with its chemical formula. The C*O contribution comes certainly from an uncompleted hydroxylation of one of the feet of the silane grafting unit. Nevertheless, part of the C*-C and C*O contributions might come from atmospheric contamination. Due to the absence of OC*F_2 bonds in the F_{13}-TMS molecule, the contribution of C*F_3 bonds (i.e. the end of chain) is spectrally well resolved and can be observed. A comparison between values obtained on silicon and fused silica substrates and values provided by the NIST (National Institute of Standards and Technology) is given in Table II. 7.

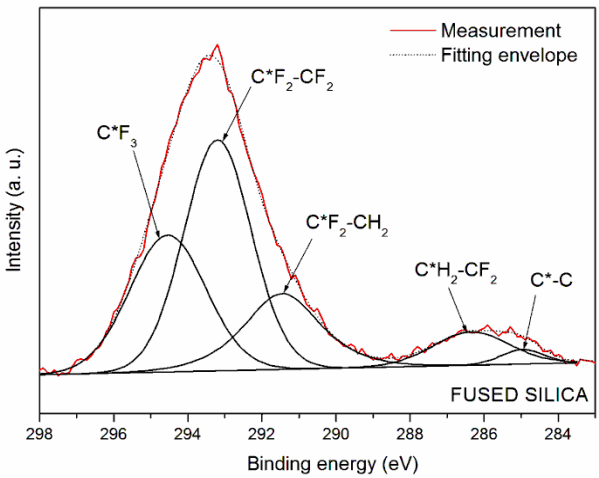


Figure II. 27: Carbon 1s XPS spectra of F_{13}-TMS grafted on fused silica (red curve) and the associated chemical bond contributions (black curves).

	Binding energy value (eV) as listed by NIST	Our results (eV) on silicon	Our results (eV) on fused silica
C*-C	285	285	285
C*H_2-CF_2	286.3	286.4	286.4
C*F_2-CH_2	290.9	291.7	291.4
C*F_2-CF_2	292.6	293.3	293.2
C*F_3	294.7	294.8	294.5

Table II. 7: Peak identification for a deposited F_{13}-TMS layer on silicon and fused silica substrates compared with NIST references.

The recorded XPS spectrum after 10 imprints is reported in Figure II. 28 with all chemical bonding contributions.

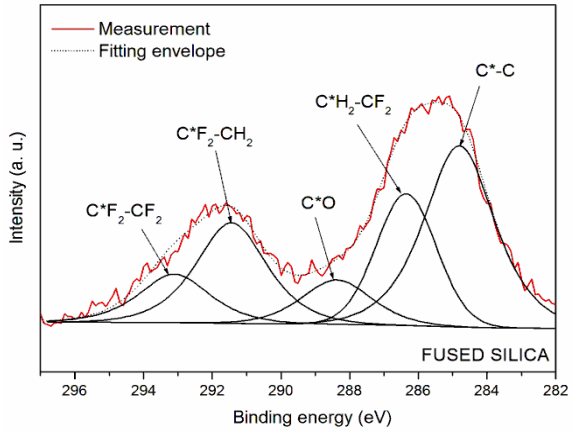


Figure II. 28: Carbon 1s XPS spectra of F_{13}-TMS grafted on fused silica (red curve) and the associated chemical bond contributions (black curves) after 10 imprints.

C*F_2–CH_2 and C*H_2–CF_2 contributions are still observed and have still the same intensity (peak area). Compared to these two contributions, the intensity of C*–C bonds (and in a lower extent of C*O bonds) is increased. This is most probably due to a surface pollution by some resist residues or atmospheric contaminants. Concerning the end of chain, C*F_2 bonds are still observed, but their relative intensity is decreased, whereas no more C*F_3 bonds (i.e. the chain end) could be measured. All these observations show that the degradation of the fluorinated treatment consists mainly in breaking the molecular chain in the fluorinated part and that the

rest of the chain remains grafted on the mold's surface. Thus, fluorinated chains are progressively degraded during the NIL process. This degradation mechanism is not necessarily the same for *Optool DSX* molecules as these molecules are "lying" on the mold's surface.

3.2.c ESR analysis

In order to see if the chemical nature of the fluorinated chains has an impact on the reactivity toward free radicals, we run ESR experiments using exactly the same experimental procedure (photo curable formulation, exposure time, UV lamp, ESR sample preparation, etc.) adopted to study *Optool DSX*, as presented in the paragraph 2.5 of this chapter. Results are listed in Table II. 8.

Sample composition	ESR intensity after 1s UV irradiation (a.u.)
Pure UV-curable resist	2800
Resist+ untreated silica beads	20250
Resist+ F_{13}-TMS treated silica beads	2850

Table II. 8: ESR signal peak height (arbitrary units) at 3474 Gauss after 1s UV irradiation for pure resist, resist mixed with untreated beads and resist mixed with F_{13}-TMS treated beads.

Here, the observed decrease in the number of free radicals with treated beads compared to untreated ones (both in contact with the resist) is even larger than for *Optool DSX*, with a 86% reduction, indicating a higher reactivity of the photocurable resist towards these fluorinated molecule. (To be compared to a reduction of 77 % for *Optool DSX*.) This can be explained by the presence of ether links C–O–C in *Optool DSX*, which have a slightly higher binding energy than C–C links (present in both *Optool DSX* and F_{13}-TMS) and which might be less reactive towards the free radicals. Furthermore, even if *Optool DSX* fluorinated chains are longer than F_{13}-TMS ones, the measured reactivity is lower. This seems to indicate that the contact area between resist and antisticking treatment is equivalent in both case i.e., confirming that long perfluoroether chains of *Optool DSX* are lying flat on the surface and not penetrating into the resist.

3.3 Conclusion

In this part, we characterized the anti-adhesive properties during UV-NIL imprints of two other F-ASL and discussed the obtained results in comparison to those obtained with *Optool DSX*. The two anchoring groups of *Fluorolink® S10* seem to minimize the mechanical interaction between the treatment and the resist. This positive effect allows to compensate the higher chemical reactivity measured, resulting in a global similar aging behavior.
Concerning F_{13}-TMS, its shorter chain length allowed us to observe more precisely the degradation mechanism that occurs during imprinting. It seems that molecules are progressively degraded along the chain in this case. As these molecules are most probably organized in a self-assembled monolayer, this seems to indicate that the mechanical contact with the resist might play an important role as well. This is what we will try to investigate in the next part where the mechanical properties of the resists are changed along with their chemical nature.

4 Impact of the UV-curable resist on the F-ASL degradation

This section will deal with the F-ASL aging issue from the resist point of view. We actually have seen in the last sections that a chemical reaction did occur between fluorosilanes and free radicals generated within the resist during UV exposure. This reactivity was observed in the case of three F-ASLs being in contact with a diacrylate-based resist. Objective of this section is to investigate in more details the influence of the resist on the ASL aging by:

- Tuning the resist's chemical and mechanical properties to give us the possibility to carefully and independently correlate them to the ASL durability.
- Investigating the role of addition of some fluorinated surfactants in the monomer solutions that can possibly prevent the mold treatment-resist interactions.

The aim is to draw first recommendations for the design of low interaction UV-NIL resists. For clarity purpose, only *Optool DSX* was considered here.

4.1 Comparison of UV-NIL and thermal-NIL

As already seen, several parameters can affect the integrity of anti-adhesive treatments, including chemical and mechanical interactions. In order to estimate the impact of each one of these two contributions, we first decided to carry out experiments involving two different resists (one involving free radicals in a UV-NIL process and a thermoplastic polymer in a thermal-NIL process) in most comparable conditions. A schematic illustration presenting the similarities and the differences between these two types of experiments is shown in Figure II. 29. An unpatterned fused silica mold treated with *Optool DSX* is used in both thermal-NIL and UV-NIL and the photocurable formulation used in UV-NIL is the same as previously.

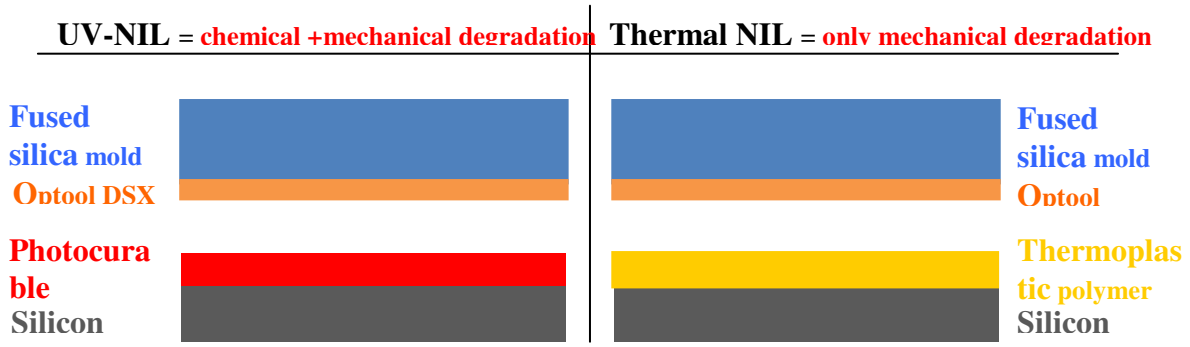


Figure II. 29: Schematic view of the comparative study between UV-NIL and thermal-NIL processes conducted in this section.

4.1.a Imprints on full 200 mm wafers

This set of experiments was conducted on 200 mm diameter wafers using the *EVG 520* imprinting tool described earlier in § 2.6. Fused silica molds were imprinted in both thin UV-curable and thermoplastic resist films coated on 200 mm diameter silicon wafers. In UV-NIL, wafers were coated with a 500 nm thick resist layer. For thermal imprints, we used a commercial electron-beam negative-tone polymer resist (*NEB22* supplied by *Sumitomo Chemicals*) coated with a thickness of 700 nm. UV imprints were done in to steps as described in § 2.6: a contact at room temperature in the *EVG 520* imprinting tool in vacuum (pressure equal to1.10^{-1} mbar) under 10 kN during 3 min and a UV exposure on the full wafer with an intensity of 0.4 mJ/cm^2 for 360 s. On the other hand, thermal imprints were run under vacuum, with an imprinting force of 40 kN during 3 minutes and at a temperature of 130°C. Once cooled down in the case of thermal-NIL, stacks (substrate / resist / mold) were demolded manually at room temperature by inserting a thin blade between the two wafers.

The surface energy of the mold was recorded for both experiments as a function of imprint number. Results are presented in Figure II. 30. Dispersive and polar components of the surface energy are also indicated.

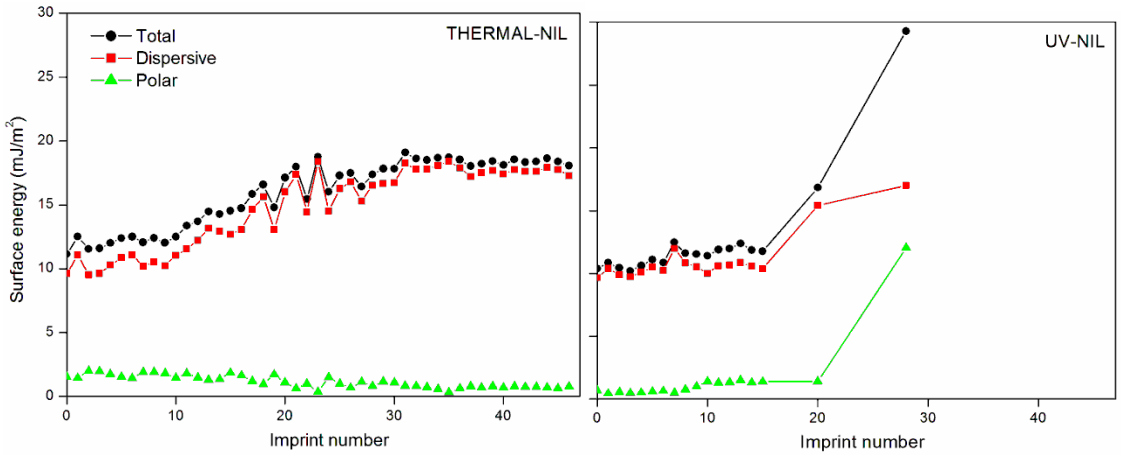


Figure II. 30: Evolution of the surface energy (and its polar and dispersive components) for fused silica molds treated with *Optool DSX* as a function of the number of imprints in thermal-NIL (left) and UV-NIL (right).

An increase in the numbers of imprints corresponds to an increase in the mold surface energy for both processes. Nevertheless, in thermal-NIL, this increase is limited to only about 8 mJ/m^2 after 45 imprints while it is of about 19 mJ/m^2 after less than 30 imprints in UV-NIL (even if, as seen before in § 2.6, we used here a full wafer UV-NIL process that is less harmful to the ASL than the standard step and repeat one). If we look at the relative components of measured surface energies, we can observe that, for thermal-NIL, only the dispersive part increases, indicating most probably a progressive degradation of the apolar fluorinated chains by mechanical friction with the resist's surface. In UV-NIL, the polar part increases also. Two reasons can be at the origin of this observation:

- Resist is present on the mold surface (diacrylate monomers used exhibits 46 % of their free surface energy under polar component). Resist molecules might react chemically with the fluorinated chains creating polar molecules or resist residues might be adsorbed on the surface.
- The F-ASL is locally degraded, exposing the bare fused silica surface.

Probably a combination of those two mechanisms is taking place during UV-NIL imprints.

4.1.b Step and repeat process in the *NPS 300* tool

To run this set of experiments, we needed an imprinting tools equipped with both thermal and UV step and repeat capabilities and eventually able to measure the force exerted at the demolding step between the mold and the substrate. Thanks to the *NaPaNIL* European project consortium, we had the possibility to access to the *NPS 300 SÜSS MicroTec* tool (illustrated in Figure II. 31) located at the *VTT Technical Research Centre* in *Espoo, Finland*, able to propose this functionality.

For thermal imprints we used here a commercial electron-beam positive tone polymer resist (PMMA *AR-P 679.04* supplied by *Allresist*, molecular weight 950K, glass transition temperature around 115°C), coated by spinning at 1000 rpm for 30 s and followed by a bake at 150°C for 1 min, to obtain a final thickness of 630nm on 4 in. silicon substrates. Unpatterned silica molds fulfilling the form factor required by the *NPS300* stepper were used, i.e. a total dimension of 50*50 mm^2 and a contact area of 10*10 mm^2 between the mold and the resist. Imprints were run at atmospheric pressure. The coated substrate was heated up to

140°C before applying a pressing force of 50 N for 60 s. The wafer was then cooled down to 70°C before separating the mold from the resist. The whole process took 410 s / die, which is a quite long process due to the heating and cooling ramps at each die. (The thermal-NIL process used here is made by heating and cooling the whole wafer at each die. Then, the previously imprinted die on the same wafer will be deleted, which is not tolerable in a normal lithography process. This is due to the fact that we wanted to use the same UV imprint head, with the same force sensor, and this head is not equipped with a stamp heating capability.)
In UV-NIL, wafers were coated with a 200 nm thick resist layer. The process was conducted at room temperature and under atmospheric pressure. We applied the same force and the same demolding process as for thermal imprints. The UV exposure was made using a broadband mercury lamp emitting from 340 to 420 nm in wavelength. The power density of the lamp was 120 mW/cm^2 at the resist surface and, for each imprint, the resist was exposed for 20 s. (We tried here to expose the formulation for a shorter time but it didn't polymerize efficiently, maybe due to the presence of residual oxygen in this case). The process for a UV imprint took 50 s / die.



Figure II. 31: a) *NPS 300* imprinting tool: overall view (left side) and zoomed view of the imprinting system; b) Schematic illustration of the automated "parallel" demolding step principle (0) and schematic evolution of the separation crack (top view, from 1 to 5).

It was mandatory to ensure a full and reproducible contact between stamp and substrate after each imprint. We paid extremely attention to this parameter and managed to get correctly imprinted dies, with well defined borders, as illustrated in Figure II. 32. Still, some particles affected printed dies although we filtered the resist before spin coating and carefully dealt with substrates and molds, showing the extreme sensitivity of the NIL process to this kind of defects. The presence of a particle impedes fully printed dies, which means a reduced contact area and consequently a lower value of demolding force. This defectiveness provoked some dispersion in the measured demolding force values and very low values were removed.

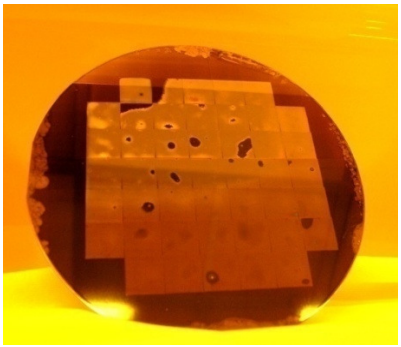


Figure II. 32: Picture of printed dies on a 100 mm diameter silicon wafer using the UV-NIL process in the *NPS300* stepper tool.

Using a scan rate of 20 measurement points per second during each imprint, it was possible to identify the demolding step in the force plot, as reported in Figure II. 33 (left). The demolding force is the force needed to separate the mold from the substrate after the imprinting step as shown in Figure II. 33 (right).

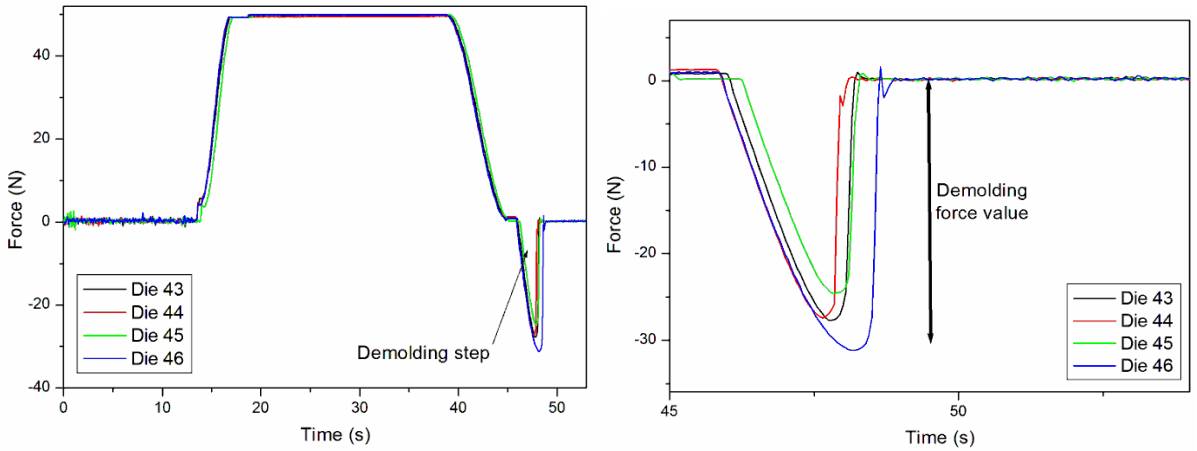
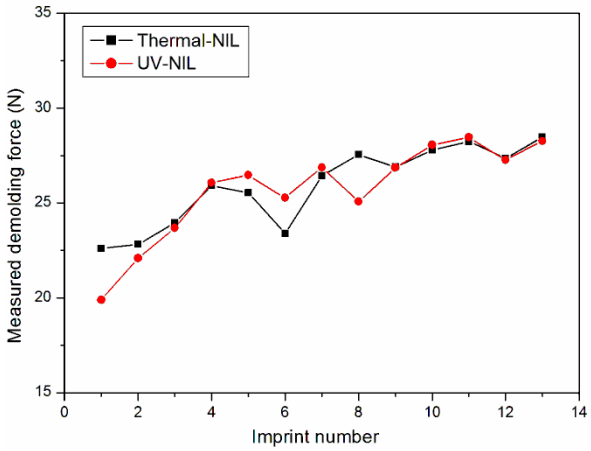


Figure II. 33: Plots of applied force vs time showing the evolution of the force applied during the whole UV-NIL sequence (left) and focusing on the spike related to the demolding step (right).

Considering that we had no access to a contact angle measurement setup in *VTT Research Centre* cleanrooms, we run imprints (recording demolding force values) and measured mold's surface energy only once back to the *CEA-LETI* cleanroom. We employed 4 different molds: for two of them we run the same number of imprints in thermal and UV mode and, for the two others, we performed imprints until we met critical adhesion problems.
In Figure II. 34 (left), we plotted the increase of the demolding force for the two first molds used to perform 13 thermal and 13 UV imprints respectively. Values and evolution of the demolding force are almost the same for both processes. Nevertheless, after the same number of imprints, the stamp used in UV mode reached a much higher value of surface energy (33.29 mJ/m^2) than the one used in thermal NIL (9.27 mJ/m^2) as reported in Figure II. 34 (right).

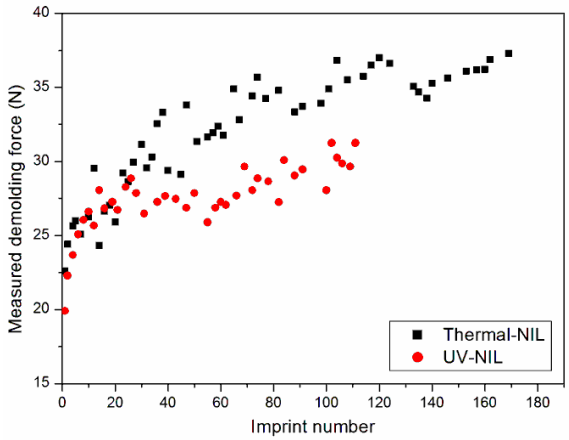


N° and kind of imprints	13 thermal-NIL	13 UV-NIL
Surface energy [mJ/m^2]	9.87	33.29
Dispersive part [mJ/m^2]	8.57	20.55
Polar part [mJ/m^2]	1.31	12.74

Figure II. 34: Evolution of the demolding force as a function of imprint number in thermal and UV imprinting modes (left) and surface energy of the mold at the end of the process (right).

With the two other molds, we performed a much larger number of imprints. 170 imprints were run in thermal-NIL, while only 110 UV imprints could be performed before reaching a two high contamination of the mold that does not allow continuing demolding force

measurements. Evolution of the demolding force amplitude for these molds is presented in Figure II. 35 along with their surface energy at the end of the process. We can observe that, after the same trend until the 30th imprint (important increase of the demolding force), the demolding force in the case of the UV mode remains then lower than the one in the case of the thermal process. Also, after the 50th imprint, the increase in the demolding force is quite limited for both processes.



N° and kind of imprints	170 thermal-NIL	110 UV-NIL
Surface energy [mJ/m^2]	9.91	41.04
Dispersive part [mJ/m^2]	7.54	19.23
Polar part [mJ/m^2]	2.37	21.81

Figure II. 35: Evolution of the demolding force as a function of imprint number in thermal and UV imprinting modes (left) and surface energy of the mold at the end of the process (right).

These results are very surprising. Indeed, we expected a higher demolding force for the UV-NIL process than for the thermal one since we know that the mold treatment is degraded very fast in UV-NIL; and, in fact, when looking to the surface energy evolution it seems that we have a degradation in the case of UV-NIL that we don't observe in the case of thermal-NIL. No correlation between the surface energy measurements and the demolding forces evolution is evidenced.

We tried to explain the apparent mismatch between demolding force values and contact angle measurements for the thermal mode. We imagined that, during first sequences of imprints, few molecules of *Optool DSX* that didn't graft correctly to the mold surface will be removed progressively, increasing the demolding force. Then, after about 50 imprints, no more fluorine molecules are removed and more stable conditions are reached where the demolding force value increases only slightly. In this hypothesis, the mold treatment degradation, which is here only due to the mechanical friction with the resist, is very limited.

A different mechanism applies most probably to imprints in UV mode. Here, from the increase of the surface energy, we can say that the degradation is very fast (surface energy higher than 33 mJ/m^2 after only 13 imprints), even faster than for our standard step and repeat process used in *Grenoble* (cf. § 2.2). This might be due to the higher UV exposure intensity (and higher dose) used, as we know that this may enhance the degradation (see § 2.6 *Impact of the UV intensity and dose*). Then, one possibility could be that, during the first 25 imprints, the surface treatment is degraded, as evidenced by the demolding force increase. After that, when a stable value of demolding force seems to be reached, a combination of a high adhesion to the silica surface and of a cohesive crack of the resist is observed. Indeed, after 110 imprints, we could not continue imprint sequences due to a too high contamination of the mold with resist's residues (microscopy experiments should have been undertaken on these molds to evaluate the separation mode).

Finally, this indicates that a low surface energy does not necessarily mean a low adherence.

4.2 Impact of type and number of polymerizable groups

Here, we carry out a precise comparative study of different resists and measure the influence of different parameters on the ASL aging. These parameters are:

- The polymerization group type (acrylate, methacrylate or vinyl ether)
- The resist's conversion rate / exposure time
- The resist's hardness and Young's modulus.

4.2.a Resist formulations and exposure

In this work, pure (composed of one monomer) photo-polymerizable resists were prepared from commercially available materials. 4 different monomers where chosen, all with the same triethyleneglycol chain, but with different ends of chain, including functions that react by free radical polymerization such as methacrylates (mono- and di-functional) and acrylates (di-functional) or by cationic polymerization like vinyl ethers (di-functional). Considered monomers are depicted in Figure II. 36. Due to their similarities, they have very close molecular weights and viscosities. To ensure a reliable comparative study, the same type and percentage of free radical photoinitiator (1 wt % of *Darocure 4265* from *Ciba*) was used in the case of methacrylate and acrylate-based resists, while 1 wt % of *UVI 6976* (*Union Carbide*) was used in the divinyl ether based resist.

Repeated imprints were then made as follows: for every formulation, a 2µl drop of solvent-free resist was manually dispensed on a 200 mm diameter silicon wafer. An unpatterned fused silica mold is then pressed onto the droplet and UV exposure is performed using a mercury lamp source emitting from 350 up to 410 nm in wavelength at a power density of 11 mW/cm^2 at the resin surface. The template was then separated from the imprinted spot, subjected to a surface energy measurement and re-used for next imprints.

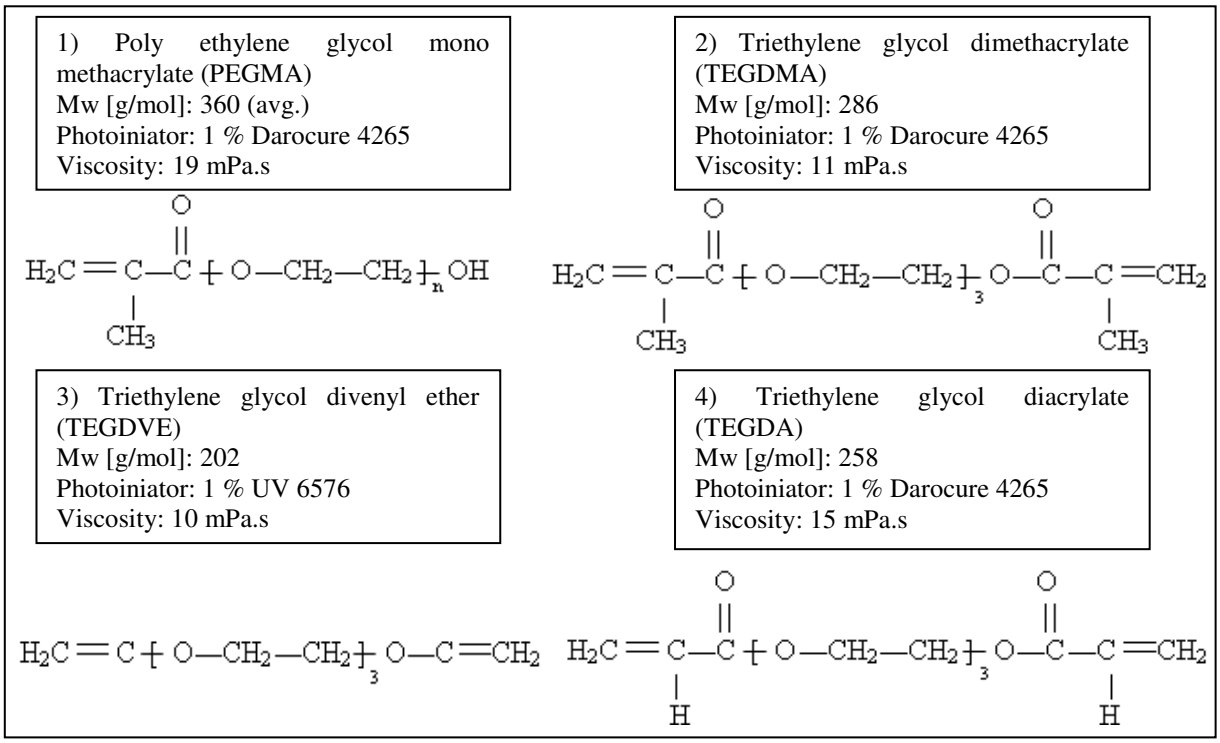


Figure II. 36: Pure monomers used in the 4 resist formulations investigated in this study.

4.2.b FTIR analysis

The conversion ratio of each resist as a function of the UV exposure time was recorded using a *Perkin Elmer*® FTIR. IR absorbance spectra of uncured and cured resists spots were recorded for each formulation. An example of a measured FTIR absorbance spectrum is given in Figure II. 37. The conversion ratio was then calculated from the decrease rate of the height of the absorbance peak of the aliphatic C=C bond (depicted in Figure II. 37 as a variable peak because the amplitude of this peak changes during the polymerization process) relative to that of a stable peak, used as internal reference (depicted in Figure II. 37 as reference peak). For methacrylate formulations, the C=C bond peak appears as a single peak at 1650 cm^{-1}, while for the other ones it appears as a double peak at 1619 and 1639 cm^{-1}. For TEGDMA, PEGMA and TEGDA based resists, the carbonyl group C=O at 1720 cm^{-1} was used as stable peak, while the methyl group C-H (with a double peak at 2890 and 2930 cm^{-1}) was used in the case of TEGDVE (due to the absence of carbonyl group in the molecular structure of the cationic formulation). Variable and stable peaks were chosen in accordance with references from the literature (TEGDMA and PEGMA,[137] TEGDA[138] and TEGDVE[139]).

Resist	Variable peak	Reference peak
TEGDMA	C=C at 1650 cm^{-1}	C=O at 1720 cm-^{1}
PEGMA	C=C at 1650 cm^{-1}	C=O at 1720 cm^{-1}
TEGDA	C=C at 1636-1619 cm^{-1}	C=O at 1720 cm^{-1}
TEGDVE	C=C at 1636-1619 cm^{-1}	C-H at 2890-2930 cm^{-1}

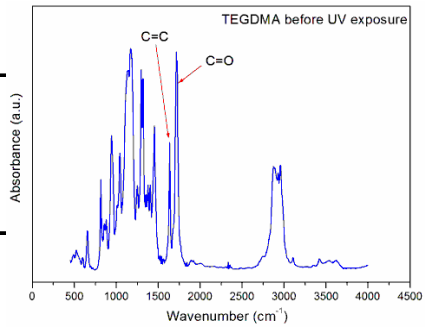


Figure II. 37: List of selected peaks used to calculate the degree of conversion for our formulations (left) and example of FTIR absorbance spectrum (right, in the case of the TEGDMA resist before UV exposure).

The degree of conversion was finally calculated by means of the following equation: $DC(\%) = 100 \times \left[1 - \frac{R_{cured}}{R_{uncured}} \right]$, where R is the height of the variable peak normalized over the stable one. Results obtained are listed and plotted in Figure II. 38:

Expo. time (s)	PEGMA	TEGDA	TEGDMA	TEGDVE
0	0	0	0	0
0.1	30	31	-	67
0.5	-	60	-	73
1	32	62	22	84
5	33	-	33	91
10	37	63	75	95
20	-	-	77	-
30	-	-	-	96
50	48	64	78	-
100	50	65	79	96
200	55	-	80	-
300	56	65	80	96
400	-	-	80	96

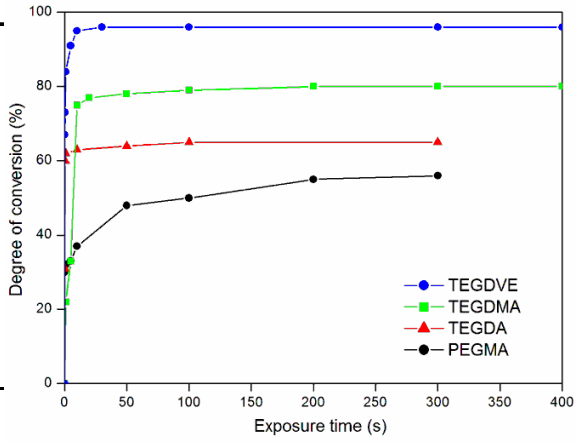


Figure II. 38: Degree of conversion (%) for each formulation, as a function of exposure time and for 1 wt % of photoinitiator.

One can notice that the studied formulations exhibit a strong increase of the conversion rate during the first seconds of exposure before reaching a plateau when the exposure duration exceeds the minute range. Formulations including two polymerisable groups per molecule (TEGDMA, TEGDA and TEGDVE) exhibit a higher degree of conversion than the mono-methacrylate one. Considering the plateau reached for high exposure doses, it is possible to rank the analyzed resists from the highest to the lowest degree of conversion as follows: TEGDVE > TEGDMA > TEGDA > PEGMA.

4.2.c ESR analysis in the case of free radical systems

The reactivity of the used UV-curable resists (acrylate and methacrylates) towards an *Optool DSX* antisticking treatment was investigated by ESR using the same experimental protocol already described in § 2.5 of this chapter. For each resist studied, we compared the ESR spectrum obtained when the resist is mixed with untreated silica beads to those obtained when the silica beads are treated with *Optool DSX*. ESR tubes containing the same weight of analysed samples were exposed to the same UV light source for the same duration and before reaching the maximum conversion degree (plateau in Figure II. 38, i.e. PEGMA: 50 s UV exposure, TEGDMA: 10 s UV exposure, TEGDA: 1 s UV exposure). Besides, all resist samples were analyzed in the dark before exposure to verify the absence of free radicals.
Recorded ESR spectra are reported in Figure II. 39. They show signatures of methacrylate free radicals (5 resonance peaks in the case of PEGMA and TEGDMA resists on Figure II. 39 a) and b)) and acrylate free radicals (3 resonance peaks in the case of the TEGDA resist on Figure II. 39 c)).[140] Resonance peak intensities, which are proportional to the concentration of free radicals, were systematically lower (red curves) in the case of resists being in contact with the antisticking product, confirming a chemical interaction between free radicals of the resist and fluorinated molecules. To estimate this reactivity, the decrease ratio of the highest and lowest resonance peak intensities was reported in Table II. 9. In the case of methacrylate based resists, resonance peaks occurring at 3485 and 3490 G were selected, while peaks located at 3482 and 3493 G were considered in the case of the di-acrylate based resist. According to this criterion, it came out that the mono-methacrylate based resist is the most reactive formulation towards *Optool DSX* molecules, followed by the di-acrylate and di-methacrylate based ones. This might be explained by a higher mobility of the free radicals during photo-polymerization in the mono-methacrylate resist due to lower resist viscosity. However, if we compare the di-functional monomers, the acrylate radicals seem to be more aggressive against *Optool DSX*.

Resist	Decrease (%) of the highest peak intensity	Decrease (%) of the lowest peak intensity	Average (%)
PEGMA	45	45	45
TEGDA	23	19	21
TEGDMA	18	14	16

Table II. 9: ESR signal decrease ratio when an *Optool DSX* anti-sticking layer treatment is used for the three free radical resists studied.

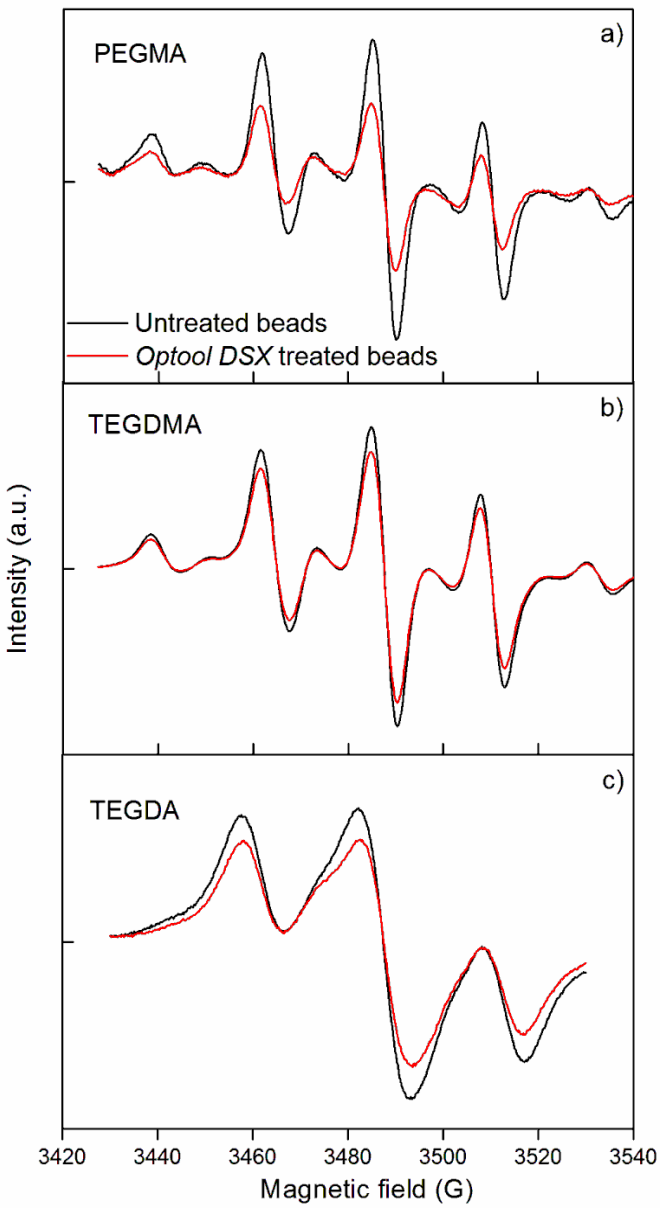


Figure II. 39: ESR spectra for the three free radical resist studied [a) PEGMA, 50 s UV exposure; b) TEGDMA, 10 s UV exposure; c) TEGDA, 1 s UV exposure] containing micrometric untreated silica beads after UV irradiation (black curve) and of resist containing micrometric *Optool DSX* treated silica beads after UV irradiation (red curve).

4.2.d Nanoindentation analysis

After this detailed analysis of the chemical reactivity of three of the four resists, we carried out a series of experiments aiming at measuring their mechanical properties as a function of the exposure dose. For each resist, we indented a rather thick UV resists film (~ 95µm) with a *Nano Indenter XP* tool from *MTS*. The principle of this measurement consists in applying an increasing load on the tip perpendicularly to the analyzed sample surface as shown in Figure II. 40. The as-applied load will induce indented material displacements that can be permanent (plastic) or reversible (elastic). When the nanoindenter tip is progressively removed, elastic displacements are recovered leaving behind only the plastic displacement visible on the material surface. A typical load / displacement curve is presented in Figure II. 40.

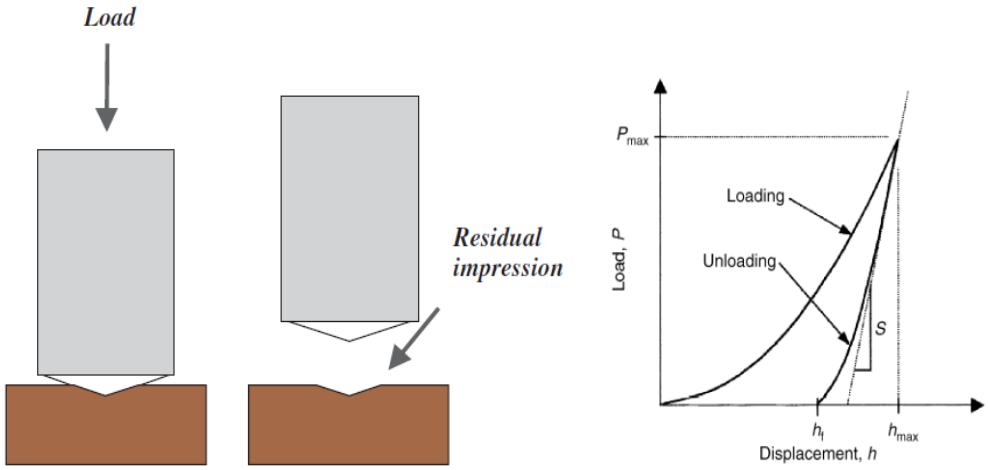


Figure II. 40: Schematic presentation of the indenter impression into the indented material (left side); Load/displacement curve showing the loading and unloading phases (right side).

An empirical consideration was taken into consideration before preparing the samples: the indentation depth doesn't have to be larger than 10 % of the coated resist. In this way, measured mechanical properties won't be affected by substrate's ones. We chose to coat about 95 µm of resist and to use an indentation depth of 2 µm. A specific procedure was followed for the preparation of the samples to guarantee a reproducible thickness of the coated resist. As illustrated in Figure II. 41, we proceeded as follows: a) Manual deposition of few drops of resist on a silicon substrate, between two parallel adhesive labels (with a thickness of 95 µm); b) Squeeze of deposed drops by contact with a fused silica mold (the resist can be evacuated in one direction); c) Illumination with the same UV lamp as for all "manual" experiments discussed before; d) Manual demolding.

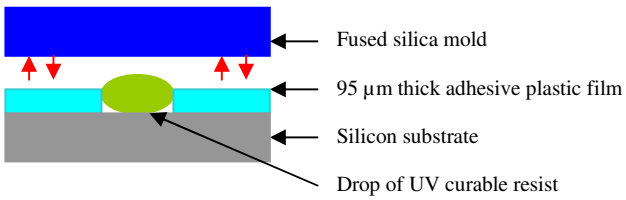


Figure II. 41: Schematic of the procedure followed for nanoindentation samples preparation.

A quantitative treatment of the load / displacement curves based on the use of the Oliver and Pharr model[141] was carried out in order to estimate the elastic modulus (E) and hardness (H) of the resists. E, was determined from the reduced modulus, E_r, given by: $E_r = (\sqrt{\pi} * S)/(2\beta\sqrt{A})$, where β is a constant that depends only on the geometry of the indenter (β=1.034 for Berkovich tip, β=1 for a round end cone one[142]); S is the slope of the initial portion of the unloading curve at the maximum peak load (as shown in Figure II. 40 where other important parameters are reported as the peak load and displacement, P_{max} and h_{max}, and the residual depth after unloading h_f); A is the projected contact area between the tip and the substrate at the peak load as it can be seen from AFM scans. For a Berkovich tip, the projected contact area was calculated as follows: $A = 24.5\ h_{max}$, while for round end cone tip with radius R, having a circular contact: $A = \pi(2Rh_c - h_c^2)$, where h_c is the contact depth at the peak load, which was estimated by $h_c = h_{max} - \varepsilon\ (P_{max}/S_{max})$, where ε is an indenter geometry constant, equal to 0.75 for spherical indenters.
According to the elastic deformation theory, the elastic modulus of the material, E, was finally calculated using the expression: $1/E_r = [(1-\nu^2)/E] + [(1-\nu_i^2)/E_i]$, where ν is the Poisson's ratio for the test material, while E_i and ν_i are respectively the elastic modulus and Poisson's ratio of

the indenter tip (for diamond, E_i = 1141 GPa and ν_i = 0.07 were used). For all tested samples Poisson's ratio was assumed equal to 0.30.
The hardness of the tested surface (H) is a measure of the material's resistance to surface penetration and was determined using the equation: H = P/A, where P is the load applied to the test surface and A the projected contact area at the load.

First, we ran experiments using a Berkovich tip. During each nanoindentation experiment, we fixed nanoindentation depth and strain rate values so that the nanoindenter had to tune the applied load depending on the response of the indented surface. As previewed by the selected standard method, once reached the depth, the load was held constant for 10s. Then; the nanoindenter head was unloaded from the indented surface till reaching a load value equal to 90% of the maximum applied load. During the analysis we monitored mechanical properties on different degree of conversion for each formulation. In Figure II. 42 we reported load / displacement curves for the 4 formulations with equivalent UV exposure time.

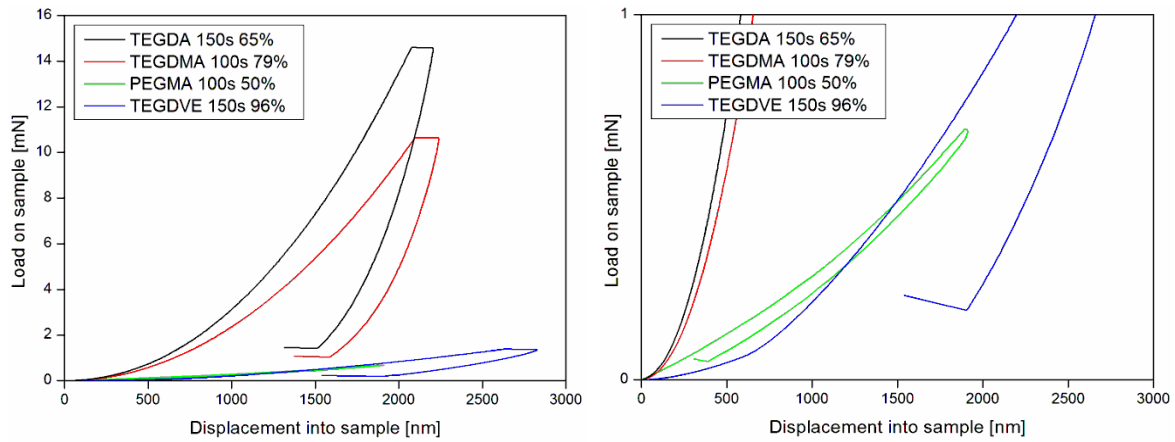


Figure II. 42: Typical load-displacement curves obtained after nanoindentation of selected resists employing a Berkovich tip and a nanoindentation depth of 2 µm (right: zoomed view for a better visualization of the PEGMA resist curve).

Considering the observable difference between the maximum displacement at maximum applied load and the residual displacement after unloading, we can estimate if the tested material has more or less recovery, i.e. elastic or plastic behavior. The PEGMA resist showed essentially an elastic behavior, as reported in zoomed view in Figure II. 42 (right), while a plastic deformation can be clearly identified in the other tested samples. Furthermore TEGDMA and TEGDA based resist could stand to a higher applied load.

Young modulus and hardness were determined for the 4 resists at different Conversion Degrees (CDs), i.e. different exposure times. Also, some of the samples were measured a second time two months later than the first measurement (they were stocked inside transparent boxes, in absence of yellow light) and in different zones (to evaluate their homogeneity). Each measurement was repeated 20 to 30 times. Obtained mean values and standard deviations are reported in Table II. 10. Results got on PolyEthyleneTerephtalate (PET) and on fused silica samples confirmed that our experimental protocol with a Berkovich tip was correct. In fact, measured mechanical properties for fused silica were in accordance with the literature (for fused silica: E = 69 to 75 GPa et H = 8.5 to 10.7 GPa) and the measured value for PET was only 4 % lower than the value announced by its supplier (heat stabilizes *Melinex ST 506* PET made by *Dupont Teijin Films*, 75µm thick, E = 4 GPa at 20°C).

# of trials	Resist (CD, expo. time)	E [GPa]	Stand. dev.	H [GPa]	Stand. dev
33 + 17 DF2	TEGDA (63%, t=10s)	2.51	0.005	0.12	0.001
25	TEGDA (64%, t= 50s)	2.8	0.051	0.13	0.007
30	TEGDA (65%, t=150s)	3.1	0.04	0.135	0.003
24	TEGDMA (70%, t= 8s)	1.95	0.087	0.09	0.001
20 + 17 DF2	TEGDMA (77%, t= 20s)	2.6	0.05	0.11	0.003
25	TEGDMA (79%, t= 100s)	2.9	0.014	0.12	0.001
20	TEGDVE (73%, t= 0.6s)	0.215	0.003	0.009	0.001
20+ 12 DF2	TEGDVE (95%, t= 10s)	0.6	0.05	0.013	0.003
30	TEGDVE (96% , t=150s)	0.61	0.018	0.014	0.002
20	PEGMA (37%, t= 10s)	0.05	0.005	0.003	0.002
29 + 10 DF2	PEGMA (50%, t= 100s)	0.13	0.008	0.04	0.004
22	PEGMA (56%, t= 300s)	0.19	0.09	0.06	0.05
Standard samples for calibration					
28 + 10 DF2	PET	3.85	0.022	0.36	0.004
29 + 10 DF2	Fused silica	74	0.113	10.65	0.009

Table II. 10: Young's modulus (E) and hardness (H) values measured by nanoindentation with a Berkovitch tip for different degree of conversion of selected resists (DF2 = in different zones after 2 months).

Considering the resists, standard deviations of E and H were really low, including measurements realized after two months and on different zones (labeled as DF2 in Table II. 10). This means that analyzed samples showed a good homogeneity and stability in the time.
Exposure time exerted clearly the same effect on analyzed specimens, i.e. an increase in the exposure time leads to an improvement in mechanical properties (higher E and H), even when the degree of conversion was almost the same.
TEGDA and TEGDMA based resists showed a similar evolution of their mechanical properties as a function of exposure time, providing higher values than TEGDVE and PEGMA based resists. Low E and H value of monomethacrylate resist compared to dimethacrylates can be logically explained considering that it had a lower degree of conversion. Furthermore, after polymerization, monofunctional monomer are entangled in only two directions, while bifunctional one will create a more rigid tri-dimensional network.

Additionally, we performed nanoindentation measurements with round end cone tips. This new geometry presents a higher contact surface especially useful for materials with low mechanical properties. The nanoindenter manufacturer, in fact, advices to use round end cone tip to run nanoindentation observation on resists with E < 1 GPa. The problem that could be met employing a Berkovich tip with resist showing E < 1GPa is the difficulty to detect the surface, leading to final indentation depth larger than expected, i.e. to incorrect data.
No standard protocol exists in the literature when round end cone tips are employed. We decided to adopt the same model (Oliver and Pharr based on elastic contact) as with Berkovich tips. The PET specimen and 3 resist samples were tested. Results are reported in Table II. 11 (20 tests per sample). H and E values obtained for the PET sample are well in accordance with those ones got with a Berkovich tip, while they were slightly lower on the other tested formulations (about 20 % lower). Nevertheless, the global trend was confirmed, with the PEGMA formulation showing lower E than TEGDVE and TEGDMA ones.

Resist (CD, expo. time)	E [GPa]	Stand. dev.	H [GPa]	Stand. dev
TEGDMA 77% 20s	2.51	0.05	0.10	0.009
TEGDVE 95% 10s	0.49	0.007	0.011	0.03
PEGMA 50% 100s	0.11	0.09	0.034	0.01
PET	3.75	0.13	0.33	0.006

Table II. 11: Young's modulus (E) and hardness (H) values measured by nanoindentation on selected resists using conospherical tip.

Nanoindentation experiments are generally corroborated by AFM observation because, in this way, it is possible to have a look on the global contact area left on the sample after indentation. Indeed, as depicted in Figure II. 43, it is possible to observe some "pile-up" (accumulation of material near the border of the indentation and impression with sharp edges) or "sink-in" (no accumulation of material near the border of the impression and impression with rounded edges), that can inform about a general plastic or elastic behavior.

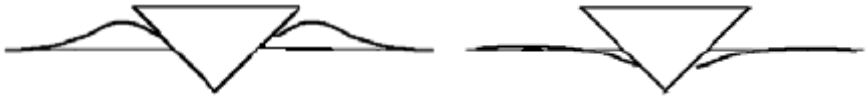


Figure II. 43: Possible profiles that can be met on indented surfaces: left: "pill-up" and right "sink-in".

AFM observations using Berkovich and round end cone tips on TEGDMA (with a degree of conversion equal to 77%) and TEGDVE (with a degree of conversion equal to 95%), are reported in Figure II. 44. TEGDMA based resist showed neither "sink-in" nor "pile-up", while TEGDVE one showed a slight "sink-in", in accordance with nanoindentation measurements where the former resist showed higher hardness than the latter.

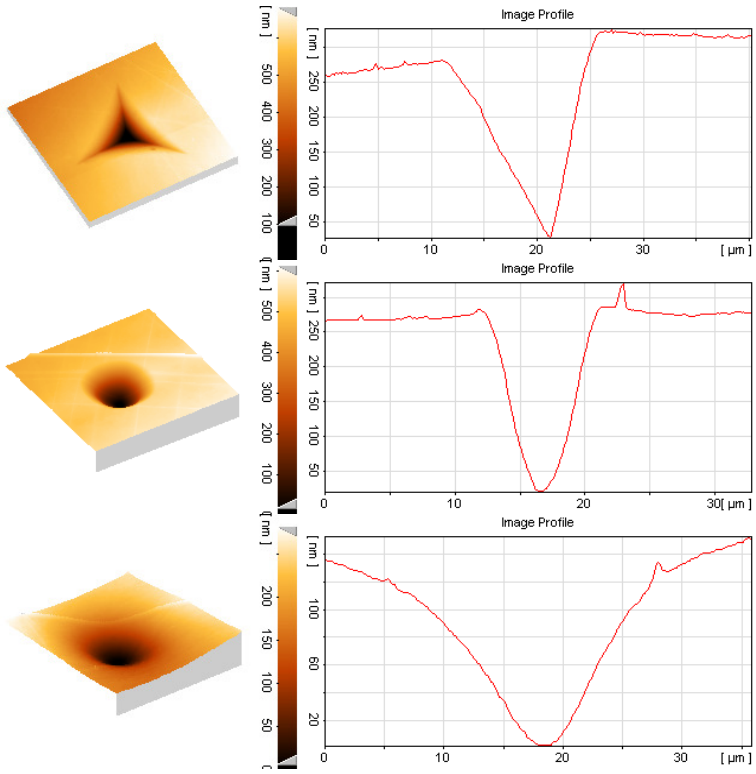


Figure II. 44: AFM images (left) and impression cross section (right) of TEGDMA cured specimen (CD 77 %) indented with a Berkovich (top) and a round end cone tip (middle), and of TEGDVE cured specimen (CD 95 %) indented with a round end cone tip (bottom).

4.2.e Contact angle measurements

Once determined, for each resist, the correspondence between the degree of conversion and the exposure time, we carried out contact angle measurements to monitor the evolution of the mold surface energy as a function of imprint number. Imprints are made manually as already presented earlier in this work. Results are reported in Figure II. 45 showing the impact of the degree of conversion on the ASL degradation for the TEGDMA and for the TEGDA resists.

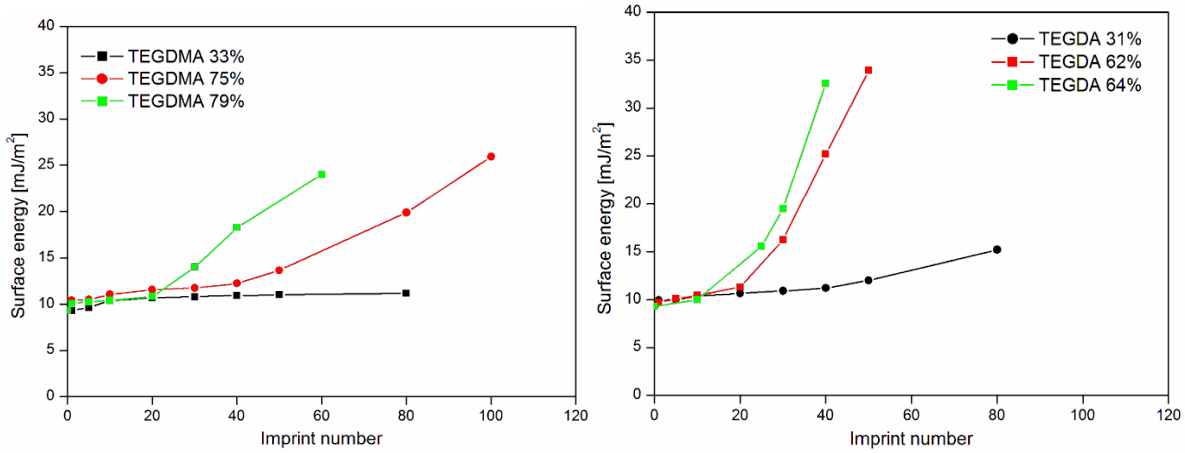


Figure II. 45: Impact of the resist's conversion degree on the mold surface energy evolution during repeated imprints for the dimethacrylate resist (left) and for the diacrylate resist (right).

It is clear that exposure time is directly correlated to the degradation of the ASL. This trend is logically explained looking at the quantity of photons sent on the resist surface. In fact, as demonstrated in § 2.5 of this chapter, free radicals generated into UV-curable resist, during radical polymerization, attack anti-adhesive molecules grafted on the mold and increase its surface energy. Keeping constant the percentage of photoinitiator and the power density of employed mercury lamp, the number of free radicals produced into the resist can be increased by only sending a higher quantity of photons, i.e. rising up the exposure time. Additionally, this trend can also be explained by a higher mechanical interaction. Indeed, as shown by nanoindentation experiments, a longer exposure time will result in higher mechanical properties for the resist.

Comparison between TEGDA and TEGDMA shows also that, in the case of TEGDA, the increase of the mold surface energy occurs earlier than in the case of TEGDMA. This is most probably due to the little higher chemical reactivity of TEGDA towards *Optool DSX* molecules (as evidenced by ESR) and to a contribution of the mechanical properties. Indeed, TEGDA was shown to be less elastic and harder than TEGDMA leading most probably to a higher mechanical interaction with *Optool DSX* molecules and to an earlier degradation of the release properties of the fused silica surface.

In a second time, we selected a comparable degree of conversion for the four different resists (i.e. an exposure time at the beginning of the plateau on the conversion curves) and run manual imprints. Results are reported in Figure II. 46. Below 20 imprints, all the resists have the same behavior but after that, the vinyl ether formulation showed the highest degradation, followed by the diacrylate, the dimethacrylate and the monomethacrylate ones.

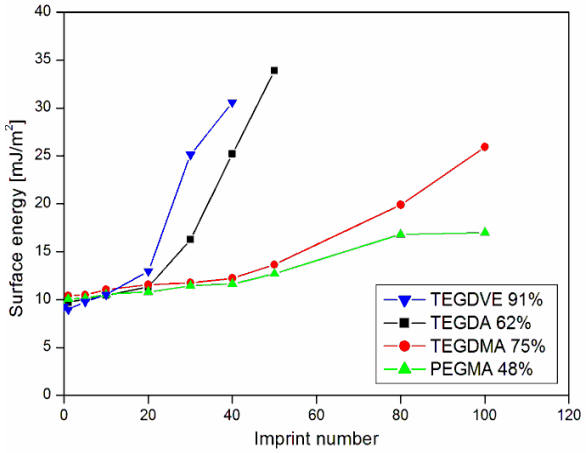


Figure II. 46: Surface energy evolution as a function of print number measured by contact angle for photo-curable monomers selected in this study, with the indication of their degree of conversion in percentage.

When the *Optool DSX* treated mold is imprinted into the mono-methacrylate based resist (PEGMA), its surface energy do not increase significantly even after hundred imprints. One can notice that although PEGMA was proven to have the higher chemical reactivity towards *Optool DSX* fluorinated molecules, the mold surface exhibits its best release properties when imprinted into this UV-curable resist. Thus, it seems that the softness of the PEGMA compensates its higher chemical reactivity and leads to an overall better antisticking performance.

Vinyl ether monomers are known in the literature for their strong adhesion to mold in the UV-NIL process.[80] This outcome is in accordance with the results shown by the TEGDVE based formulation during contact angle observations. In fact, TEGVE based resist degraded the most the anti-adhesive mold treatment although it didn't have the highest mechanical properties (these were much lower than those of TEGDA and TEGDMA formulations). As a consequence, it seems that for this cationic resist, the chemical reactivity dominates the mechanical interaction.

4.2.f Conclusion

Thanks to the tuning of their chemical and mechanical properties, four types of UV curable, low viscosity resists were proven to be very interesting for a detailed and comparative analysis of the antisticking layer degradation mechanisms. We first demonstrated that, for each UV-curable resist used, the longer is the exposure duration, the more rapid is the degradation of the antisticking molecules.

In the case of free-radical resists, we showed that 3D entangled networks (di acrylate and di metacrylate based resists) degrade much more the release properties of the quartz mold than mono methacrylate based one, although this later was shown to exhibit the higher chemical reactivity towards the antisticking fluorinated molecules. However, if we compare the di-functional monomers, the acrylate radicals seem to be more aggressive than methacrylate ones. In conclusion, the mechanical interaction between fluorinated mold treatments and free-radical UV-NIL resists seems to be dominating in the degradation mechanism for resists with $E > 1$ GPa.

In the case of the vinylether system, a high chemical interaction between the resist and fluorinated molecules is most probably at the origin of the very rapid enhancement of the mold's surface energy after repeated imprints.

4.3 Impact of fluorinated additives in the UV curable resist

4.3.a Introduction

As mentioned in Chapter I, an additional strategy to reduce the mold-surface interfacial energy is the use of fluorinated surfactant additives in the resist formulation. It has been shown that such additives are efficient when they can diffuse towards the resist-mold interface. Migration is facilitated by a fluorinated mold treatment (i.e. when the surfactant molecules have an affinity with the mold surface) and when those additives do not have any photopolymerizable groups and therefore do not participate in the photopolymerization process.[76,143,130] When the mold is not treated, almost no surfactant segregation occurs at the resist-mold interface[76] and no surfactant contribution is expected.
Here, we study the influence of fluorinated resist surfactants on the mold treatment degradation. In a first part, we compare the performance of two different surfactant products. Then, detailed XPS experiments are conducted with one of these surfactants to get more insight on its working mechanism. Finally, the effect of the concentration of this surfactant is studied.
The resist used here is the same diacrylate monomer as in § 2 & 3 and the imprinting process is the one described in § 2.4 and used in almost all the work presented previously.

4.3.b Tests with two different surfactants

The chosen surfactants are taken with a silane end-group having the ability to react with the mold surface in order to possibly regenerate the initial mold treatment. Two different products are used: 1H,1H,2H,2H-perfluorooctyl-TriMethoxySilane (called F_{13}-TMS before) and 1H,1H,2H,2H-perfluorooctyl-TriEthoxySilane (called F_{13}-TES). As shown in Figure II. 47, both had the same fluorinated chain, but a different silane end-group.

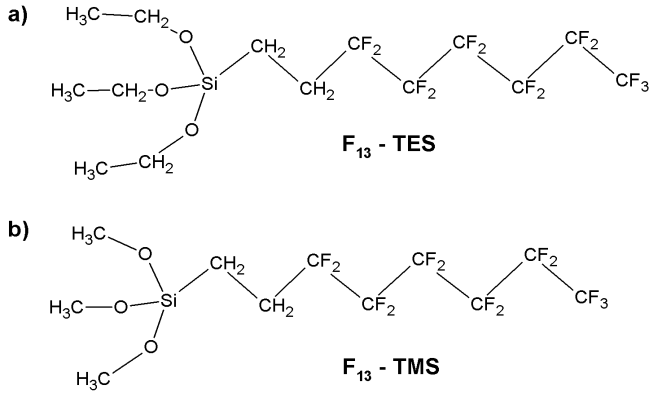


Figure II. 47: Chemical formulae of the two surfactants used. Top a): F_{13}-TES; bottom b): F_{13}-TMS.

In a first stage, we have compared a resist without surfactant with the same resist containing respectively 3 % of F_{13}-TMS and 3 % of F_{13}-TES. As illustrated in Figure II. 48, one can see that the surface energy of the mold pressed in the resist with no surfactant increases very fast: it has reached the surface energy of an untreated mold after only 40 imprints. When introducing a surfactant in the resist formulation, the increase is much slower. It is still significant with F_{13}-TMS, but there is only a slight increase after 100 imprints with F_{13}-TES where the surface energy reaches 15 mN / m. Surfactants may act by different ways: they may reduce the mechanical adherence between the mold and the resist, they may protect the initial mold treatment from a chemical attack by the resist's free radical, they may form a fluorinated deposited layer onto the mold (mold treatment regeneration or mold contamination), or most probably a combination off all those mechanisms. The fact that the surfactant benefit is very

different for the two products is surprising since they have almost the same chemical composition. One explanation might be that the two products have a different diffusion coefficient in the resist, leading to a different surfactant concentration at the mold-resist interface. Another probable reason might come from the different silane end-group reactivity. The methoxy-silane end-group is more reactive than the ethoxy-silane end-group. Then, the use of F_{13}-TMS may lead to an increased mold contamination by surfactant residues, and then by resist residues, leading to a larger increase in the mold's surface energy. To try to understand how surfactants are working, we have investigated in more details the mold and resist's surfaces by XPS in the case of the F_{13}-TES surfactant.

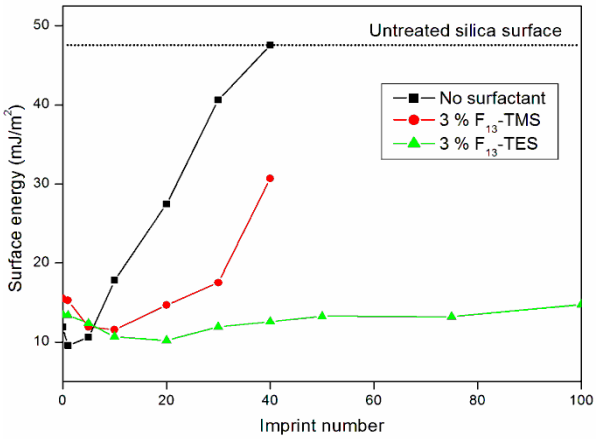


Figure II. 48: Surface energy of an *Optool DSX* treated fused silica mold as a function of the number of imprints in a resist with no surfactant and in resists with 3 % of the two different surfactants.

4.3.c XPS analysis with the F_{13}-TES surfactant

First, we have analyzed the imprinted resist surface. Carbon 1s XPS spectra of the resist surface after the 10^{th} imprint for both a resist with and a resist without surfactant are reported in Figure II. 49. Peaks with the larger binding energies, from 290 eV to 295 eV, are due to the presence of fluorocarbon bonds. Peaks centered at 294.5 and 292.1 eV are related to C*F_3 and C*F_2-CF_2 environments, respectively. Below 290 eV, all the peaks are attributed to aliphatic carbon environments. For the resist with surfactant, some fluorinated species are observed on the resist surface. These fluorinated species come from the surfactant and not from the initial mold treatment as no fluorinated species are observed in the same conditions on the resist without surfactant (no transfer of *Optool DSX* from the mold to the resist surface is observed). It is the presence of these fluorinated species at the mold-resist interface that either limits the mold's surface degradation or confers to the mold a low surface energy.

We have then analyzed the mold surface after 75 imprints in the surfactant-containing resist case. On the carbon 1s XPS spectra (Figure II. 50, left), we observe a large amount of fluoro-carbon bonds that corresponds perfectly to the composition of the F_{13}-TES surfactant. This means that F_{13}-TES molecules are adsorbed at the surface of the mold and enable to maintain its surface energy to a low value. Furthermore, these molecules remain grafted on the surface even under ultra-high vacuum in the XPS setup. No O-C*F_2 bonds (corresponding peak at 293.5 eV, characteristic of the *Optool DSX* molecule) are observed, indicating that no *Optool DSX* molecules are present at the extreme surface of the mold. This is confirmed by the oxygen 1s XPS spectra reported in Figure II. 50 (right). We observe *Optool DSX* on a newly treated mold (presence of O*-CF_2 bonds) but not after 75 imprints. After 75 imprints, we observe only O*-Si bonds coming either from the fused silica and or from the surfactant. Unfortunately, we were not able to distinguish Si*$(OC_2H_5)_3$ bonds (surfactant) from Si*O_2 bonds (mold) using the Si 2p XPS spectra (no sufficient spectral resolution in the used

conditions). Finally, this means that either the *Optool DSX* layer is degraded and or completely covered with a layer of F_{13}-TES.

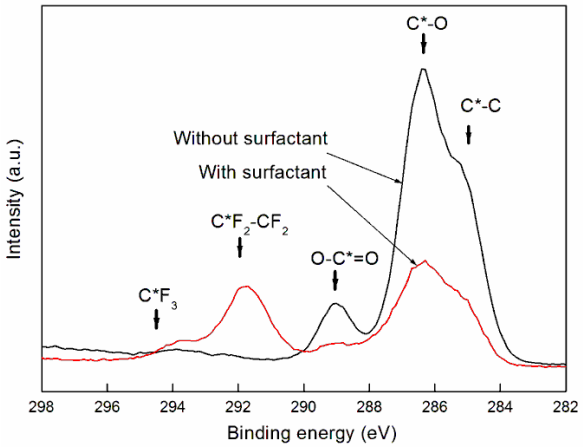


Figure II. 49: Carbon 1s XPS spectra of the resist surface (black curve: without surfactant; red curve: with F_{13}-TES surfactant) after the 10th imprint with an *Optool DSX* treated fused silica mold. Arrows indicates the positions of the different bond contributions.

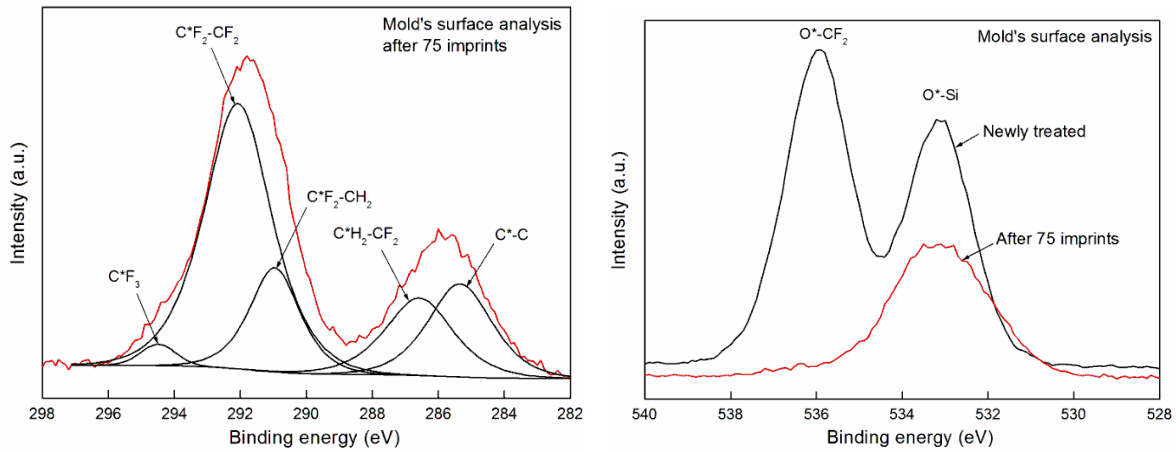


Figure II. 50: Right: Carbon 1s XPS spectra of a fused silica mold surface (initially treated with *Optool DSX*) after 75 imprints in a resist containing 3 % of F_{13}-TES and the associated chemical bond contributions (dashed curves); Left: Oxygen 1s XPS spectra of a fused silica mold surface (initially treated with *Optool DSX*) newly treated (black curve) and after 75 imprints in a resist containing 3 % of F_{13}-TES (red curve).

To try to answer to this question and to have an idea of the thickness of the newly deposited F_{13}-TES layer (spectroscopic ellipsometry is of no help here), we have recorded the Carbon 1s XPS spectra after 20 imprints only, before and after dipping the mold in a good solvent for F_{13}-TES molecules (perfluorohexane). These curves are reported in Figure II. 51. We observed that before the perfluorohexane rinse, we have a combination of both *Optool DSX* and F_{13}-TES spectra. Presence of O*-CF_2 bonds is visible at 293.5 eV. This means that the deposited F_{13}-TES layer onto the mold is extremely thin at this stage (< 5 nm, otherwise no signal would be recorded from the *Optool DSX* layer by XPS). After perfluorohexane rinse, bond contributions related to F_{13}-TES molecules are reduced and the contribution of *Optool DSX* is increased. This confirms the presence of a thin layer of F_{13}-TES at the surface and indicates also that these molecules are not all covalently grafted to the surface. Nevertheless, we do not end up with the spectra of a new *Optool DSX* treatment, meaning that this treatment is degraded and or that some F_{13}-TES molecules are well grafted to the surface.

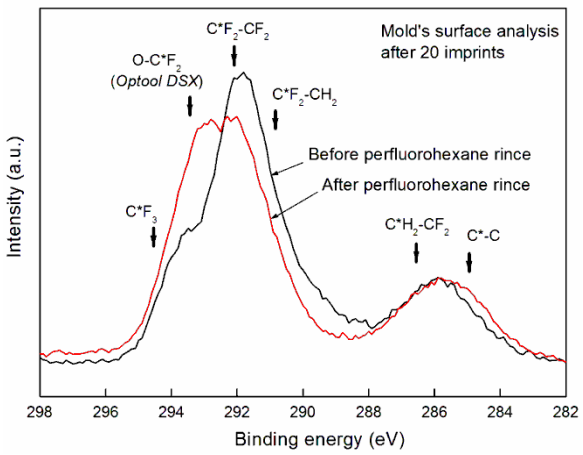


Figure II. 51: Carbon 1s XPS spectra of a fused silica mold surface (initially treated with *Optool DSX*) after 20 imprints in a resist containing 3 % of F_{13}-TES before (black curve) and after (red curve) rinsing with perfluorohexane. Arrows indicates the positions of the different bond contributions.

When pursuing the experiment up to a larger number of imprints (150), we observed that some contamination appears on the mold's active surface without increasing too much its surface energy and that these residues are not completely soluble in perfluorohexane, as illustrated in Figure II. 52. This means that, indeed, F_{13}-TES molecules can be grafted to the mold surface but that this grafting mechanism in not well controlled now.

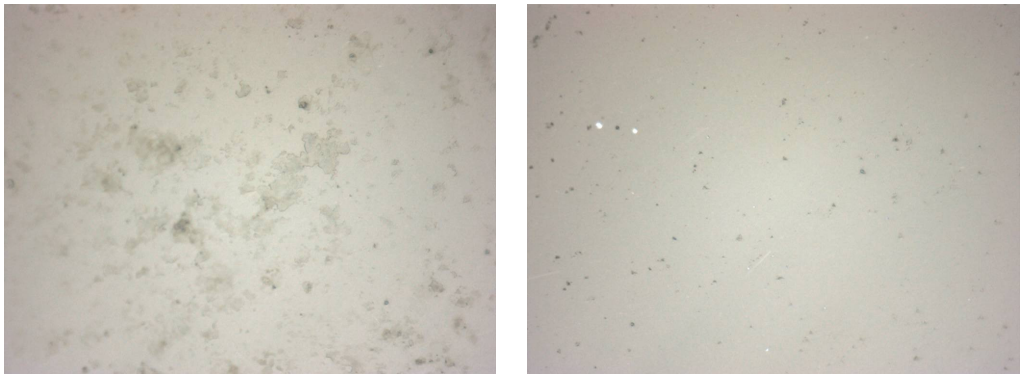


Figure II. 52: Images of fused silica mold surface after 150 prints, respectively before (left) and after (right) perfluorohexane rince. Field of view is 60*80 µm.

4.3.d Surfactant's concentration effect

Up to here, we used 3 % of surfactant in our resist formulations. This is a large amount for a component that does not participate to the cured resist polymer network. In Figure II. 53, we have reported the surface free energy of the mold surface pressed in a resist containing 0.1, 1 and 3 % of F_{13}-TES. We observe that a larger quantity of surfactant will lead to a lower surface energy increase. Nevertheless, even with 0.1 %, the benefit of the presence of a surfactant is very important compared to a resist without surfactant.

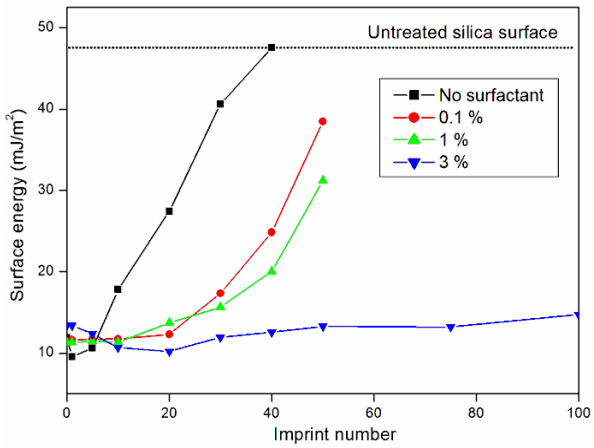


Figure II. 53: Surface energy of an *Optool DSX* treated fused silica mold as a function of imprint number in a resist with no surfactant and in resists containing 0.1 %, 1 % and 3 % of F_{13}-TES.

4.4 Conclusions

By using same tools for UV and thermal NIL in otherwise very comparable conditions, we confirmed that F-ASL are degraded much faster in the UV-NIL process, involving chemical and mechanical interactions. Nevertheless, it seems quite difficult to quantify the respective amount of chemical and mechanical contribution to the ASL degradation from these results.

By tuning the monomer's chemical and mechanical properties, we were able to say that the mechanical part of the degradation is important if we use resists with high mechanical properties (E > 1 GPa). Also, we observed a higher reactivity for the acrylate free-radicals, than for the methacrylate ones in regards to the mold treatment and showed that an over-exposure of the resist (longer exposure time that does not increase that much the conversion rate) will affect the ASL. Finally, the overall mold treatment degradation rate for the vinylether formulation is higher than the acrylate or methacrylate one, even if the mechanical properties of this resist is much lower, indicating a probable higher chemical interaction.

In a final part, we demonstrated that, by using well chosen fluorinated surfactants in nanoimprint lithography resists, it was possible to renew a perfluorinated layer at the surface of fused silica molds. Nevertheless, we showed that the created layer might lead to mold contamination after a larger number of imprints. Most probably, a balance has to be found between the reactivity of the surfactant (that seemed to increase the risk of mold contamination), quantity (0.1 % had already a significant effect) and surface grafting mechanism for an improved efficiency. Furthermore, it seemed that fluorinated surfactants did not suppress the degradation of an initial mold treatment, but, combined with low reactivity resists; it should lead to a very efficient antisticking solution.

5 Conclusions of chapter II

In this chapter, we tried to understand and overcome the degradation of fluorinated antisticking layers that are deposited on fused silica molds in the UV-NIL process. Indeed, in a classical step and repeat process, only a few wafers can be imprinted without sticking problems. By adapting our XPS measurement procedure, performing original ESR and nanoindentation experiments, tuning the resist's mechanical and chemical properties and proposing original resist formulations with reactive surfactants, we were able to:

- Demonstrate a correlation between resist's high mechanical properties and a high degradation rate of the ASL
- Quantify the reactivity between a F-ASL and a resist (free radical case)
- Demonstrate a correlation between a high UV intensity (more free radicals available at the same time) and a high degradation rate of the ASL
- Demonstrate a correlation between a high UV dose (longer reaction time + higher mechanical properties of the resist) and a high degradation rate of the ASL
- Propose a degradation mechanism of the fluorinated chains that starts at the end of the chain in the case of short self-assembled F-ASL molecules
- Demonstrate the possibility of regenerating the mold treatment by using reactive surfactants in the resist
- Demonstrate a higher chemical reactivity of vinylether resists than free-radical systems toward the ASL
- Demonstrate a higher reactivity of acrylate free radicals than methacrylate ones toward the ASL

Finally, to minimize the degradation of fluorinated mold treatments in a UV-NIL process, it appears that one should use a monofunctional methacrylate resist with a well chosen surfactant (that will regenerate the mold treatment), a low intensity UV-light source and should not over-expose the resist.

Chapter III. Application of UV curable resists in a reverse UV-NIL process

1 Introduction

This chapter is centered on the work I carried out in *Spain*, in the *Phononic and Photonic Nanostrocture group* (directed by Professor *Clivia M. Sotomayor Torres*) at the *Catalan Institute of Nanotechnology* (*ICN*, *Bellaterra* campus, *Barcelona*). The aim of this stay was to address an innovative application including UV-NIL patterning steps issued from *LTM*'s knowledge and skills. The targeted demonstration consists in fabricating 1D and 2D templates made of organic-inorganic material that can be used to improve the self organisation of di-block copolymers (BCP).

In this chapter, I will described the whole sequence of technological processes conducted in order to demonstrate the capabilities of UV-NIL combined with BCP self organisation for the fabrication of multi-scale structures. A first section will be dedicated to a brief review of BCP self assembly mechanisms and how they could be used for nanopatterning. Emphasis will be put on their high potential in term of ultimate resolution capabilities and also on their inherent limitations for large scale device fabrication. Graphoepitaxy, as a solution to circumvent this major limitation will be presented and discussed at the end of this first section. The second section will show how the UV-NIL concept was put in practice in order to fulfill the demonstration's constraints. The principle of Reverse UV-NIL (RUV-NIL), capable of features imprinting without any residual layer, will be firstly presented. Afterwards the description of the developed RUV-NIL process is given, presenting the hybrid mold fabrication procedure, the used imprinting parameters and the processed UV curable resist.

2 Block copolymers for nanopatterning

2.1 Nomenclature

When a polymer is made by linking only one type of small molecule, or monomer, together, it is called a homopolymer. When two different types of monomers are joined in the same polymer chain, the polymer is called a copolymer. Taken two different monomers, *A* and *B*, they can be made into a copolymer in many different ways, as indicated in Figure III. 1.

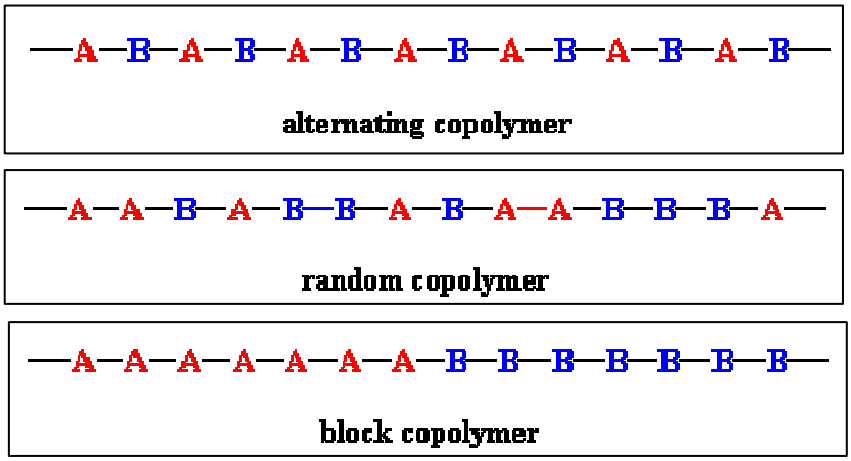


Figure III. 1: Sketches indicating different kind of copolymers that can be obtained taking two different starting monomers A and B.

When the two monomers are arranged in an alternating way, the polymer is called *alternating copolymer*. When the two monomers are arranged in an irregular way, the polymer is called *random copolymer*. Finally, when all of one type of monomers are grouped together and all of the other as well, the polymer is called *block copolymer* (BCP).

2.2 Microphase separation

Block copolymers, include two or more copolymer units covalently bonded together, can undergo microphase separation, progressing from a homogenous mixture of the constituent blocks (phase mixed) into discrete heterogonous polymer domains (microphase separated), when thermally annealed above the glass transition temperature (Tg). A wide variety of nanostructures with feature sizes close to 7 – 10 nm have been reported.[144,145] Microphase separation can also be induced by swelling the polymer films in a saturated solvent environment.[146] The final morphology for an A–B block copolymer film is governed by three parameters: the mole fraction of one block (f) with respect to the other block, the degree of polymerization for the entire polymer (N) and the segmental interaction parameter, known as the Flory–Huggins interaction parameter (χ). Figure III. 2 displays the rich variety of nanostructures which can be formed by tailoring the mole fraction (f) and the degree of polymerisation (N) for a given A–B block copolymer, based on the self-consistent-mean-field (SCMF) theory. According to SCMF theory and experimental analysis of a symmetric block copolymer phase diagram, by decreasing the concentration of an A-block dominant system towards an equal molar fraction for both blocks, phases such closed packed spheres (CPS), body centred cubic spheres (S), hexagonally packed cylinders (C), bicontinuous gyroid structure (G) and lamellae (L) should be obtainable.[147] Closed packed sphere structures have yet to be demonstrated experimentally.

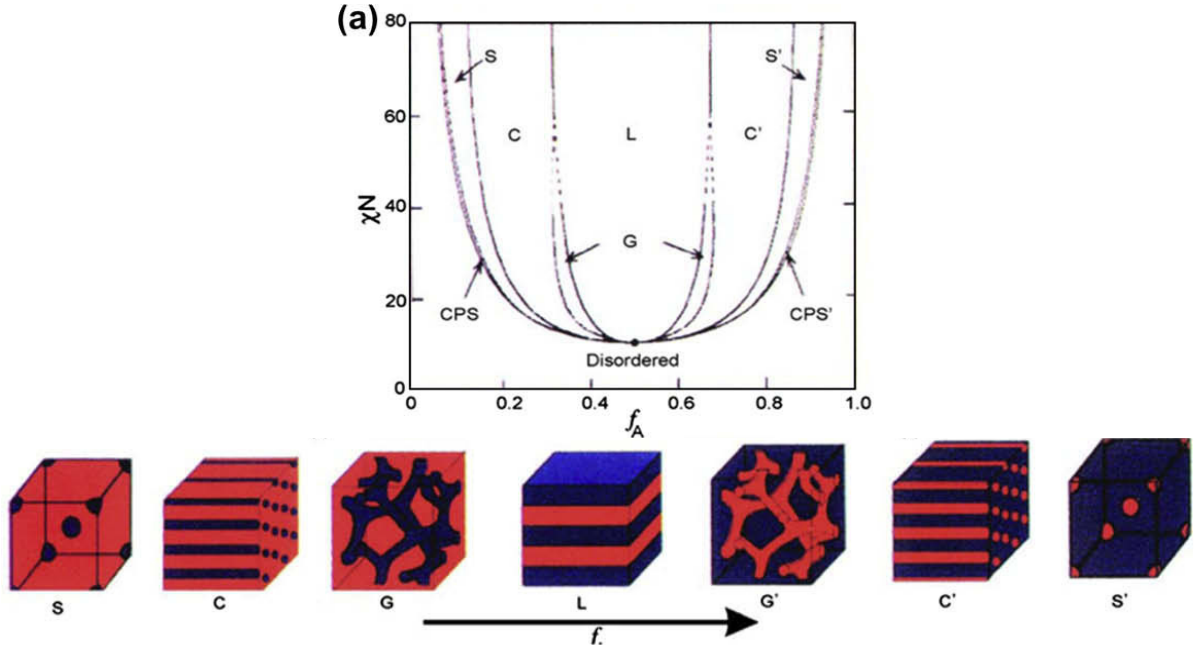


Figure III. 2: SCMF phase diagram for an A–B diblock copolymer, different microdomain structures are predicted to exist as a function of mole fraction.[148]

Undergoing microphase separation, diblock copolymers generate regular self-assembled nanostructures, whose arrangement is conditioned by the interaction with the interfaces in their proximity. For instance, a lamellar PS-b-PMMA copolymer when deposited on silicon will undergo microphase separation, with the PMMA segment preferentially wetting the native oxide of the substrate, and as a result, the PMMA and PS form alternating layers normal to the substrate (the vertical orientation of the lamellar structure is not accessible). Depending on the surface where separated BCPs are deposited, it is possible to modify their orientation. In fact, C.T. Black from *IBM* reported that the same starting material (70 % PS and 30 % PMMA) generated a matrix of hexagonal packed cylinders perpendicularly oriented to the surface but also lines parallel to surface with random orientation depending on the choice of surface pretreatment, as illustrated in Figure III. 3.[149]

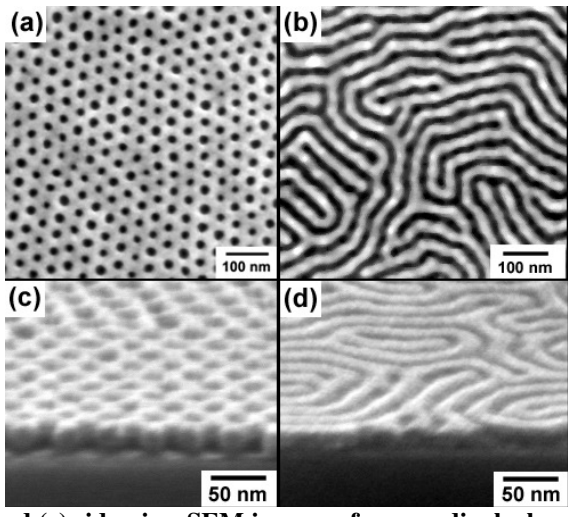


Figure III. 3: (a) Top-view and (c) side-view SEM images of perpendicularly oriented cylindrical phase (70 % PS and 30 % PMMA) diblock copolymer thin film, where PMMA was chemically removed by immersion in acetic acid. (b) Top-view and (d) side-view SEM images of the same kind of diblock copolymer but deposed on a differently treated silicon surface.

Regularity ensured by microphase separation in BCPs is becoming a subject of research for potential commercial development. Applications for BCP films in the general area of materials science include solid state battery electrolytes[150] and membrane separation technologies.[151] Park and co-workers have provided an extensive review of technologies that might be developed using BCP thin films including nanoscale electronics, magnetics and photonics.[152] By far the most researched area for use of these materials is as potential alternatives to conventional mask-based photolithography for fabrication of nanoelectronic circuitry.

Depending on the kind of application, block copolymers allow to transfer ordered features on the substrate in different ways. The schematic flow in Figure III. 4 is useful to explain the steps necessary to finally pattern the substrate. The first strategy consist on (a) self assembling BCPs (for example PS-b-PMMA), than (b) removing one of two blocks (PMMA) by plasma etching or chemical dissolution, and (c) removing an eventual under layer. After this, metal features with an ordered geometry might be fabricated by metal evaporation as depicted in Figure III. 4.

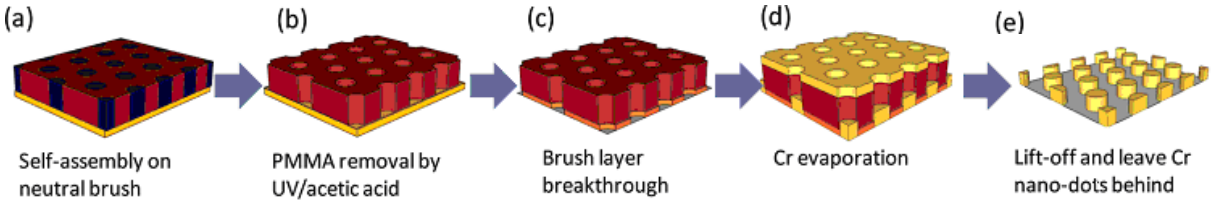


Figure III. 4: Schematic process flow showing how it is possible to fabricate ordered features on a substrate using microphase separated diblock copolymers (PS-b-PMMA).[153]

2.3 How can we align thin film diblock copolymers?

Block copolymers ensure access to high resolution features but present only a short range order after microphase separation. Indeed, the microphase separation of BCPs produces regular structures but the size of the region where the pattern displays high regularity is dependent on the thermodynamics and kinetics that describe the phase separation process. Often the patterns have 'domain' where the phase separated microstructure has a well-defined arrangement. The neighboring domains will have the same periodic microstructures but between each domain alignment of features will be random. Domain sizes can range from tens of nm to micron dimensions. A typical example is given in Figure III. 5.

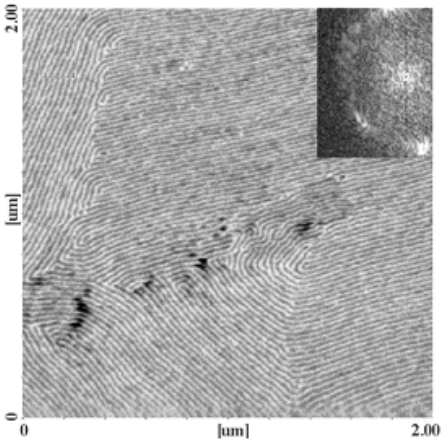


Figure III. 5: Tapping mode AFM phase image showing typical microphase separated BCP structures (cylindrical arrangement of polystyrene-block-polyethyleneoxide, PS-b-PEO, with the PEO cylinders orientated parallel to the substrate surface) formed in 50 nm thick films on silicon substrate.[154]

The presence of grain boundary type structures can arise for two main reasons. Firstly, during microphase separation, the ordered structure will nucleate at many points and these ordered regions will grow until a grain boundary wall is formed. Secondly, extrinsic defects such as substrate defects or impurities can precipitate domain structures. For practical use in electronics the feature alignment direction must be strictly controlled to allow subsequent lithographic steps to define device and interconnect structures. Thus, in recent years, control of alignment in these nanopatterns has been of pivotal importance.
Several methods have been adopted to control the microphase separation of these systems. They include electric fields,[155] where a careful design of the electrodes may lead to alignment areas of > 1 cm^2.[156] Flow fields have also been widely used and shear forces have been shown to preferentially align structures.[157] Long-range alignment aided by a directional crystallisation process has also showed significant promise for this application. In this technique a molten crystalline organic material is used as the solvent for the BCP and, during processing, the polymer microdomains align in the direction of growth of the organic crystallites.[158]
However, two techniques have become dominant because the methodology may be transferable to industrial environments for generation of large area aligned nanopatterns. These are chemical patterning and graphoepitaxy. The former, as the name suggests, involves pre-patterning the substrate surface with chemical functionality that selectively chemically interacts with one block. The microphase separated structure will then tend to align to the pre-pattern. Provided that the feature size of the chemically patterned substrate surface is matched to the feature size of the polymer pattern then the chemical interactions between the blocks and the substrate can be such as to produce almost ideal pattern of polymer.[159] The latter will be presented most in details in the following paragraph as it concerns the application on which I worked during my experiments at *ICN* in *Barcelona*.

2.4 Graphoepitaxy

In the graphoepitaxy of block copolymer assembly, a thin film is assembled within the microscale confinement imposed by a topographically patterned substrate that can endure the temperature annealing required to accomplish directed block copolymer assembly. Upon the deposition of block copolymer thin film over a prepatterned substrate and subsequent temperature annealing, as showed in Figure III. 6, the physical confinement imposed by the side wall of the topographic pattern enforces lateral ordering of self assembled nanodomains along the pattern edge.

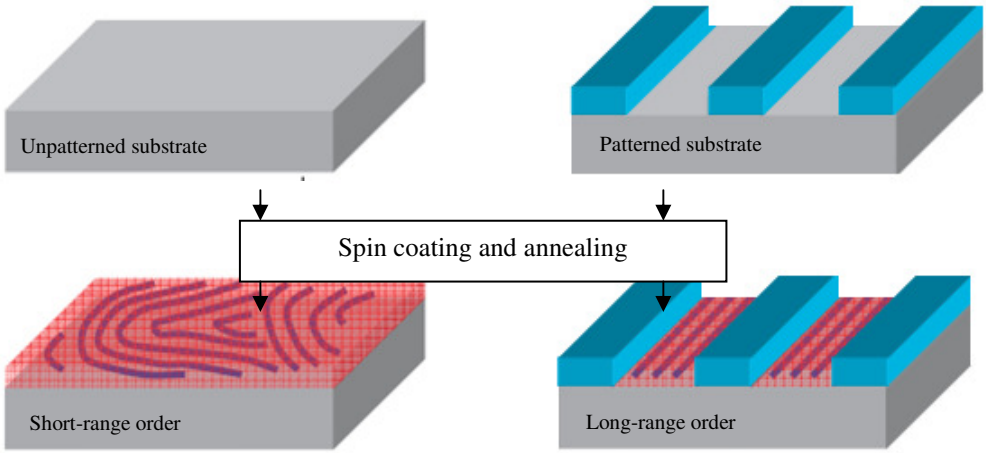


Figure III. 6: Sketch of self assembly process over an unpatterned substrate (left) and directed-assembly over a patterned substrate (right) for monolayers of horizontal cylindrical block copolymers.

The spontaneous close packing of neighboring nanodomains raises the propagation of laterally ordered morphology throughout the film plane such that a highly ordered nanopattern can be generated within the topographic confinement.[160]
It is important to underline that several parameters contribute to the arrangement of BCP in long-range order. Those concerning the BCP are essentially the thickness, the molecular weight and the annealing temperature. Another parameter concerns the interaction of BCP with the patterned substrate (named also template): the surface energy of the different patterns components (sidewalls, top and bottom surfaces as illustrated in Figure III. 7). Also the template can influence BCP arrangement through the trench width. It is, in fact, possible to have templates for which the length scale (Ls) is compared, or slightly bigger (around 10 times), or bigger (more than 10 times) than the characteristic periodicity of the block copolymer (Lo, ranging from 10 to 100 nm). Templates can be classified not only depending on the length scale (Ls) but also on the wall profile (planar or non planar). Several methods can be adopted for creating templates, depending on the dimensionality (1D, 2D, or 3D, as illustrated in Figure III. 7), length scale, and pattern requirements.

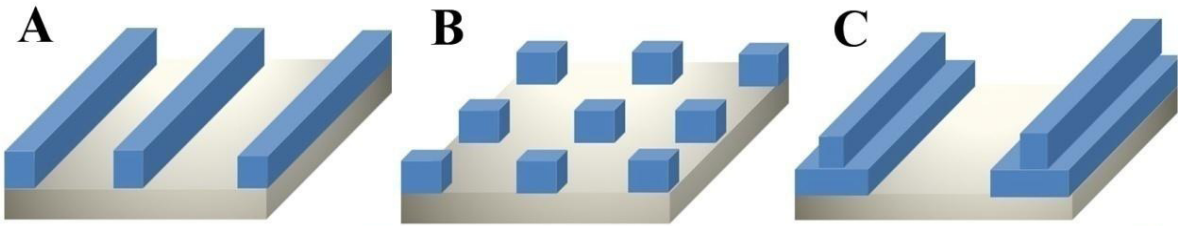


Figure III. 7: Templates for graphoepitaxy with different dimensionality, respectively 1D, 2D and 3D from (A) to (C). The different colours indicate that in templates there are elements (substrate and patterns) made by different materials and having therefore a different surface energy.

Direct-write (maskless) lithography methods are particularly suitable for fundamental directed self-assembly block-copolymer research because these methods provide patterns in the deep sub-micrometer region as well as arbitrary geometries. Imprint and soft lithography are also very useful to mold polymers and to make chemical patterns.

3 Reverse UV-NIL experiments

This paragraph is focused on the reverse UV-NIL process, which is the selected technique for the realization of templates for the long-range ordering of BCP. First, the principle of this process is presented, followed by the description of the developed RUV-NIL process (hybrid mold fabrication, imprinting parameters and UV curable functional resist synthesis).

3.1 Description of the process used

As already introduced in paragraph 2.5 of Chapter I, in the reverse UV-NIL process, the resist is spin-coated on the mold's surface (instead of the substrate surface, as done for the conventional process) and then transferred by contacting the substrate. The interest of RUV-NIL is mainly the possibility to fabricate 3D complex features by repeating the process on the same substrate and fabricating a multilayer structure.
A variant of the RUV-NIL process, called "selective transfer" RUV-NIL is used here.[161] In this case, a hybrid stamp is employed, presenting a quartz body with incorporated metal protrusions (opaque to UV-light). The principle of this technique is illustrated in Figure III. 8. An additional advantage of this technique is that features with no residual layer can be obtained, and, for BCP graphoepitaxy, it is very interesting to be able to tune independently the surface properties of the sidewalls and of the bottom surface, as depicted in Figure III. 7, and, etching the residual layer by plasma etching may change the surface chemistries.

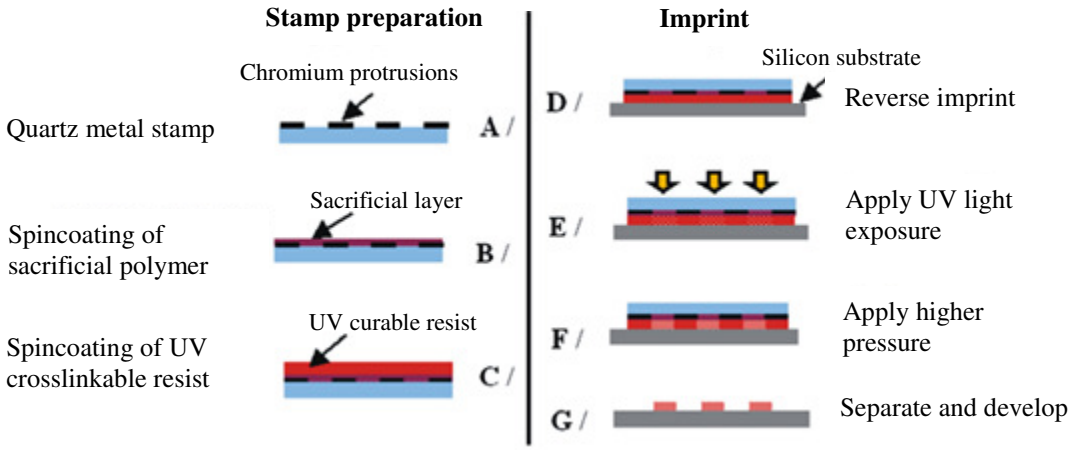


Figure III. 8: Schematic process of RUV-NIL using "selective transfer" mode.

First, (B), a sacrificial polymer layer is spin coated on a hybrid stamp with Cr protrusions (A) and successively baked to remove the residual solvent. This sacrificial polymer layer is very thin (down to 20 nm) and is used as an adherence promoter, a planarization layer and to protect the stamp from contamination by the photocuring resist. Then (C), a photosensitive resist is spin coated on the sacrificial polymer layer. Subsequently, (D), the bilayer coated stamp is reverse-imprinted onto a flat silicon substrate or on a prepatterned surface (in this case, the photosensitive resist has to be solid at room temperature in order not to flow into the prepatterned topography). Finally, (E) samples are expose to UV light, (F) a higher pressure is applied for a specific time to assist the adhesion between polymer and substrate, and (G), mold and substrate are separated and unexposed polymer areas as well as the lift-off resist are removed, leaving behind the negative features of the original stamp. By repeating this procedure three-dimensional structures can be fabricated, as illustrated in Figure III. 9 (right side). An example of a one layer grating, showing no resist residual layer, got after selective transfer RUV-NIL is presented in Figure III. 9 (left side); in this case, the oxygen plasma-etching step, usually necessary in standard NIL, is avoided.

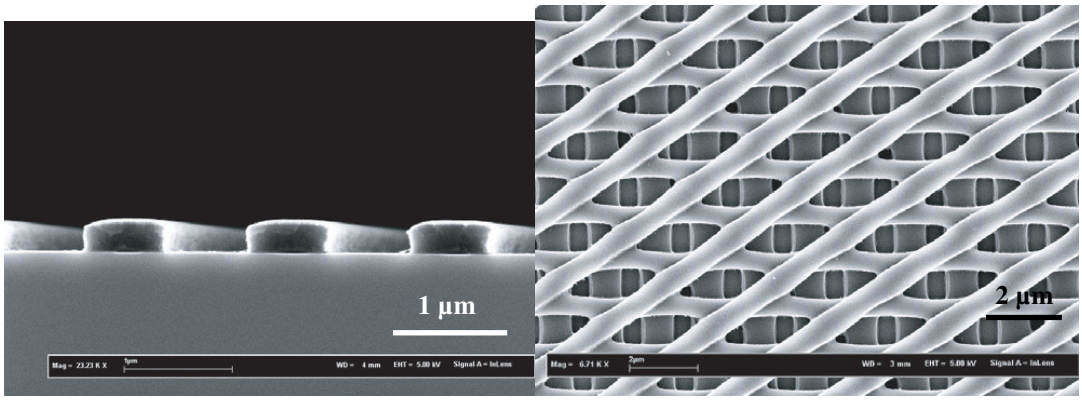


Figure III. 9: Scanning electron microscopy (SEM) image of gratings fabricated by "selective transfer" RUV-NIL (left) and SEM image of a three layer structure fabricated by "selective transfer" RUV-NIL (right).[162]

In our case, found optimized process parameters were as follow. We used a 130 nm thick commercial lift off resist (*LOR* from *Microchem* (polyimide polymer)) as sacrificial layer. The reverse imprinting of the functional hybrid UV curable resist (that will be presented later) was performed onto a flat silicon substrate at 40 °C and UV light was applied for 5 seconds. After UV exposure, a 63 bar pressure is applied for 100 s to assist the adhesion of the polymer layers to the substrate. Finally, the stamp is removed and the unexposed polymer areas are rinsed away (Shipley remover 1165).
Imprints were performed using a 2.5 inch *Obducat* nanoimprint system including a broadband mercury UV exposure lamp (emitting from 250 to 400 nm in wavelength with a power density of 420 mW/cm^2 on the whole spectrum). A screen snapshot of the imprinting tool software is given in Figure III. 10, where we can see the evolution of substrate temperature, imprint pressure and UV exposure as a function of time.

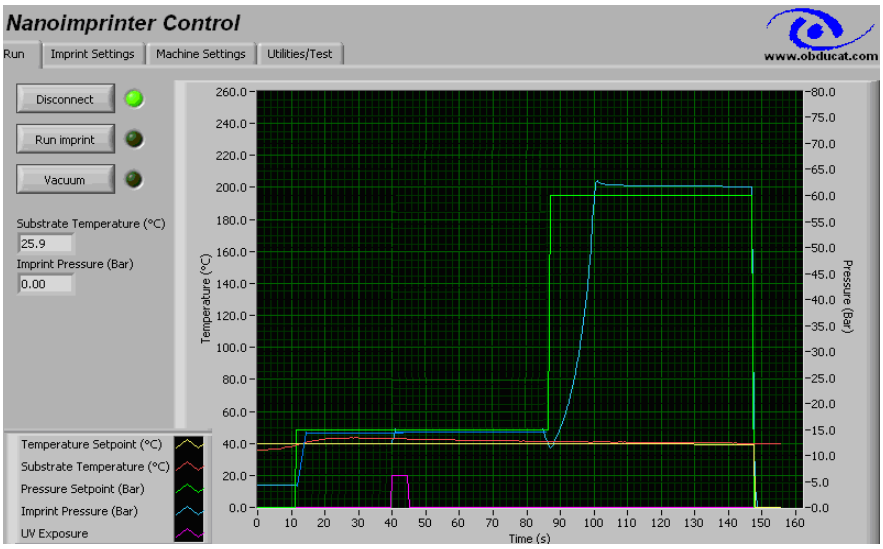


Figure III. 10: *Obducat* tool working window indicating imprinting parameters.

Description of the hybrid mold fabrication is presented in the next paragraph, while the description of the used UV-sensitive resists is given in the following one.

3.2 Hybrid mold fabrication

We fabricated hybrid molds in *Grenoble*, by using thermal NIL in the *LTM* facilities. Followed process steps are illustrated in Figure III. 11:

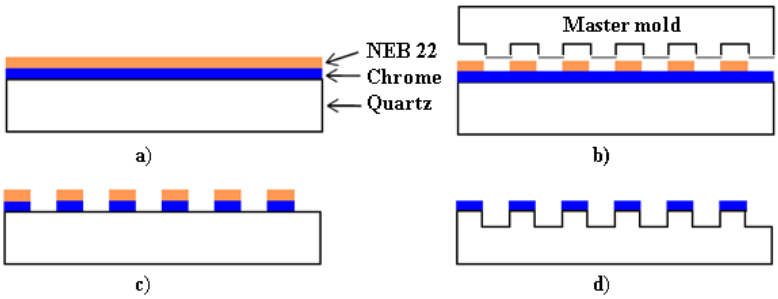


Figure III. 11: Flowchart of the hybrid mold fabrication for RUV-NIL.

Fused silica substrates (100 mm diameter, 550 µm thick), were covered with 60 nm of chrome. Then, a 300 nm thick layer of thermoplastic polymer, (*NEB22* from *Sumitomo Chemicals*), with a glass transition temperature of 80°C, was spin coated on the chrome layer (step a) layer and baked for 1 min at 90°C to remove the residual solvent. Afterwards, a master silicon mold was employed to perform a thermal NIL process at 130°C (imprinting temperature) and 15 kN (applied force) for 5 minutes, followed by polymer residual layer etching (step b). Thermal imprints were performed employing the *EVG 520* imprinting tool. Chromium etching (step c) and quartz etching (step d) were performed using an *Applied Materials Centura 5300* etching equipment into two different chambers. The chromium etching was performed in the *DPS+* chamber (60 nm of chromium were etched in 80 s in a Cl_2/O_2 plasma chemistry), while the residual resist layer and the quartz etching were performed in the *EMAX* chamber (420 nm of silica were etched at an etching rate of 3 nm/s, while 100 nm of resist residual layer were etched in 35 s, both in a CF_4 plasma chemistry). Finally, chromium/silica protrusions were 500 nm deep. Fabricated hybrid molds presented features of different shapes (lines and dots, as presented in Figure III. 12) and dimensions (for both shapes, the smallest width / space ratio was 0.2 µm / 0.2 µm, while the biggest one was 1.5 µm / 1.5 µm).

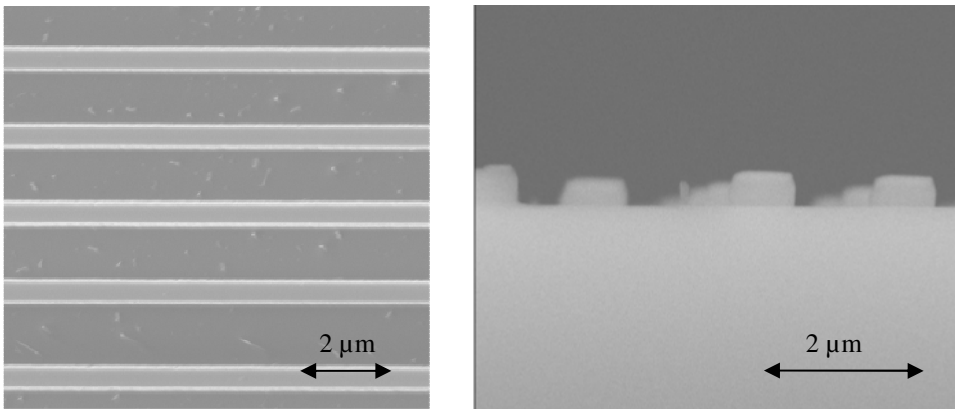


Figure III. 12: SEM pictures showing different profiles (line, top view at the left side; dots, side view at the right side) of a fabricated hybrid chromium/silica mold.

3.3 UV-curable functional resist

UV-curable resists used and developed here are organic-inorganic materials based on SilSesQuioxanes (SSQs). SSQs refer to molecules whose chemical structure follows the basic composition $R_nSi_nO_{1.5n}$. Their molecular architecture can be classified into two categories: (a) non caged structure (which includes (i) random, (ii) ladder and (iii) partial-cage structure) and

(b) caged structure (which includes (i) T8, (ii) T10 and (iii) T12 structure), as illustrated in Figure III. 13.

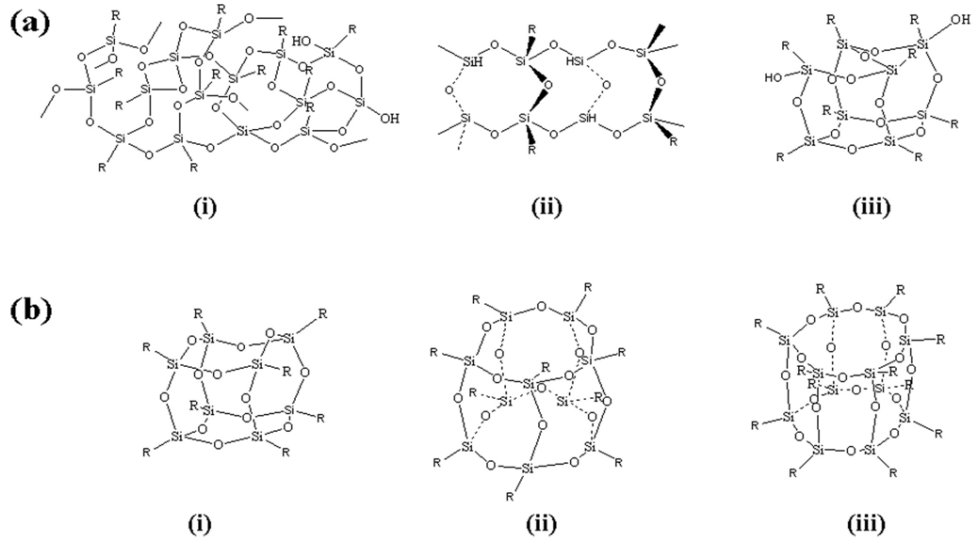


Figure III. 13: Chemical structures of silsesquioxanes. (a) non-caged silsesquioxanes: (i) random, (ii) ladder, (iii) partial caged structures, and (b) caged silsesquioxanes: (i) T8, (ii) T10, (iii) T12 structures.[163]

Cage-like silsesquioxanes are usually called Polyhedral OligoSilSesquioxanes (POSSs). POSS molecules with a T8 cubic silicon-oxygen inorganic core ($R_8Si_8O_{12}$) are the most prevalent system studied. Silsequioxanes have found uses in different applications, most notably as a direct write negative tone electron-beam resist and a low-*k* dielectric insulator material[164] in the microelectronics industry.

A recent work on aligning block copolymer nano-patterns within electron beam patterned SSQ-type templates has shown that linear and concentric hexagonal arrays of PS-*b*-PMMA lamellae can be obtained with high precision.[165] The combination of using a neutral brush layer at the base and hydrogen silsesquioanxe (HSQ) sidewalls allowed the researchers to create hexagonal arrays of parallel cylinders and concentric rings of PS-b-PMMA cylinders with low defect content. (Nano-ring shapes are particularly attractive for ferromagnetic nanostructures fabrication to be used in magnetic RAM applications.[166])

Using SSQ-based resists in a "selective transfer" RUV-NIL process appears advantageous over electron-beam in terms of time and cost. Indeed, as mentioned above, this process allows getting no residual layer between the gratings and the surface properties of the bottom surface and of the sidewalls can then be tuned independently. Also, one can play on this resist's properties to induced an improved self-organization of the BCP. Therefore, we decided to adopt RUV-NIL in selective transfer mode for fabricating 1D and 2D templates for graphoepitaxy. To achieve this target, resist's specifications are as follows:

- The resist has to present a good wetting of the sacrificial layer deposited on the hybrid stamp, giving a homogenous film after spin coating.
- The resist film should be solid at room temperature after solvent evaporation to enable reverse imprints over topography.
- The resist has to be photocurable and sufficient solubility contrast should exist after exposure to facilitate the development step.
- The cured resist should sustain the long (> 10 h) annealing time at elevated temperature (typically around 170 °C) needed for the BCP self-assembly.

It is not straightforward to have all these specification in the same resist. To fulfill these requirements, we worked on the synthesis and formulation of epoxy / T8 SSQ based hybrid materials. Indeed, organic epoxies will bring UV sensitivity and have already, in general,

correct mechanical and thermal properties. On the other hand, SSQ cages will bring more thermal[167] and mechanical[168] resistance and give a core to which it is possible to graft almost any chemical function or organic ligand.[169,170,171] The functionalization of the cages can be only partial to maintain the possibility to functionalize the material after cross-linking. A multiple functionalization is also possible. Indeed, one can think of various combinations in order to tune the surface properties (wettability, surface tension), the viscosity, the process-ability (both thermal and UV-crosslinkable functions) or the mechanical properties (hardness, flexibility).
Relatively few reports have described the successful fabrication of SSQ-based nanostructures using NIL. HSQ have been used as imprint resist materials but this material is solid and has to be imprinted before solvent evaporation and or at very high imprinting pressure.[172,173] Despite the numerous advantages mentioned above, very few commercial products exists and one has to synthesize its proper products.

4 First results

4.1 Graphoepitaxy on SSQ resists

Several formulations based on SSQ monomers were synthesized in *LTM* in the past years. They were tested as stamp replication materials[108] and evaluated as electrical interconnect dielectrics in microelectronics.[75] SSQ cages bearing eight dimethylsilyloxy groups (PSS-octakis[dimethylsilyloxy] substituted) were functionalized with polymerizable epoxy groups of different chain lengths, giving molecules called C4 (four carbons attached to the cage), C6, C8 and C10, as illustrated in Figure III. 14:

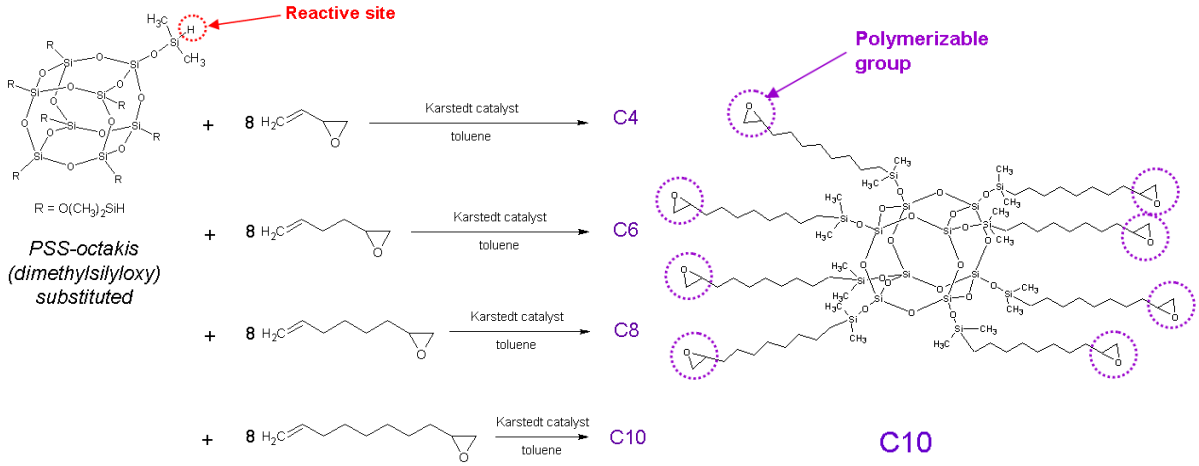


Figure III. 14: Preparation of photo-polymerizable aliphatic epoxy-silsesquioxane resists obtained by grafting epoxy alkenes chains (centre) on the PSSQ cage (left side). The final structure of C10 is presented (right).

These synthesized materials were taken into consideration as starting point for the conception of resists for BCP template fabrication. They present the expected properties as listed above; expect that they are liquid at room temperature. Then, they were imprinted in a standard UV-NIL process (presence of a residual layer) with a transparent fused silica mold and tested for graphoepitaxy experiments. First results, obtained on our templates at *University College Cork*, in *Ireland*, are presented in Figure III. 15 in the case of the C6 resist. A regular dewetting process is observed, making possible to obtain nanorings and organized droplets of different sizes.

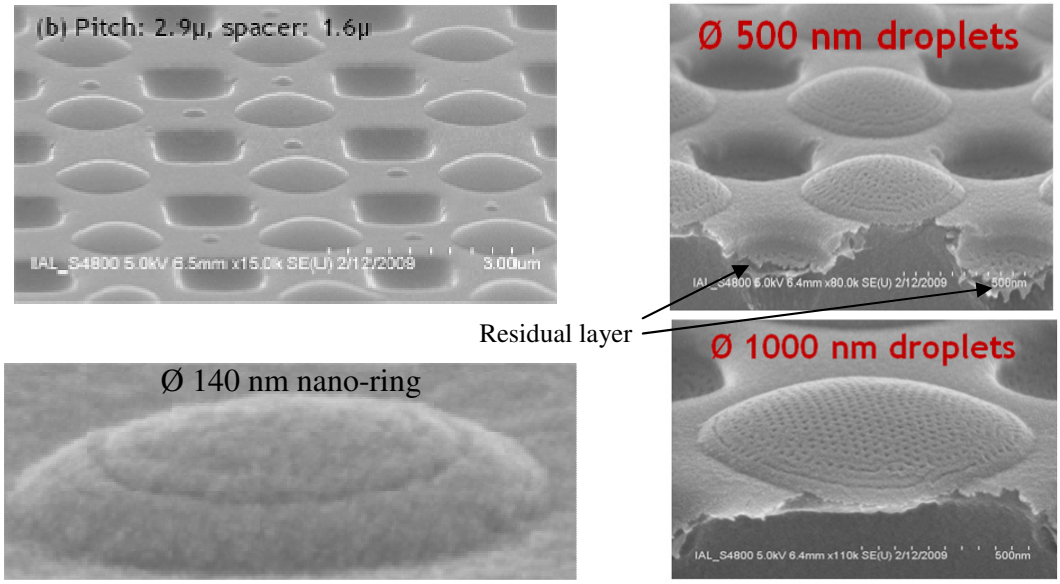


Figure III. 15: SEM images of self-organized PS-b-PMMA nano rings and micro-droplets obtained on a patterned C6 resist layer.

4.2 Development of a dedicated solid SSQ resist

Good self-organization results were obtained before, even with the presence of a residual layer on our SSQ-based templates. Nevertheless, in order to test different BCP geometries, it is necessary to have a process fabrication technique that does create directly a pattern with no residual layer (to avoid plasma etching). For this, a solid SSQ resist has to be synthesized, to be used in the "selective transfer" UV-NIL process.

Several formulations were tested, containing now also cycloepoxy functions. These materials were synthesised by Dr. *Mustapha Chouiki* (ancient collaborator of the *LTM* and partner of the new European project *LAMAND*), working in *Profactor GmbH*, *Austria*, using the general chemical reaction presented in Figure III. 16. Materials are labelled according to the number of cycloepoxies (CE) and aliphatic epoxies (C*n* in Figure III. 14).

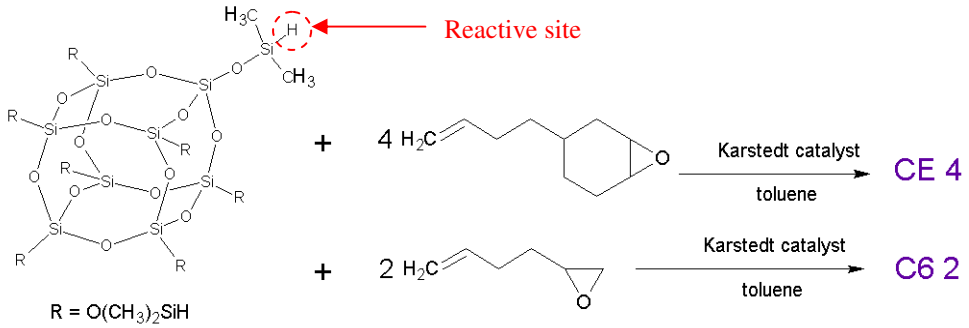
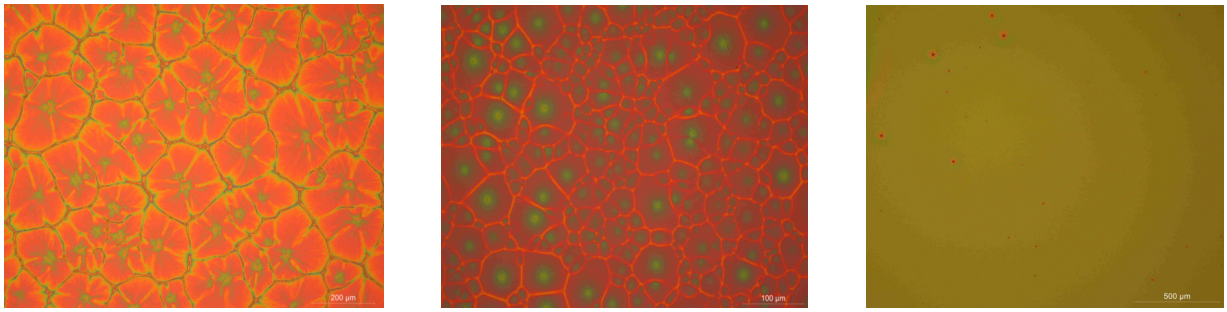


Figure III. 16: Preparation of the photo-polymerizable epoxy-silsesquioxane resist CE_4C6_2.

Solid SSQ films could be obtained with the CE_5C6_3, the CE_4 and the CE_4C6_2 resists. Nevertheless, it is in general difficult to obtain a uniform film after spincoating since solid SSQs undergoes easily crystallization as depicted in Figure III. 17.



CE_5C6_3 CE_4 CE_4C6_2

Figure III. 17: Pictures showing films generated on a silicon substrate after spincoating for three of the synthesized solid SSQ resists. Field of view is 60*80 µm.

The most interesting formulation was CE_4C6_2, which presented a good film after deposition. This formulation presents correct characteristics to be used in the "selective transfer" RUV-NIL process. It was then tested to fabricate BCP templates.
Imprinting parameters adopted where those presented before. *Darocure ITX* and *Irgacure 250* (*Ciba*) where added to the formulation as sensitizer and photoinitiator respectively. First results of the obtained templates are reported in Figure III. 18. Features seem to be well replicated into the resist. Nevertheless, these are preliminary results and a final optimization of the process with this resist (in order to get uniform zero residual layer even on sub 500 nm features for example) was not possible due to time constrains.

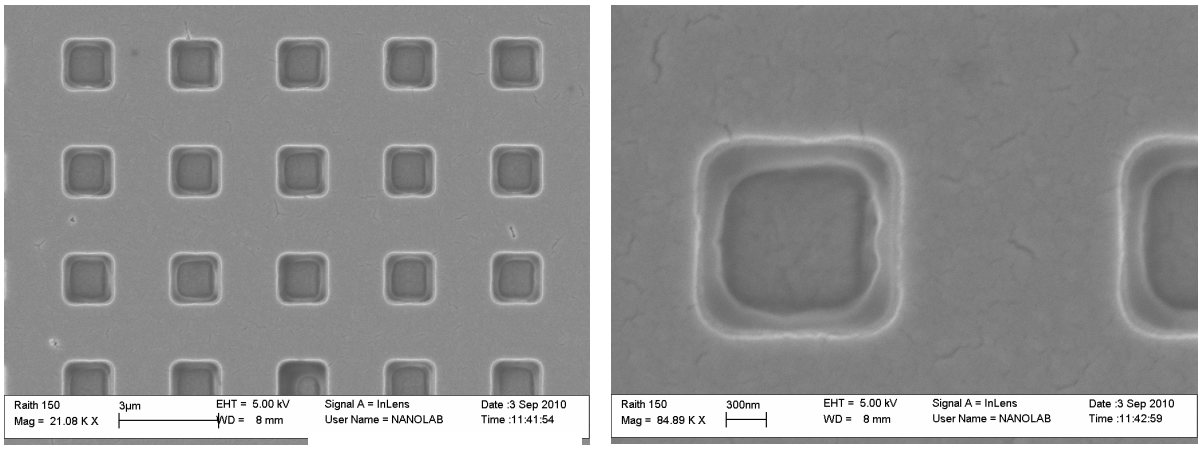


Figure III. 18: Top view scanning electron microscope image of CE4 C62 template for graphoepitaxy.

5 Conclusion

Block copolymers ensure access to very high resolution features (10 nm scale) but present a short range order after microphase separation. Several methods exist to control the microphase separated structures. Graphoepitaxy is one of these, but the template fabrication has to be made with low-cost and large area techniques to benefit completely from this kind of self-assembled processes. UV-NIL is an excellent candidate for that, especially the "selective transfer" reverse UV-NIL process presented here, where features without resist residual layers can be fabricated, avoiding the plasma etching step that is supposed to alter the template's surface properties. Also, the use of silsequioxane-type resist make possible to fabricate high mechanical and thermal resistance graphoepitaxy templates and to tune the resist's properties.

In this chapter, results are presented concerning the hybrid mold fabrication need for the RUV-NIL process and an optimization of silsequioxane resists was done in order to fulfil the requirements of this technique. The dewetting behavior of PS-b-PMMA diblock copolymers was tested on existing silsesquioxanes, and has still to be tested with the CE_4C6_2 formulation. This work will be part of a new European project called *LAMAND* which started last August 2010.

General conclusion and perspectives

This manuscript is the result of a constant work of research, aimed at supplying a contribution to critical issues concerning UV nanoimprint lithography. Thanks to its limited cost of ownership, high resolution and high throughput, this process represents a promising technique for transistor production in microelectronics industry but also for other fields of application like magnetics or photonics. Two main critical issues threaten the spreading of UV-NIL at large scale. Those are the defectivity after the imprint step and the short lifetime of the mold treatment necessarily to avoid adhesion between the mold and the resist. In my work I addressed almost only the second point.

Concerning the defectivity due to an uncontrolled resist flow, the impact of the mold treatment and of resist's viscosity and chemistry on the flowing behaviour was investigated during my work. Nevertheless, this evaluation, and a proper comparison of the used conditions, was very difficult and partial results obtained were not included in this manuscript. However, in the future, a research concerning real time scatterometry, ongoing at *LTM*, is certainly a very elegant technique to study the resist flow.

In Chapter II, we tried to understand and overcome the degradation of fluorinated antisticking layers that are deposited on fused silica molds in the UV-NIL process. Indeed, only a few wafers can be imprinted without sticking problems in a standard step and repeat process. By using at best *LTM*'s technical environment and collaborations, I was able to demonstrate that these fluorinated mold treatments undergo:

- A chemical degradation during the UV exposure
- A faster degradation with higher UV exposure intensity or dose
- A faster degradation with stiffer and harder polymerized resists
- A degradation starting at the chain end in the case of short self-assembled F-ASLs
- A partial regeneration when surface-reactive surfactants are used in the resist
- A faster degradation with vinylether resists, than with acrylate ones
- A faster degradation with acrylates then with methacrylate ones
- A faster degradation in a UV-NIL process than in a thermal-NIL process.

Nevertheless, it remains quite hazardous to think about the possibility to use non-stop the same treated mold to run an unlimited number of imprints. Most likely, a combination of low reactivity resists, resist surfactants and or mold copies will be needed to overcome this issue. Direct measurement of demolding forces, implemented in some of the prototype step and repeat systems, should allow to follow the stamp degradation and to predict the need of change or re-treatment, using then for example an automated mask cleaning sequences.[174]

Due to its low cost and high resolution on large area, UV-NIL is an extremely interesting process in combination with (low cost) self-assembled processes. In the last chapter of this manuscript, preliminary results are presented concerning a reverse UV-NIL process intended at fabricating smart templates for the long range ordering of diblock copolymers by graphoepitaxy. The dewetting behavior of PS-b-PMMA diblock copolymers was demonstrated on the type of resists developed and further work is now undergoing on this topic, mainly in the framework of the European project *LAMAND*.

In the future, NIL is still considered as a next generation lithography technique in microelectronics, but will most probably be a generic technique developed for specific

applications with specific processes and tools in the fields of optics, data storage[175] and applications requiring three-dimensional fabrication or imprinting in a functional material. In the microelectronics industry, the Cost of Ownership (CoO) of NIL was calculated not to be systematically below the CoO of photolithography. Furthermore, even if the CoO of NIL is lower, industrials are quite conservative and would like to change completely their technology only if the gain is above 30%.[176] In any case, *Hewlett-Packard Labs* claims that perfection in NIL will be too expensive and suggest the development of alternative integrated circuits technologies that are defect-tolerant.[177]

Résumé en français

Introduction

Durant les dernières décennies, la réduction incessante des dimensions caractéristiques des circuits intégrés a permis à l'industrie microélectronique de connaître un formidable essor technologique et une réelle réussite économique. En effet, la miniaturisation des composants élémentaires, tels que les transistors, a permis d'accroître considérablement la densité d'intégration des circuits fonctionnels (il y avait un seul transistor dans le premier circuit intégré en commerce en 1961, alors que en 2010 le processeur Xenon 7500 en contenait jusqu'à 2.3 milliards) mais aussi leurs performances en terme de rapidité et de complexité.
Dans ce contexte de réduction des dimensions et d'augmentation de la densité d'intégration des composants électroniques, des techniques de lithographie de nouvelle génération (ou NGL) sont constamment à l'étude. Parmi ces techniques de lithographie alternative, les techniques de lithographie basées sur la nanoimpression, sont considérées, depuis quelques années, comme une NGL pour le nœud technologique de 32 nm. Le principe de la lithographie par nanoimpression consiste à répliquer des motifs tridimensionnels sur un moule, par pressage de ce moule dans la résine, qui en remplit ses cavités. Plusieurs variantes de cette technique ont été proposées, tels que la nanoimpression thermique (NIL thermique) (où les résines utilisées sont essentiellement des polymères thermoplastiques) et la nanoimpression assistée UV (UV-NIL) (où les matériaux utilisés sont des monomères photosensibles). Cette thèse est une contribution au développement des connaissances sur l'UV-NIL, avant d'envisager son utilisation à large échelle comme un outil lithographique performant et économiquement viable. Certains points faibles peuvent empêcher l'adoption de l'UV-NIL au niveau industriel, notamment: i) une faible disponibilité de résine commerciales, ii) la production compliquée de moules en quartz de haute résolution, iii) la compréhension de l'écoulement de la résine et iv) les problèmes d'adhésion moule/résine pendant impression.

Cette thèse a été menée principalement au sein du Laboratoire des Technologies de la Microélectronique, à Grenoble, France. Il s'agit d'un laboratoire du CNRS situé à l'intérieur du site du CEA-LETI-Minatec. J'ai réalisé aussi une partie de mes travaux de thèse à l'étranger. Plus en détail : a) six mois au sein de l'Institut Catalan de Nanotechnologie (ICN), à Barcelone (Espagne) dans le Phononic and Photonics Nanostructures Group du Prof. C.M.Sotomayor Torres; b) dix jours au VTT Technical Research Centre à Espoo (Finlande).

Ce manuscrit s'articule en trois chapitres, plus précisément:

- Dans le Chapitre I j'ai présenté le contexte général de la lithographie en microélectronique et la raison pour la quelle il y a la nécessité de développer des techniques de lithographie alternatives. De plus, j'ai décrit dans le détail l'UV-NIL.

- Le Chapitre II représente le cœur de mon manuscrit. Il contient les résultats concernant la problématique d'adhésion moule/résine. On a cherché à quantifier et à comprendre la dégradation du traitement antiadhésif du moule pendant le procédé. De plus, des voies originales ont été proposées pour chercher à limiter l'impact néfaste de cette dégradation efficacement cette problématique.

- Le Chapitre III présente les résultats relatifs l'optimisation d'une résine hybride organique-inorganique que nous avons structurée par UV-NIL en vue d'une application spécifique, qui consiste à fabriquer des motifs fonctionnels permettant l'organisation à longue distance de copolymère di-blocs. Ces derniers résultats ont été obtenus en collaboration avec ICN in Espagne et l'University College-Cork en Irlande.

Chap. 1 La lithographie et la nanoimpression assistée par UV

La lithographie en micrélectronique

L'industrie microélectronique impose une réduction constante des dimensions des motifs afin d'augmenter les performances des circuits intégrés, leur densité d'intégration, et de réduire leur coût de fabrication. La lithographie étant l'étape qui définit la dimension des motifs à fabriquer, c'est aussi elle qui régit la réduction des dimensions ainsi que l'augmentation de la densité d'intégration des composants sur une puce.

Ainsi, la lithographie a permis de réduire la dimension des grilles des transistors de quelques microns à des dimensions submicroniques puis sub-100 nm, en utilisant des systèmes optiques d'exposition fonctionnant avec des longueurs d'onde (λ) de 436 nm puis 365 nm, 248 nm et 193 nm. A l'heure actuelle, les motifs de plus petites dimensions (aussi appel´es Dimensions Critiques ou Critical Dimensions : CD) fabriqués en production sont des grilles de transistor de 45 nm. Ils sont fabriqués par lithographie optique par immersion dans l'eau, fonctionnant à λ = 193 nm. Cependant, ces techniques de lithographie ne peuvent pas permettre la réalisation des nœuds technologiques futurs. C'est pourquoi des nouveaux systèmes lithographiques sont en développement pour que les nœuds technologiques 32 nm puis 22 nm puissent être produits. Ces systèmes lithographiques incluent l'extrême UV (ou EUV) qui, en utilisant une longueur d'onde plus courte (13.4 nm), devrai permettre d'obtenir des dimensions plus petites encore. Par contre, quasiment tous les matériaux absorbent les rayonnements EUV, ce qui empêche l'utilisation de systèmes optiques en transmission. On doit alors utiliser des optiques entièrement réflectives dans une enceinte sous vide, ce qui rend le prix de ces outils de lithographie EUV relativement élevé.

La lithographie électronique, basée sur l'écriture avec un faisceau d'électrons est également envisagée. Cette méthode permet de définir des dimensions de quelques nanomètres mais à cause de son type d'écriture (en série), elle souffre d'une vitesse de traitement extrêmement lente et, en tous cas, incompatible avec les contraintes de production.

La nanoimpression est une technique qui semble offrir un excellent compromis entre la résolution et la vitesse de traitement.

La mise au point de ces nouvelles technologies complexes, appelées "lithographies émergentes", doit suivre un calendrier strict (instauré par la feuille de route de l'ITRS. Selon les grandes lignes données par la version du 2009 de cette feuille de route, la nanoimpression est une des solutions envisagées pour le nœud technologique de 22 nm, prévu en production pour 2016.

La nanoimpression

Dans le domaine de la nanofabrication, la nanoimpression a été introduite par S. Chou en 1995 ; il s'agit d'une technique de lithographie dans laquelle on utilise un moule présentant une topographie de surface pour venir, par contact, déformer une résine. La résolution de cette technique peut atteindre celle de la lithographie électronique puisqu'elle ne dépend que des dimensions des motifs sur le moule, que l'on définit par lithographie électronique.
Plusieurs variantes de cette technique ont été proposées, telles que la nanoimpression thermique (NIL) et la nanoimpression assistée UV (UV-NIL), qui sont illustrées en Figure 1.1.

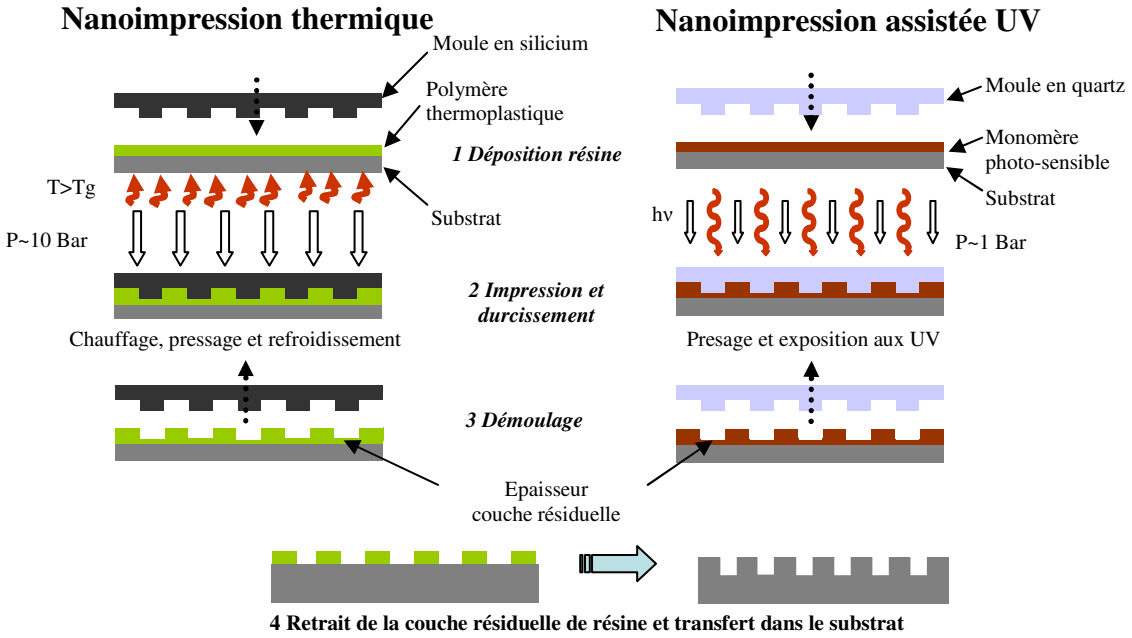


Figure 1.1: Illustration des différentes techniques de nanoimpression: NIL thermique (sur la gauche) et UV-NIL (sur la droite).

Dans la nanoimpression thermique on utilise un moule en silicium qui présente des structures gravées sur une de ses faces et un substrat en silicium recouvert d'un film de polymère thermoplastique (avec une viscosité de l'ordre de milliers de Pa s).
Le moule et le substrat sont ensuite mis en contact et chauffés à une température supérieure à la température de transition vitreuse (Tg : glass transition température) du polymère afin de transformer ce dernier à l'état liquide. Le moule est ensuite pressé dans le film de polymère en appliquant une pression de l'ordre de 10-100 bars, qui en remplit les cavités. Enfin, le moule et le substrat sont refroidis à une température inférieure à la température de transition vitreuse puis séparés. La couche de résine résiduelle en fond des motifs est alors retirée et ensuite les motifs sont éventuellement transférés dans le substrat par gravure plasma.
La nanoimpression assistée par UV prévoit aussi quatre étapes principales (déposition de la résine sur le substrat, impression et durcissement par photo-polymérisation, séparation moule/substrat et enfin retrait de la couche résiduelle), mais présente des différences importantes du point de vue des matériaux adoptés. En fait, au départ on utilise un moule en quartz, et un substrat en silicium recouvert avec un film de monomères photosensible (avec une viscosité de l'ordre de centaines de mPa s). Ensuite le moule est mis en contact avec le substrat en appliquant une pression de l'ordre de 1 bar et la polymérisation de la résine se produit après exposition aux rayons UV.
Une fois le démoulage effectué, on obtient le négatif du moule dans la résine avec une épaisseur résiduelle en fond des motifs. Cette couche résiduelle est inhérente au principe de la

nanoimpression. En effet, les résines, même très fluides, ne peuvent s'écouler sur des distances très importantes (au mieux de quelques millimètres pour les résines à base de monomères et de l'ordre de quelques microns pour les thermoplastiques) lorsqu'elles sont en couche très fines comme c'est le cas en nanoimpression (avec des épaisseurs de l'ordre du nm ou μm). Si l'on voulait atteindre une épaisseur résiduelle nulle, il faudrait appliquer une force de pression infinie. D'autre part, cette couche résiduelle protège les motifs du moule puisque ceux-ci ne sont jamais en contact avec le substrat. En revanche, il importe que cette épaisseur résiduelle soit la même sur une grande surface et quelques soient les motifs pour une raison évidente d'homogénéité des structures que l'on veut transférer par la suite dans le silicium. Une variation d'épaisseur trop importante engendrerait un non respect des dimensions des motifs après transfert dans le substrat.

Les techniques de lithographie par nanoimpression peuvent varier entre elles suite à la variation de certaines paramètres, tels que :
a) le matériau du moule : on peut en fait utiliser des moules « durs » avec un module de Young important (environ 130 GPa pour le silicium et 75 GPa pour le quartz) ou « mous » avec un faible module de Young (inferieur à 2 GPa - pour le poly(dimethylsiloxane)) ;
b) le profil du moule : il peut être plan ou cylindrique. Ce deuxième cas peut être réalisé en présence d'un substrat plan (on parle de « roll to plate lithography ») ou cylindrique (on parle de « roll to roll lithography ») ;
c) la taille du moule : il peut être plus petit ou avoir la même grandeur que le substrat ;
d) la surface où l'on dépose la résine : les variantes de nanoimpression décrites dans le schéma de la figure 1.1 prévoient que la résine soit déposée sur le substrat. Il y aussi la possibilité de déposer la résine sur la surface du moule et de la renverser sur le substrat lors de l'impression. Cette technique (appelée génériquement Reverse NIL) peut être utilisée pour la fabrication de motifs en 3D à travers l'empilement de différents niveaux.

Un autre aspect non négligeable est qu'étant donné la simplicité du procédé, l'équipement nécessaire est bien moins coûteux qu'un équipement de photolithographie conventionelle à 193 nm. Ceci rend les procédés de nanoimpression abordable pour de nombreuses applications (éventuellement hors microélectronique). Actuellement, cette technique est viable pour des applications ciblées en biologie, en optique, domaines qui ne nécessitent pas encore une grande résolution. Pour la microélectronique, les contraintes de rendement et de débit imposent des jalons difficiles à atteindre, portant essentiellement sur les problèmes de défectivité. Cette défectivité provient principalement de la mise en contact du moule et de la résine.

L' UV-NIL

Plusieurs variantes de cette technique ont été développées :

- Le procédé UV-NIL "pleine plaque" ou "full-wafer", dans lequel le moule et le substrat ont la même dimension.
- Le procédé d'UV-NIL "step and repeat" dans lequel le moule est de petite dimension (typiquement entre 2 et 5 cm de côté) comparé au substrat (typiquement 100 ou 200 mm de diamètre).
  Le principe d'UV-NIL est alors répété un grand nombre de fois sur la plaque en silicium afin de la recouvrir de motifs. Son avantage principal consiste dans le prix moins cher du moule, vu que les motifs sont contenus sur une surface plus petite. Pour ce type de procédé, deux approches de dépôt de résine sur le substrat ont été proposées :
  - La première méthode consiste à étaler la résine par centrifugation sur toute la plaquette. C'est la méthode de "dépôt par centrifugation" ou "spin-coating".
  - La deuxième variante consiste à déposer des gouttes de résines sur la puce à imprimer avant chaque pressage. C'est la méthode de "dispense de gouttes" ou "drop-dispense". Ces deux procédés sont schématisés en Figure 1.2.

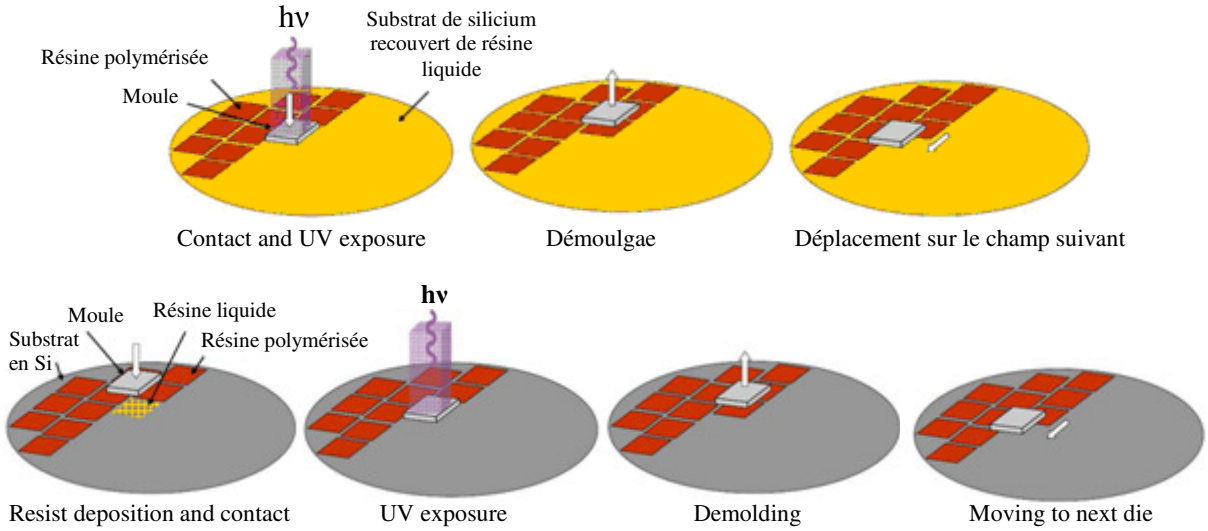


Figure 1.2: Deux différentes méthodes pour déposer la résine pour l'UV-NIL en modalité "step and repeat" : "spin-coating" (en haut) et "drop-dispense" (en bas).

Au cours de ma thèse j'ai conduit mes travaux de recherche en utilisant des moules de taille plus petite que celle du substrat et la résine était étalée sur le substrat par "spin-coating".

Résines photosensibles pour l'UV-NIL

En général la composition d'une résine pour l'UV-NIL prévoit la présence de certains élements, plus précisément: a) un photoinitiateur, responsable d'initier la polymerization de la résine après exposition aux UV ; b) un solvant, utilisé comme diluant afin d'optimiser l'épaisseur de résine qu'on souhaite déposer ; c) un (ou plusieurs) monomère(s), qui représentent les unités répétitives (peuvent être mono ou multifunctionnelles) des résaux creés après polymérisation (2D ou 3D selon la fonctionnalité des monomères) ; d) des additifs éventuels, rajoutés par exemple afin de moduler les propriétés mécaniques du réseau polymérisé (présence de groupements aromatiques) ou encore de baisser le valeur de l'énergie de surface de la résine (présence de groupements fluorés).
Les principales familles de monomers utilisés dans l'UV-NIL sont :

- les acrylates, qui se caractérisent par i) une importante disponibilité commerciale, ii) une faible viscosité, iii) une polymérisation (radicalaire) rapide, mais pouvant être inhibée en présence d'oxygène) ;
- les époxydes, qui se caractérisent par i) une insensivité à l'oxygène, ii) des proprietés mécaniques importantes, iii) une photo-polymérisation (cationique) plutôt lente) ;
- les vinyl éthers, qui se caractérisent par i) une insensibilité à l'oxygène, ii) polymérisation (cationique) plutôt rapide, iii) propriétés mécaniques importantes et iv) une disponibilité commerciale limitée).

Il faut remarquer qu' il n'y a pas beaucoup de résines UV-NIL à l'échelle commerciale. Les producteurs actuellement présents sur le marché sont Nanonex, Micro resist technology, Molecular Imprint, AMO, Toyo Gosei et AGC.

Points forts de l'UV-NIL

a) Le premier point est qu'utilisant un moule en quartz, transparent aux longueurs d'ondes du spectre visible, on a la possibilité d'aligner plus facilement plusieurs niveaux de lithographie, ce qui ouvre la voie à plus de domaines d'applications qu'en nanoimpression thermique.

b) Ensuite, la polymérisation se faisant sous UV, on utilise une résine photosensible constituée de monomère et d'un photo-amorceur. Ces résines, qui ont un poids moléculaire bien plus faible que les thermoplastiques, peuvent fluer sur de grandes distances (de l'ordre du mm). L'influence de la répartition des motifs sur le moule est donc moins critique qu'en nanoimpression thermique et les pressions utilisées pour le pressage sont bien plus faibles (typiquement 1 bar).

c) De plus, le procédé de « step and repeat » adopté en UV conduit à un moule ayant une surface active plus petite. Sa fabrication est ainsi facilitée et on aura des motifs plus homogènes. En effet, le fait de devoir fabriquer un moule de 200 mm de diamètre en nanoimpression thermique alourdi l'étape de lithographie et en augmente le coût.

d) Enfin, il n'y a pas de cycle thermique, d'où un débit de fabrication potentiellement plus rapide et pas de problèmes de distorsions ni de défauts dus à des différences de coefficients d'expansion thermique entre le moule et le substrat.

Limites de l'UV-NIL

A l'heure actuelle, l'état de développement de la nanoimpression thermique est suffisant pour des applications dans le domaine, de la photonique, de la microfluidique et de la biologie. En effet, cette technique est une alternative intéressante à la lithographie électronique et cela en apportant une économie financière ainsi qu'un gain de temps. En revanche, pour une application en microélectronique, seule l'UV-NIL peut être envisagée mais il reste encore de deux jalons principales à franchir pour qu'elle soit intégrée dans la feuille de route de la microélectronique:

a) Tout comme en thermique, le moule vient en contact avec la résine ce qui rend la technique très sensible à la contamination particulaire. Contamination qui est un frein réel pour atteindre une défectivité raisonnable. Ce problème est d'autant plus important que l'on utilise généralement ici des pressions d'impression plus faibles.

b) Pour aider au démoulage, un revêtement antiadhésif est déposé sur le moule (en NIL thermique comme en UV-NIL). Cependant, celui-ci se dégrade plus vite en UV-NIL qu'en thermique. Il faut donc retraiter le moule plus souvent, ce qui diminue le rendement de la technique et amène des défauts supplémentaires. Le nombre d'impressions réalisées avant de retraiter le moule avec l'antiadhésif est beaucoup trop faible. Il faut arriver à multiplier le nombre d'impressions par 1000 pour que l'UV-NIL devienne intéressante en microélectronique.

Chap. 2 La problématique d'adhésion moule/résine

Introduction et contexte

Le collage entre le moule et la résine durant l'étape de démoulage est un réel problème puisqu'il conduit à l'arrachage des motifs de la résine comme on peut le voir sur la figure 2.1.

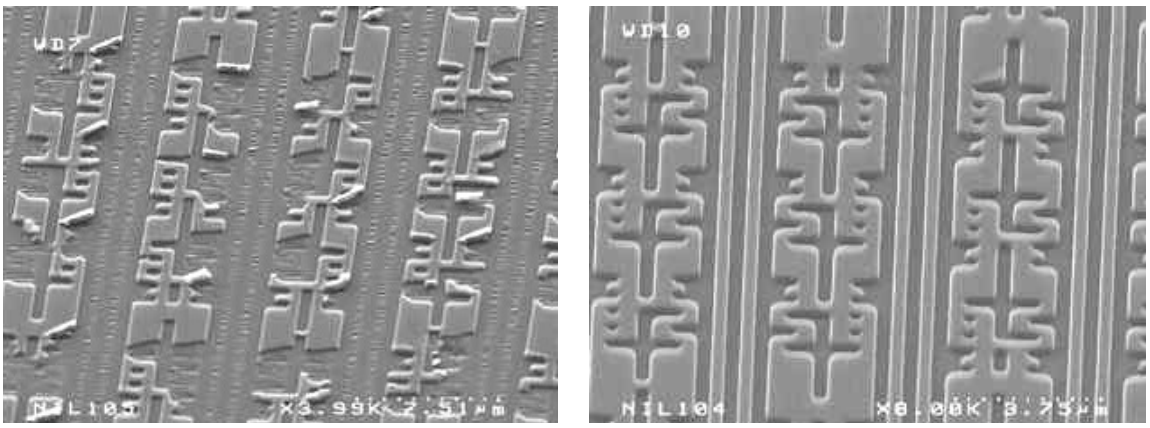


Figure 2.1: Motifs de résine imprimés par UV-NIL, après démoulage: avec arrachage (sur la gauche) et sans arrachage (sur la droite).

Ce problème est un point bloquant pour un procédé qui doit être viable, aussi bien à court terme qu'à long terme. Plusieurs possibilités ont été envisagées pour rendre le démoulage le plus propre et le moins destructif possible. Le principe étant toujours de minimiser les interactions entre la résine et le moule de façon à ce qu'il n'y ait pas d'affinité entre les deux et ainsi que la séparation des deux soit aisée. Pour cela, on cherche à minimiser leur énergie de surface soit en traitant la résine, soit en traitant le moule, soit en jouant sur la composition des résines, soit finalement en combinant toutes ces approches.

Différentes solutions peuvent être envisagées pour résoudre cette problématique.
a) Le traitement de la résine. Par la littérature on sait qu'un traitement plasma fluoré (CF_4 ou SF_6) sur des résines thermoplastiques à l'état solide avant impression provoque la dégradation des liaisons carbone-oxygène pour créer des liaisons carbone-fluor. De cette façon on diminue l'énergie de surface et les forces d'adhérence, mais cette solution n'est pas indiquée pour des résines pour l'UV-NIL (qui sont liquide à température ambiante). De plus, elle ajoute une étape supplémentaire dans le procédé et demande la mise au point d'une recette plasma pour chaque résine.
b) Le traitement du moule. Deux possibilités sont envisagées pour traiter le moule. Le but de ces traitements est de diminuer l'énergie de surface du moule. Pour cela, on peut déposer une fine couche de matériau inorganique de faible énergie de surface comme le $SiO_{(1-x)}C_x$ ou le carbone cristallisé (carbone possédant un arrangement cristallographique différent de celui du diamant) sur le moule. Le problème avec ces matériaux est qu'il est difficile de les déposer en couche très fine de quelques nanomètres. Une alternative est de déposer une couche épaisse de ces matériaux et de définir les motifs dans cette couche. Le deuxième traitement consiste à greffer une monocouche auto-assemblée de molécules fluorées à la surface du moule, ce qui permet d'obtenir une énergie de surface de l'ordre de 10 $mN.m^{-1}$. L'expérience montre que le greffage de cette couche permet effectivement de séparer le moule de la résine sans arracher de motifs pour un nombre d'impressionnes limités.
c) L'optimisation de la composition de la résine. Il est possible de traiter la résine avec des molécules fluorées (surfactants). Dans la littérature, il a été montré que ces petites molécules migrent en surface au plus près du moule, en diminuant le risque d'arrachage. Il existe

également des résines à base de monomères fluorés (NIF, Asahi Glass Company, Japon) qui montrent des bons résultats après démoulage. La surface d'un moule traité avec une molécule fluorée permet un démoulage plus facile avec des résinés contenant du fluor vu la forte compatibilité entre les deux surfaces.

Dans tout les cas, il s'avère indispensable de traiter le moule afin d'assurer un démoulage optimum. Le choix d'une molécule fluorée présente plusieurs avantages. Le traitement est assez facile à mettre en œuvre et il peut être réalisé plusieurs fois, ce qui permet de recycler le moule. De plus, ce traitement est indépendant de la composition chimique de la résine. Le recyclage est très intéressant car il permet de réutiliser les moules dont le traitement a été dégradé. Malgré cette dégradation, il est possible d'effectuer un certain nombre d'impressions (variable selon les résines utilisées, étude en cours au laboratoire) mais cela reste un gros problème. Il faut donc comprendre cette dégradation afin de trouver des solutions pour limiter le vieillissement du traitement. Le but à atteindre étant de traiter une seule fois le moule pour toute sa durée de vie.

Aperçu de la littérature

Le nombre de publications portant sur l'antiadhésif dans le procédé UV-NIL est en augmentation depuis 2007. Elles traitent aussi bien d'hypothèses concernant la dégradation de la couche antiadhésive, que d'alternatives permettant de se passer de ce traitement. En ce qui concerne les hypothèses, certains parlent d'une dégradation purement mécanique entre la résine et le traitement antiadhésif lors du démoulage, alors que d'autres mentionnent une dégradation provenant d'une interaction chimique entre le traitement et la résine. Les méthodes de caractérisation principalement utilisées pour ces études sont la spectroscopie de photoélectrons X, la mesure d'angle de contact et d'énergie de surface. Globalement, il en ressort que le problème est complexe parce qu'il dépend aussi bien de l'antiadhésif utilisé que de la résine photosensible. C'est pourquoi des alternatives comme la réplication de moule dans des polymères permettant de faire des moules jetables bon marché commencent à être étudiées. Ce survol de la littérature montre bien l'importance de compréhension des mécanismes de dégradation de la couche antiadhésive.

La stratégie suivie pendant cette thèse pour analyser la problématique d'adhésion moule/résine a été la suivante : on a dans un premier temps adopté une molécule commerciale fluorée largement utilisée dans la littérature (Optool DSX fourni par la compagnie Daikin) pour traiter la surface du moule en quartz. On a évalué les propriétés physico-chimiques du traitement avant impression et puis après impression, suite à la mise au point d'un protocole expérimentale pour chaque différent technique d'analyse. Dans un deuxième temps on a adopté d'autres molécules fluorées et mené une étude comparative avec l'Optool.

Analyse de la couche antiadhésive avant impression

La molécule Optool DSX, illustrée en figure 2.2, est un perfluoro-polyéther tri-methoxy silane que l'on dépose en phase liquide. A l'issue de ce traitement on va créer des liaisons covalentes siloxanes (Si-O-Si) entre la surface du moule et les groupements d'ancrage methoxy silanes de la molécule d'Optool.

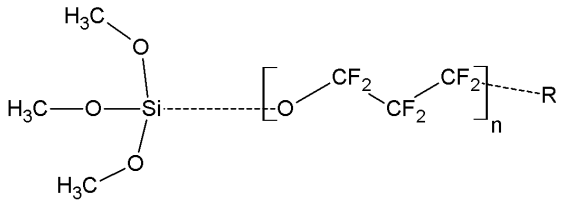


Figure 2.2: Formule chimique de l'Optool DSX.

La couche antiadhésive a été caractérisée après déposition par ellipsométrie montre une épaisseur de l'ordre de 3 nm (vu que la longueur théorique de la molécule calculée est égale à 15 nm, ceci signifie que les molécules sont pliées sur elle mêmes). Puis par angle de contact on a mesuré l'énergie de surface d'une surface en silicium et d'une autre en quartz après traitement, en obtenant la même valeur pour le deux substrats (au tour de 10 mJ/m^2). On a mesuré aussi l'angle de contact formé par des gouttes d'eau sur chaque substrat, égal à environ 115° et indiquant en effet une surface très idrophobe. On a même analysé les deux surface traitées du point de vue chimique par spectroscopie de photoélectrons X (XPS). La mise en place d'une procédure d'acquisition correcte par XPS n'a pas été très simple pour ce qui concerne le substrat en quartz. La nature isolante de ce matériau provoque une accumulation de charge positive en surface venant de la disparition des électrons photo-émis. Cette accumulation représente une barrière d'énrgie supplémentaire, qui se traduit par une perte d'énergie cinétique des électrons. Par conséquence on obtient des énergies de liaison plus importantes lors de la mesure. Pour s'affranchir de ce problème un canon à électron est utilisé : il permet de compenser l'excès de charges positives (durée de la compensation entre 20 min et 2 heures). Il est donc nécessaire effectuer correctement la compensation de charge (qui se fait sous rayonnement X) avant de démarrer l'acquisition des spectres XPS. En suivant l'évolution du spectre de Carbone de l'Optool DSX en fonction de différents temps d'exposition aux rayons X on a constaté une dégradation (diminution d'intensité des pics) due aux rayons X. Une nouvelle procédure d'acquisition a été donc élaborée : la compensation de charges est effectuée sur une zone de l'échantillon et, pour l'acquisition, on se déplace d'une distance équivalente à la taille du faisceau des rayons X (400 μm). La mesure est ainsi effectuée sur une zone non altérée.

En observant les spectres du carbone de l'Optool DSX déposé sur un substrat en quartz et un autre en silicium on constate que le greffage de la molécule se produit de la même façon (vu qu'on retrouve des spectres qui présentent les mêmes énergies de liaisons et des pics d'intensité pratiquement identiques, en largeur et hauteur), comme illustré en figure 2.3.

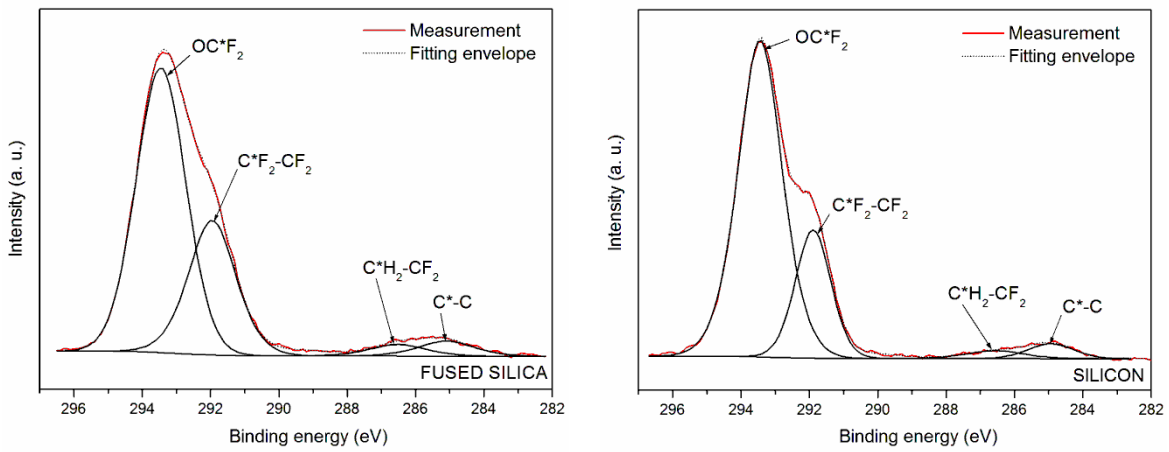


Figure 2.3: Spectre XPS du carbone 1s pour une surface en quartz (sur la gauche) et en silicium (sur la droite) après déposition de la molécule Optool DSX. Les liaisons chimiques correspondantes sont indiquées (courbes noires).

Analyse de la couche antiadhésive après impression

Après avoir identifié des techniques capables de caractériser le traitement antiadhésif après déposition et avoir mis au point un protocole expérimental pour chacune entre elles, on a étudié le comportement de telle couche après plusieurs impressions.

Pour les impressions on a utilisé une résine (étalée sur un substrat en silicium de 200 mm) à base de monomère diacrylate (Laromer 8765), de photo-initiateur radicalaire (Irgacure 379) et l'ethyl lactate en tant que solvant. Le stepper EVG770 a permis de réaliser des impressions comparables entre elles ; après polymérisation la résiné présentait un taux de conversion de 75% (mesuré par spectroscopie infrarouge à transformée de Fourier (FTIR)). Les moules en quartz utilisés pendant les impressions sont de petite taille (25x25 mm^2 de surface en contact avec la résine).

Avec un même moule traité Optool on a réalisé plusieurs impressions; son énergie de surface augmentait au fur à mesure qu'on augmentait le nombre d'impressions, comme illustré en figure 2.4.

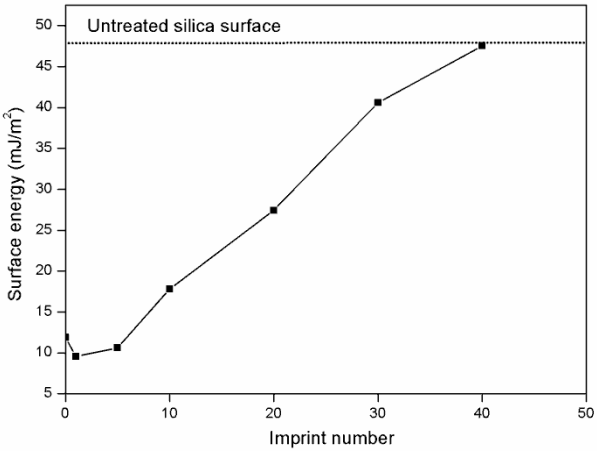


Figure 2.4: Energie de surface en fonction du nombre d'impressionnes pour un moule en quartz traité avec Optool DSX.

Cette augmentation d'énergie de surface se traduit par une dégradation de la couche antiadhésive avec une séparation moule/résine de plus en plus difficile pendant le démoulage. On a suivi, par XPS, l'évolution du spectre carbone de l'Optool DSX pour la surface d'un moule traité et ainsi que sur la surface de résine après 10 impressions. Ce qu'on en déduit est

que la dégradation de la couche antiadhésive est due à la progressive diminution des composantes fluorés de l'Optool DSX (OCF_2 et CF_2-CF_2). Par contre on n'a pas distingué des variations chimiques importantes (capables de nous renseigner sur le mécanisme de la dégradation) en observant la surface de la résine à cause de la longueur de la molécule fluorée.

Après avoir démontré l'existence d'une détérioration du traitement antiadhésif, on a cherché à mieux comprendre l'origine de cette dégradation. Pour cela on a évalué l'impact possible de plusieurs paramètres.
1) L'exposition du traitement anthiadhésif du moule aux rayons UV n'induit pas de changements. En effet l'exposition aux UV pour une durée variable (entre 0 et 2000 s) de la surface en quartz traités avec l'Optool a été démontrée comme n'ayant aucun effet sur la longévité du caractère hydrophobe de ces moules : l'angle de contact formé par une goutte d'eau sur la surface est resté constant (et égale à 115°).

2) La procédure de recyclage d'un moule traité peut impacter la durée de vie du traitement. La procédure de recyclage adoptée consistait à enlever les résidus d'un traitement dégradé et d'en déposer un autre «comme à nouveau » (correctement greffé et avec des valeurs d'énergie de surface bien reproductibles). Une suite de traitement plasma et de nettoyage « humide » a été mise en œuvre et validée par une analyse physico-chimique de l'état de surface après nettoyage et après retraitement.

3) Les radicaux produits dans la résine lors de l'exposition ont un impact direct sur la dégradation de la couche antiadhésive. Pour pouvoir analyser ces espèces on a utilisé de façon innovante la résonance paramagnétique électrique (RPE). Les échantillons analysés par RPE doivent être contenus à l'intérieur de petits tubes en verre. A fin de reproduire l'interaction entre un moule en quartz traité avec une molécule antiadhésive et une résine photosensible on a formulé des mélanges composés par billes en silice (de taille micrométrique) et la même résine utilisée lors des impressions (mais dans ce cas sans solvant). Plus précisément, comme illustré en figure 2.5, on a comparé les spectres RPE obtenus par 3 tubes différents : un (spectre en verte) contenant de la résine et des billes non traitées avant exposition; un autre (spectre en noire) contenant de la résine et des billes non traitées après exposition ; un autre (spectre en rouge) contenant de la résine et des billes traitées avec Optool après exposition.

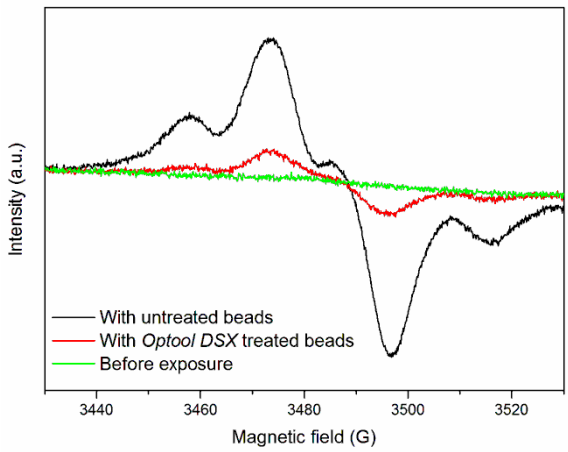


Figure 2.5: Superposition de spectres obtenus par analyse RPE de mélanges de résines UV-NIL avec des billes de silice, répresentative du matériau du moule, vierge ou traitée avec Optool DSX.

Le spectre vert confirme l'absence de radicaux en l'absence d'exposition aux UV. Vu qu' on observe une diminution entre l'intensité du signal obtenu après exposition en présence de billes non traitées par apport au mélange contenant des billes traitées, on peut affirmer que le traitement antiadhésif est attaqué chimiquement par les espèces radicalaires produites lors de la polymérisation.

Evaluation d'autres traitements antiadhésifs

Après avoir évalué l'impact de plusieurs paramètres sur la dégradation de la molécule Optool DSX, nous avons choisi d'observer le comportement d'autres traitements effectués avec d'autres molécules commercialisées lorsque le nombre d'impression croît.

La molécule Fluorolink S10, fournie par Solvay Solexis et illustrée en figure 2.6, a été testée dans un premier temps. Elle se dépose en phase liquide et sa particularité est la présence de 2 groupements d'ancrage (un pour chaque extrémité, de type ethoxysilane) par apport à l'Optool DSX, caractérisé par la présence d'un seul groupe d'ancrage.

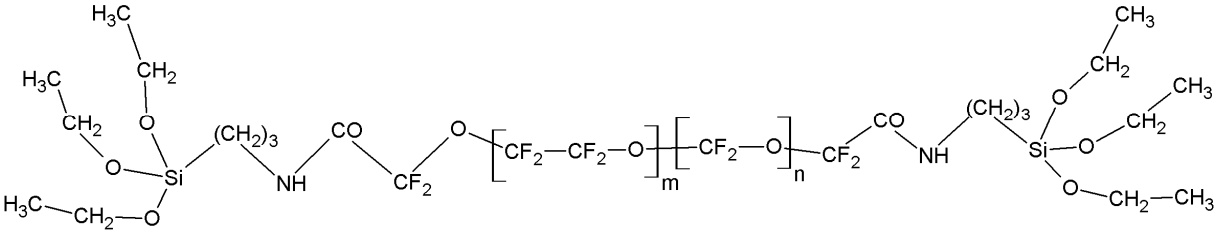


Figure 2.6: Formule chimique du *Fluorolink® S10* (m/ n= 1.5 - 2.5, 2 < n < 5, 5 < m < 9).

Dû à la présence d'un double ancrage, on pense que les chaines de la molécule se greffent en formant des ponts sur la surface du moule en quartz.
L'étude de l'évolution de l'énergie de surface en fonction du nombre d'impressions (qu'il permet d'observer le comportement global d'un traitement antiadhésif, compte tenu de toutes les causes possibles de dégradation) montre que le FLK S10 et l'Optool DSX ont un comportement similaire. Par contre selon les observations par RPE le FLK S10 est plus attaqué chimiquement par les radicaux libre. Donc, le comportement similaire entre les deux différents antiadhésifs lors des mesures d'énergie de surface est expliqué avec une meilleure stabilité mécanique du FLK S10 lors du démoulage. Cette hypothèse est plausible en raison de la présence du double greffage.

La deuxième molécule étudiée est le F_{13}-TMS, fournie par ABCR et illustrée en figure 2.7. Elle se dépose en phase liquide également, présente un seul groupement d'ancrage (de type methoxy silane) et sa particularité est le fait d'avoir une molécule plus courte que celle de l'Optool DSX (longueur théorique : 3 nm). Les chaines de F_{13}-TMS sont donc disposées de façon verticale sur la surface du moule.

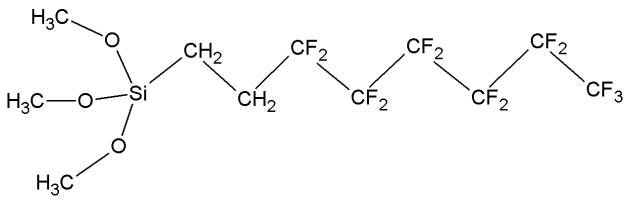


Figure 2.7: Formule chimique du F_{13}-TMS.

Les observations par XPS ont donné des résultats très pertinentes- En effet il a été possible d'identifier et de suivre l'évolution de toutes les liaisons chimiques présentes dans la molécule

(même la liaison CF_3, qui représente la queue). En observant le spectre XPS du carbone on a pu mieux comprendre le mécanisme de dégradation : la molécule se dégrade progressivement tout le long de la chaine (on observe en fait la disparition de la liaison CF_3, puis la diminution de CF_2- CF_2 et CH_2- CF_2).

Evaluation de l'impact de la résine photosensible sur la dégradation de la couche antiadhésive

On s'est intéressé à savoir si les propriétés de la résine photosensible pouvaient influer sur la dégradation de la couche antiadhésive et si oui, quels en étaient les mécanismes.
1) On a étudié l'influence du nombre et de la typologie des fonctions polymérisables en formulant les résines illustrées en figure 2.8.

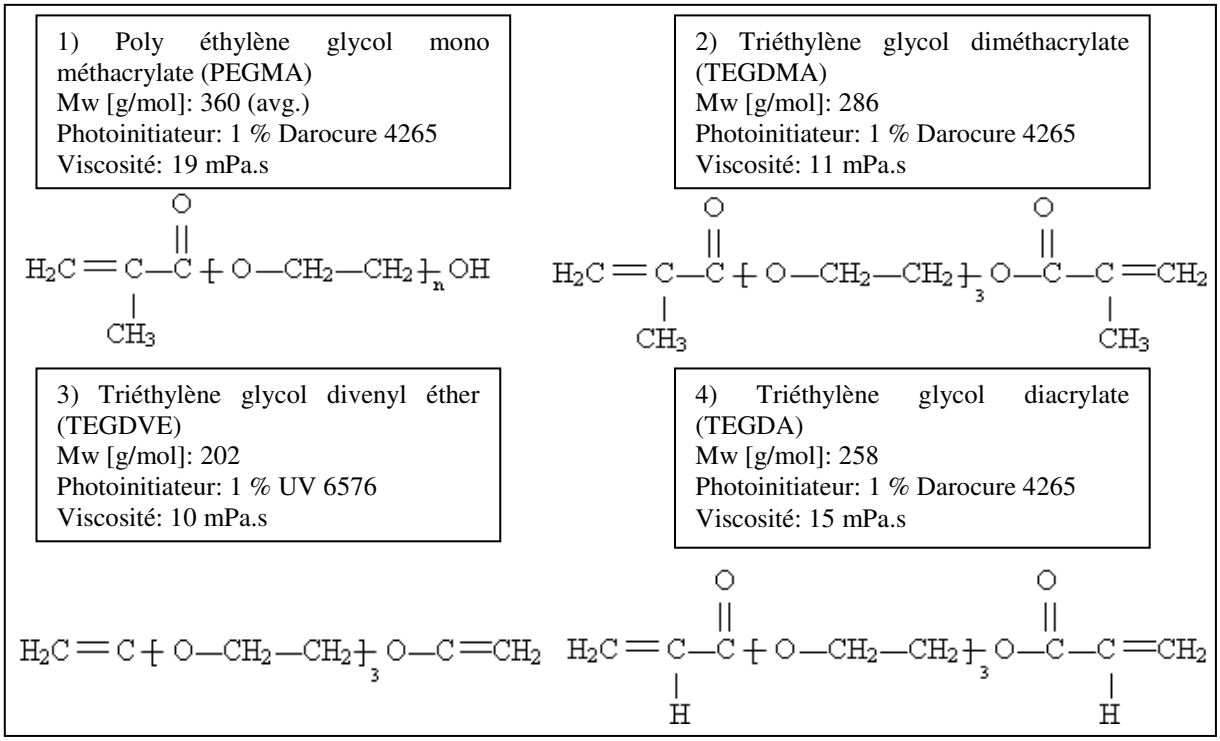


Figure 2.8: Formulations des résines utilisées dans cette étude.

Les résines formulées présentent la même chimie (de type triéthylène glycol), une viscosité et un poids moléculaire assez proches. Nous avons choisi d'utiliser pour les résines radicalaires le même pourcentage du même photo-initiateur (1% Darocure 4265) afin de rester dans des conditions expérimentales permettant une étude comparative. Une résine à polymérisation cationique (di-vinyl éther) a également été intégrée dans cette étude.
Les résines sélectionnées ont été caractérisées par FTIR (détermination du taux de conversion en fonction de la dose d'exposition aux UV), par RPE (détermination de la réactivité chimique vis-à-vis de billes de silice traitées avec Optool DSX), par nanoindentation (détermination de la dureté et du module élastique en fonction de la photopolymérisation), par angle de contact (afin de suivre l'évolution de l'énergie de surface en fonction du nombre d'impressions).
Après avoir corrélé les résultats des différentes analyses on a obtenus des informations importantes, jusqu'à présent jamais publiées dans la littérature. On a tout d'abord démontré que pour toutes les résines analysées plus la durée de l'exposition aux UV est longue, plus la dégradation du traitement antiadhésif est rapide. Ceci s'explique par la croissance du nombre

De radicaux libres générés dans la résine en fonction de nombre de photons incidents.
La résine qui dégrade plus fortement la couche antiadhésive est celle à base de vinyl éther, en raison d'une très forte interaction chimique (vu que les propriétés mécaniques sont moins importantes que celles des résines radicalaires di-fonctionnelles).
En ce qui concerne les résines de type radicalaire, les résines di-fonctionnelles, capables de générer après polymérisation un réseau 3D, dégradent le traitement du moule de façon plus importante que la résine à base de mono-méthacrylate même si ce dernier avait montré une plus grande réactivité chimique vis-à-vis de la molécule d'Optool DSX (par contre ses propriétés mécaniques sont plutôt faibles, juste supérieures à celles de la résine cationique) .
La résine à base de diacrylate montre une plus grande réactivité chimique que celle de type di-méthacrylate, alors que les propriétés physiques sont comparables entre les deux résines.
On peut donc conclure que pour les résines de type radicalaire difonctionnelles, l'interaction mécanique résine/molécule fluorée lors du démoulage a un impact plus important par apport à l'attaque chimique.

2) On a modifié la formulation de la résine à base de monomères de type diacrylate (déjà adopté lors de l'étude de la dégradation de la molécule Optool DSX en fonction du nombre d'impressions), en ajoutant un surfactant fluoré. Sa formule chimique est illustrée en figure 2.9.

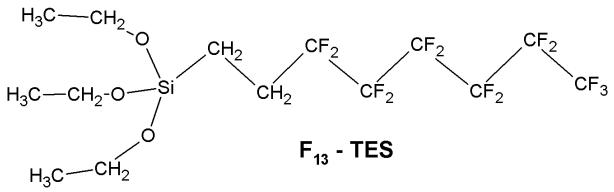


Figure 2.9: Formule chimique du surfactant fluoré F_{13}-TMS.

Les surfactants fluorés sont connus dans la littérature pour leur capacité de migrer à la surface de la résine et d'interagir avec la surface d'un moule traité (avec une molécule fluorée). Cette interaction, due à la forte affinité entre la surface du moule d'un côté et la surface de la résine de l'autre, permet de baisser l'énergie de surface du moule.
La particularité du surfactant F_{13}-TES est qu'il présente un fonction d'ancrage de type ethoxy silane, capable de se greffer, après migration, à la surface du moule.
Pour connaître le pourcentage de surfactant à rajouter, on a suivi, grâce aux mesures de l'angle de contact, l'évolution de l'énergie de surface d'un moule traité Optool après plusieurs impressions dans des formulations de résine contaminant un pourcentage variable de surfactant (respectivement 0.1, 1 et 3% en masse). La formulation qui a abouti à une croissance moins rapide de l'énergie de surface a été celle contenant 3% de F_{13}-TES.
On a donc étudié par XPS la surface du moule traité et de la « résiné modifiée » après plusieurs impressions. On a pu bien reconnaître la présence du surfactant sur la surface de la résine imprimée et surtout sur celle du moule (ceci signifie qui il a réussi à se greffer à la surface du moule). Grâce à ce greffage, il a été possible de réaliser un nombre d'impressionnes (150) bien supérieur à celui obtenus en son absence (environ 50). Par contre après 150 impressions on a assisté à la parution de contaminations sur la surface du moule : il reste donc à optimiser et mieux comprendre le mécanisme de greffage de ce surfactant.

Chap. 3 Application d'une résine photo-sensible dans le procédé UV-NIL reversible.

La grapho-épitaxie

La grapho-épitaxie est une technique qui permet d'arranger à longue distance (de l'ordre du cm) de façon ordonnée les copolymères à bloc (il s'agit de polymères contenant différent monomères liés par liaisons covalentes, par exemple A et B, qui se répètent régulièrement le long de la même chaine, -AAAAA-BBBBB-). Les copolymères à bloc ont la capacité de se dissocier en microphases séparées (avec une taille de l'ordre du nm) à partir d'une phase mixte après avoir suivi un traitement thermique approprié). Après séparation, ils présentent un ordre à courte distance (de l'ordre du nm ou µm). L'intérêt de pouvoir arranger les copolymères à bloc à longue distance réside dans le fait que l'ordre ainsi obtenu peut être utilisé pour structurer, à bas coût, des grandes surfaces permettant la fabbrication de dispositifs de très forte densité d'intégration sans faire appel à aucune technique de lithographie conventionelle.
Afin d'arranger les copolymères à bloc par grapho-épitaxie, il faut disposer d'un substrat présentant une topographie, comme illustré en figure 3.1. De cette façon il est possible d'obtenir, après leur déposition et réchauffement, un arrangement avec ordre à longue distance (au lieu d'en avoir un à courte distance en présence d'un substrat sans topographie).

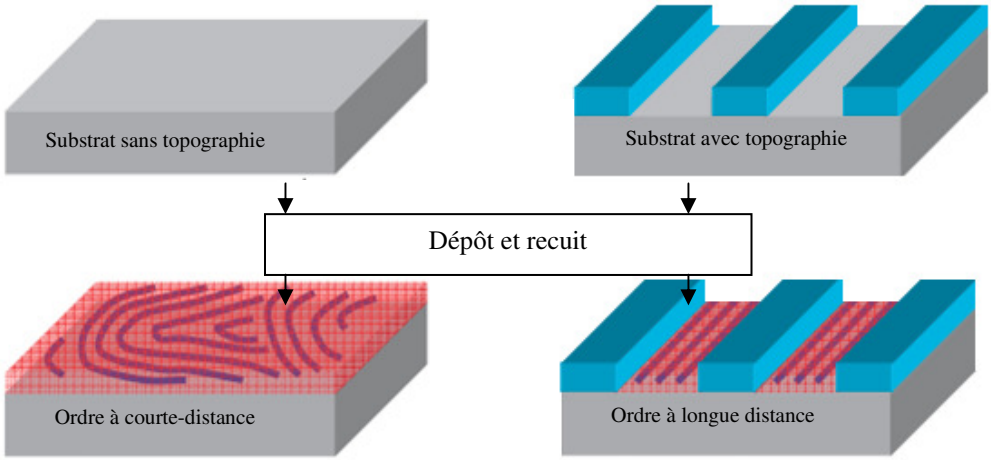


Figure 3.1: Schéma du procédé d'auto-assemblage sur un substrat sans topographie (sur la gauche) et d'assemblage-dirigé (sur la droite) avec des copolymères à bloque.

Un des paramètres importants pour l'arrangement des copolymères à bloc par grapho-épitaxie est la présence d'une valeur différente d'énergie de surface entre les deux surfaces avec les quelles ils sont en contact (le profile vertical du motif et le substrat).

L'UV-NIL renversé

L'UV-NIL renversé est une variante de l'UV- NIL. Les différentes étapes du procédé sont illustrée en figure 3.2. Il faut utiliser un moule hybride (en quartz avec des protrusions opaques vouvertes de chrome) sur le quel on dépose un polymère sacrificiel, qui a la fonction de promoteur d'adhérence et de protection de la surface du moule Puis on dépose une résine photosensible. L'étape suivante consiste à renverser le moule hybride recouvert, en le mettant en contact avec le substrat. Pour la suite on a l'exposition aux UV à travers le moule hybride, puis l'application d'une pression afin d'assister l'adhésion entre la résine et le substrat. On termine avec la séparation et le développement des zones qui n'avaient pas polymérisées lors

de l'exposition car protégées par les protrusions parque que masquées par les protrusions opaques.

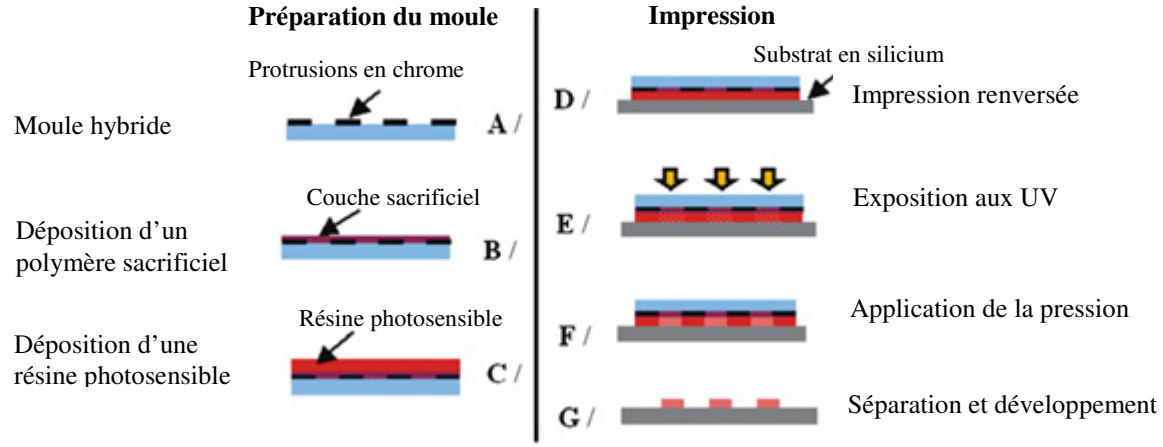


Figure 3.2: Schéma du procédé UV-NIL renversé.

L'UV-NIL renversé représente une technique capable de produire les substrats avec une topographie adéquate pour la grapho-épitaxie, les quels sont habituellement réalisés par lithographie électronique. Les avantages de l'UV-NIL renversé pour cette application sont plusieurs : a) la rapidité du procédé dans la structuration du substrat ; b) il n'est pas nécessaire de traiter la surface du moule hybride avec un revêtement antiadhésif ; c) il permet d'obtenir, après développement, une topographie sans aucune épaisseur résiduelle de résine (il garanti donc une différence entre l'énergie de surface du profile vertical du motif et le substrat).

La résine photosensible

Je me suis occupé d'optimiser les paramètres du procédé UV-NIL renversé (afin d'obtenir un substrat avec topographie pour arranger les copolymères PS-PMMA) en utilisant une résine hybride organique-inorganique. La résine sur la quelle j'ai travaillé est illustrée en figure 3.3.
Il s'agit d'une résine à base de monomères de sislsesquioxane avec une structure chimique en forme de cage, contenant à chaque sommet un atome de silicium (formule $R_8Si_8O_{12}$, avec R qui indique un substituant). La cage a été fonctionnalisée avec 4 chaines contenants 6 atomes de carbone et une fonction ciclo-époxie (CE_4), mais aussi avec 2 chaines contenants 6 atomes de carbone et une fonction époxie ($C6_2$).

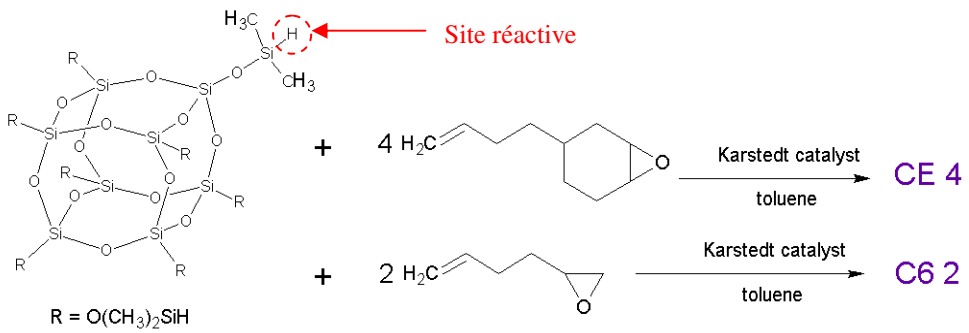


Figure 3.3: Préparation de la résine photosensible de type epoxie-silsesquioxane, CE_4C6_2.

La résine utilisée devait satisfaire des conditions imposées par l'utilisation du procédé UV-NIL renversé. En particulier :
- avoir une bonne mouillabilité avec le polymère sacrificiel déposé sur le moule hybride, en donnant un film homogène après dépôt ;

- être solide à température ambiante après dépôt sur la surface du moule, afin de permettre son décollement sur le substrat sans couler ;
- être photosensible et présenter un bon contraste afin de pouvoir être développée ;
- résister au recuit avec longue durée (température d'environ 170°C pour une durée supérieure à 10 heures) nécessaire pour pouvoir arranger à longue distance les copolymères à bloc après dépôt sur le substrat avec topographie.

Ultérieures analyses doivent être faites afin de vérifier si la résine utilisée permet d'atteindre totalement les critères requises par le cahier des charges de la grapho-épitaxie

References

[1] http://spectrum.ieee.org/semiconductors/design/shrinking-possibilities/0
[2] G. E. Moore, "Cramming more components onto integrated circuits", Electronics 38(8), 1965.
[3] http://www.organdi.net/article.php3?id_article=82
[4] P.B. Meggs, "A history of graphic design", book ISBN 0-471-291-98-6, John Wiley & Sons Inc, p. 146, 1998.
[5] L. J. Guo, "Recent progress in naoimprint technology and its applications", J. Appl. Phys. D 37(11), p. R123-R141, 2004.
[6] http://www.almaden.ibm.com/st/chemistry/lithography/process/
[7] http://www.ece.gatech.edu/research/labs/vc/theory/photolith.html
[8] R. F. Pease and S. Y. Chou, "Lithography and Other Patterning Techniques for Future Electronics", Proc. IEEE 96(2), p. 248-270, 2008.
[9] B. Fay, "Advanced optical lithography development from UV to EUV", Microelectron. Eng. 61, p. 11-24, 2002.
[10] http://www.nikon.com/products/precision/society/story0203/index.htm
[11] R. H. French and H. V. Tran, "Immersion lithography: photomask and wafer-level materials", Annu. Rev. Mater. 39, p. 93-126, 2009.
[12] W. Hinsberg, G. Wallraff, C. Larson et al., "Liquid immersion lithography-evaluation of resist issues", Proc. SPIE 5376, p. 21-33, 2004.
[13] http://willson.cm.utexas.edu/Research/Sub_Files/DoubleExposure/index.php
[14] http://www.itrs.net/Links/2009ITRS/2009Chapters_2009Tables/2009_Litho.pdf.
[15] W. Trybula, "Directions in maskless lithography", Future FAB International, Sect.5, p. 74-76, 2005.
[16] D. Henry, J. W. Gemmink, L. Pain et al., "Status and future of maskless lithography", Microelectron. Eng. 83, p. 951-955, 2006.
[17] H. Kinoshita and O.Wood, "EUV lithography: An historical perspective," in EUV Lithography, V. Bakshi, Ed. SPIE Press, 2008.
[18] S. Sivakumar, "R&D Status and key technical and implementation challenges for EUV HVM", Workshop Proceedings of 2009, International Workshop on EUV Lithography.
[19] R. M. Hudyma and R. Soufli, "Projection systems for extreme ultraviolet lithography," in EUV Lithography, V. Bakshi, Ed. SPIE Press, 2008.
[20] B. LaFontaine, Y. Deng, R.-H. Kim et al., "The use of EUV lithography to produce demonstration devices", Proc. SPIE 6921, p. 69210P-69210P-10, 2008.
[21] G. F. Lorusso, J. Hermans, A. M. Goethals et al., "Imaging performance of the EUV alpha semo tool at IMEC", Proc. SPIE 6921, p.69210O, 2008.
[22] H. Meiling, E. Boon, N. Buzing et al., "Performance of the full fiels EUV systems", Proc. SPIE 6921, p. 69210L-13, 2008.
[23] S. Uzawa, H. Kubo, Y. Miwa et al., "Canon's development status of EUVL technologies", Proc. SPIE 6921, p. 69210N-8, 2008.
[24] S. Y. Chou, P. R. Krauss, and P. J. Renstrom, "Imprint of sub-25 nm vias and trenches in polymers", Appl. Phys. Lett. 67(21), p. 3114-3116, 1995.
[25] A. Fuchs, M. Bender, U. Plachetka et al., "Lithography potentials of UV-nanoimprint", Curr. Appl. Phys. 8(6), p. 669-674, 2008.
[26] J. Haisma, M. Verheijein, K. van den Heuvel et al., "Mold-assisted nanolithography: a process for reliable pattern replication", J. Vac. Sci. Technol. B 14(6), p.4124-4128, 1996.
[27] J.-L. Masson and P. F. Green, "Viscosity of entangled polystyrene thin film melts:film thickness dependence", Phys. Rev. E 65, p. 031806, 2002.
[28] H. Shift, "Nanoimprint lithography: an old history in modern times?A review", J. Vac. Sci. Technol. B 26(2), p. 458-480, 2008.
[29] A. Fuchs, B. Vratzov, T. Wahlbrink et al., "Interferometric in situ alignement for UV-based nanoimprint", J. Vac. Sci. Technol. B 22(6), p. 3242-3245, 2004.
[30] S. D. Schuetter, G. A. Dicks, G. F. Nellis et al., "Controlling imprint distorsions in step-and-flash imprint lithography", J. Vac. Sci. Technol. B 22(6), p. 3312-3317, 2004.
[31] J. A. Rogers and H. H. Lee, "Unconventional nanopatterning techniques and applications", book ISBN 978-0-470-09957-5, John Wiley & Sons, Inc., p. 598, 2009.
[32] S. H. Ahn and L. J. Guo, "Large-area-roll-to-roll and roll-to-plate nanoimprint lithography: a step toward hight-throughput application of continuous nanoimprinting", ACS NANO 3(8), p. 2304-2310, 2009.

[33] X. D. Huang, L.R. Bao, X. Cheng et al., "Reversal imprinting by transferring polymer from mold to substrate", J. Vac. Sci. Technol. B 20(6), 2872-2876, 2002.
[34] N. Kehagias, V. Reboud, G. Chansin et al., "Reverse-contact UV nanoimprint lithography for multilayered structure fabrication", Nanotechnology 18(17), p. 175303, 2007.
[35] N. Kehagias, M. Zelsmann, C. M. S. Torres et al., "Three-dimensional polymer structures fabricated by reversal ultraviolet-curing imprint lithography", J. Vac. Sci. Technol. B 23(6), p. 2954-2957, 2005.
[36] X. Sun, L. Zhuang, W. Zhang et al., "Multilayer resist methods for nanoimprint lithography on nanoflat surfaces", J. Vac. Sci. Technol. B 16(6), p. 3922-3925, 1998.
[37] J. Hao, M. W. Lin, F. Palmieri et al., "Photocurable silicon-based materials for imprinting lithography", Proc. SPIE 6517, p. 651729/1-651729/9, 2007.
[38] E. K. Kim, J. G. Ekerdt and C. G. Willson, "Importance of evaporation in the design of materials for step and flash imprint lithography", J. Vac. Sci. Technol. B 23(4), p. 1515-1520, 2005.
[39] S. V. Sreenivasan, X. Lu, A. Cherala et al., Abstract Book, EIPBN 2007 Conference, Denver, CO, 29 May–1 June 2007.
[40] D. J. Resnick, S. V. Sreenivasan, and C. Grant Willson, "Step & flash imprint lithography", Materials Today 8(2), p. 34-42, 2005.
[41] http://www.molecularimprints.com/Technology/technology2.html
[42] M. Colburn, B. J. Choi, S. V. Sreenivasan et al., "Ramifications of lubrification theory on imprint lithography", Microelectron. Eng. 75(3), p. 321-329, 2004.
[43] D. D. Cheam, P. S. Kumar Karre, M. Palard et al., "Step and flash imprint lithography for quantum dots based room temperature single electron transistor fabrication", Microelectron. Eng. 86(4-6), p. 646-649, 2009.
[44] Y.-S. Sim, K.-D. Kim, J.-H. Jeong et al., "Wafer deformation in ultraviolet-nanoimprint lithography using an element-wise patterned stamp", Microelectron. Eng. 82(1), p. 28-34, 2005.
[45] D. Lentz, G. Doyle, M. Miller et al., "Whole wafer imprint patterning using step and flash imprint lithography: a manufacturing solution for sub-100-nm patterning", Proc. SPIE 6517, p. 65172F, 2007.
[46] J. Viheriälä, J. Tommilaa, T. Leinonena et al., "Application of UV-nanoimprint soft stamps in fabrication of single-frequency diode lasers", Microelectron. Eng. 86(3), p. 321-324, 2009.
[47] M. J. Stefan, "Versuche uber die scheinbare adhesion", Akad. Wiss. Math-Natur. 69(2), p. 713-735, 1874.
[48] H. Schift and L. J. Heyderman, "Alternative Lithography: unleashing the potential of nanotechnology", book ISBN 978-0-306-47858-1, Springer, p. 425, 2003.
[49] K. Perez Toralla, J. De Girolamo, D. Truffier-Boutry et al., "High flowability monomer resists for thermal nanoimprint lithography", Microelectron. Eng. 86(4-6), p. 779-782, 2009.
[50] M. D. Austin, H. Ge, W. Wu et al., "Fabrication of 5 nm linewidth and 14 nm pitch features by nanoimprint lithography", Appl. Phys. Lett. 84, p. 5299-5301, 2004.
[51] F. Hua, Y. Sun, A. Gaur et al., "Polymer imprint lithography with molecular-scale risolution", Nano Lett. 4(12), p. 2467-2471, 2004.
[52] W. J. Dauksher, D. Mancini, K. Nordquist et al., "Fabrication of step and flash imprinting lithography templates using a variable shaped-beam exposure tool", Microelectron. Eng. 75(4), p. 345-351, 2004.
[53] International Technology Roadmap for Semiconductors (ITRS), http://www.itrs.net/.
[54] J. Healey, "Current technical trends: dual damascene & low-k-dielectrics", Threshold system report, p. 1-6, 2002.
[55] G. M. Schmid, M. D. Stewart, J. Wetzel, et al., "Implementation of an imprint damascene process for interconnect fabrication", J. Vac. Sci. Technol B 24(3), p. 1283-1291, 2006.
[56] N. Nagai, H. Oro, K. Sakuma, et al., "Copper multilayer interconnection using ultraviolet nanoimprint lithography with a double-deck mold and electroplating", Jpn. J. Appl. Phys. 48, p. 115001-115005, 2009.
[57] G. M. Schmid, M. Miller, C. Brooks, et al., "Step and flash imprint lithography for manufacturing patterned media", J. Vac. Sci. Technolog. B 27(2), p. 573-580, 2009.
[58] http://www.onversity.net/image/actual/hamr.png
[59] M. Meier, C. Nauenheim, S. Gilles et al., "Nanoimprint for future non-volatile memory and logic devices", Microelecton Eng. 85(5-6), p. 870-872, 2008.
[60] A. Gaston, A. Z. Khokhar, L. Bilbao et al., "Nanopatterned UV curable hydrogels for biomedical applications", Microelectron. Eng. 87(5-8), p.1057-1061, 2010.
[61] I. Yoneda, S. Mikami, T. Ota et al., "Study of nanoimprint lithography for application toward 22 nm node CMOS devices", Proc. SPIE 6921, p. 692104, 2008.
[62] T. Ando, K. Kuwabara, C. Haginoya et al., "Developments of nanoimprint technologies and applications", Proc. SPIE 5931, p. 59310B, 2005.
[63] X. Liang, H. Tan, Z. Fu et al., "Air bubble formation and dissolution in dispensing nanimprint lithography", Nanotechnology 18(2), p. 25303, 2007.

[64] K.-D. Kim, J.-H. Jeong and Y.-S. Sim, “Minimization of residual layer thickness by using the optimized dispensing method in S-FIL process”, Microelectron. Eng. 83(4-9), p. 847-850, 2006.
[65] H. Hiroshima, M. Komuro, N. Kasahara et al., “Elimination of pattern defects of nanoimprint under atmosferic conditions”, Jpn. J. Appl. Phys. 42, p. 3849-3853, 2003.
[66] A. Fuchs, M. Bender, U. Plachetka et al., “Ultraviolet-based nanoimprint at reduced environmental pressure”, J. Vac. Sci Technol. B 23, p. 2925-2928, 2005.
[67] S. Landis, N. Chaix, D. Hermelin et al., “Investigation of capillary bridges growth in NIL process”, Microelectron. Eng. 84(5-8), p. 940-944, 2007.
[68] I. McMackin, W. Martin, J. Perez et al., “Patterned wafer defect density analysis of step and flash imprint lithography”, J. Vac. Sci. Technol. B 26(1), p. 151-155, 2008.
[69] T. DiBiase, M. Ahamdian, and I. Malik, “Comprehensive defect analysis methodology for nanoimprint”, Microelectron. Eng. 84(5-8), p. 989-993, 2007.
[70] I. Yoneda, S. Mikami, H. Tokue et al., “A study of filling process for UV nanoimprint lithography using a fluid simulation”, Proc. SPIE 7271, p. 72712A, 2009.
[71] http://www.mufong.com.tw/Ciba/ciba_guid/rz_uv_curing_brosch%EE%BB%AAe07%5B1%5D.pdf
[72] http://www.eclogiteskincare.com/blog/wp-content/uploads/2009/07/uv-light-spectrum.gif
[73] http://pslc.ws/mactest/radical.htm
[74] http://pslc.ws/macrog/cationic.htm
[75] J. De Girolamo, M. Chouiki, J.-H. Tortai et al., “Epoxy sislsesquioxane resists for UV nanoimprint lithography”, J. Vac. Sci Technol. B 26(6), p. 2271-2275, 2008.
[76] K. Wu, X. Wang, E. K. Kim et al., “Experimental and theoretical investigation on surfactant segregation in imprint lithography”, Langmuir 23(3), p. 1166-1170, 2007.
[77] E. P. Chan, and A. J. Crosby, “Quantifying release in step-and-flash imprint lithography”, J. Vac. Sci. Technol. B 24, p. 2716-2722, 2006.
[78] X. Cheng, L. J. Guo, and P.-F. Fu, “Room temperature and loz pressure nanimprint based on cationic photopolymerization of novel epoxysilicone monomers”, Adv. Mater. 17, p. 1419-1424, 2005.
[79] E. K. Kim, N. A. Stacey, B. J. Smith et al., “Vinyl ethers in ultraviolet curable formulations for step and flash imprint lithography”, J. Vac. Sci. Technol. B 22, p. 131-135, 2004.
[80] B. K. Long, B. K. Keitz, and C. G. Willson, “Materials for step and flash imprint lithography”, J. Mater. Chem. 17, p. 3575-3580, 2007.
[81] E. K. Kim, M. D. Stewart, K. Wu et al., “Vinyl ether formulations for step and flash imprint lithography”, J. Vac. Sci Technol. B 23, p. 2967-2971, 2005.
[82] W. Jiang, Y. Ding, H. Liu et al., “Two-step curing method for demoulding in UV nanoimprint lithography”, Microelectron. Eng. 85(2), p. 458-464, 2008.
[83] P. Voisin, M. Zelsmann, H. Ridaoui et al., “Photopolymerization kinetic study of UV nanoimprint lithography dedicated resists”, J. Vac. Sci Technol. B 25, p. 2384-2387, 2007.
[84] B. Viallet, P. Gallo, and E. Daran, “Nanoimprint process using epoxy-silane low-viscosity prepolymer”, J. Vac. Sci. Technol. B 23, p. 72-75, 2005.
[85] M. D. Stewart, J. T. Wetzel, G. M. Schmid et al., “Direct imprinting of dielectric materials for dual damascene processing”, Proc. SPIE 5751, p. 210, 2005.
[86] V. Reboud, N. Kehagias, C. M. Sotomayor Torres et al., “Spontaneous emission control of colloidal nanocrystals using nanoimprinted photonic crystals”, Appl. Phys. Lett. 90, p. 11115-11117, 2007.
[87] M. Li, H. Tan, L. Kong et al., “Four-inch photocurable nanoimprint lithography using NX-200 nanoimprinter”, Proc. SPIE 5374, p. 209-212, 2004.
[88] G. Y. Jung, W. Wu, Z. Li et al., “Surface engineering for resolution enhancement in nanoimprint lithography”, Proc. SPIE 5751, p. 952, 2005.
[89] P. Voisin, M. Zelsmann, R. Cluzel et al., “Characterisation of ultraviolet nanoimprint dedicated resists”, Microelectron. Eng. 84(5-8), p. 967-972, 2007.
[90] M. B. Chan-Park, Y. Yan, W. K. Neo et al., “Fabrication of high aspect ratio poly(ethylene glycol) containing microstructures by UV embossing”, Langmuir 19(10), p. 4371-4380, 2003.
[91] M. B. Chan-Park, Y. C. Lam, P. Laulia et al., “Simulation and investigation of factors affecting high aspect ratio UV embossing”, Langmuir 21(5), p. 2000-2007, 2005.
[92] H. Lee and G.-Y. Jung, “Wafer to wafer nano-imprinting lithography with monomer based thermally curable resin”, Microelectron. Eng. 77(2), p. 168-174, 2005.
[93] N. V. Le, W. J. Dauksher, K. A. Gehoski et al., “Selective dry etch process for step and flash imprint lithography”, Microelectron. Eng. 78-79, p. 464-473, 2005.
[94] J. Y. Kim, D.-G. Choi, J.-H. Jeong et al., “UV-curable nanoimprint resin with enhanced anti-sticking properties”, Appl. Surf. Sci 254(15), p. 4793-4796, 2008.

[95] Y. Kawaguchi, F. Nonaka and Y. Sanada, " Fluorinated materials for UV nanoimprint lithography", Microelectron. Eng. 84(5-8), p. 973-976, 2007.
[96] W. H. Heath, F. Palmieri, J. R. Adams et al., "Degrdable cross-linkers and strippable imaging materials for step-and-flash- imprint lithography", Macromolecules 41, p. 719-726, 2008.
[97] W. J. Dauksher, K. J. Nordquist, D. P. Mancini et al., "Characterization of and imprint results using indium tin oxide-based step and flash imprint lithography templates", J. Vac. Sci. Technol. B 20, p. 2857-2861, 2002.
[98] M. Komuro, Y. Tokano, J. Taniguchi et al., "Improvement of imprinted pattern uniformity using sapphire mold", Jpn. J. Appl. Phys. 41, p. 4182-4185, 2002.
[99] K.-I. Nakamatsui, N. Yamada, K. Kanda et al., "Fluorinated diamond-like carbon coating as antisticking layer on nanoimprint mold", Jpn. J. Appl. Phys. 45, p. L954-L956, 2006.
[100] A. O. Altun, J.-H. Jeong, J.-J. Rha et al., "Boron nitride stamp for ultra-violet nanoimprint lithography fabricated by focused ion beam lithography", Nanotechnology 18(46), p. 465302, 2007.
[101] D. P. Mancini, K. A. Gehoski, E. Ainley et al., "Hydrogen sislsesquioxane for direct electron-beam patterning of step and flash lithography templates", J. Vac. Sci. Technol. B 20, p. 2896-2901, 2002.
[102] D. J. Resnick, D. Mancini, W. J. Dauksher et al., "Improved step and flah imprint lithography templates for nanofabbrication", Microelectron. Eng. 69(2-4), p. 412-419, 2003.
[103] G. M. Schmid, E. Thompson, N. Stacey et al., "Template fabrication for the 32 nm node and beyond", Microelectron. Eng. 84(5-8), p. 853-859, 2007.
[104] S. Sasaki, T. Hiraka, J. Mizuochi et al., "UV-NIL template making and imprint evaluation", Proc. SPIE 7271, p. 72711M-72711M-7, 2009.
[105] P. Voisin, M. Zelsmann, C. Gourgon et al., "High-resolution fused silica mold fabrication for UV-nanoimprint", Microelectron. Eng. 84(5-8), p. 916-920, 2007.
[106] D. R. Barbero, M. S. M. Saifullah, P. Hoffmann et al., "High resolution nano imprinting with a robust and reusable polymer mold", Adv. Func. Mat. 17, p. 2419-2425, 2007.
[107] W.-S. Kim, D.-G. Choi and B.-S. Bae, "Ultraviolet-nanoimprint of 40 nm scale patterns using functionally modified fluorinated hybrid materials", Nanotechnology 17(13), p. 3319-3324, 2006.
[108] N. Kehagias, V. Reboud, J. De Girolamo et al., "Stamp replication for thermal and UV nanoimprint lithography using a UV-sensitive silsesquioxane resist", Microelectron. Eng. 86(4-6), p. 776-778, 2009.
[109] M. Bender, U. Plachetka, J. Ran et al., "High resolution lithography with PDMS molds", J. Vac. Sci. Technol. B 22, p. 3229-3232, 2004.
[110] J. Viheriälä, M.-R. Viljanen, J. Kontio et al., "Soft stamp UV-nanoimprint lithography for fabrication of laser diodes", Proc. SPIE 7271, p. 72711O, 2009.
[111] M. Beck, and B. Heidari, OnBoard Technology, p. 52, 2006, www.Onboard-Technology.com.
[112] H. F. Hess, D. Pettibone, D. Adler et al., "Inspection of templates for imprint lithography", J. Vac. Sci. Technol. B 22, p. 3300-3305, 2004.
[113] W. J. Dauksher, K. J. Nordquist, N. V. Le et al., "Repair of step and flash imprint lithography templates", J. Vac. Sci. Technol. B 22, p. 3306-3311, 2004.
[114] M. Pritschow, J. Butschke, M. Irmscher et al., "Evaluation of the CD-SEM Vistec LWM90xx for line-with measurement of nanoimprint templates", Proc. SPIE 7271, p. 72711U, 2009.
[115] K. Selinidis, E. Thompson, I. McMackin et al., "High-resolution defect inspection of step-and-flash imprint lithography for 32-nm half-pitch patterning", Proc. SPIE 7271, p. 72711W, 2009.
[116] W. J. Dauksher, N. V. Le, K. A.Gehoski et al., "An electrical characterization of wafers imprinted with step and flash imprint lithography", Proc. SPIE 6517, p. 651714, 2007.
[117] S. Ramachandran, L. Tao, T. H. Lee et al., "Deposition and patterning of diamondlike carbon as antiwear nanoimprint templates", J. Vac. Sci. Technol. B 24, p. 2993-2997, 2006.
[118] A O Altun, J. H. Jeong, J. J. Rha et al., "Fabrication of fluorine-doped diamond-like carbon stamps for UV nanoimprint lithography", Nanotechnology 17(8), p. 4659-4663, 2006.
[119] F. A. Houle, S. Raoux, D. C. Miller et al., "Metal-containing release layers for use with UV-cure nanoimprint lithographic template", J. Vac. Sci. Technol B 26, p. 1301-1304, 2008.
[120] H. Sun, J. Liu, P. Gu, and D. Chen et al., "Anti-scticking treatment for a nanoimprint stamp", Appl. Surf. Sci. 254(10), p. 2955-2959, 2008.
[121] U. Srinivasan, M. R. Houston, R. T. Howe et al., "Alkytrichlorosilane-based self-assembled monolayer films for stiction reduction in silicon micromachines", J. of Micro Electro Mech. Syst. 7(2), p. 252-260, 1998.
[122] M. Beck, M. Graczyk, I. Maximov et al., "Improving stamps for 10 nm level wafer scale nanoimprint lithography", Microelectron. Eng. 61-62, p. 441-448, 2002.
[123] H. Schift, S. Saxer, S. Park et al., "Controlled co-evaporation of silanes for nanoimprint stamps", Nanotechnology 16(5), p. S171-S175, 2005.

[124] G.-Y. Jung, Z. Li, W. Wu et al., "Vapor-phase self-assembled monolayer for improved mold release in nanoimprint lithography", Langmuir 21(4), p. 1158-1161, 2005.
[125] Y. Tada, H. Yoshida and A. Miyauchi, "Analysis on deterioration mechanism of release layer in nanoimprint process", J. Photopolym. Sci. Technol. 20(4), p. 545-548, 2007.
[126] L. C. Lloyd and M. Malloy, "SEMATECH's nanoimprint program: a key enabler for nanoimprint introduction", Proc. SPIE 7271, p. 72711Q-72711Q-10, 2009.
[127] F. A. Houle, C. T. Rettner, D. C. Miller et al., "Antiadhesion considerations for UV nanoimprint lithography", Appl. Phys. Lett. 90, 213103-213105, 2007.
[128] F.A. Houle, E. Guyer, D.C. Miller et al., "Adhesion between template materials and UV-cured nanoimprint resists", J. Vac. Sci. Technol. B 25, p. 1179-1185, 2007.
[129] H. Schmitt, M. Zeidler, M. Rommel et al., "Custom-specific UV nanoimprint templates and life-time of antisticking", Microelectron. Eng. 85(5-6), p.897-901, 2008..
[130] M. W. Lin, D. J. Hellebusch, K. Wu et al., "The role of surfactants in adhesion reduction for step and flash imprint lithography", J. Micro/Nanolith. MEMS MOEMS 7(3), p. 33005, 2008.
[131] Briggs and M. P. Seah, "Practical surface analysis by Auger and X-ray photoelectrons pectroscopy", book ISBN 0-471-95340-7, Wiley, 1983.
[132] N. Yamada, K. Nakamatsu, K. Kanda et al., "Surface evaluation of fluorinated diamond-like carbon thin film as an antisticking layer of nanoimprint mold", Jpn. J. Appl. Phys. 46, p. 6373-6374, 2007.
[133] Y. Hirai, S. Yoshida, A. Okamoto et al., "Mold surface treatment for imprint lithography", J. Photopolym. Sci. Technol. 14(3), p. 457-462, 2001.
[134] M. Okada, M. Iwasa, K. Nakamatsu et al., "Durability of antisticking layer against heat in nanoimprint evaluated using scanning probe microscopy", Microelectron. Eng. 86(4-6), p. 657-660, 2009.
[135] C. Decker, "Polymérisation sous rayonnement UV", Techniques de l'Ingénieur, AM 3044, 2000.
[136] X. Gao and J. Nie, "Low temperature photopolymerization and post cure characteristic"Polym. Int. 56 (2007) 707.
[137] J. D. N. Filho, L. T. Poskus, J. Guilherme, et al., "Degree of conversion and plasticization of dimethacrylate-based polymeric matrices: influence of light-curing mode", J. Oral Sci. 50(3), p. 315-321, 2008.
[138] http://hal.archives-ouvertes.fr/docs/00/04/84/93/PDF/5d_Partie_IV.pdf
[139] http://www.fo.usp.br/portal/materiaisp/arquivos/Finer2004.pdf
[140] D. C. Doetschman, R. C. Mehlenbacher and D. Cywar, "Stable free radicals produces in acrylate and methacrylate free radical polymerization: comparative EPR studies of structure and effects of cross-linking", Macromolecules 29(5), p. 1807-1816, 1996.
[141] W. C. Oliver, and G. M. Pharr, "An improved technique for determining hardness and elastic modulus using load and displacement sensing indentation experiments", J. Mater. Res. **7**(6), p. 1564-1583, 1992.
[142] F. Carrillo, S. Gupta, M. Balooch et al., "Nanoindentation of polydimethylsiloxane elastomers: effect of crosslinking, work of adhesion, and fluid environment on elastic modulus", J. Mater. Res., 20(10), p. 2820-2830, 2005.
[143] M. Bender, M. Otto, B. Hadam et al., "Multiple imprinting in UV-based nanoimprint lithography: related material issues", Microelec. Eng. 61–62, p. 407-413, 2002.
[144] J. K. Bosworth, M. Y. Paik, R. Ruiz et al., "Control of self-assembly of lithographically patternable block copolymer films", ACS Nano 2(7), p. 1396-1402, 2008.
[145] S. Park, D. H. Lee, J. Xu et al., "Macroscopic 10-terabit-per-square-inch arrays from block copolymers with lateral order", Science 323(5917), p. 1030-1033, 2009.
[146] G. Kim and M. Libera, "Morphological development in solvent-cast polystyrene-polybutadiene-polystyrene (SBS) triblock copolymer thin films", Macromolecules 31(8), p. 2569-2577, 1998.
[147] F. S. Bates and G. H. Fredrickson, "Block copolymers-designer soft materials", Phys. Todays 52(2), p. 32-38, 1999.
[148] R. A. Farrell, N. Petkov, N. Morris et al., "Self-assembled templates for the generation of 1 arrays of 1-dimensional nanostructures. From molecules to devices", J. Colloid Interface Sci. 349(2), p. 449-472, 2010.
[149] C. T. Black, "Integration of self assembly for semiconductor microelectronics", Proc. IEEE, Custom integrated circuits conference, p. 87-91, 2005.
[150] P.P. Soo, B.Y. Huang, Y. I. Jang et al., "Rubbery block copolymer electrolytes for solid-state rechargeable lithium batteries", J. Electrochem. Soc. 146(1), p. 32-37, 1999.
[151] M. Ulbricht, "Advanced functional polymer membranes", Polymer 47, p. 2217-2262, 2006.
[152] C. Park, J. Yoon and E. L. Thomas, "Enabling nanotechnology with self assembled block copolymer patterns", Polymer 44(22), p. 6725-6760, 2003.
[153] A. J. Hong, C. Liu, Y. Wang et al., "Metal nanodot memory by self-assembled block copolymer lift-off", Nano Lett. 10(1), p. 224-229, 2010.

[154] R. A. Farrell, T. G. Fitzgerald, D. Borah, et al., "Chemical interactions and their role in the microphase separation of block copolymer thin films", Int. J. Mol. Sci. 10(9), p. 3671-3712, 2009.
[155] T. Thurn-Albrecht, J. DeRouchey, T. P. Russell et al., "Pathways toward electric field induced alignment of block copolymers", Macomolecules 35(21), p. 8106-8110, 2002.
[156] P. Mansky, J. DeRouchey, J. Mays et al., "Large-are domain alignment in block copolymer thin films using electric fields", Macromolecules 31(13), p. 4399-4401, 1998.
[157] D. E. Angelescu, J. H. Waller, D. H. Adamson, et al., "Macroscopic orientation of block copolymer cylinders in single-layer film by shearing", Adv. Mater. 16, p. 1736-1740, 2004.
[158] C. Park, C. D. Rosa, B. Lotz et al., "Molecular and microdomain orientation in semicrystalline block sopolymer thin films by directional crystallization of the solvent and epitaxy", Macromol. Chem. Phys. 204(12), p. 1514-1523, 2003.
[159] M. P. Stoykovich, M. Müller, S. O. Kim et al., "Direct assembly of block copolymer blends into nonregular device-oriented structures", Science 308(5727), p. 1442-1446, 2005.
[160] R. A. Segalman, A. Hexemer and E. J. Kramer, "Edge effects on the order and freezing of a 2D array of block copolymer spheres", Phys. Rev. Lett. 91, p. 196101-1-196101-4, 2003.
[161] N. Kehagias, G. Chansin, V. Reboud et al., "Embedded nano channels fabricated by non-selective reverse contact UV nanoimprint lithography technique", Microelectron. Eng. 84(5-8), p. 921-924, 2007.
[162] N. Kehagias, V. Reboud, G. Chansin, et al., "Reverse-contact UV nanoimprint lithography for multilayered structure fabrication", Nanotechnology 18(17), p. 175303-1-175303-4, 2007.
[163] J. Wu and P. T. Mather, "POSS polymers: physical properties and biomaterials applications", J. Macromol. Sci. Polymer Rev. 49, p. 25-63, 2009.
[164] A. T. Kohl, R. Mimna, R. Shick et al., "Low k, porous methyl silsesquioxane and spin-on-glass", Electrochem. Solid State Lett. 2(2), p. 77-79, 1999.
[165] T. Yamaguchi and H. Yamaguchi, "Two-dimensional patterning of flexible designs with high half-pitch resolution by using block copolymer lithography"Adv. Mater. 20(9), p.1684-1689, 2008.
[166] A. Subramani, D. Geerpuram, A. Domanowski et al., "Vortex state in magnetic rings", Physica C 404(1-4), p. 241-245, 2004.
[167] J. J. Schwab and J. D. Lichtenhan, "Polyhedral oligomeric silsesquioxane (POSS)-based polymers", Appl. Organomet. Chem. 12(10-11), p. 707-713, 1998.
[168] S. Bizet, J. Galy and J.-F. Gerard, "Structure-property relationships in organic-inorganic nanomaterials based on methacryl-POSS and dimethacrylate networks", Macromolecules 39(7), p. 2574-2583, 2006.
[169] G. M. Schmid, M. D. Stewart, J. Wetzel, et al., "Implementation of an imprint damascene process for interconnect fabrication", J. Vac. Sci. Technol. B 24, p. 1283-1291, 2006.
[170] Y.-L. Liu, M.-C. Tseng and M.-H. Fangchiang, "Polymerization and nanocomposites properties of multifunctional methylmethacrylate POSS", J. Polym. Sci., Polym. Chem. 46(15), p. 5157-5166, 2008.
[171] Y. Xu, X. Zhu and S. Yang, "Crack-free 3D hybrid microstructures from photosensitive organosilicates as versatile photonic templates", ACS Nano 3(10), p. 3251-3259, 2009.
[172] S. Matsui, Y. Igaku, H. Ishigaki et al., "Room temperature replication in spin on glass by nanoimprint technology", J. Vac. Sci. Technol. B 19(6), p. 2801-2805, 2001.
[173] Y. Igaku, S. Matsui, H. Ishigaki et al., "Room temperature nanoimprint technology using hydrogen silsesquioxane (HSQ)", Jpn. J. Appl. Phys. 41, p. 4198-4202, 2002.
[174] S. Singh, S. Chen, K. Selinidis et al., "Automated imprint mask cleaning for step-and-flash imprint lithography", Proc. SPIE 7271, p. 72712H-1-72712H-9, 2009.
[175] C. Brooks, G. M. Schmid, M. Miller et al., "Step and flash imprint lithography for manufacturing patterned media", Proc. SPIE 7271, p. 72711L, 2009.
[176] *STMicroelectronics* in European MEDEA+ project *Fantastic*, 2007-2010.
[177] Q. Xia, W. Wu, J.J. Yang et al., "On the integration of memristors with CMOS using nanoimprint lithography", Proc. SPIE 7271, p. 727106, 2009.

Résumé

La nanoimpression assistée par UV (UV-NIL) est une technique de lithographie émergente permettant de fabriquer des motifs de très petites dimensions (de l'ordre du nanomètre) par simple pressage d'un moule transparent (contenant dans sa surface des nanostructures) dans une résine fluide (déposée en film mince sur un substrat en silicium par centrifugation). L'étape suivante au pressage est l'exposition aux rayonnements UV qui photo-polymérise la résine, avant de séparer le moule de la résine durcie. En raison de son fort potentiel, l'UV-NIL est considéré comme un candidat possible pour réaliser l'étape lithographique dans la fabrication des circuits intégrés du futur. Deux aspects critiques peuvent empêcher l'adoption de l'UV-NIL à une échelle industrielle. Il s'agit des défauts générés après l'étape de pressage (liés à l'écoulement de la résine) et la courte durée de vie du moule traitée (il est en fait nécessaire de déposer une couche antiadhésive sur la surface du moule pour éviter que la résine s'y colle). La première problématique a été abordée à travers la proposition d'un model qui semble permettre de estimer la longueur d'écoulement des résines fluide pour l'UV-NIL.
Les recherches menées au tour de la deuxième problématique représentent le cœur de ce manuscrit. Une meilleure compréhension des mécanismes de dégradation de la couche antiadhésive ont été acquis. La dégradation est le résultat d'une attaque chimique (exercé par les radicaux produits dans la résine polymérisée contre la molécule fluorée et conditionné aussi par la nature chimique de la résine photo-sensible) et d'une dégradation mécanique (due aux stresses exercés pendant le démoulage et liée à la qualité du greffage de la molécule antiadhésive sur le moule). La rajoute de surfactants fluorés dans la formulation de la résine représente une solution valable pour augmenter le nombre d'impressions faites avec un même moule traité.
Enfin une résine hybride (organique-inorganique) a été synthétisée pour une application concrète : la réalisation de moules qui permettent d'organiser à longue échelle (quelque millimètre) des di-bloc copolymers (avec un taille de quelque nanometer) par graphoepitaxie.

Abstract

The UV curing nanoimprint lithography (UV-NIL) is a next generation lithography technique that can produce very tiny patterns (in the nanometer scale) by a simple imprinting step performed with a patterned and transparent template in a flowable resist (deposed par spin-coating on a silicon substrate as thin layer). The imprinting step is then followed by UV exposure (that cures the resist) and demolding. Due to its high potential in replicating patterns with high resolution, UV-NIL is considered nowadays as a possible candidate to perform the lithographic step in the next generation integrated circuits. Two critical issues threaten the spreading of UV-NIL at large scale: defects generated during imprinting step (depending on the resist flowing behaviour) and short life-time of a treated mold (a fluorinated self assembled monolayer, F-SAM, is deposed on the mold surface to avoid the sticking of the resist). Concerning the first issue, a model potentially capable to predict the flowing distance of liquid photo curable resist is presented.
The experiments performed over the second issue were really profitable and gave interesting results. In fact, a better understanding on the mechanisms of ASL degradation was achieved. This aging is due to a chemical attack (exerted by free radicals, which was generated into the uv curable resist during polymerization step, toward the fluorinated molecule, and conditioned as well by the chemical nature of the resist) and a mechanical degradation (caused by the stress exerted during demolding step and linked to the quality of F-SAM grafting on the mold surface). The add of fluorinated surfactants in the chemical formulation of the resist represent an effective solution for improving the number of imprints performed employing the same mold.
At the end of this manuscript there is the presentation of a hybrid (organic-inorganic) resist, that was synthesized for a real useful application: the creation of templates to arrange at large scale (few millimetres) di-bloc copolymers (sized of few nanometres) by graphoepitaxy.

Mots-clé

Lithographie, nanoimpression, UV-NIL, écoulement, anti-sticking layer, dégradation, graphoépitaxie

Key-words

Lithography, nanoimprint, UV-NIL, flowing, anti-sticking layer, degradation, graphoepitaxy